IAEA-TECDOC-1412

Integration of tracing with computational fluid dynamics for industrial process investigation

Final report of a co-ordinated research project
2001–2003

IAEA
International Atomic Energy Agency

November 2004

IAEA-TECDOC-1412

Integration of tracing with computational fluid dynamics for industrial process investigation

Final report of a co-ordinated research project
2001–2003

IAEA
International Atomic Energy Agency

November 2004

The originating Section of this publication in the IAEA was:

Industrial Applications and Chemistry Section
International Atomic Energy Agency
Wagramer Strasse 5
P.O. Box 100
A-1400 Vienna, Austria

INTEGRATION OF TRACING WITH COMPUTATIONAL FLUID DYNAMICS
FOR INDUSTRIAL PROCESS INVESTIGATION
IAEA, VIENNA, 2004
IAEA-TECDOC-1412
ISBN 92–0–114504–7
ISSN 1011–4289

© IAEA, 2004

Printed by the IAEA in Austria
November 2004

FOREWORD

The Coordinated Research Project on Integration of Residence Time Distribution (RTD) Tracing with Computational Fluid Dynamics (CFD) Simulation for Industrial Process Visualization and Optimization began in January 2001 and was completed in December 2003. Five research agreement holders from Australia, France, Germany, Norway and the United States of America were involved, providing their expertise and know-how. Six research contract holders from Brazil, Cuba, Czech Republic, India, Republic of Korea and Poland with recognized experience in radiotracer methodology and technology as applied to industrial processing also participated in the project.

The overall objective of the CRP, which is the basis for the present TECDOC, was to develop and validate an integrated methodology for radiotracer and fluid dynamics modelling in investigation of engineering processes selected from chemical and petrochemical industries, energy production, mineral ore processing and wastewater treatment sectors. The main scope of the CRP was to elaborate a combined experimental-computational method for obtaining reliable quantitative results about process insight in industrial vessels and process units to improve and optimize their design and efficiency.

The first research coordination meeting (RCM) held in Vienna on 5–8 May 2001 defined the detailed technical content for each of the participating groups in order to meet the objectives of the CRP.

The second RCM was held in Saclay, France on 15–19 July 2002. This meeting evaluated the research work during the first year. Good progress was made. The experiments also highlighted some difficult issues to be addressed in more detail. Simplified experimental set-ups were defined in order to further study some basic principles. A first version of an educational package for CFD was presented and evaluated.

The third and final RCM took place at the International Atomic Energy Agency in Vienna on 1–5 December 2003. The RCM summarized the participants' experiences in using RTD and CFD together on a variety of different industrial problems. The educational package introducing the concepts of CFD and RTD was finalized and tested.

The participants amply demonstrated the beneficial role of RTD-CFD integrated method in analysing and optimizing industrial processes with many case studies from chemical and petrochemical industries, from mineral ore processing and waster water treatment plants.

The CRP participants from developing countries are becoming more confident in introducing CFD simulation in tracer investigations. The CFD educational package provides basic information about the CFD approach. The CFD-RTD educational package will play an important role in the training of tracer specialists in developing countries, thereby improving their performance and accreditation in industrial problem solving.

This TECDOC summarizes the main achievements of the CRP, provides basic information about the CFD simulation of industrial processes, gives the main lines of the CFD-RTD software and illustrates their use through many case studies. It will help the radiotracer and chemical engineering specialists in introducing modern modeling methods to industry and in transferring the technology from developed to developing countries. The CFD-RTD software is attached to the TECDOC.

The IAEA wishes to thank all the participants in the CRP for their valuable contributions. The IAEA officers responsible for this publication were J. Jin and J. Thereska of the Division of Physical and Chemical Sciences.

EDITORIAL NOTE

This publication has been prepared from the original material as submitted by the authors. The views expressed do not necessarily reflect those of the IAEA, the governments of the nominating Member States or the nominating organizations.

The use of particular designations of countries or territories does not imply any judgement by the publisher, the IAEA, as to the legal status of such countries or territories, of their authorities and institutions or of the delimitation of their boundaries.

The mention of names of specific companies or products (whether or not indicated as registered) does not imply any intention to infringe proprietary rights, nor should it be construed as an endorsement or recommendation on the part of the IAEA.

The authors are responsible for having obtained the necessary permission for the IAEA to reproduce, translate or use material from sources already protected by copyrights.

CONTENTS

SUMMARY 1

Advanced CFD & radiotracer techniques — A complementary technology — for industrial multiphase applications 23
J.Y. Tu

Modelling the internal flow in a photo-reactor for wastewater irradiation 35
R.M. Moreira, A.M.F. Pinto, B.G. Batista,C.V. Alves

Applications of CFD and tracer stimulus response techniques in complex flow analysis 49
J. Thýn

Tracer experimental techniques for CFD model verification and validation in sugar crystallizer 67
J. Griffith, J. Borroto, J. Domínguez, M. Derivet, J. Cuesta, P. Flores
D. Fernández, A. Amor, B. Franklin

Simulation of a radiotracer experiment by flow and detection chain modelling: A first step towards better interpretation. 85
P. Berne

Investigation of transport behaviour of selected organic compounds in electrochemical remediation of contaminated soils 109
T. Jentsch

Validation of CFD models and integration of CFD-RTD methods for industrial process visualization and optimization..... 119
H.J. Pant, A. Patwardhan, A.K. Mahendra, V.V. Ranade

Radiotracer assisted visualization and CFD modelling of multiphase fluid flow in porous media..... 147
T. Bjørnstad, A. Haugan, C. Chatzichristos, Ø. Dugstad, J. Sagen

Combining CFD simulation with experimental RTD function for hydrocyclone separator studies. 161
Z. Stegowski, E. Nowak, L. Furman

Application of radiotracer technology and CFD for diagnosis of wastewater treatment plant 179
J.H. Jin, S.H. Jung, J.B. Kim
D.S. Jang, H.S. Kim, M.S. Shin

Contributions to the CRP integration of RTD tracing with CFD simulation for process visualization and optimization..... 203
R. Gardner, A. Shehata, Ch. Huffman, V. Metwally, W. Guo

ANNEX: CFD&RTD EDUCATIONAL PACKAGE 209

LIST OF PARTICIPANTS 221

SUMMARY

1. BACKGROUND ON RTD AND CFD

Two major methods used for investigation of industrial complex processes are the radiotracer residence time distribution (RTD), which is an experimental method, and computational fluid dynamics (CFD), which is a numerical simulation method.

Residence time distribution (RTD)

Residence time distribution (RTD) analysis by radiotracer derives important information from process units, such as flow pattern, back mixing, bypassing. A sharp pulse of a suitable radioactive tracer is injected into the inlet of a process unit or vessel. The response curve from the outlet detector is known as the residence time distribution (RTD) function (Fig. 1). This RTD function provides rich information about the process stream dynamics.

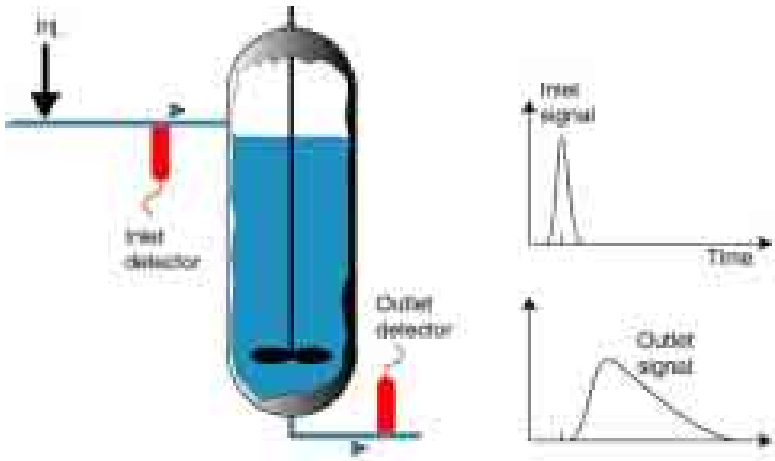

FIG. 1. Principle of RTD tracing method.

The residence time distribution (RTD) method has been continuously developed and used. The treatment of RTD curves for extracting important parameters of industrial processes has achieved a good standard. Efficient RTD software was validated for modeling of various chemical engineering reactors. However, the RTD method remains a global approach. RTD systemic analysis requires the choice of a model, which is often semi-empirical and rather idealized (combination of perfect mixers, dead volumes, etc.). There are some situations in which the RTD approach can not be applied (non-linear systems).

Computational fluid dynamics method

Industry is looking for more predictive techniques. Computer Fluid Dynamic (CFD) method provides detailed spatial distribution of flow fields (Figs. 2&3). Computational fluid dynamics (CFD) uses advanced computer software to model the flow of fluids through a processing facility. Increasing computer power in the last decade is a dominant factor determining the rapid growth of industrial utilization of CFD. CFD can be easily coupled to modern tools for three-dimensional visualization, creating maps of velocity vectors, streamlines, iso-value contours, etc.

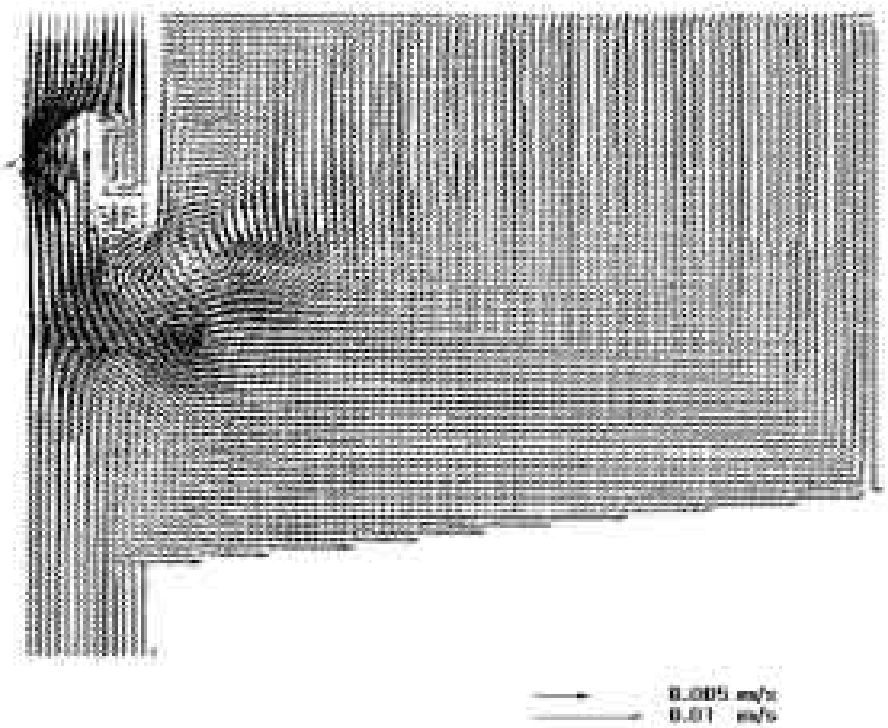

FIG. 2. CFD modelling of a wastewater treatment plant: map of flow and velocity patterns.

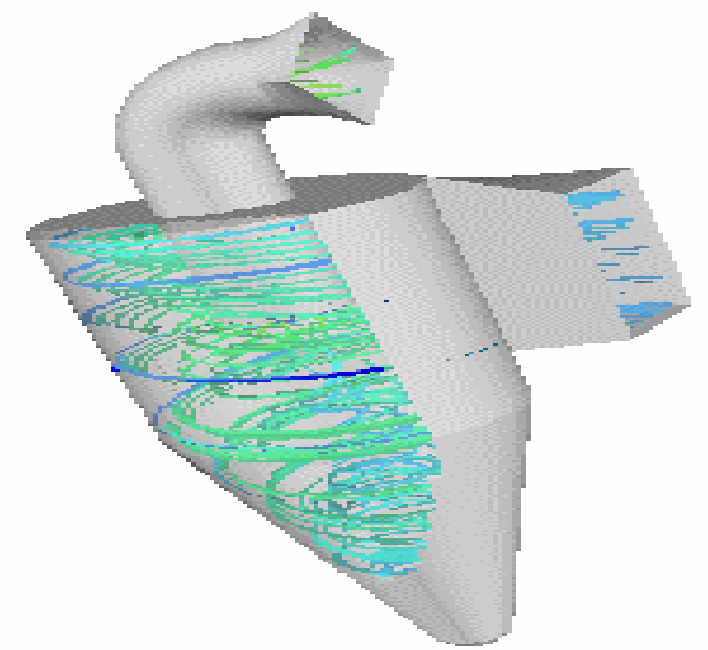

FIG. 3. CFD modelling of particle flows map inside a cyclone.

At present, both RTD and CFD methods are used for investigation of hydrodynamics in engineering processing reactors. Experimental RTD tracing is reasonably simple and reliable; it provides various important hydrodynamic parameters but it is not able to visualize the flow pattern inside the flow containment.

The numerical simulation of industrial processes through Computational Fluid Dynamics (CFD) method is a relatively new approach more powerful for process visualization. CFD simulation is performed by sophisticated CFD software. The most known in the market is FLUENT software package. It is quite heavy in use, so only computer specialists and well specialized engineers can use it. Moreover, it is rather expensive and only few institutions and universities in developed and more advanced developing countries could afford it cost for research and education activities.

The CFD simulation consists in solving transport equations for known geometrical configuration of a reactor. This is a calculation exercise that could provide deformed maps especially in systems with strong interaction of hydrodynamics with physico-chemical reactions. The exciting CFD results (Figs. 2&3) are being questioned by industries about reliability of their models due to lack of experimental techniques for model verification and validation This is the reason why CFD models have to be verified and validated by experimental tracer RTD results.

The RTD-CFD interaction is both sides. The CFD can be used also to complement the information obtained from the RTD systemic approach. CFD provides data that can quantify RTD systemic model, which means the CFD model, can "degenerate" into more quantitative RTD systemic analysis, providing more comprehensive results for chemical engineers. In fact, these two approaches, experimental and numerical, are complementary to each other. The RTD systemic approach detects and characterizes main features of the flow (mixing and recirculations) while CFD enables to locate them. The trend is to combine experimental and numerical approaches in order to obtain reliable quantitative results for industrial complex processes.

There is a need is to elaborate an integrated RTD-CFD experimental-computational method for obtaining reliable quantitative results about process insight in industrial vessels and process units to improve and optimize their design and efficiency.

The industrial processes under investigation in the frame of this CRP were:

- Hydrocyclone in copper ore enrichment (Poland)
- Clarifier in wastewater treatment plant (Korea)
- Crystalliser in sugar processing plant (Cuba)
- Stirred tank in petrochemical and chemical industry (India)
- Photo reactor in wastewater purification installation (Brazil)
- Heat exchanger in petrochemical industry (Czech republic)

2. SUMMARY OF CRP PARTICIPANTS' REPORTS

Australia

In the framework of the CRP research on computational fluid dynamics (CFD) modeling of various industrial multiphase flows, including gas-solid particle flow in power utility boilers and heat exchangers, liquid-bubbly flow due to sub-cooled boiling in nuclear reactors, and water-sediment two-phase flow in rivers was carried out. A number of CFD codes including commercial software, FLUENT and CFX, and in-house research codes have been used for these applications. Comparisons of numerical predictions with experimental data from radiotracer techniques were performed.

In cooperation mainly with Mr. Berne, France and other CRP participants a CFD&RTD Education Package was developed, in which lecture notes, tutorials and computer software for both CFD and RTD are included.

CFD for multiphase flow has made significant strides in recent years and is rapidly becoming a useful tool for system design, scale-up and optimisation. However, detailed, non-intrusive experimental data are still lacking for comprehensive validation of mathematical models in CFD software for solving complex industrial multiphase flow problems. Through this CRP it has been demonstrated that radiotracer techniques could play an important role in addressing this problem through RTD analysis due to its advantages over many conventional techniques. CFD simulation could also be used for RTD analysis in characterising the basic flow behaviour of the processing units or plants.

The numerical tracer tests using CFD, based on the calculated flow field, could be an effective tool in combination with the tracer experiment/field-scale measurements. RTD analysis, together with the detailed knowledge of flow and temperature distribution throughout the system, can give a more complete picture or visualisation of the flow characteristics of the multiphase processing system. The integration of CFD with radiotracer RTD techniques may become a complementary technology to be greatly beneficial for industrial applications (cost-effectively consulting and services

Brazil

The photo reactor (PR), which is fairly simple geometry and flow pattern, was selected and has shown to be a good choice. A laboratory unit especially designed for tracer tests was built up.

A multipoint data acquisition system and the basic RTD software package DTSPRO from France were used for tracer experimental work and data processing and modeling. A commercial software package for CFD simulation, the CRX code, has been acquired. There was rather difficult for tracer group to make use of CFD software for numerical modeling. The experience obtained during the CRP allows pursuing the RTD-CFD integrated work.

The tracer group has profited from the exceptional opportunity of networking with researchers throughout the world working at the border of the RTD and CFD techniques together with the consolidation of the cooperation with local researchers in the process and water treatment areas. The choice of a particularly adequate system for flow modeling studies, and the combination of the experimental methodologies for this task comprising actual visualization, flexibility for parameter tuning, and operational simplicity is the main achievement of Brazilian tracer group.

Cuba

In the framework of this CRP the Cuban team has worked on the improvement of the experimental design for RTD tests at a pilot sugar crystallizer and on the selection of the proper tracer for that kind of studies in order to achieve reliable results for CFD flow simulation at this installation. As a result of these tests, the redesign of the crystallizer was performed. A new approach for RTD studies in non-Newtonian fluids for flow patterns characterization at the pilot crystallizer was carried out showing the complexity of this system. With the same purposes, batch mixing process was also tested and a homogenization time for massecuite fluid close to seven hours was found out. This evidences that the crystallizers that the Cuban sugar industry is trying to develop will achieve low exhaustion efficiency with significant sugar losses due to their relative low residence time.

Because of a lack of the powerful CFD code Fluent, the flow simulation was carried out by the CFD code Flotran in the ANSYS 5.4 package. The possibility of RTD prediction on the basis of numerical solution of transport equations for fluid dynamics in a more simplified geometry of the crystalliser with molasses as fluid using transient analysis of temperature pulse spreading was tried. This is a necessary step for further validation of flow simulation by the RTD function of a real massecuite fluid at crystalliser. It was concluded that for complex flow structure, the more general Stimulus Response Method (SRM) based in point source response (PSR) is more suitable for CFD verification than the, in some cases, ambiguous, RTD function.

Hence, the design and preparation of a multipurpose point source consisting of a mini-version of the generator system $^{99}Mo/^{99m}Tc$ has been performed and a special PC-program has been prepared for the interpolation of detector responses function.

Czech Republic

The activities of Czech research group can be divided into three categories:

- Prediction of RTD model changes by CFD;
- CFD verification by RTD;
- Methodology of CFD verification by RTD and by local responses.

CFD application for prediction of RTD model changes was demonstrated on gas flow analysis in electron beam cylindrical chamber with baffles. RTD was effectively simulated in 2D modeling by using a Finite Element method. A salt tracer coupled with conductivity detection as well radiotracers were used in the experiments and the best comparison was obtained for the real value of the parameter. This solution exemplifies how the problem can be solved even with more simple 2D description of the real system. Special software, a so-called integral zonal model, was developed and tested for heating conditions. The model is able to predict the influence of heater geometry, fluid properties and operational parameters.

The methodology for successful simulation of Stimulus Response experiment by special post-processing data treatment was suggested. This method uses detection chain description and enables simulation of the local responses registered by the detector from the tracer concentration field evaluated by CFD code. Application of this methodology was demonstrated on parallel flow analysis on an Ohmic heater and on the analysis of time homogenization in a vessel with mechanically stirring.

RTD & CFD are suitable methods for flow analysis in industrial equipment. As there are some difficulties in simulation of tracer experiments in laminar flow (e.g. numerical dispersion) and similar numerical problems can be expected also in transient or turbulent flows, the verification on the basis of velocity measurements is recommended if possible.

CFD codes are powerful tools, which are used for prediction of heat, mass and momentum of complicated flows in industrial equipment. However, application of CFD models in the process control or in detail analysis of biological or chemical kinetics is impracticable. In contrary, the system analysis by RTD modeling is easy to implement. Approach of “Simplified Fluid dynamic by Combined Model Network” is recommended and the solution is based on a two step procedure. The first step is the complex flow by 3D CFD simulation and the next step is simplification of the flow behavior to a network of plug flow or ideally mixed regions strictly interconnected.

France

Two contributions have been made during the CRP.

Firstly, the response of a wall detector placed in a backward-facing step flow has been calculated (using CFD and a Monte Carlo code) as a function of location, tracer energy and flow regime.

Secondly, a routine for RTD model optimization has been provided for the educational package.

The idea with the first contribution was to see if the detector signal could give some information on the flow pattern and velocity. Numerical routines have been developed along the same lines as those used by the Czech group.

Although only moderate success has been achieved with respect to the initial objective, the results obtained highlight the pitfalls in exploiting data from local (as opposed to outlet) detectors.

Progress in this area would require development and qualification of reliable methods for peak decomposition.

The objective of the second contribution was to have a simple tool with a limited number of models for the purpose of demonstration and education.

Germany

Two basic radiotracer applications were carried out during the CRP:

- Lab scale transport behavior investigations of selected organic compounds at the electrochemical soil remediation facility
- Gas RTD and gas distribution measurements in a cross sectional area of a reactor for batch pyrolysis of waste wood particles.

Regarding the first application the following results were achieved:

- Transport behavior of model contaminants in several electrical fields and different kinds of soil could be quantified,
- Competitive influence of the different electrokinetical transport phenomena electro migration and electro osmosis could be made "visible"

The radiotracer method, which is well suited for the investigations, allows a non-intrusive monitoring without taking samples and, thus, without any influence on the transport processes. RTD measurements were executed with the two different gas tracers inactive helium gas (^{4}He) and radioactive ^{41}Ar. Results from measurements with both gases show a sufficient conformity; differences can be explained by the different detector positions for the output signal.

For the tomographic reconstruction of the tracer distribution in one cross sectional area a transport matrix was created. It includes the calculation of the total efficiency of each detector. This calculation is based on the summation of the contribution from each voxel to the signal of each detector. The results achieved are not only the basis of the tomographic reconstruction procedure but also for the CFD modeling.

India

The knowledge of flow parameters such as mixing time, mean residence time, residence time distribution etc. is of utmost importance for accessing and optimizing the performance of chemical reactors. In addition to this, these parameters also play an important role in designing new reactors or modification of the exiting reactors.

Computational fluid dynamic (CFD) models are finding increasing applications in characterization of flow behavior and predicting the characteristic parameters (mixing time and RTD) of chemical reactors. However, these models are based on a number of mathematical equations and assumptions, and thus needs to be validated before applying them to real life industrial situations. In addition to this, the integration of radiotracer measurements with the validated CFD simulation provides local flow pattern inside the investigated system.

In the framework of the present CRP, radiotracer experiments were carried out to measure mixing time and residence time distribution in different batch and continuous type reactors, respectively.

During the first year, radiotracer experiments were carried in batch type sludge hygenisation irradiator for measurement of process parameters such as circulation time, mixing time, breakthrough

time, flow rate and estimation of degree of backmixing. $^{82}Br^-$ as ammonium bromide was used as a tracer. The measured tracer data were treated and process parameters were obtained. The treated data were analyzed using classical modeling approach and information about the flow behavior of the irradiator was obtained. In addition to this, the CFD modeling of the flow behavior of the irradiator was also carried out. The experimentally measured tracer concentration data were compared with the CFD simulations and fairly good agreement was observed between the two. Based on the results obtained from radiotracer measurements and CFD simulations flow dynamics of the irradiator could be visualized.

During second year, the experiments were carried out for mixing time measurement in a jet-mixer at different operating and process condition using three different radiotracers (^{82}Br, ^{113m}In-EDTA and $^{99m}TcO_4$-). Some of the experiments were also carried out using chemical tracer. The measured tracer concentration curves were treated and mixing times were estimated. The measured data were simulated using CFD models based on turbulence. The CFD simulations were compared with the experimentally measured tracer concentration. Reasonably good agreement was observed between the measured tracer concentration profiles and estimated mixing times. This led to the conclusion that the CFD model was able to predict the flow behavior of the Jet Mixer reasonably well: The CFD model has been validated and will be used to design full scale industrial Jet Mixer.

During the third year, experiments were carried out in continuously stirred tank reactors (CSTRs) using radiotracer techniques. The measured RTDs were treated and analyzed using classical modeling approach and CFD based models. The experimentally and CFD simulated RTD curves were compared. In some cases, it was observed that the CFD predicted RTD curves did not match well with the experimentally measured RTD curves, indicating that the CFD model was not adequate enough to predict the true flow behavior of the investigated system and need to be improved. However, in some investigations, good match between experimentally measured and CFD simulated RTD curves were observed. However, some more work is still required to validate the models.

Good agreement between radiotracer measurements and CFD simulations has been observed in some cases. However, in few cases, the agreement between the two was poor. This discrepancy may be because of inherent errors in CFD models and solution of the associated model equations.

The CRP introduced a new area to the tracer technologists to validate the CFD simulations using radiotracer techniques and integrate the results of experimental measurements with the validated CFD simulations for flow visualization. The work carried out in the framework of this CRP could also help to promote the use of tracer techniques in industry and chemical engineering research. The Indian Process Industry and chemical engineers involved in research in different academic institutions will be enormously benefited by this new approach in near future.

Republic of Korea

Three radiotracer experiments were carried out on a rectangular clarifier in wastewater treatment to measure local concentration-time curve (RTD profiles) of the radiotracers.

Radiotracers ^{113m}In in complex compound with EDTA and $^{131}I^-$ in NaI solution were used for tracer tests. A CFD model was produced and successfully used for predicting the flow behavior in a clarifier. The phenomena such as density-induced waterfall and strong bottom current were observed from the radiotracer experiments and clearly described in CFD model as well.

The first attempt to compare the field measurement with the CFD simulation showed the potential of the radiotracer technique as a powerful tool for validating the numerical description. In order to simulate the flow pattern in the complicated weir outlet geometry, which strongly affects the particle removal efficiency of the clarifier, three-dimensional approach is definitely required.

The RTD curves obtained from 3-D CFD model have been compared with the radiotracer results for quantitative analysis. Based on the validated CFD model, the modification on the internal structure of the clarifier would be followed to investigate the influence of the modification into RTD curves.

Norway

The Norwegian group has been occupied mainly with two subjects during the three years of the present CRP:

- Industrial radionuclide generators for RTD applications,
- Radiotracer assisted visualization and CFD modeling of multiphase fluid flow in porous media.

For the first subject a questionnaire was answered by the CRP participants on their use of radionuclides and radionuclide generators in their own RTD experiments. The answers revealed that the commercial availability of proper radiotracers for various types of RTD experiments seems rather limited. In several cases experiments are carried out using tracers labeled with "medical" radionuclides because of easy access. Often this may work well but sometimes these tracers are not the right ones.

An example is the frequent use of $^{99m}TcO_4^-$ for tracing of the water phase. In situations with moderate temperature and non-reducing conditions this may work well, but it may be useless at higher temperatures and under chemically reducing conditions. It is concluded, however, that an effort should be undertaken to develop a larger selection of industrial radionuclide generators, which should be made available on commercial terms to the tracer community.

The second subject constitutes one element in a series of experimental and theoretical development on tracer technology for oil field implementation. The objective has been to study experimentally and theoretically the basic principles in simultaneous application of passive water tracers and water/oil partitioning tracers for measurements of remaining oil saturation in oil reservoirs. Results are encouraging. Simulations matched reasonably well the experimental results although improvements should be attempted. Details about this work are given in the country report from Norway in the present TECDOC.

Poland

The radiotracer experimental tests were performed in hydrocyclones' classification process. Nine radiotracer experiments were conducted for different grain sizes of solid mineral particles. Preliminary analysis of these data has been performed using the moment method, RTD-models and z-transform. The French DTS software has been used for the deconvolution and macromodelling. RTD software analysis allowed estimation of the degree of particle separation from the RTD curves.

The results showed that some grain sizes have an optimal mean residence time. This result has been very interesting for CFD verification.

The CFD models for turbulent flow description and solid material flow with have been investigated. Finally the CFD simulation has been done.

For CFD simulation the commercial software GAMBIT and FLUENT has been used. The GAMBIT software has been used for hydrocyclone geometry and the mesh preparation. The FLUENT software has been used for flow simulation. At first step the modeling of one-phase flow (water), in the hydrocyclone, has been done. At second step solid particles flows in the hydrocyclone have been simulated. For water flow simulation the turbulent model k-ε has been used. For solid particles flow

simulation the turbulent dispersion model has been used. This has allowed simulating the separation curve and RTD function for solid particles.

The obtained CFD results compare to the experimental RTD data fit well. The description of the solid particles separation in the hydrocyclones using the CFD simulation seems reliable.

United States of America

Four contribution areas have been treated during the three years of this CRP. In the first year the contribution was entitled "On combining and experimentally verifying the CFD and RTD approaches by Monte Carlo Simulation". That work was based largely on the paper that appeared earlier in Nuclear Science and Engineering. In the second year the contribution was entitled "Improving the radioactive particle tracking (RPT) technique by dual energy and non-linear inverse analysis approaches". That work was done largely by a number of graduate students as a project in the course NE 726 Radioisotope Applications. In the third year the two contributions were on: "RTD and other tracer experiments in a single vessel for CFD evaluation" and "Dynamic radioactive particle tracker".

The contributions made either are or will be useful in future work in this area. The Monte Carlo simulation approach may be useful in simulating particle trajectories for RTD determination. The RPT experimental approach may be useful in the future for benchmarking CFD calculations of flow streamlines. The experimental results for the tracer experiment on a single right circular cylindrical vessel should be valuable later for benchmarking CFD simulations.

3. TECHNICAL ISSUES ON CFD AND RTD

The hydrodynamics of an industrial reactor plays decisive role in its performance. The product quality and the efficiency of the process depend upon the flow dynamics of the fluid. Most of the industrial reactors are designed to behave either as a plug flow or well mixed flow. However, the real flow behaviors tend to deviate from these conditions and thus it becomes necessary to quantify this deviation. The residence time distribution (RTD) method is commonly used to quantify the deviation of the fluid flow from ideal condition simulating a model.

Radioactive tracer techniques are widely used for the measurement of RTD of flowing fluid in industrial process systems. The technique involves injection of a suitable radiotracer into the inlet stream and measurements of the tracer concentrations at the outlet or strategic locations of the system. The measured tracer concentration distribution is treated and analyzed using physically representative models. The main drawback of this classical approach is that it gives only global hydrodynamic behavior of the flow in the system and does not give any local information i.e. flow details inside the system.

Prediction of RTD using CFD

The global information obtained from the classical RTD approach is sufficient in many simple situations. However, in most of the complex industrial systems, the knowledge of local velocity profile or flow field is required to operate them at their full efficiency. Computational Fluid Dynamics (CFD) method provides complete flow field map and enables the visualization of the process flow. Based on the flow visualization, necessary corrective measures could be taken to operate the system according to its optimal regime.

The RTD function, f(t), can also be obtained from the CFD simulation. The RTD function is derived from the velocity field of CFD code either (1) by particle tracking method or (2) by stimulus-response simulation method. The particle tracking method can distort the RTD integral distribution function considerably, especially at later parts of the time scale, because sometimes it is difficult to avoid particle trapping in recirculation regions or in turbulent whirls. The CFD stimulus-response simulation method gives probably better results, though it is a more time consuming procedure. It is

based upon modeling of transient temperature or concentration field for introduction of a short tracer pulse at the inlet. Below, two case studies are reported where the CFD simulation approach was used for RTD predictions.

Case study: Prediction of RTD in a chamber with baffles

The RTD prediction for simple geometry of a gas flow through a chamber with baffles was investigated by using the commercial software Fluent for a broad range of Reynolds numbers (by the model for laminar or turbulent regions). The velocity field inside the chamber was obtained using the CFD code for a constant inlet velocity and for different Re.

The calculation of the RTD from the velocity field was performed simulating the concentration field by setting a short pulse at the inlet. In this case study, a triangular concentration pulse having mean duration of 1 sec (0.5% of the mean residence time) was used in order to obtain the RTD function, which is the impulse response f(t) at the outlet of the chamber.

Steady incompressible flow was considered in the numerical analysis. Numerical CFD simulation provided the RTD function, which fits better with the model of dead volumes with cross flow. This simple combined model, in fact, fits better the calculated RTD of the flow in turbulent regime quite well as it is shown on Fig.4.

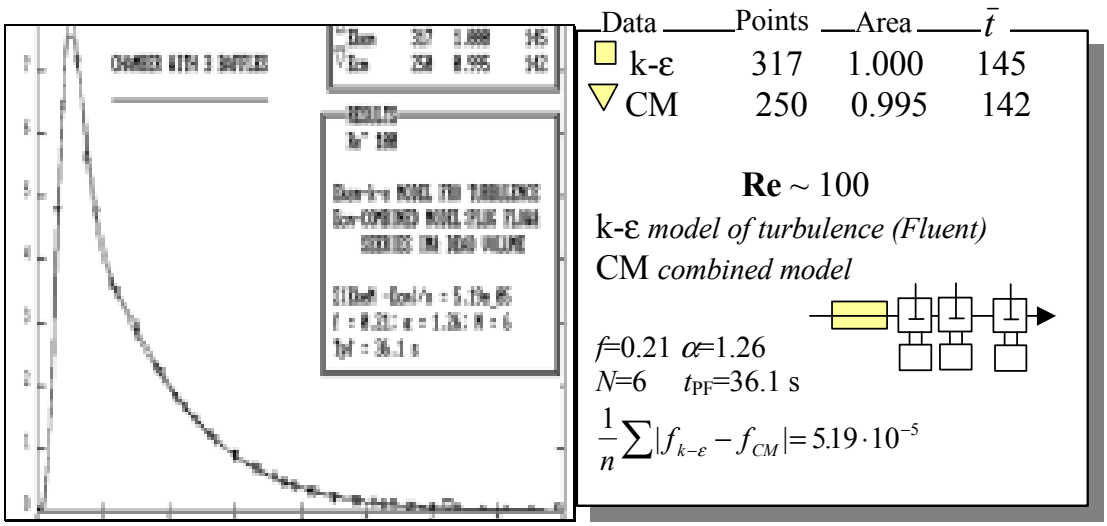

FIG. 4. Impulse responses f(t) of 3D cylindrical chamber with 3 baffles. Laminar flow.

The influence of Re and baffles on the RTD function was investigated using the Fluent 3D simulation. The RTD curves for different Re numbers predicted by Fluent 3D software are shown in Fig. 5. Molecular diffusion of tracer was not neglected because the role of diffusion is significant (D = 2.49.10-5 m2s-1), especially at low Re.

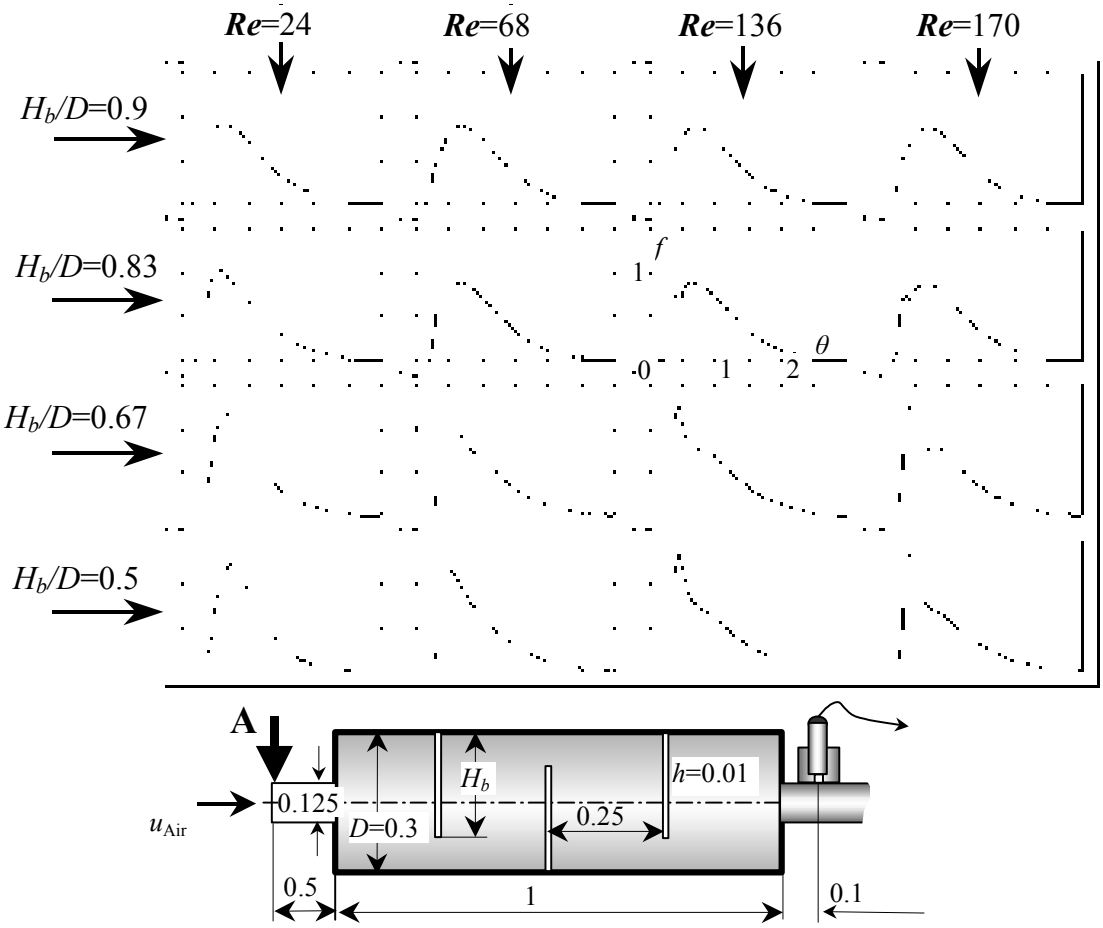

FIG. 5. Impulse responses f(t) of 3D cylindrical chamber with 3 baffles. Laminar flow.

The calculated RTD functions are characterized by two peeks for Re>40. This is probably caused by the fact that the swirls behind baffles are not ideally mixed regions. Using N-perfectly mixed tanks in series model better fitting of the calculated RTD with the model is obtained (Fig. 6).

The RTD model parameters represent main integral characteristics of the chamber-reactor, such as the relative volume of dead region and the mass exchange between the main stream and this dead zone. These parameters are related with the design parameters (geometry (Hb/D) and Re) as shown in Fig. 6. Thus the general trends (e.g. an expansion of dead region with increasing Re and Hb) can be quantified.

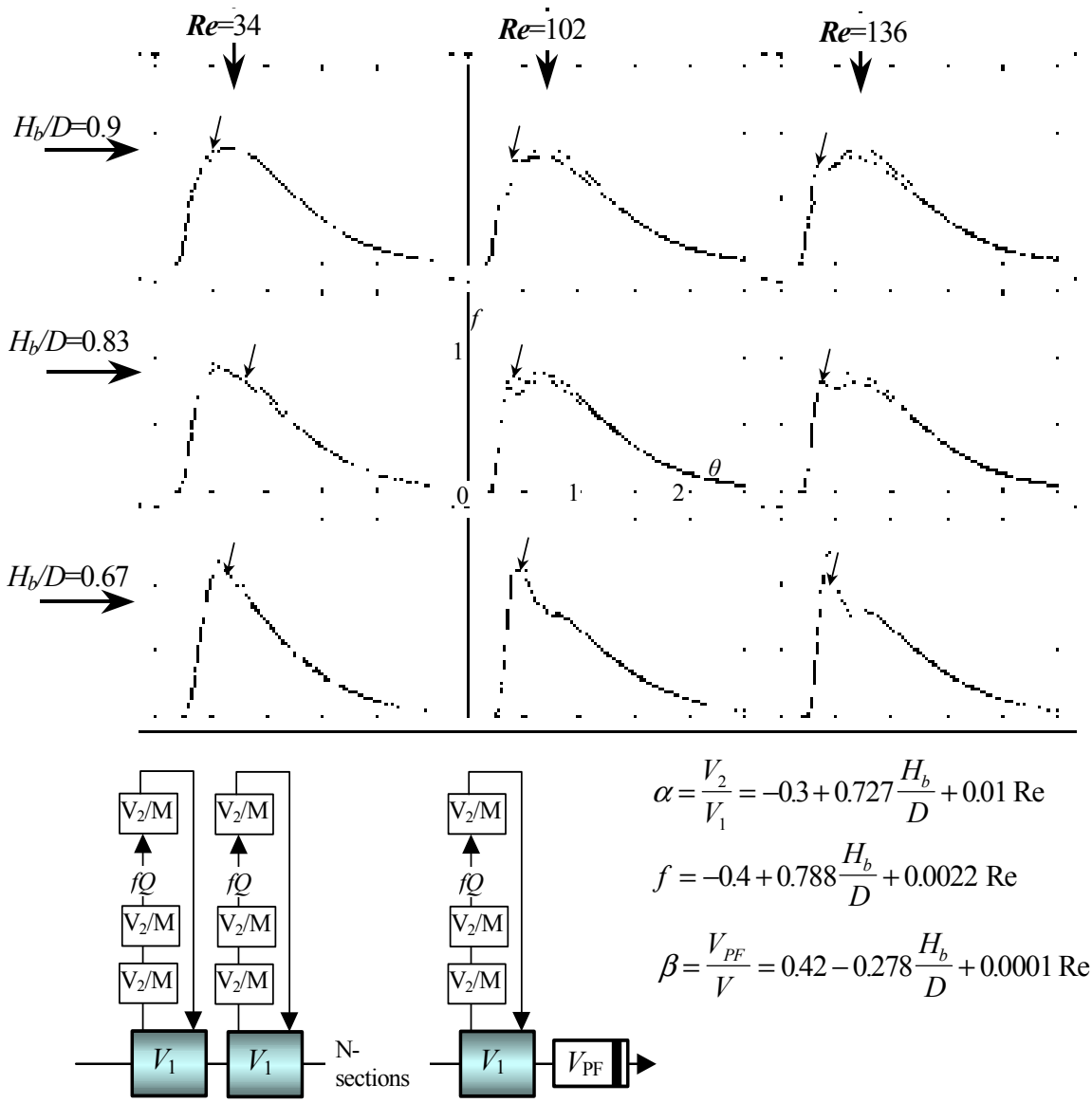

FIG. 6. Impulse responses calculated by improved combined model (denoted by arrows) and by Fluent 5.3. N=4, M=3. Parameters α, β, f are calculated as functions of Re and H_b/D (relative height of baffles) according to simple linear relationships identified by regression.

Case study: RTD prediction for studying homogenization in a Liquid Sludge Hygienization Irradiator (SHRI)

Irradiation of sludge is aimed at reducing the microbial load. Each element of liquid sludge should receive the appropriate minimum required dose while undergoing the irradiation process. Liquid sludge irradiators may operate in batch or continuous mode. Details of the considered irradiator are shown in Fig. 7. The sludge in the irradiator is kept under constant circulation using an external circulation via a pump. Obviously the flow rate through the external circulation loop controls the fluid dynamics and mixing within the irradiator. Intuitively it can be said that the higher the flow rate, the better will the mixing be. However, higher flow rate requires higher energy consumption. In order to optimize the irradiator, it is essential to identify an optimum circulation flow rate, which will minimize the energy consumption without jeopardizing the mixing within the irradiator.

FIG. 7. Schematic diagram of irradiator and source assembly.

CFD simulations of the sludge flow in the irradiator were carried out. The flow results obtained from the CFD model were then used to predict the RTD function. It was assumed that addition of a tracer does not affect the underlying flow field.

Therefore, while simulating mass balance equation for the tracer mass fraction, the momentum equations were not solved. A square pulse of a tracer was introduced in the computational model for the duration of 0.5 s. It must be noted that since the SHRI is a closed system, the tracer mass fraction outgoing from SHRI re-enters SHRI after the delay time of the process piping outside SHRI. In the present work, such a delay time was neglected since it was much smaller than the mean residence time. Equivalence of mass fractions of entering and outgoing fluids was mapped on to FLUENT using the 'user defined subroutine'. CFD simulations were then carried out to understand local and overall mixing in SHRI under different circulation flow rate. Typical results in the form of contours of mass fraction of tracer are shown in Fig 8.

CFD simulations indicate that about three circulations through the reactor lead to reasonable mixing within the contents of the vessel. In order to obtain the RTD function from CFD simulations the variation of tracer mass fraction in the outlet of the system with time was calculated. Typical predicted C-curve (RTD function) from the CFD model for the case of 1 m3/hr and 0.33 m3/hr are shown in Fig. 9.

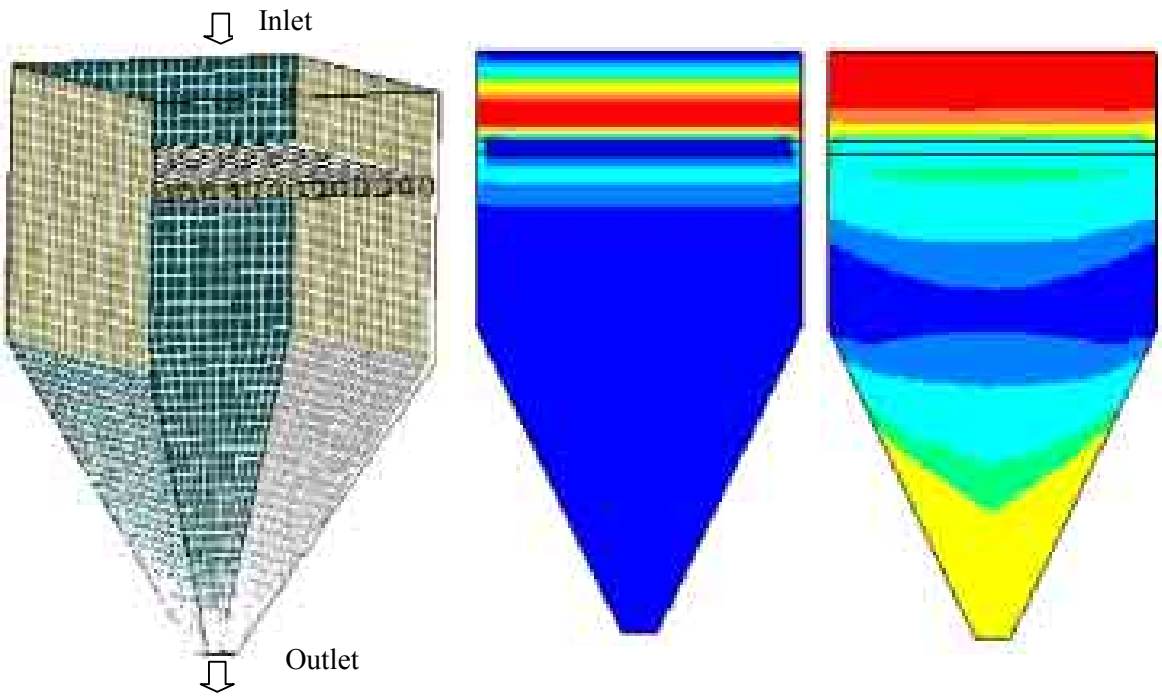

FIG. 8. CFD simulations of the sludge flow in the irradiator. Typical results in the form of contours of mass fraction of tracer are shown.

In order to bring the predicted responses for two flow regimes on uniform basis, the predicted values were normalized using the maximum tracer concentration observed during the mixing simulations. The normalized tracer concentration response was plotted against the dimensionless time normalized by residence time. It can be seen that normalized tracer responses for the two values of circulation flow rate are almost the same.

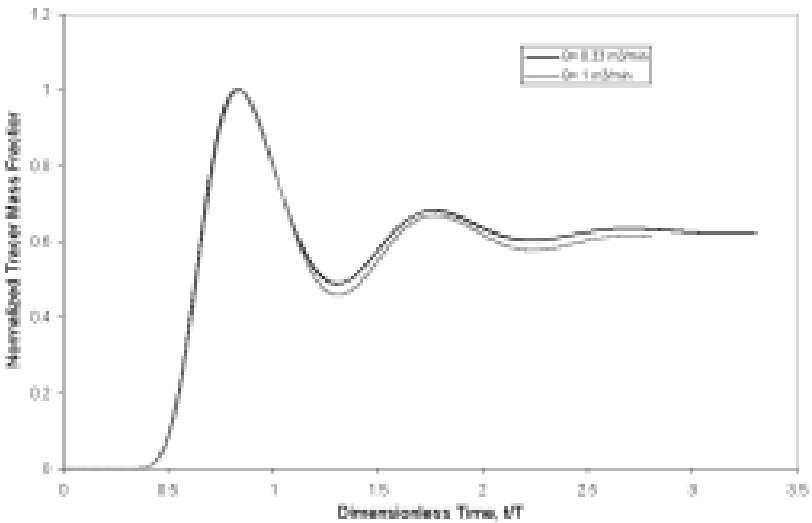

FIG. 9. Normalized tracer distribution RTD curves predicted by CFD model.

The predicted variation of the calculated RTD functions (curves) can then be compared with the experimental tracer response studies to verify the CFD simulation reliability, because the CFD code can give any kind of RTD functions depending on the initial conditions and software requests. The verification of the CFD simulation with tracer experiment, that means the comparison of the RTD function predicted from CFD code with the RTD experimental curve, is always necessary to carry out to ensure the reliability of results.

Verification of CFD model by tracer experiments

The CFD models are based on solution of numerous fluid dynamic equations. However, the ability of these models to predict the flow behavior of a system depends upon the accuracy of the solution of the model equations. Exact solutions are extremely difficult for most of the engineering flows. Furthermore, it must be remembered that the numerical solution of the equations will always be approximate. There can be various reasons for differences between the computed results and the reality. Errors may arise from each part of the process used to generate results:

- approximation in the fluid dynamic equations,
- inadequate accuracy of input data,
- approximations in the numerical techniques,
- computational constraints,
- interpretation of the results and etc.

The reliability of CFD results is often to be questioned because there are many different CFD models available for one system. For example, Fluent CFD software suggests several codes, such as Reynolds stress model, standard k-ε model, RNG modification of k-ε model, turbulent viscosity transport model and etc., for the approximation of boundary conditions at the wall in modeling of turbulent flows. It is not an easy task to choose the best model for a specific problem. Some of these models are known as low Reynolds number models, enabling to predict even the transition from the laminar to the turbulent flow regime, but this prediction is rather unreliable. Taking into account above approximation errors, it is not surprising that quite different results of simulations are obtained with different model, differing by several tens of percent.

It is indeed necessary to develop a CFD model and exploit its potential for design of industrial systems or improvement and troubleshooting in the existing systems despite these limitations. Thus there is a strong need to verify or validate these CFD models before they are applied in practice for prediction of flow behavior of the industrial systems in order to provide accurate and reliable results. This is the reason why the CFD model should be validated with the RTD obtained by tracer experiment.

There are two radioactive techniques to verify CFD by RTD: Radioactive particle tracking technique and radioactive tracer technique. The radiotracer RTD method is used for verifying the CFD models in this CRP.

Case study: CFD-RTD comparison for a hydrocyclone

A hydrocyclone is a device where the grain material classification proceeds in the field of the centrifugal force action. The centrifugal forces are generated by flowing liquid on spiral trajectory in a motionless vessel. This spiral flowing is generated by tangential inlet of the suspended solids with a proper velocity. The physical differences of the grains, size and specific gravity, offers possibilities to separate the grains in a hydrocyclone. Inside the hydrocyclone two countercurrent rotating streams are generated. One rotates close to the hydrocyclone wall and flows downwards with bigger and heavy grains to the underflow. The second rotates inside the wall stream and flows upwards with small and lightweight grains to the overflow (Fig. 10).

The radiotracer experiment was performed for a hydrocyclone that worked inside the beneficiation process of the copper ore enrichment process. In this case it was not possible to carry out

a pulse injection of the radiotracer and the scintillation probes were placed in three positions: At the inlet of the hydrocyclone, at the outlet of the underflow and at the outlet of the overflow. Radiotracer experiments have been conducted by injection of different grains sizes.

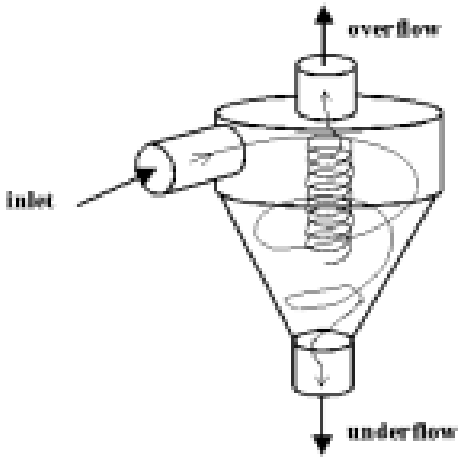

FIG. 10. Sketch of the hydrocyclone.

In the first step the CFD modeling of one-phase flow (water) in the hydrocyclone has been done. In the second step the flow of solid particles in the hydrocyclone has been simulated. For water flow simulation the turbulent model k-ε has been used. For simulation of the flow of solid particles the turbulent dispersion model has been applied. Fig. 11 shows the results for water flow CFD simulation.

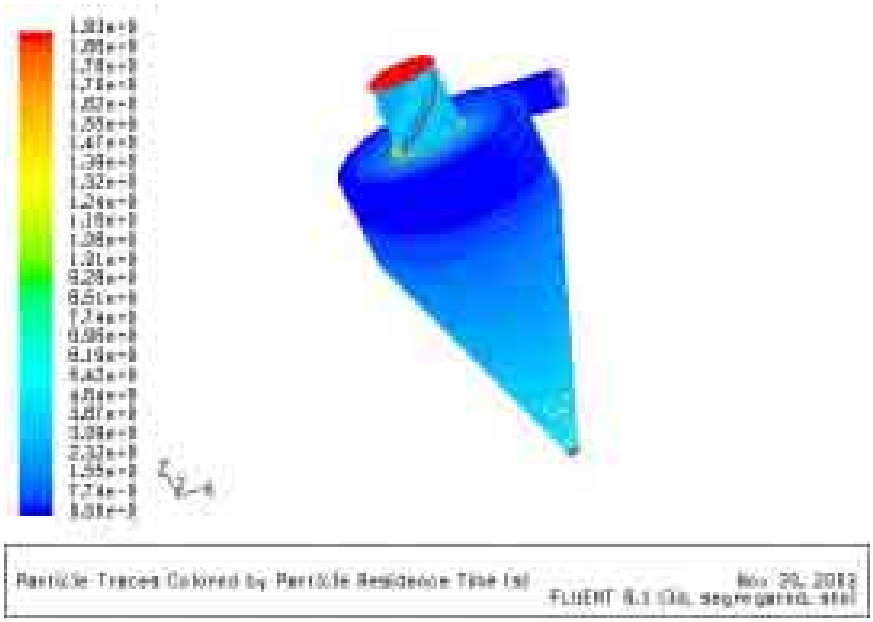

FIG. 11. All path lines flowing from the inlet.

The RTD function for solid particles was predicted from the CFD calculation. In Fig. 12 the RTD function obtained from CFD simulation and RTD experimental separation curves are shown. Relatively good agreement was observed between measured and simulated tracer response curves.

This comparison of CFD simulation with RTD tracer measurement showed that the chosen CFD model was reasonably correct.

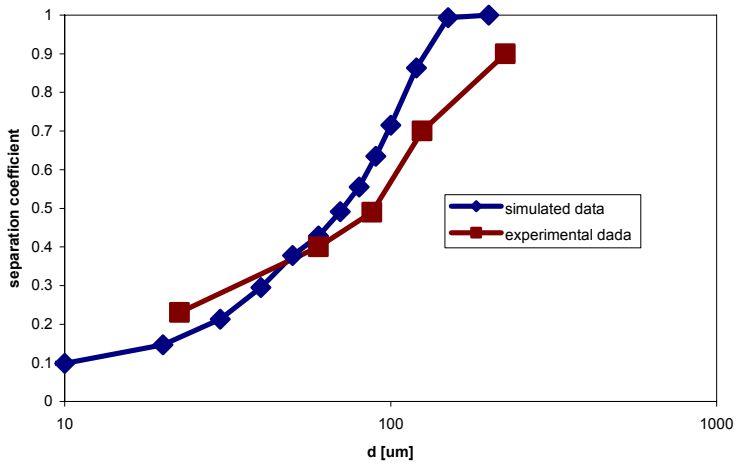

FIG. 12. Simulated and experimental separation curves.

Use of local responses for the verification of CFD model

Sometimes the RTD information obtained at the outlet of a system is not sufficient for the analysis of complicated flow structures inside the system. For example, the shape of the outlet RTD for parallel flow may be similar to that for recycled flow. To verify CFD results of such a complex system, it is necessary to have stimulus "local" responses in addition to the response at the outlet. The local stimulus responses can be measured with detectors positioned inside or at the wall of the vessel. The data can provide additional information so that the flow structure can be sufficiently and unambiguously determined.

Case Study: Verification of local responses in the clarifier of wastewater treatment plant

The radiotracers ^{113m}In-EDTA and I-131 were used to obtain the mass transport response curves in order to investigate the hydrodynamic behavior of water flow in a rectangular clarifier of a wastewater treatment plant. The clarifier and the detection positions are shown in Fig. 13. The data for the response curves were introduced as a reference to a numerical modeler that simulates the flow by means of CFD using the standard k-ε turbulence model.

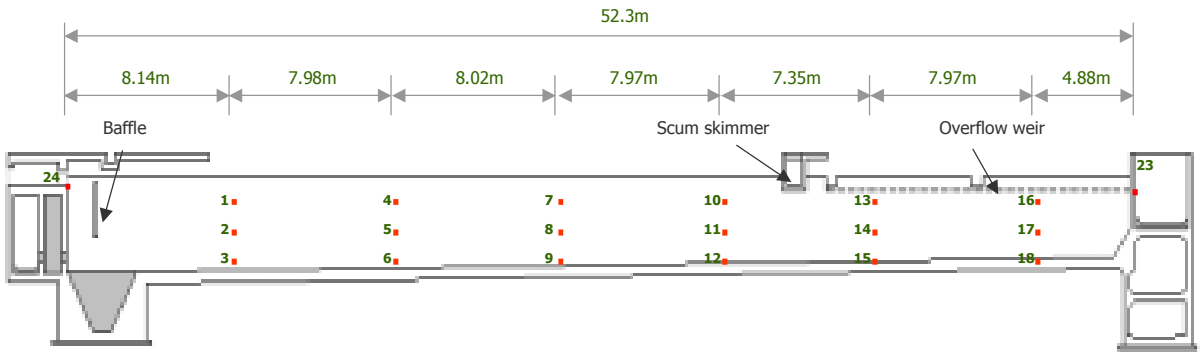

FIG. 13. The clarifier for RTD experiment and CFD simulation.

For validation purposes, the response curves predicted from the CFD simulation were compared with reference radiotracer experimental curves. Fig. 14 shows some examples of the comparison of the response curves obtained from radiotracer experiments and those calculated from CFD simulations. The CFD simulated RTD profiles are generally in a reasonable agreement with the experimental RTD curves at the upstream and the middle-stream sections but a substantial difference was observed at the area of discharge weirs. One of the reasons for this discrepancy could be found from the fact that the radiation detectors were installed near the wall in order to keep the detectors from being disturbed by the continuously moving scrapper. But the major reason would be the simplification of the complicated discharge weir section in 2-D CFD model.

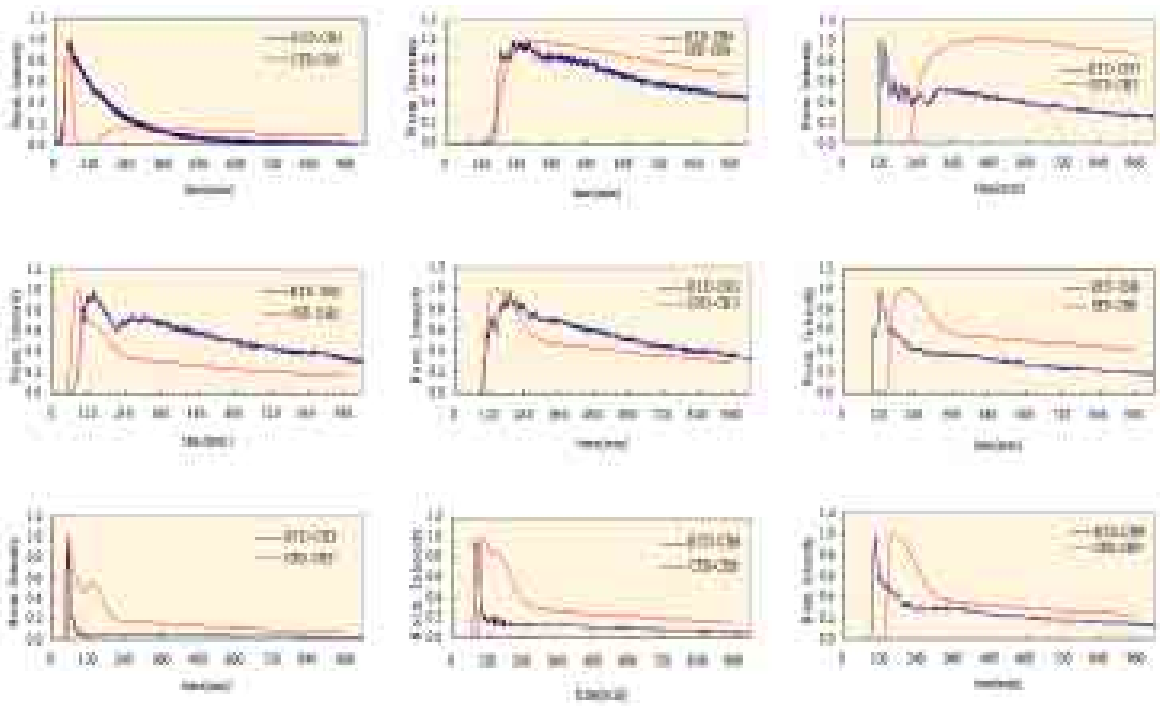

FIG. 14. Comparison of CFD results with radiotracer local responses.

Despite this discrepancy in some parts, the simulation clearly showed the typical characteristics such as the density flow driven by the waterfall phenomenon at the front end of the clarifier, the bottom density current in the settling zone and the upward flow in the withdrawal zone as shown in Fig. 15. A three-dimensional approach is highly recommended for the better agreement between the RTD profiles from both radiotracer experiment and CFD simulation.

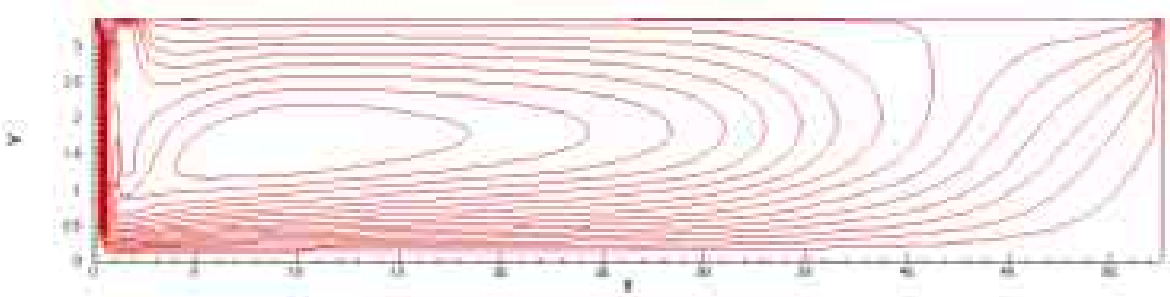

FIG. 15. The contour plot of predicted streamlines from the CFD simulation. (Uin=3cm/sec, Cin=1300ppm).

Simulation of local responses from CFD model in complex flows

However, in the case where there are remarkable gradients of tracer concentration in a detection volume, the response characteristics (algorithm) of a detector to the radiation have to be identified for the exact comparison between RTDs of tracer experiment and the CFD simulation.

The combination of local tracer impulse response measurement and CFD modeling offers the opportunity for evaluation of each voxel of the detection volume to the integral detector signal. CFD modeling simulates the tracer concentration for each voxel. On a differential basis the local response of a collimated detector is given by

$$R(t) = \iiint_V e(x, y, z) \cdot c(t, x, y, z) dxdydz$$

where *c(t,x,y,z)* is the distribution of tracer concentration obtained from CFD calculations and *e(x,y,z)* is total efficiency function. A useful practical equation for making this calculation is

$$R(t) = \sum_{i=1}^{n} e_i \cdot c_i(t)$$

where c_i is tracer concentration and e_i is the total efficiency for voxel i.

The efficiency can be obtained from various methods for the specific detector, detector collimation, sample material, and gamma-ray energy for a specific case. By comparing the measured and calculated detector signals one can change the conditions of the CFD modeling to obtain the correct results.

Three methods for evaluation of the *e(x,y,z)* function are possible:

- measurement of response to a point source as a function of its position in the appropriate experimental rig,
- analytical calculations taking into account solid angles and attenuation
- Monte-Carlo simulations.

The first method is to be preferred whenever possible, which may not be the case outside the laboratory environment. It has been applied by the Czech group for various radionuclides (^{99m}Tc, ^{137}Cs, ^{198}Au, ^{82}Br and ^{24}Na) and by the Cuban group for ^{99m}Tc. The analytical calculations method is chiefly applicable when the photopeak only is considered. It has been used by the Czech group for the same radionuclides and by the German group for ^{41}Ar. The Monte-Carlo method is in theory of very general use. In practice, care must be taken to include all the relevant physical phenomena (detector crystal non-linearity, electron channeling, etc.) especially if gamma spectra are to be predicted. This approach has been used by the Czech group for ^{99m}Tc and ^{137}Cs and by the French group for ^{99m}Tc and ^{82}Br. At the present time, validation of this method against experimental data is not completed, even though some data are available.

One should be aware that the detector signal may not be unique in that the response to a small concentration close to the detector may give the same response as from larger concentration farther from the detector. So, unique differences in tracer concentration distributions may not be detectable with simple individual collimated detectors. In the future, more sophisticated detection approaches are possible that could give unique responses. For example, one might use pairs of collimated detectors that are operated to obtain coincidence counts from a tracer that emits gamma rays in coincidence. This would tend to restrict the response to a relatively small sample volume at a position specified by the collimation.

It could also be used gamma-ray spectroscopy on tracers that emit two or more gamma rays with different energies so that different attenuation in the sample can be used to delineate the effective distance of the detected tracer from the detector.

Finally, a full blown tomographic approach could be used to obtain the detailed tracer spatial concentration at any time.

All of these more sophisticated techniques, while yielding much more detailed information, suffer from requiring much more expensive and complex equipment and from yielding much lower counting yields per unit tracer intensity.

Conclusion on RTD-CFD interaction

RTD and CFD are suitable methods for flow analysis in industrial apparatuses. They are complementary and verify each other. They can be used for micro and maxcro modeling of different industrial processes.

As there are some problems in the simulation of tracer experiments in laminar flow (e.g. numerical diffusion) and similar numerical problems can be expected also in transient or turbulent flows, the verification on the basis of velocity measurements is recommended.

CFD code is powerful tool, which is used for prediction of heat, mass and momentum of complicated flows in industrial apparatuses. However application of CFD models in the process control or in detail analysis of bio, or chemical kinetics is impracticable. In contrary the global system analysis by RTD model is easy to use. Approach of Simplified Fluid Dynamic by Combine model Network is recommended and solution is based on a two step procedure. Starting from the complex flow by 3D CFD simulation and simplification of the flow behavior is reduced to a network of plug flow or ideally mixed regions strictly interconnected. The analysis of complicated kinetics is evaluated then in these units.

4. CRP CONCLUSIONS AND RECOMMENDATIONS

The RTD approach provides an excellent basis for the flow and dispersion aspects of lumped parameter models of continuous, steady-state industrial processes, but is not capable of directly providing information or insight into the detailed (micro scale) complex flow and dispersion in these processes. The participants generally agree that CFD simulation will eventually be useful to obtain better insight into this complex flow distribution in industrial process units.

The efforts that have been made by the participants in using CFD techniques for various real industrial applications in this CRP have given a positive impact to the need to better understand and use CFD codes. Although the use of CFD calculations on specific processes produced positive qualitative results, they were not able to yield accurate quantitative results for experimental RTD's or tracer responses. It is felt that there may be a number of reasons causing this problem, such as lack of CFD knowledge by the participants, inexperience in using commercial CFD codes, relying on the CFD results from other groups, and inconsistency of experimental conditions between CFD simulations and tracer experiments. In addition to these general problems, which are common for most beginning CFD users, the participants believe that there are at least two technical problems with obtaining accurate quantitative results for RTD comparison. These are numerical dispersion and inadequacy of the turbulence models in the CFD codes. An additional non-technical problem is the high cost of the CFD codes.

When these problems are solved, it would be expected that the CFD simulations would become more accurate and, therefore, even more important for industrial process research and development. In particular, the visualization and fundamental understanding of these processes in complex industrial

processing units through CFD simulations will greatly benefit the tracer community and processing industry as a whole.

The participants have amply demonstrated the beneficial role of RTD-CFD combination in analyzing and optimizing the industrial processes with many case studies from chemical and petrochemical industries, from mineral ore processing and waster water treatment plants. The main results (output of the CRP) generated by the individual participants include:

(1) CFD modeling of liquid-bubbly two-phase flow due to sub-cooled boiling in nuclear reactors and development of an Educational Package for CFD and RTD (Australia),
(2) Modeling of the internal flow in a photo-reactor for wastewater irradiation (Brazil),
(3) Application of RTD and CFD approaches to heat transfer processes (Czech Republic),
(4) Modeling a sugar crystallizer (Cuba),
(5) Treatment of a backward facing flow experiment with CFD (France),
(6) Investigations of the transport behavior of selected organic compounds in electrochemical soil remediation and gas RTD and distribution measurements in the cross section of a batch pyrolysis waste wood reactor (Germany),
(7) Investigation of radiotracer and CFD approaches to various industrial processes (India),
(8) Multiphase radiotracer assisted visualization and CFD modeling of multiphase fluid flow in porous media (Norway),
(9) Combining RTD and CFD approaches for the study of hydrocyclones (Poland),
(10) Application of radiotracer technology and CFD simulation for the diagnosis of a wastewater treatment plant (Korea),
(11) Improvement to the radioactive particle tracking approach (USA).

In addition to these results generated on individual processes by the participants, a number of general contributions were made. This included the data generated on a fundamental tracer experiment in which the flow in a single right circular cylindrical vessel was investigated with dye and radioactive tracers.

It was recognized in this CRP that the lack of CFD knowledge and inexperience of using CFD codes might limit the capability of exploring the use of CFD simulations. Therefore, a CFD & RTD Educational Package with lecture notes, tutorials, and both CFD and RTD software through a user-friendly web-based interface has been developed as an output of the CRP through the cooperation of the participants. This package can be used for training and education for using CFD and RTD techniques and their interactions.

Also available is a software package that includes both RTD tracer and CFD codes that can be used for describing various single-phase processes. Finally, this TECDOC, which has been prepared based on the work performed during this CRP, will help radiotracer group and their end users' institutions to establish a working partnership to develop further and make operational the RTD-CFD method for problem solving.

ADVANCED CFD & RADIOTRACER TECHNIQUES — A COMPLEMENTARY TECHNOLOGY — FOR INDUSTRIAL MULTIPHASE APPLICATIONS

J.Y. TU
Australian Nuclear Science & Technology Organisation (ANSTO),
Menai, New SouthWales, Australia

Abstract

A CFD&RTD Education Package was developed, in which lecture notes, tutorials and computer softwares for both CFD and RTD are included. A user-friendly web-based interface has been prepared to allow lecturers more effectively conducting their training courses or workshops, and to provide students or users more easily learning the CFD and RTD knowledge and practising computer softwares. This report gives an overview of the advances in development and use of CFD models and codes for industrial, particularly multiphase processing applications. Experimental needs for validation and improvement of CFD models and softwares are highlighted. Integration of advanced CFD modelling with radiotracer techniques as a complementary technology for future research and industrial applications is discussed. The features and examples of the developed CFD&RTD Education package are presented.

1. INTRODUCTION

Many industries make products or provide services that are connected with fluid flow and associated multiphase (gas, liquid and solid particles) processes, which are fundamental to national economy in all countries because they are central to all major process industries - energy, minerals, chemical engineering, pharmaceuticals, food and metallurgical processing. Throughout industry, fluid-solid two-phase flow unit operations are some of the most troublesome to operate. The flow behavior of these two-phase systems is too complex in order to reliably scale-up, design or optimize them. Typically, experimental testing is performed on expensive, larger-scale units for “effective” new designs or new units mimic existing units.

CFD uses advanced computer models and software to simulate the flow of fluids or multiphase through a processing facility or unit. The use of CFD models and codes by the industry and engineering community has increased dramatically in the last few years. This rise in interest and the use of CFD codes has resulted from improvements in the predicting capabilities of CFD models, reductions in the cost of computer hardware, and inflation of the costs to perform experiments and to maintain experimental facilities.

The development of reliable CFD models would reduce the need for expensive large-scale test facilities. Evaluation of key variables and flow parameters such as particle concentration, flow velocity, particle material and size distribution, inlet flow conditions and geometry, etc. could be explored without elaborate testing equipment. In addition, turn around time for troubleshooting an existing unit could be reduced and more efficient operation could be achieved. CFD modeling for multiphase flow based on two-fluid model is rapidly becoming a typical tool used for the prediction of flow behavior in many industrial processes, such as power utility boilers, fluidized beds, chemical reactors, transport lines, etc. CFD modeling or simulation typically contributes to the design and optimization of industrial components having the potential to save companies many millions of dollars per year.

At present, there are two methods currently being used for investigation of industrial complex processes, radiotracer residence time distribution (RTD) experimental technique (systemic analysis), and CFD simulation. The RTD is almost a well-established methodology with universal applications. Protocols, procedures and software were prepared for validating RTD system analysis in many

industrial processes from petrochemical and chemical engineering. The RTD methodology has been introduced to almost all radiotracer groups.

The numerical simulation of complex systems through CFD methods is a new approach and more powerful for process visualization. The real time experimental RTD tracing is simple and reliable; it provides various important hydrodynamic parameters but it cannot localize and visualize flow pattern inside the systems. The CFD is a fine and predictive analysis, which provides nice spatial pictures of the insight of a process, such a flow patterns and velocity map. Due to lack of physical experimental data the CFD calculation provides qualitative results only, especially in systems with strong interaction of hydrodynamics with physico-chemical reactions. This is the reason that CFD models have to be verified and validated by experimental tracer RTD results.

The RTD-CFD interaction is both sides. The CFD can be used also to complement the information obtained from the RTD systemic approach. CFD provides data that can quantify RTD systemic model, which means the CFD model can "degenerate" into more quantitative RTD systemic analysis, providing more comprehensive results for engineers. In fact, these two approaches, experimental and numerical, are complementary to each other. The RTD systemic approach detects and characterizes main features of the flow (mixing and recirculation) while CFD enables to locate them. The trend is to combine experimental and numerical approaches in order to obtain reliable quantitative results for industrial complex processes.

Then, user-friendly and versatile software would be more useful for tracer people; but often these two requirements are hard to satisfy simultaneously. Besides that, one should be able to know the limitations of the numerical procedures used (error propagation, instabilities, etc.), and hopefully how to take them into account. Hardware with the required capabilities must also be available. Then, the cost of both software and hardware might hinder applications, especially in developing countries. Finally, it is felt that the CFD methodology could and should be extended to other modeling fields, besides the simulation of industrial equipment. These could be environmental systems, hydrology, pollution and contaminant transport; or anywhere else tracers are applied. In view to promote integration of CFD and RTD tracer techniques, a recommendation was made in the first CRP meeting to develop an education package on CFD-RTD with simple case studies that will be very helpful for many CRP participants and other tracer groups.

2. CFD IN INDUSTRIAL MULTI-PHASE FLOW APPLICATIONS

Gas-solid particle flow in power boilers

Burning coal, for electricity generation, creates products of combustion, which contain solid particles (flyash). These small solid particles are carried by the hot (flue) gas flow through the heat exchangers in power utility boiler. The transported flyash can cause severe erosion to the heat exchanger boiler-tubes. The annual cost of erosion to a plant operator can be as high as several million dollars. A method of reducing erosion by appropriate modifications during the maintenance or design stage of power utility boilers is crucial for their safe and more efficient operation. Therefore, it is important to understand the hydrodynamics of gas-solid two-phase flow in power boilers and around heat exchanger tube banks.

The complexity of the flow generated within a power utility boiler (three-dimensional, two-phase and turbulent) has compelled designers to make use of empirical information, often complemented by pilot plant experiments, in order to tackle problems associated with the erosion reduction and the design of new boilers1. Such a design procedure is rather expensive and inefficient, and more importantly, it is often valid only for a very restricted parameter range. It is very important for designers to have information about the location of the maximum erosion rate and its causes. Therefore, a computer code that accurately predicts the detailed flow and particle distributions within power boilers under different operating conditions would be a desirable tool.

A CFD code specially developed for power utility boilers [2,3] has been applied to simulate the flue gas and fly ash flows in a real-scale boiler configuration, currently operating in the State of New South Wales, Australia. The computational grid consists of 117,000 computational cells (30 x 130 x 30 in the x, y, z directions). Stretched grids are used to obtain an acceptable distribution of points near wall surfaces. Since erosion tends to be localized in particular areas of the boiler, failures have generally been experienced in the economizer [4] where non-uniform flue gas and fly ash flow distributions occur and were predicted by CFD. The flyash concentration contours (normalized) and velocity vector plots of the particle flow are shown in Figure 1 for the symmetry plane. One may see that both size particles are centrifuged due to 180 degree bend and more flyash particles are flung to the outside of the bend. Due to the different inertia a larger particle-free zone can be identified at inside of the bend for high inertial particles (d_p = 80μm) than for lower inertial particles (d_p =30μm).

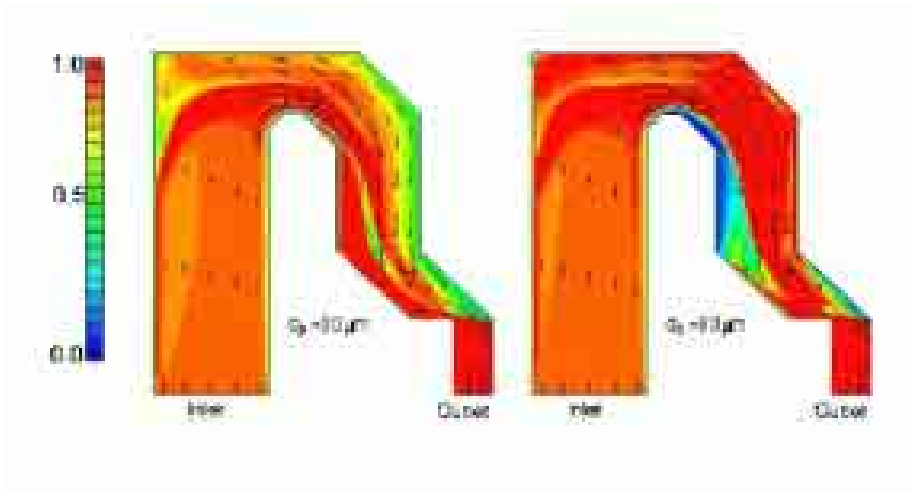

FIG. 1. Flyash concentration contours (normalised) and velocity vector plots of the particle flow.

The estimate of erosion rate from the global flow solution indicates that the area of maximum erosion rate at the economizer inlet can be predicted with reasonable accuracy when compared with measurements of erosion rate on operational plants. The quality of the solutions in boilers is sufficient to provide an insight into the flow phenomena and erosion patterns within coal-fired boilers so that CFD codes may be employed in future to generate designs in order to reduce the incidence of tube failures due to fly ash erosion.

Bubble-liquid boiling flow in nuclear reactors

Flow instability is an important consideration in the design of nuclear reactors because of the possible occurrence of flow excursion during a postulated accident. Static flow instability may arise in narrow cooling channels due to steam formation in the case of loss of coolant accidents. The formation of steam in a heated channel can have a significant effect on the overall pressure drop along the channel.

A schematic of the experimental test rig is shown in Figure 2. The test loop consists mainly of the test channel, water storage tank, circulating pump, preheater and water purification unit. The test channel contains a heated section where the subcooled boiling flow occurs. The measuring plane is located at 1.61 m downstream of the beginning of the heated section. Demineralised water was used as the working fluid.

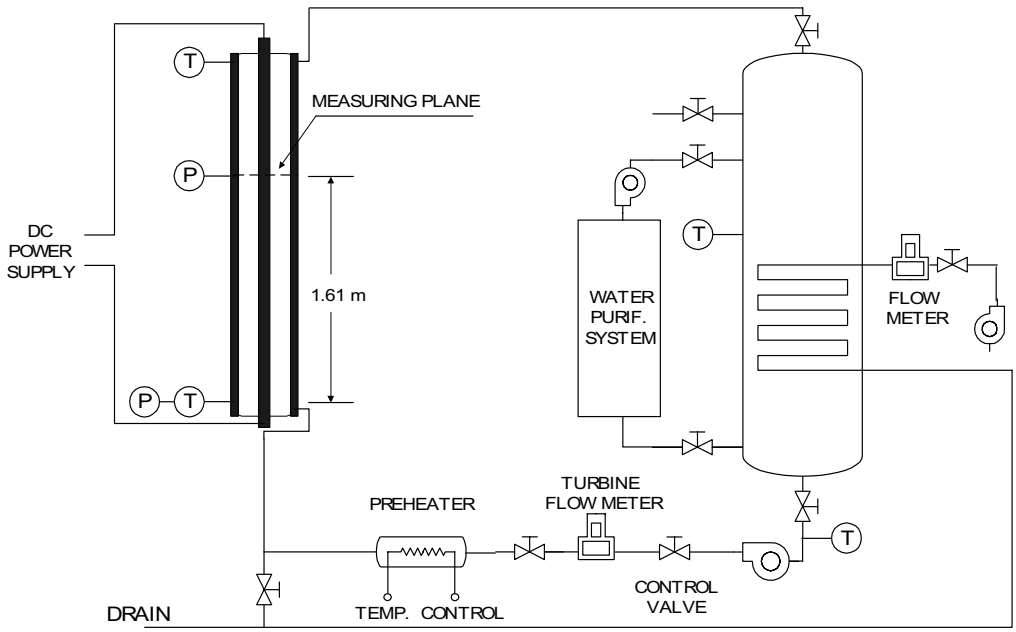

FIG. 2. Experimental test rig.

During the experiments, observations made through high-speed photography revealed the presence of large bubbles away from the heated wall. The bottom vapor bubble at upstream was seen sliding along the heated surface until it was impeded by the downstream bubble.

Experiments have clearly indicated the presence of bubbles sliding shortly after being detached from the heated cervices before lifting into the liquid core. These upstream bubbles traveling closely to the heated wall have the tendency of significantly colliding with any detached bubbles downstream and subsequently forming bigger bubbles due to the bubbles merging together. Here, the condensation phenomenon dominated and the bubbles gradually decreased in size due to the increased condensation as they migrated towards the opposite end of the unheated wall of the annular channel. This supposition of the phenomenon predominant in subcooled boiling flows has been further confirmed by experimental observations of Gopinath et al. [5] (see Figure 3), which illustrated a bubble gradually being condensed in a subcooled liquid away from the heated surface.

In the commonly used two-fluid CFD model for multi-phase flow applications, the phase interaction terms appear in the field equations, which represent the contribution of the mass, momentum and energy transfers through the interface between the phases. As the bubble Sauter diameter appears in the interfacial terms between the liquid and gas phases, an accurate determination of the bubble Sauter diameter is important as the bubble size significantly influences the inter-phase momentum such as the drag force and heat and mass transfer through the interfacial area concentrations.

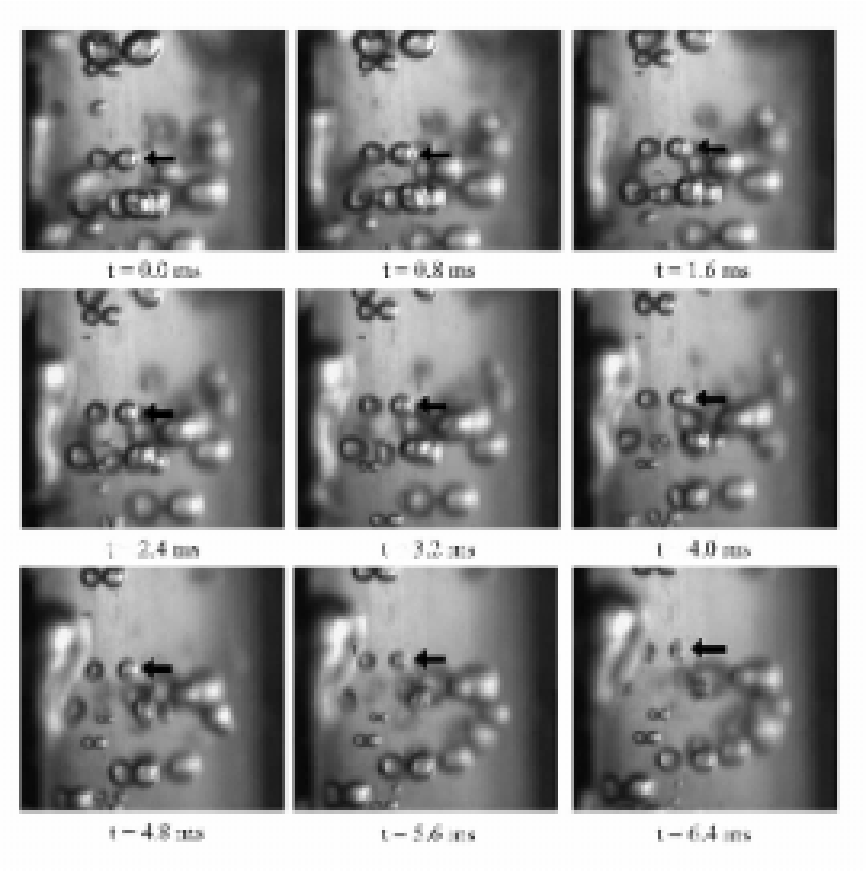

FIG. 3. A bubble undergoing condensation in a subcooled liquid (Gopinath et al, 2002).

An investigation on the capability of using the population balance approach for subcooled boiling flows was conducted. In this study, our aim is to develop a better understanding of complex phenomena associated with hydrodynamics, heat and mass transfer, and bubbles coalescence and condensation in subcooled boiling flow through experimental observations. Numerical simulations using population balance approach based on the MUSIG (MUltiple-Size-Group) model coupled with the two-fluid CFD boiling model in the generic computer code CFX4.4 are also conducted. This new MUSIG boiling model is evaluated through comparisons against experimental measurements of local two-phase quantities.

Figure 4 presents the locally predicted void fraction profiles against radial measured values. Good agreement was achieved between the predictions and measurements. The peak local void fraction was always observed in the vicinity of the heated surface in a typical subcooled boiling flow. This high local void fraction found here was explicitly due to the large number of bubbles generated from the active nucleation sites on the heated surface. Here, large amount of bubbles were generated from these nucleation sites when the temperature on the heated surface exceeded the saturation temperature. A proper prediction of the nucleation site densities is therefore crucial as already confirmed from the parametric study above. As these bubbles reached a critical size, they detached from the heated surface and migrated laterally toward the subcooled liquid core under the competing process of bubble coalescence and condensation as aforementioned.

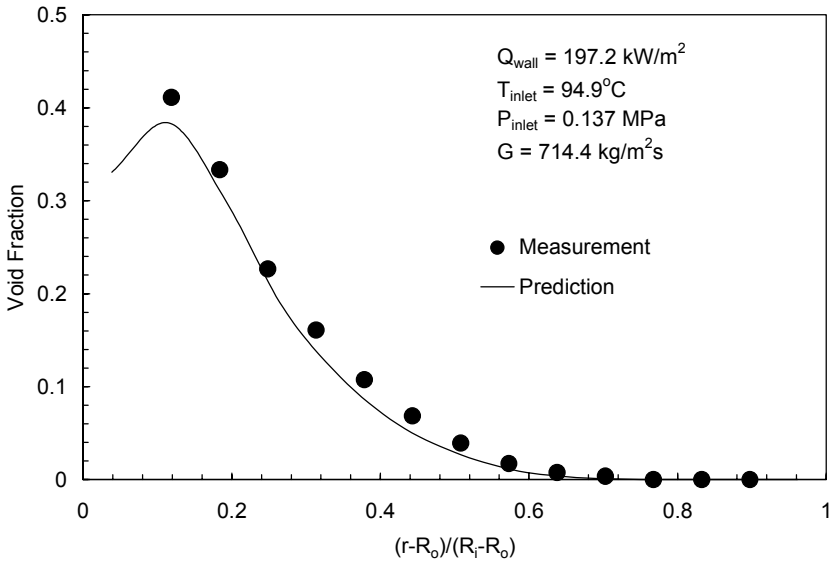

FIG. 4. Comparison of local radial void fraction between prediction and measurement.

The two-fluid CFD boiling model predictions are compared against a series of comprehensive experiments performed at CEA-Grenoble in a vertical rectangular channel of 600 mm in height. The width and thickness of the channel flow area are 38 mm × 3.6 mm respectively. Heat was applied around the outer test section wall. These experimental data were chosen because of the requirement to validate the model against the configuration of the eventual replacement of the present research reactor at ANSTO similar to those of the CEA test section geometry.

3. CURRENT ISSUES IN CFD MODEL VALIDATION FOR INDUSTRIAL MULTIPHASE FLOW

When being excited by CFD simulations used extensively for a variety of industrial problems as illustrated earlier, researchers and industry are also being perplexed by the question on the reliability and confidence of mathematical models due to the lack of sophisticated experimental techniques, in particular, in plant-scale measurements for model validation. It happens that researcher obtain completely different results when using different numerical models.

Obviously, further model refinement and thorough model validation necessitates the acquisition of detailed, non-intrusive flow measurements. Some techniques are available for non-intrusive measurements in two-phase flows. These include Gamma densitometry tomography for solids volume fraction, radioactive particle tracking techniques, capacitance imaging, cinematography, and NMR, to name a few. Each of these techniques, however, has limitations in terms of cost, speed of measurement, indirect measurement, and/or resolution. There is also a critical need to explore, in a controlled fashion, the factors which are known to influence flow behavior such as particle size distribution, particle shape and density etc.

Radiotracer technology

Radiotracer techniques could play an important role in addressing this problem due to its advantages over many conventional techniques. For instance, the radiotracer technique:

- can have both technical and economic benefits for plant-scale measurements due to the high sensitivity and stability of radioisotopes and modern nuclear radiation detection equipment;

- can allow non-contact, remote analyses of dynamic processes, thus avoiding any perturbations that might arise from direct sampling and working under the severe and hazardous physical and chemical conditions;
- enables investigations of particular elements and uniquely defined material within the experiment.

Therefore, it is important for nuclear organizations to make considerable efforts on exploration of industrial utilization of this technology. ANSTO and its collaborating partners at Australian National University have been working on developing new radioactive tracers for medical and intended industrial applications [9].

Figure 5 shows a process developed for creating such new tracers, which can have the following new features:

FIG. 5. New tracer

- wide range of suitable radiotracers
- will sustain high temperatures (>1200°C)
- ~10nm dimension, can emulate gas flow
- particles with specified size, shape and density for particular applications
- can be made hydrophobic or hydrophilic proven technology.

CFD & RTD methodology – a complementary technology

Residence time distribution (RTD) analysis plays an important role in multiphase processing industry. It characterizes the main flow features in non-ideal flow units, which is very useful to determine the mixing behavior and conversion rate of a processing system. Traditionally, RTD analysis is carried out by performing tracer experiments in either field scale units or laboratory scale physical models.

An alternative to the conventional experimental approach is to perform CFD simulation of numerical tracer experiments for RTD information in both macroscopic and microscopic levels. The flow pattern is calculated throughout the unit, and tracers can be set-up at different inlets and purely carried over to the outlet by convective flow. Not only the standard RTD curves of integral and

differential forms could be obtained, but also more detailed distribution of the residence time of different fluids since their entry into the system could be calculated throughout the system. In combination of temperature and species distribution, more reaction information could be deduced, which will be very useful for the processing operation. Eventually, the simulation could provide a possibility to answer the question whether the residence time is sufficient for the off-gases in the operation system at sufficiently high temperatures.

Numerical tracers can be simulated by CFD by solving the following transport equations for concentration

$$\frac{\partial}{\partial t}(\overline{\rho}_g C_i) + \frac{\partial}{\partial x_i}(\overline{\rho}_g \tilde{u}_g^i C_i) = 0$$

Figure 6 shows an example of RTD curve obtained from CFD simulation in a reactor system.

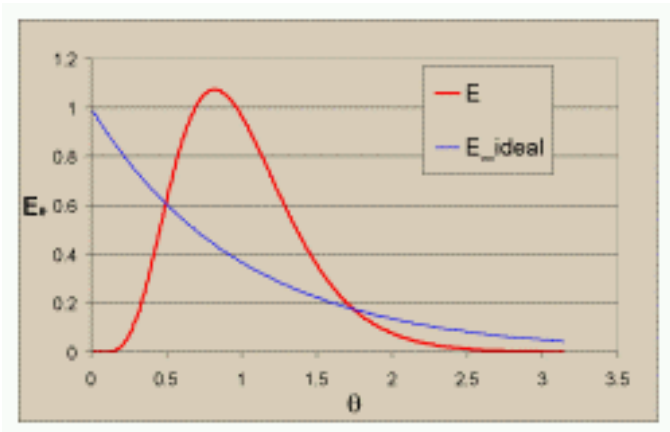

FIG. 6. RTD curve from CFD

Because the development of new CFD models currently for research and industrial applications is particularly active, the integration of CFD development with radiotracer techniques may invent new radiotracers and new experimental procedures, becoming a sophisticated experimental technique for research (model verification) and for industrial applications (consulting and services). By working closely with CFD modeling, the radiotracer technique could also be advanced using comprehensive CFD interpretation or visualization to enhance the quality of experimental data.

4. CFD & RTD EDUCATION PACKAGE

Overview of features of the package

In view to promote integration of CFD and RTD tracer techniques, a recommendation was made in the first CRP meeting to develop an education package on CFD-RTD with simple case studies that will be very helpful for many CRP participants and other tracer groups.

In this respect, the features of the package have included:

- a simplified CFD computer code for solving the partial differential equations for flow fields including the flow velocities, pressure and temperature and tracer concentrations;
- a simplified RTD computer code for solving the mathematic equations based on RTD concepts for studying flow fields in various configurations;
- a user-friendly interface for using both CFD and RTD computer codes;
- basic knowledge of CFD and RTD in the form of lecture notes using simplified terms integrated into the user-friendly interface (web-based);
- five flow cases as examples in tutorials for practising the use of the CFD code and learning about CFD;
- several flow cases as examples in tutorials for practising the use of the RTD code and learning about RTD.

Examples of the package

A CD contains the developed CFD-RTD Education Package with the instruction of installation. The package includes both lecture and tutorial materials and computer codes as well as built in a web-based environment as shown in Figure 7.

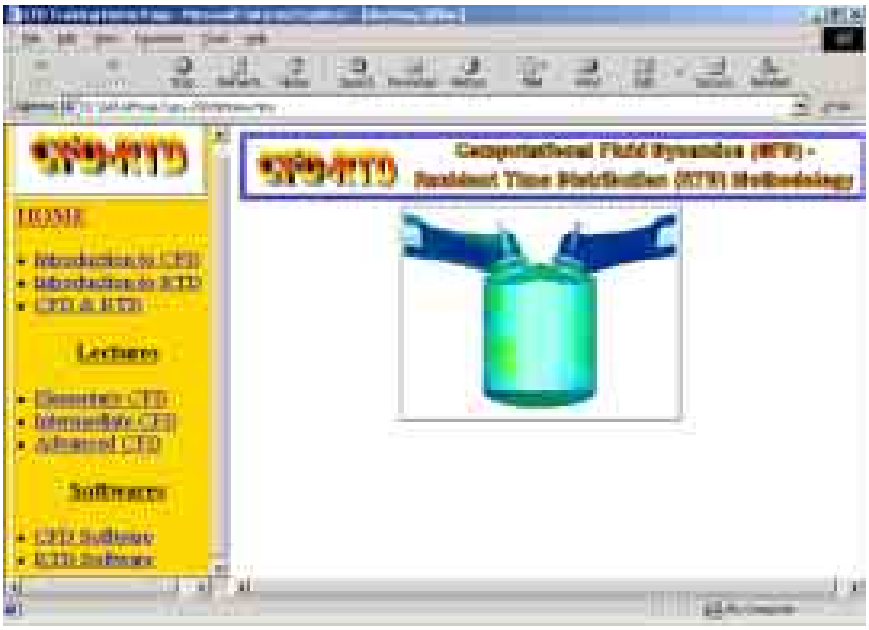

FIG. 7. Home page of CFD-RTD Education Package.

When you click “Introduction to CFD”, a sub-web page with a list of lectures allows the participants or users to learn about the CFD, such as, What is CFD, Why CFD, What CFD provides

and How CFD works? The package also provides the basic concept about the integration of CFD with RTD and their interaction. In the lectures, the package provides three levels of CFD lecture notes. The following five lectures can be delivered in order to teach the counterpart to learn the basic knowledge of CFD by using the package:

- Introduction to CFD
- Fundamentals of CFD (Elementary CFD)
- How to use a CFD code (Elementary CFD)
- Turbulence Modelling (Intermediate CFD)
- Modelling of Industrial Multi-Phase Flows (Advanced CFD)

It is important that the participants or users can learn how to use a CFD computer code through the hand-on tutorials for practice. Thus, the following five tutorials were also given to the participants to practice the use of CFD4RTD (short for "CFD for RTD") computer code built in the package:

- Laminar flow in a pipe
- Turbulent flow in a pipe
- Pipe flow with heat transfer
- Turbulent flow past a backward facing step
- Modeling of multi-phase flow in a ventilation room

5. CONCLUDING REMARKS

CFD for multiphase flow has made significant strides in recent years and is rapidly becoming a useful tool for system design, scale-up and optimization. However, detailed, no-intrusive experimental data are lacking for comprehensive validation of mathematical models in CFD software for solving complex industrial problems. Radiotracer techniques could play an important role in addressing this problem through RTD analysis due to its advantages over many conventional techniques. CFD simulation could also be used for RTD analysis in characterizing the basic flow behavior of the processing units or plants.

The numerical tracer tests by using CFD, based on the calculated flow field, could be an effective tool in combination with the tracer experiment/field-scale measurements. RTD analysis, together with the detailed knowledge of flow and temperature distribution throughout the system, can give a more complete picture or visualization of the flow characteristics of the multiphase processing system.

The integration of CFD with radiotracer RTD techniques may become a complementary technology to be greatly beneficial for industrial applications (cost-effectively consulting and services).

In the framework of the CRP a CFD&RTD Education Package has been developed to promote the integration of these two methods. The package includes lecture notes, tutorials and computer software for both CFD and RTD. A user-friendly web-based interface was developed to allow more effectively conducting the training courses or workshops, and to allow students or users to more easily learn and practice the CFD and RTD knowledge and computer programs. Further developments of computer codes and validation techniques are needed to enable to solve real complex industrial multiphase flow problems.

REFERENCES

[1] ECNSW (Electricity Commission of New South Wales), 1988, "Liddell Power Station Unit 6: Boiler Rehabilitation," Specification and contract No. 3824.

[2] TU, J. Y., C.A.J. Fletcher, M. Behnia, J. A. Reizes, D. Owens and P. Jones, 1997, Prediction of Flow and Erosion in a Coal Fired Power Boiler and Comparison with Measurement, *Transactions ASME Journal of Engineering Gas Turbines & Power*, Vol. 119, July, pp. 709–716.

[3] TU, J. Y., C.A.J. Fletcher and M. Behnia, 1997, Numerical Modelling of Three-Dimensional Flyash Flow in Power Utility Boilers, *International Journal of Numerical Methods in Fluids*, Vol.24, pp.787–807.

[4] JONES. P and Owens, D., 1995, "Wallerawang Power Station Units 7 & 8 Economiser Erosion and Replacement Investigation," Report No. pp/M/1266/1, Power Engineering Boiler, Fuel & Water Systems, Pacific Power, New South Wales, Australia, April.

[5] GOPINATH, R., Basu, N. and Dhir, V. K., 2002, "Interfacial heat Transfer during subcooled flow boiling", *Int. J. Heat Mass Transfer*, 45, 3947–3959.

[6] TU, J. Y. and YEOH, G. H., 2002, "On numerical modelling of low-pressure subcooled boiling flows", *Int. J. Heat Mass Transfer*, 45, 1197–1209.

[7] YEOH, G. H. & J. Y. Tu, 2002, "Implementation of a two-phase boiling model into the RELAP/MOD2 computer code to predict void distribution in low-pressure subcooled boiling flows", *Nuclear Science and Engineering*, 140, 182–188.

[8] YEOH, G. H., TU, J. Y., LEE, T. H. and PARK, G.-C., 2002, "Prediction and measurement of local two-phase flow parameters in a boiling flow channel", *Num. Heat Transfer, Part A: Applications*, 42, 173–192.

[9] BURCH, B., 2000, Private communication.

[10] YANG, Y.X., Reuter, M.A. and Hartman, D.T.M., 2000, Residents time distribution (RTD) analysis of a hazardous waste rotary kiln incinerator by way of CFD simulation, Proceedings of International Conference on Applied Computational Fluid Dynamics, Beijing, pp. 492–499.

MODELLING THE INTERNAL FLOW IN A PHOTO-REACTOR FOR WASTEWATER IRRADIATION

[A]R.M. MOREIRA, [A]A.M.F. PINTO, [A].B.G. BATISTA, [B].C.V. ALVES
[a]National Nuclear Energy Commission,
Center for the Development of Nuclear Technology,
[b]Federal University of Minas Gerais,
Department of Sanitary and Environmental Engineering,
Belo Horizonte, Brazil.

Abstract

The photo-reactor (PR) was investigated. The ultraviolet (UV) rays sweep all the liquid volume but its intensity decreases exponentially with distance. The key to a good performance is a combination of optimum irradiation dose and fluid residence times. Tracer tests were accomplished in a transparent mock up of the PR to determine the flow pattern within it. Instantaneous injections of ^{99m}Tc and ^{113m}In tracers provided the information required on residence time distribution (RTD). Simultaneous dye injections allowed the visualization of non-ideal flow behaviour, and aided in the construction of a conceptual model for the reactor. The RTD measurements were recorded under the several flow and exit-outflow combinations and processed later on using an *ad hoc* code. These measurements, together with a 3D mapping of the internal radiation dose distribution will provide the designer with the tools required for the calculation and optimization of the reactor yield.

1. BACKGROUND

Many Departments of Sanitary Engineering of Latin American Universities are active in prospecting, developing and optimizing innovative equipment and schemes for urban wastewater treatment. Taking into consideration the socio-economical and cultural environments in this part of the world, these efforts have been directed to develop technologies that are both simple and reliable. At the Federal University of Minas Gerais (UFMG) attention has been focused in treatment systems that can be incepted in communities with scarce resources, both material and manpower. The Center for the Development of Nuclear Technology of the Brazilian Nuclear Energy Commission (CDTN/CNEN) in Belo Horizonte has been associated with UFMG in many of these projects and has been instrumental in supporting this research, propping it with the tools of tracer applications, analytical data processing and modeling.

An innovative wastewater treatment system for small communities was designed as an alternative system to kill bacteria through ultra violet (UV) irradiation. It consists of a Photochemical Reactor (PR), which can be easily constructed in small mechanical shops with cheap materials and, besides, are easily controlled by non skilled personnel in far away locations.

The residence time of the wastewater inside the active zone and the absorbed UV energy doses are the two fundamental parameters controlling the yield of such reactors. The objective of the present work has been the measurement of the residence time distribution and its related moments. Besides, a modeling effort was carried with the tracer data obtained during the experiments carried. At a later stage this will be combined with the UV doses measurements in order to optimize the reactor design.

The specific approach to wastewater treatment studied takes advantage of irradiation in the short wave range. Some of the energy carried by the radiation is absorbed by the several DNA molecules of the microorganism species present, thus disrupting vital cellular processes in the cells.

Although the UV source is designed to sweep all the liquid volume, the intensity of the radiation decreases exponentially with distance. Thus uniformity of exposition requires some degree of transversal mixing to produce flow paths that push the fluid particles both near the outer walls and to the lamps during equilibrated amounts of time. As is well known, transversal dispersion resulting in mixing can be caused by velocity and concentration gradients in the direction transversal to the flow

axis [1]. The net result is a net flow pattern which is nearer to the plug flow ideal situation. This pattern can be modeled by the axially dispersed plug flow model [2].

A Plexiglas mock up of the PR has been constructed, at the 1:1 scale, provided with entrance and exit ports at different positions which allows different combinations of flow geometries. The flow rate can also be easily varied.

Tracer tests were accomplished to determine the flow pattern and the existence of dead volumes within the PR. ^{99m}Tc and ^{113m}In instantaneous injections and collimated scintillation detectors placed at the entrance and exit ports and a data acquisition system provided the required information. Dye tracers were injected simultaneously with the radiotracer so that the flow visualization could also be directly observed and recorded by photos whenever desired. Small GM detectors could also be placed at any height inside hollow tubes corresponding to the position the lamps.

The key to a good performance of the reactor is a combination of optimum irradiation dose and fluid residence times. The residence time distributions recorded at the several flow patterns tested can supply this information to the designer.

Besides this the dynamical modeling of the internal flow is attempted using the full tracer information recorded. Some experimental difficulties are then met, stemming from the rather short mean residence times inside the PR of the order of 90 s or less. Both the injection setup and procedure had to be optimized to assure a minimum dispersion between the injection port and the reactor entrance. Also a minimum of influence on the detectors of the radiotracer away from the measuring stations had to be ensured by means of a quite effective shielding. An ^{113m}In generator and scintillation probes with smaller diameters (1 in.) have been used in the experimental work. The DTS-PRO software package (PROGEPI-Nancy) has been used for the data processing and modeling work.

Optimizing the flow in the PR places a challenging task to the designer. Similarly to other chemical reactors it has to approximate plug flow behavior to attain the best reaction yield, although a good degree of transversal mixing is desired so that all the liquid parcels are equally irradiated during the short time period they take to travel through the equipment. It is hoped that tracer information will provide an efficient guidance to the optimum hydrodynamic design, avoiding with the recourse to higher UV doses, larger equipment and lower flowrates.

2. DESCRIPTION OF THE PHOTOREACTOR

Inside the photochemical Reactor, UV emitting lamps are used to disrupt or someway alter the DNA structure of microorganism cells. Common commercially available low-pressure mercury vapor lamps emitting light at the 253,7 nm wavelength constitute an effective disinfection agent. Besides the low initial and operational costs, one other remarkable advantage is that they don't introduce any chemical products into the effluent. Thus, neither chlorinated nor any other reaction products are produced that might hurt the biota or any other water quality parameters in the natural systems into which the treated flow is discharged.

The field PR is constituted of a PVC tubing with 200 mm nominal diameter and 900 mm length. Four vertical 30 W nominal power low-pressure mercury vapor lamps are installed inside it at equal spacing. A cleaning device (brushes fixed by a handle manually operated from outside the reactor has been devised for preventing decay of the emitted energy due to fouling at the lamp surfaces. Both the incoming and outgoing flows are horizontal. In Fig. 1 these features are clearly displayed.

Thus the PR physically consists of nothing more than a small vertical tube inside which an upward flow of the wastewater is established. During its residence period in the PR the flowing fluid is thus exposed to the UV rays generated by the set vertically mounted lamps inside the reactor.

Two problems are inherent to this method: (1) the diminution of the range of UV light penetration in the turbid waste flow; (2) the non uniform irradiation as the light intensity exponentially decreases with the distance from the lamp. Both problems are aggravated by an increase in the turbidity. Placing settling tanks upstream the PR may provide a reduction in the organic residue content and in the suspended solids of the incoming flow, but this to the detriment of the simplicity and low cost desired for applications to small communities sited far away from larger centers. This is why information on the performance of the system is looked for to optimize the design in terms of dimensions and proportions, flow pattern and residence time control in such a way as to maximize the exposure of the liquid to the UV radiation. Improvements in these variables may result in significant gains in the long run. The other factor affecting the PR performance is related to the irradiation efficiency; the cleaning of the outer surfaces of the lamps is a major concern in this connection, and this subject is being tackled by one other team.

Three experimental PR's have been installed in municipal sewage treatment in the State of Minas Gerais. The first one, now decommissioned, was at the town of Itabira (population: ~100.000, ca. 100 km northeast of the capital Belo Horizonte). The complete system includes an upstream UASB (Upflow Anaerobic Sludge Blanket) reactor, as well as screens and a grit chamber, as shown in Fig. 2. This PR was fed with an aliquot diverted from the effluent flow exiting the UASB reactor, corresponding to the sewerage of a community of about 150 people, and in this special application it was in place of a facultative pond, which is the usual treatment.

The other two test reactors were placed in a tandem arrangement to allow tests covering a larger span of parameters. They are still running in the Belo Horizonte plant (population 3.500.00), where the Department of Sanitary and Environmental Engineering of UFMG has set up a complex of pilot plants aiming at research purposes. One of them has an aluminum cask and was constructed at the CDTN mechanical shops.

Figure 1 shows the PR construction in Itabira. Figure 2 shows the PR operating at the wastewater treatment plant in Belo Horizonte. Tracer tests have been performed in both of them.

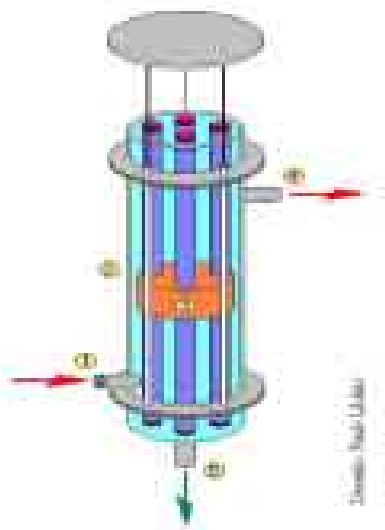

FIG. 1. Photoreactor in Itabira. Left: (1) entrance port, (2) external structural pins, (3) moving lamp scrubber, (4) exit port, (5) bottom flushing port. Right: photo of the reactor and control panel at its rear.

FIG. 2. Field PR assembled in tandem at the wastewater plant in Belo Horizonte.

Table I lists the operating characteristics of these field photoreactors.

TABLE I. MAIN CHARACTERISTICS OF THE PHOTOCHEMICAL REACTOR

Active volume: 20.3 L	Number of lamps: 4
Geometry: cylindrical	Power of the lamps: 30 W
Structural material: PVC	Power of the radiation at 253,7 nm: 8.3 W
Total length: 900 mm	Lamp model: G30T8 (Philips)
External diameter: 200 mm	Average irradiated area: 0.5027 m^2
Internal diameter: 196 mm	Thickness of the irradiated layer: 412 mm
Diameter of the lamps: 26 mm	Flow direction: upwards, parallel to lamps

3. RADIOTRACER EXPERIMENTS

Given the data in Table I, the mean residence time inside the PR should be θ = 50 s, corresponding to a radiation dose D_M = 17 MW.s.cm^{-2}. This figure meets the requirements of a population of 150 people. i.*e*. it corresponds to a population equivalent *PE* = 150.

Test runs have been performed both at this low mean residence time and using a lower flow-rate that rose to θ = 90 s. This last value allowed the higher dose D_M = 30.4 MW.s.cm^{-2} to be delivered to the wastewater flow, but it corresponds to a smaller *PE* = 85 people. These two *PE* values were deemed to correspond to two phases in the development of a small community

The operational characteristics during the test runs are shown in Table II, in which I_M is the average irradiation rate: $D_M = I_M . \theta$.

TABLE II. AVERAGE OPERATIONAL CHARACTERISTICS IN TEST RUNS

Phase	PR operational characteristics			
	θ (s)	*PE* (Inhabitants)	I_M (mW.cm^{-2})	Dose (mW.s.cm^{-2})
1	90	85	0.338	30.4
2	50	150	0.338	16.9

Besides the hydrodynamic characteristics determined with the tracer, other physical-chemical parameters were monitored in the runs: temperature, pH, total suspended solids, COD, nitrate, TKN, total coliforms, and *Escherichia coli.* The average efficiency of the PR, expressed in terms of *Escherichia coli* inactivation amounted to 91 % in the UASB reactor and to 99.92 % in the PR (i.e.: a total average efficiency of 99.9996 %, or 5.4 logarithm units).

Tracer tests

Tracer tests were performed both in the field reactors and in the laboratory, the later making use of a mock up of the PR, especially built to serve the study of the internal flow in this equipment.

Field tests

Pulse injections of radioactive tracer were done with a hypodermic syringe through a rubber septum built as near as feasible to the PR entrance port. Shielded scintillation probes were placed both at the entrance and ports. The use of the entrance probe recorded the tracer signal effectively entering the reactor. Since a true Dirac impulse is never attained no matter how quickly the injection is performed, its imperfections on the response of a system with such a short residence time may not be negligible. This contamination could then be approximately corrected by deconvolution.

In the initial tests ^{99m}Tc (E_γ = 0.14 MeV) that could be obtained at medical clinics in Belo Horizonte was used as the tracer. Later on ^{113m}In (E_γ = 0.40 MeV) produced by a ^{113}Sn → ^{113m}In generator that was supplied by IAEA advantageously substituted the ^{99m}Tc. Injected activities are of the order of 1 mC (3.7 MBq).

The main interest of the UFMG design engineers were the mean residence time and information about the degree of mixing or dispersion, or alternatively the Peclet number. Anyway, eventual anomalies in the internal flow could be detected and quantified by a simple analysis of the recorded residence time distribution.

Laboratory tests

Since field work with tracers is limited by logistic and safety constraints, it was decided to build an exact replica of the PR and put it inside the controlled area at CDTN where work with radioactive material is no hindrance. This allowed a row of tests to be run, either changing the flow conditions or repeating them whenever necessary.

For this purpose a mock-up of the reactor at the 1:1 scale has been constructed with transparent acrylic. This material could allow actual visualization of the internal flow doing dye injections. Besides the structural material the other only difference from the real reactor was the lack the cleaning brush and its guide, but this piece normally stays out of the active volume when the real reactor is running. Tubes with the outer dimensions of the lamps were inserted in the exact positions occupied

by them, even though the actual lamps were not needed. A photo of the whole set up is shown in Fig. 3.

FIG. 3. Acrylic mock-up reactor, 1:1 scale, mounted in laboratory, showing the peripherals.

As is shown in the photo, there are three horizontal entrance ports at the bottom of the reactor, besides a vertical port in place of the vertical drain of the real reactor. In the laboratory tests this last port can also be used to feed the flow into the reactor, thus creating a fourth alternative for the entrance geometry. At the top only one exit port is needed, so that the different combinations of entrance and exit positions allow the test of four combinations of flow patterns through the active volume. The flowrate can changed and measured with the help of a rotameter. The tracer injection septa are placed inside tees just upstream the entrance ports.

In order to visualize the internal flow a Rhodamine WT dye was used. This possibility is quite useful for defining the model characteristics and even making the initial guesses of the parameters to be used. The dye can also be mixed with the radiotracer solution, and injected together with it; thus both tracers will have exactly the same pulse characteristics. Fig. 4 shows different moments of the displacement through the reactor of an instantaneously injected dye tracer pulse. From the upward bound tracer front is apparent that a rather flat velocity profile is obtained with the Peclet numbers used in the runs.

Also shown at the top left of the last four photos in Fig. 4 is the shielded detector placed right after the exit port; the detector at the entrance is hidden by the reactor. Other probes can be placed at any vertical position along the external wall, and small GM detectors can be introduced in the hollow cylindrical compartments where the lamps would be in the real reactor.

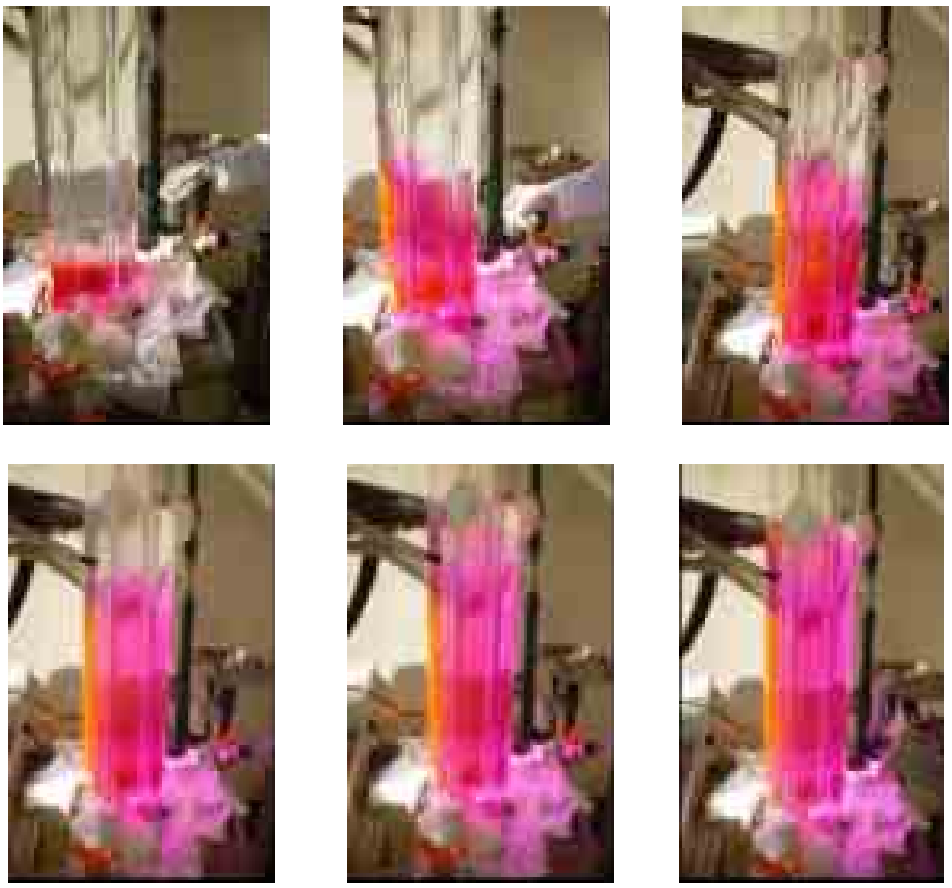

FIG. 4. Different moments of the transit of the fluid through the reactor visually indicated by a dye tracer.

However, when the feed flow was introduced through the bottom port, the behaviour changed drastically, as can be appreciated in the photos shown in Fig. 5.

FIG. 5. Dye transit through the PR the flow being fed through the central bottom port; photos from left to right shot at 1 s, 5 s and 100 s after the injection.

Two experimental problems related with a good signal detection had to be considered in this setup, and both stem from the small dimensions of the reactor. The first one is the shielding and collimation of the probes; only the tracer that is just passing in front of them should be recorded.

The second has to do with the distance between the injection septum and the reactor entrance. An effort was made to minimize these influences as much as possible, but the very recorded signals

indicated that perfect conditions were not obtained. Actually perfect conditions cannot be secured in such measurements and a posteriori corrections must be applied on the recorded signals [3, 4].

Modeling Approach

Practical recipes for reactor performance evaluation are very simple. The United States Environmental Protection Agency (U.S.E.P.A.), for instance rates the performance upon some straightforward indexes, such as [5]:

- q : feed flow rate
- τ : theoretical mean residence time (reactor volume divided by flowrate)
- $\bar{t}$: experimental mean residence time
- t_b : time of tracer breakthrough
- t_{90} : time at which de 90% of the tracer has passed through the reactor
- t_{50}: time at which de 50% of the tracer has passed through the reactor
- t_{10}: time at which de 10% of the tracer has passed through the reactor
- t_p: time of the peak
- N_{Pe}: Peclet number
- N_{Re}: Reynolds number

These parameters have been in use by the design group at UFMG, and tracer tests can easily determine them. However they tell nothing whatsoever about the internal flow structure and other meaningful parameters that allow scale up to be performed. That is why modeling was considered necessary to provide a better design basis.

The ideal flow conditions for reactors are those that approximate the plug flow ideal, since these provide the highest yields no matter the reaction kinetics. The nearer the flow gets to plug flow, the flatter will be the velocity profile. But the inverse is not necessarily true: the more turbulent a flow, the flatter its velocity profile, but also the higher its turbulence and the resulting mixing. Of course plug flow is an unattainable ideal.

What is aimed at in any tubular reactor with unavoidable dispersion is the maximization of the Peclet number. In the case of the PR one further condition is desired. Since the irradiation dose decreases with the distance from the lamps, the bacterial activity in a particle of the fluid flowing near to the outer wall all the way from entrance to exit will suffer a much lower depression than one flowing near the lamps. It is desirable that they should be exchanging positions all the time and this calls for a high radial dispersion.

The 1-D axially dispersed plug flow (DPF) model translates in mathematical terms exactly this situation. Thus it was thought that this model would better suit the situation at hand. Since there are large variations in the flow section at the entrance and at the exit of the PR, the boundary conditions of the DPF model should take this into account. Besides, due to design reasons there is a quiescent region above the exit port of the PR, and the dye neatly indicated that some fraction of the flow gets into it and only slowly returns back, going directly to the exit channel. This calls for a dead zone with a low interchange rate with the main flow to make up the whole model.

The preliminary results obtained with the field PR's, as shown in Table III were useful in evincing shortcomings in items considered important for the performance of the reactor. They pointed to the existence of dead zones and preferential paths; these should not be left out of the conceptual model. Following these hints the basic model has been conceived with the modular structure shown in Fig. 6. The French software DTSPRO [6] has been used to perform the model fit. In this conception the PR is assumed composed of two parts:

- An axially dispersed plug flow compartment closed to diffusion at both extremities;

- Perfect mixing cells exchanging flow with dead zones. These cells are assumed in parallel with the main flow from which a lesser derivation makes a detour through the quiescent volume on the top of the PR.

The parameters of this model are:

- V_{DPF} = the volume swept by axially dispersed plug flow (alternatively the mean residence time $\tau = V_{DPF}/q$ in this region);
- N_{Pe} = the Peclet number in this compartment;
- V_{MD} = the total volume of the mixing cells exchanging flow with dead zones (alternatively the mean residence time τ in this region);
- J = the number of mixing cells
- t_m = exchange time constant ($t_m = V_D/q_{ex}$, where V_D is the volume of the truly dead space, q_{ex} is the flow rate being exchanged between the mixing cells and the dead space; thus t_m is the residence time in the truly dead space);
- $K = V_D/ V_M$ is the volume ratio between the dead and mixed space
- φ = the fraction of the flow rate that is deviated to the mixing cells plus dead zones volume.

It is seen that even though the conceptual model with its only two modules is rather simple, the number of parameters is large since the mixing cells with dead zones module requires four parameters. It will be seen that the model quite insensitive to J , t_m , and K. However leaving out the dead spaces might be an oversimplification. The model structure is depicted in Fig. 6. Now, the runs with the feed through the bottom port were modeled simply by a plug flow and one perfect mixed tank in series.

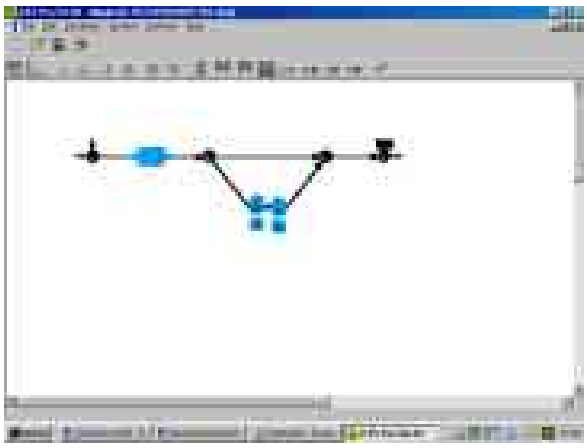

FIG. 6. Conceptual structure of the PR model: (1) axially dispersed plug flow module; (2) mixing cells exchanging with dead volumes module.

It is clearly seen that there is axial dispersion even though the flow approximately laminar. Of secondary importance, but not altogether negligible, is the influence of dead volumes together with their natural consequence: preferential paths. At UFMG these hydrodynamic indexes are being correlated with the performance indexes utilized by sanitary engineers such as UV dose and size distribution of suspended particles in the effluent being processed. A remarkable reaction yield in terms of coliform abatement was achieved by the PR with its present hydrodynamic parameters.

Table III indicates how the tests results evaluate the PR performance in the sewage plants. Shown in the second column are the EPA recommended values [5].

TABLE III. INTERPRETATION OF HYDRODYNAMIC TEST RESULTS

Index	Recommendation	1.1.1.1.1.1 Ita bira	Belo Horizonte	Indication from RTD
q	–	0,23 L·s^{-1}	0,69 L·s^{-1}	–
τ	–	90 s	30 s	–
$\bar{t}$	–	89,8 s	34,6 s	better flushed at lower flowrates
t_b / τ	> 0,5	0,01	0,03	occurrence of de preferential paths
t_p / τ	> 0,9	0,70	0,83	occurrence of de preferential paths
t_{90} / t_{10}	< 1,0	4,0	3,8	divergence from plug flow
$\bar{t} / \tau$	≈ 1,0	1,0	1,2	dead volume at higher flowrates
$t_{50} / \bar{t}$	≈ 1,0	1,2	1,1	occurrence of dead volumes
N_{Pe}	> 20	4.5	5.3	axially dispersed plug flow
N_{Re}	> 6000	952	2858	nearly laminar flow

The tracer injection pulse is not perfect Dirac (instantaneous) but has a finite duration. The injection pulse is not at all negligible at the scale of the response signal. Hence, the conceptual model cannot be directly fit to the tracer response and deconvolution must be applied to find the real RTD function of the PR. The software DTSPRO allows this to be accomplished (Fig. 7).

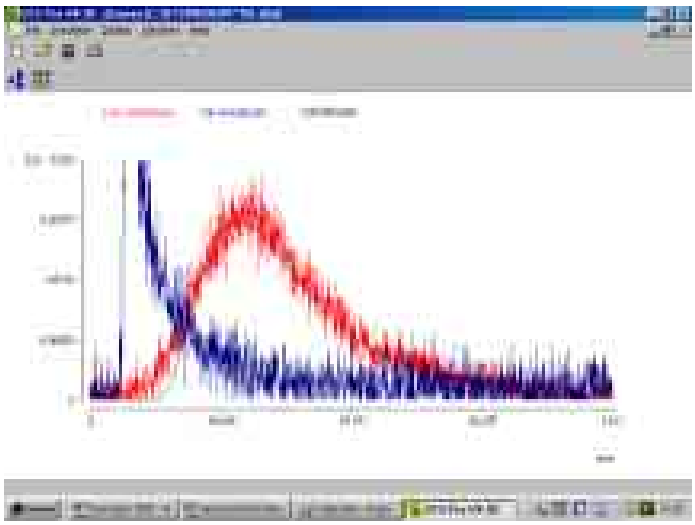

FIG. 7. Normalized input and output signals (wavering curves), and best fit obtained by convoluting entrance and RTD of model (smooth curve), Run 26.

Figs. 7 shows the recorded entrance and exit signals, $x(t)$ and $y(t)$ respectively, and a smooth line overlapping the recorded exit signal. This is the response of the model to the recorded inlet signal, it is not the RTD, which is the response to a Dirac δ – impulse at the entrance. The RTD, or response of the model to the δ – impulse, or transfer function, hereafter noted as $h(t)$, is shown as the intermediate smooth line in Fig. 8.

Using the conceptual model shown in Fig. 6 together with the data of the tracer runs the parameters were estimated in the deconvolution mode of the software, and their values are shown in Table IV.

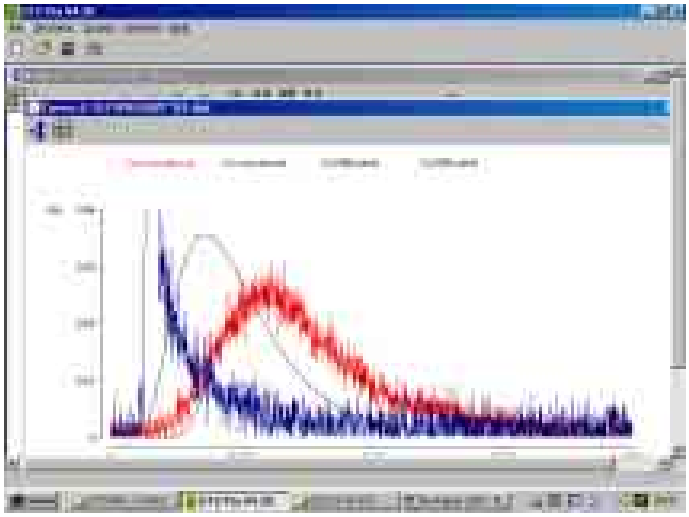

FIG. 8. Graph showing the calculated impulse response or RTD as the intermediate smooth line between the entrance and exit signals, Run 26.

TABLE IV. RTD MODEL PARAMETERS

Entrance port	I2	I2	I2	I2	I2	I0	I2	I3
Experiment	4	5	10	11	12	17	20	26
q (L·s^{-1})	0.21	0.21	0,84	0.87	0.29	0.46	0.21	0,46
V_{DPF} (L)	15.0	13.0	18.0	16.3	13.0	–	15.0	13.8
N_{Pe}	6.5	7.0	6.5	7.5	8.0	–	6.5	8.5
V_{MD} (L)	5.3	7.3	2.3	3.0	7.3	–	5.3	6.5
J	20	20	20	20	20	–	20	20
t_m (s)	9	9	9	9	9	–	9	9
K	2	2	2	2	2	–	2	2
φ (%)	4.8	4.8	2.5	2.9	5.3	–	7.9	2.2
V_{Plug} (L)	–	–	–	–	–	3.0	–	–
V_{Mixed} (L)	–	–	–	–	–	18.3	–	–
N_{Re} at inlet	8905	8820	35230	36952	12421	20259	9092	19503
N_{Re} inside PR	244	242	965	1012	340	555	249	534

The Reynolds numbers at the inlet and inside the PR have been added to Table IV, even though they are not strictly parameters of the model. Nonetheless, they are indicative of the flow behavior and can help in its diagnosis. Its calculation accounts for the fraction of the cross section occupied by the lamps.

The totally distinct behavior of the flow fed is shown in Fig. 9.

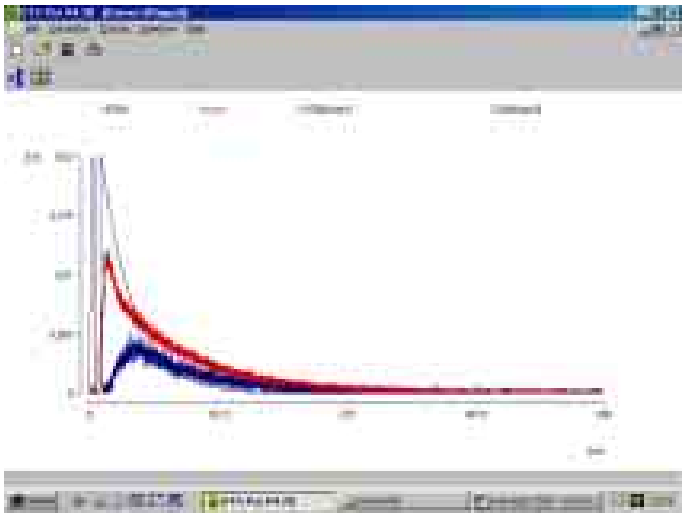

FIG. 9. RTD (smooth line in between entrance and exit pulses) for a flow that is fed through the central port I0, Run 17.

4. COMMENTS AND CONCLUSIONS

It is concluded from Table IV that as the flowrate increases the dead volume decreases, but the intensity of the dispersion as measured by N_{Pe} does not change much. Also, the fraction of the flow entering into the dead zones decreases with the flowrate.

The variation of the entrance and exit positions does not cause any appreciable changes when the entrance ports are equidistant from the exit. This was to be expected, however the behavior is dramatically altered when the entrance is at I0, the central bottom position.

It must be stressed that the RTD function obtained by this method is the calculated impulse response $h(t)$ of the model, and not the actual RTD of the system. The correction of $h(t)$ depends on the faithful conformity of the model to the real system, on the accuracy of the values of its parameters, and on the quality of the recorded signals $x(t)$ and $y(t)$:

$$\hat{y}(t) = \int_0^t \hat{x}(\theta)\,\hat{h}(t-\theta)\,d\theta$$

The hats indicate that all these functions are subject to either experimental or computational errors. Anyway, $h(t)$ is the function that will have to be used to compare with the results of the CFD simulation. Hence a lot of effort has to be dedicated to its accurate calculation so that a reliable validation gauge is effectively made available.

The most detrimental characteristics in PR reactors are dead zones and preferential paths. These demand more potent lamps for the same degree of disinfection, and electrical power represents the most important capital item in UV disinfection systems. This is why provision for such zones was included in the model. But it proved to be quite mild in the PR, as indicated by the small fraction of the flow diverted to it. Due to this the model was quite insensitive to parameters J, t_m , and K. However not only the dye visualization but also the response of the model to a step impulse as displayed in Fig. 10 indicate that it takes a long time for the marked fluid parcel to leave the system.

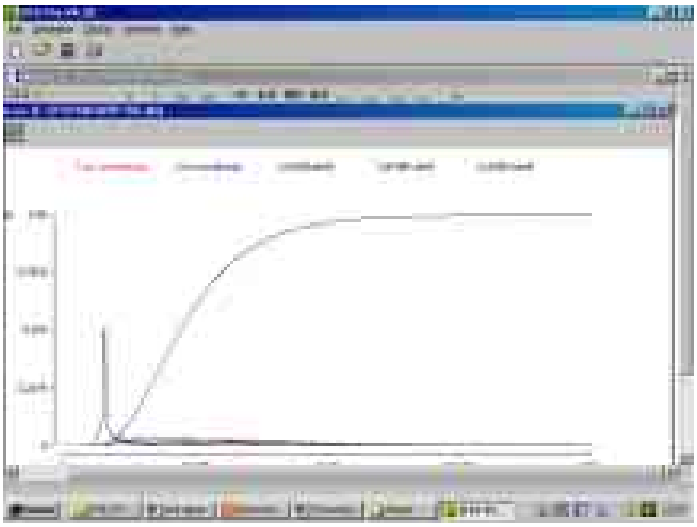

FIG. 10. Response of the PR model to a step impulse indicating the long time it takes for the final concentration to reach steady state.

It is also seen that, despite the seemingly high reaction yield as measured by the decimation of the bacterial concentration, there is a lot o deviation from plug flow; the Peclet number is rather poor and the Reynolds number inside the PR definitely in the laminar range

Laminar flow is normally undesirable because the radial velocity gradients result in large variances of the RTD function. However one might speculate about the effect of low Reynolds numbers in photoreactors. In a laminar flow the particles further away from the lamps would receive a lesser dose but would be irradiated for longer times. But the interpretation of tracer results under laminar flow conditions is not straightforward since the response depends on both the mode of injection and of detection and these are never quite perfect [7]. To attain laminar flow conditions, $N_{Re} < 2000$, with the dimensions shown in Table I, the mean residence time in the PR would need to be $\bar{t} \geq 73$ s, or the flowrate $q \leq 28$ mL·s^{-1}. Some of the tracer runs were performed at flowrates lower than this value, but there was not enough length for the laminar flow to be established, especially with the harsh entrance effects in the PR.

Dye observation showed that right after entering the reactor the feed flow suffers an intense mixing action, due to sudden expansion and abrupt change of direction. Compounded with this is the high Reynolds number in the inlet tube. Actually this is one of the reasons for never attaining perfect pulse shapes; the other reason being the strong turbulence caused by the injection jet itself. As a result of both these factors the entrance pulse looks like the response of a perfect mixer. It is felt that the modeling of the PR, either by RTD or CFD models, will have to include the section between the injection and the entrance to the reactor.

Although versatile and easy to operate as well as avoiding complexities in the shape that might hamper CFD investigative work, the very asset of the PR size places some difficulties for radiotracer detection. It is difficult to suppress the influence of the tracer inside the system on the probes that need to be placed very close to the reactor walls. Shielding and collimation have limits in this suppression; only detector models may improve the quality of such measurements.

REFERENCES

[1] JIRKA, G.H, SOCOLOFSKY, S.A., Environmental Fluid Mechanics – Part I: Mass Transfer and Diffusion, Engineering – Lectures, 2nd. Edition, Institut für Hydromechanick – Universität Karlsruhe, Karlsruhe (2002) 150 pp.

[2] LEVENSPIEL, O., Chemical Reaction Engineering, 3rd. Edition, John Wiley & Sons, Inc., New York (1999) 668 pp.

[3] THÝN, J., ZITNÝ, R., KLUSON, J., CECHÁK, T., Analysis and Diagnostics of Industrial Processes by Radiotracers and Radioisotope Sealed Sources, Vydavalteství CVUT, Praha (2000) 329 pp.

[4] SABINO, C.V.S., MOREIRA, R.M., LULA, Z.L., CHAUSSON, Y., MAGALHÃES, W.F., VIANNA, M.N., "Contaminant transport in aquifers: Improving the determination of model parameters", in: Application of Isotope Techniques to Investigate Groundwater Pollution, IAEA-TECDOC-1046, Vienna (1998).

[5] UNITED STATES ENVIRONMENTAL PROTECTION AGENCY (USEPA), Municipal Water Desinfection – Design Manual, EPA 625/1–86/021, Cincinnati (1986) 247 pp.

[6] LECLERC, J. P., Antoine, B., Software "DTSPRO V4.2", PROGEPI LSGC – CNRS – ENSIC, Nancy (2000).

[7] GARDNER, R.P., FELDER, R.M., DUNN, T.S., "Tracer concentration responses and moments for measurements of laminar flow in circular tubes", Int. J. Appl. Radiation Isotopes 24 (1973) 253 – 270.

APPLICATIONS OF CFD AND TRACER STIMULUS RESPONSE TECHNIQUES IN COMPLEX FLOW ANALYSIS

J. THÝN
Czech Technical University, Prague.

Abstract

The activities of the Czech research group can be divided into three categories: a) RTD model changes prediction by CFD; b) CFD verification by RTD; and c) Methodology of CFD verification by RTD and by local responses. CFD application for prediction of RTD model changes was demonstrated on gas flow analysis in electron beam cylindrical chamber with baffles. RTD simulation was effectively solved as 2D modelling by using the Finite Element method. The conductivity method as well radiotracers were used in the experiments and the best comparison was obtained for the real value of the parameter. This solution is an example on how the problem can be solved even with more simple 2D description of the real system. Special software, so called integral zonal model, was created and tested for heating conditions. The model is able to predict the influence of heater geometry, fluid properties and operational parameters.

1. INTRODUCTION

While the RTD method is based on the mass balance, the basis of CFD methods is also balance of movement and heat. As CFD describes processes in terms of spatially localized flow units (control volumes, or finite elements) interconnected by mass, momentum and heat streams the results are more precise and have greater information content. However this approach needs no additional information only in the case of for small flowrate in laminar one phase flow. Semiempirical models of momentum, heat and mass transfer have to be used in most of applications concerning turbulent or multiphase flows.

Several models are offered by commercial CFD software and their choice can influence the results. For example different ratio of maximal and mean velocities of flow in a tube can be obtained for different Re number calculated by different models offered by FLUENT. Generally, the proper choice of the model is based on the experience or on the experimental verification of results. Tracer RTD function provides information about flow structure, thus can be used for the CFD verification.

Once the proper CFD model is known for a regime, it can be used for prediction of changes of flow structure for different values of flow rate and viscosity. This important advantage of CFD was used in analysis of gas flow in a chamber with three baffles.

The RTD curve is not sufficient for analysis of complicated flow structure, while the same shape provides several models [1]. This is reason that not only RTD but also stimulus “local” responses should be used for a verification of CFD results. The stimulus responses measured by detectors mounted inside or at wall of vessel can complete missing RTD global information providing together un unambiguously flow structure. However the response characteristics (algorithm) of collimated “wall” detectors have to be included to identification procedure.

Two algorithms for collimated scintillation detector have been suggested and used in parametrical analysis of RTD from Fluidized Catalytic Cracking reactor [1].

During first period of research, work was concentrated on the CFD verification by RTD. The second and third year CFD results were verified on the basis of local responses of detectors placed around vessel.

2. DESCRIPTION OF RESEARCH CARRIED OUT

RTD simulation by CFD

Real tracer experiments are typically based on instantaneous injection of tracer (radiotracer, salt, fluorescent, dye) into inlet stream and monitoring concentration of tracer at outlet (using scintillation detectors, conductivity probes). This impulse response is a time curve *f(t)*, which can be interpreted as a residence time distribution (*RTD*) of material flowing through the investigated system. Residence time distributions *f(t)* can be obtained also from calculated velocity field either by particle tracking method or by simulation of stimulus-response experiment, i.e. by solving non-stationary concentration field of a "tracer".

Particle tracking

The particle tracking explores capability of CFD programs to predict trajectories of dispersed phase particles (the particles must have the same properties, e.g. density, as the continuous phase). The trajectories and residence times are integrated on the basis of known velocity field of continuous phase (Lagrangian method). This approach is straightforward in laminar (convective) flows, on contrary to turbulent flows, where random fluctuations of velocities must be superposed to the mean velocity of continuous phase (discrete or continuous random walk models).

Tracer RTD function

Stimulus function is usually prescribed as a short pulse or a step change of tracer concentration at inlet. Then the corresponding mass-averaged concentrations of tracer at outlet provides the residence time distributions f(t), or integral distribution F(t) respectively. Impulse injection instead of step change is preferred because is easy and the RTD represents better the system than F(t).

Reliability of CFD results

There is a number of similar CFD models available in commercial packages. The commercial program Fluent 5.3 suggests for modeling of turbulent flows several options, such as Reynolds Stress Model, standard k-ε , RNG modification of k-ε model, turbulent viscosity transport model Spalart and Allmaras, Large Eddy Simulation and others, with different boundary conditions at the wall. It is not an easy task to decide which one of these models is the best for a specific problem. Some of these models are declared as low Reynolds number models, enabling to predict even the transition from the laminar to the turbulent flow regime, but this prediction is very unreliable. Taking into account also approximation errors, i.e. influence of computational mesh and selected approximation formula it is not surprising that several quite different results of simulations, differing by several tens of percent, are typically obtained.

Prediction of RTD changes by CFD

The prediction of RTD for different steady state conditions can be done on the basis of numerical solution of transport equations for fluid dynamics using particle tracking method or transient analysis of temperature or tracer concentration pulse. The RTD prediction for a broad range of Reynolds numbers (by the model for laminar or turbulent regions) simulated for simple geometry of the gas flow in the chamber with and without baffles was realized by using the commercial software Fluent. Velocity fields were evaluated for a constant inlet velocity and variation of *Re* was accomplished by changing viscosity.

Prediction of RTD in a chamber

Steady, incompressible flow was considered in the numerical analysis. Numerical experiments were used for identification of RTD model of dead volumes with cross flow. This simple combined model was able too fit impulse response calculated by CFD in turbulent region quite well as it is shown on Fig.1.

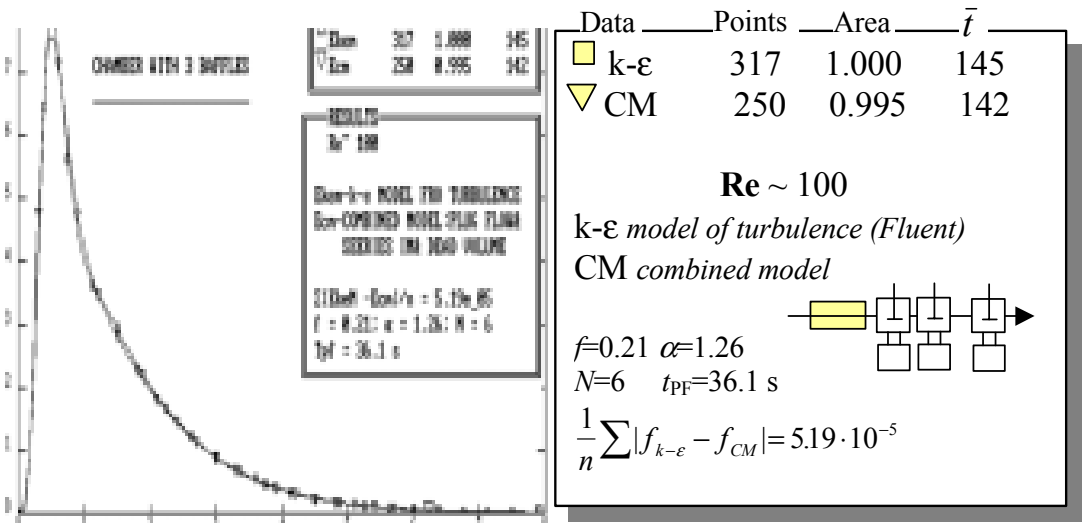

FIG. 1. Impulse responses f(2) of 3D cylindrical chamber with 3 baffles. Laminar flow.

Influence of *Re* and the relative height of baffles, predicted by 3D model (by Fluent) is shown in Fig.2. Molecular diffusion of tracer was not neglected (D = 2.49.10^{-5} m^2.s^{-1}), because the role of diffusion is significant, especially at low *Re*.

Calculated impulse responses are characterized by two peeks at Re>40. This is probably caused by the fact that the swirls behind baffles are not ideally mixed regions and this assumption seems to be acceptable only at turbulent flows. Slightly improved combined model takes into account this characters of swirls replacing the single tank in a "dead zone" by a series of M-perfectly mixed tanks (this series represents a circulation loop), see Fig. 3.

The improved combined model is physically substantiated and its parameters represent main integral characteristics of the reactor: Number of sections N equals number of regions between baffles, parameter ∀ characterizes relative volume of dead region and f is mass exchange between the main stream and this region. Parameters of model ∀, f, ∃ can be related to the design parameters - geometry (H_d/D) and Re, as shown in Fig.3. Thus the general trends (e.g. an expansion of dead region with increasing Re and H_b) can be quantified.

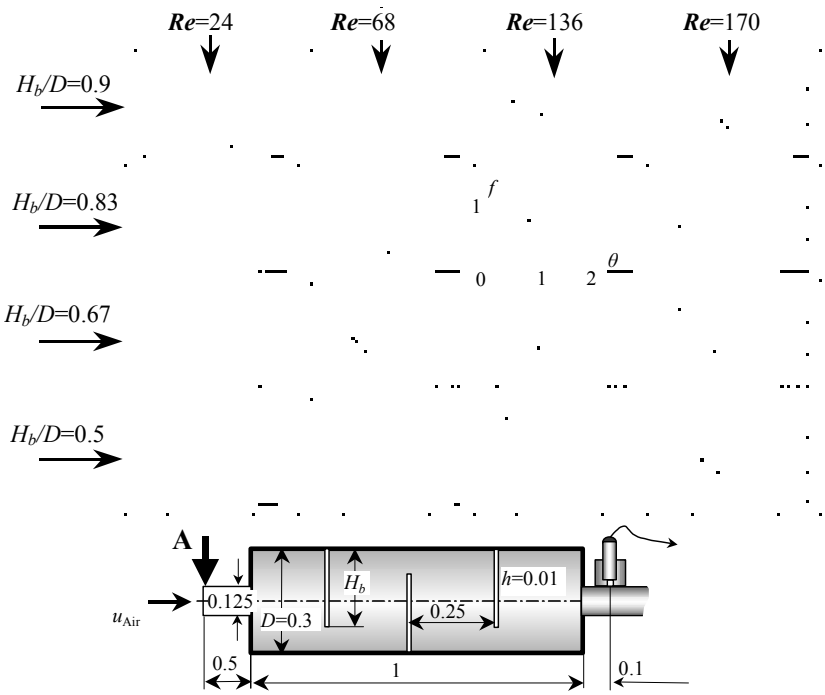

FIG. 2. Impulse responses f(2) of 3D cylindrical chamber with 3 baffles. Laminar flow.

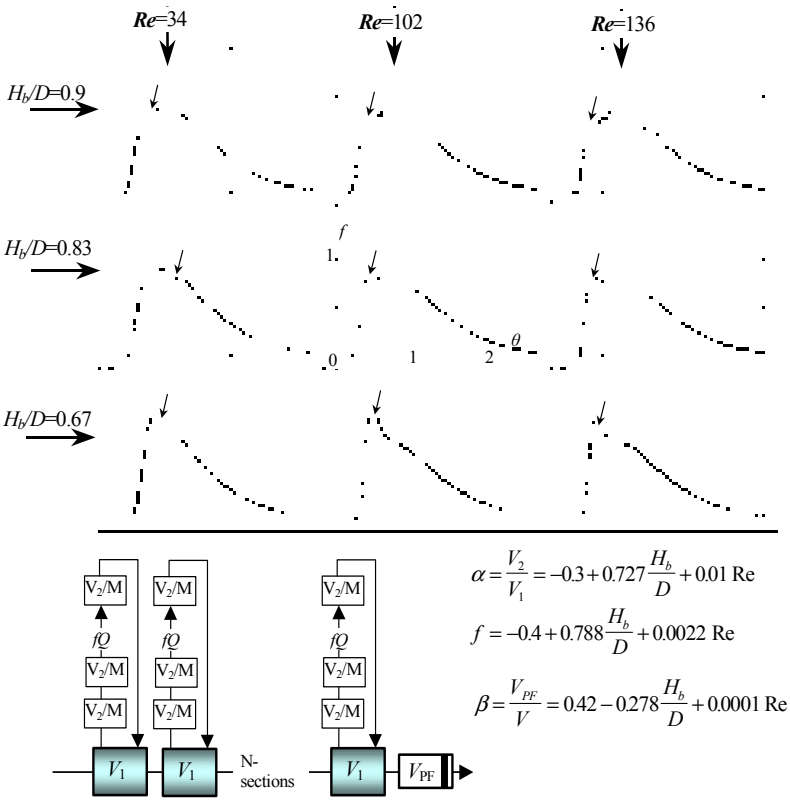

FIG. 3. Impulse responses calculated by improved combined model (denoted by arrows) and by Fluent 5.3. N=4, M=3. Parameters ∀, ∃, f are calculated as functions of Re and H_b/D (relative height of baffles) according to simple linear relationships identified by regression.

Verification of CFD by RTD

The response numerically evaluated by CFD code as mass average of concentration at the output tube can be compared with the experimentally measured RTD. A suitable CFD model can be chosen (from the set of the models offered by commercial CFD software) on the basis of this comparison. As the experiment can be easily implemented even in industrial equipment, RTD seems to be a good means for verification of CFD numerical evaluations in such cases.

Direct ohmic heater

Numerical modeling and experiments are tested on a continuous direct ohmic heater, shown in Fig.4. The reason why this continuous heater has been selected for tracer experiments lies in the fact, that the flow pattern – counter current parallel flows – is frequently encountered in mass transportation equipment (not only heat exchangers but also for example core annulus flow pattern in cracking units).

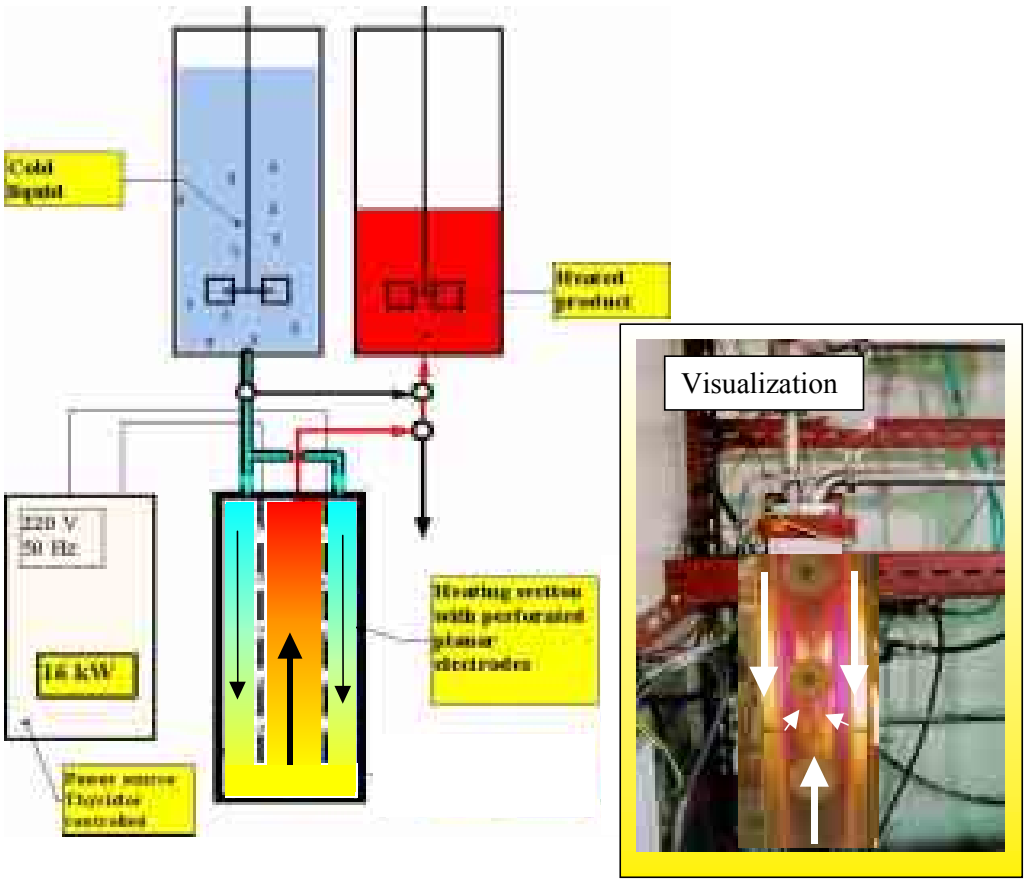

FIG. 4. Sketch of the Direct Ohmic Heater

Liquid flow from top to bottom in lateral channels (preheating) was reversed at the bottom of heater. Electrodes can be perforated thus allowing a part of cold liquid in lateral channel flows directly to the central channel.

RTD was measured with conductivity and with radiotracers. Fluent software was tried for 3D modeling of the system with cross flows without success because of the density of the mesh. 2D modeling with commercial software COSMOS (using Finite Element method) was used instead. Of course 2D modeling provides the response, which is not a fully realistic description of the flow field, but this response can be used for comparison of CFD numerical prediction with RTD experimental impulse response (Fig.5).

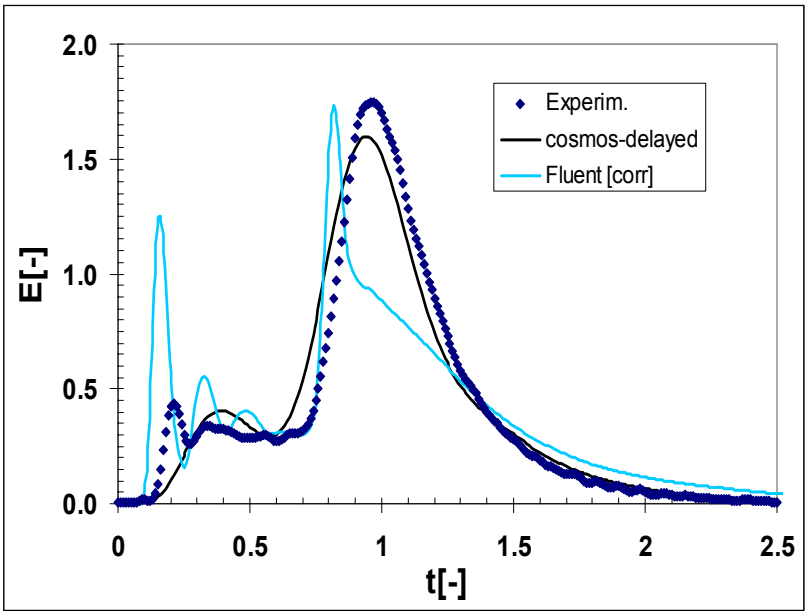

FIG. 5. RTD measured (by conductivity) and calculated by CFD 3D (Fluent) and 2D Cosmos.

3. METHODOLOGY OF CFD VERIFICATION BY RTD AND BY LOCAL RESPONSES

The most important parts of methodology for validation of results of CFD method by radiotracers are:

a) successful simulation of tracer experiment by CFD code (numerical solution of tracer dispersion in the system), which results in tracer concentration field in several time intervals;

b) postprocess data treatment, which use detection chain description and which enable to simulate the local responses detected by detector from the tracer concentration field evaluated by CFD code.

While the evaluation of RTD is possible to receive directly from commercial software (Fluent e.g.) as a mass average of tracer at the cross section of outlet tube, the local response must be evaluated by

$$J(t,x,y,z) = \iiint_V D(x,y,z)c(t,x,y,z)dxdydz$$

where *c(t,x,y,z)* is the distribution of tracer concentration obtained from CFD calculations and *D(x,y,z)* is transfer (weight) function.

Two ways of evaluation ware suggested for *D(x,y,z)* function:

- by using of algorithms for collimated detectors (see [1]);
- by interpolation of values determined as the detector response to Point Source which is situated inside of the apparatus. Point Source Response PSR can be realized directly by experiment (if possible), or by numerical simulation by using MC code.

Algorithms of collimated wall detectors

The tracer measurement should correspond to the tracer concentration in the volume, which "sees" collimated detector. However, measurements are influenced by qualities of radiation collimation, way of detection, physical qualities of flowing materials and surroundings etc. The relation between measured value and tracer concentration is solved by special algorithm for collimated scintillation detector. This algorithm should be as much as possible realistic but also simple, as it will be used several times in many nodal points, which are used for description of flow by numerical methods (by Finite Elements (COSMOS) or Control Volume (FLUENT).

Two algorithm are formulated [1]. Perfect absorption of radiation in detector is supposed in both of them. The first algorithm is more suitable for tracer with "soft" γ-radiation, the second is for "hard" γ- radiation.

FIG. 6. Water barrel used for evaluation of point source responses.

The algorithms were tested on the basis of collimated detector characteristics, which were evaluated from the **P**oint radioactive **S**ource **R**esponses in the water. (see Fig.6). Experimental responses to so called "point" source (^{99m}Tc (140keV) or ^{137}Cs (662 keV)), which was situated in the water, were evaluated for different distance from the frontal area of lead block with the collimation hole with diameter of 1.4 cm and depth 3 cm, with scintillation crystal (NaI(Tl)) with diameter 5 cm and high of 3 cm..

Monte Carlo code (program INSPECT, Tola [5]) was also used for evaluation PSR under the same conditions

Verification of CFD by PSR experiment and by stimulus response method.

PSR method is used in steady state conditions of the system, with the same detector and gamma collimator.

Point Source Response in the system.

The experiments with a point source inside the apparatus at no-flow conditions yields information about the actual collimator characteristic and information about absorption and reflection characteristic of the media and internals inside the vessel (Fig.7).

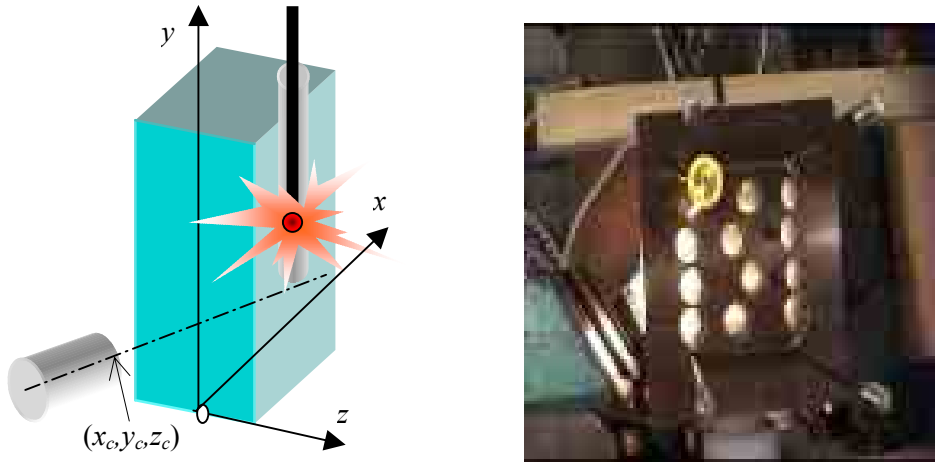

FIG. 7. Point source response measurement in the system.

Interpolation

By monitoring count rate of the collimated detector at different positions of radiation source, the response function D (x,y,z), corresponding to unit activity at a general point x,y,z can be obtained. For interpolation of N measured points in three dimensional space (m=3) can be used relation:

$$D(x,y,z) = \frac{\sum_{i=1}^{N} \frac{D_i}{l_i^3}}{\sum_{i=1}^{N} \frac{1}{l_i^3}}$$

The detector response to a general distribution of activity c(t,x,y,z) can be calculated by integration across the whole volume of apparatus

$$J(y,x,y,z) = \iiint_V D(x,y,z)c(t,x,y,z)dxdydz = \int_0^{2H_x}\int_0^{H_y}\int_{-H_z}^{H_z} D(x,y,z)c(t,x,y,z)dzdydx$$

The distribution of tracer c(t,x,y,z) is obtained from CFD calculations.

As there is great difference between the density of measured point response and density of mesh used in Fluent evaluation interpolation formula has to be tested as well.

Examples of PSR measured with four scintillation detectors with different collimation holes on the test rig of direct ohmic heater are presented in the Fig. 8. Experiment performed with ^{137}Cs (3.6mCi) in the test rig for direct ohmic heater gave the contours shown in Fig. 8: The contours were obtained by using the method of interpolation.

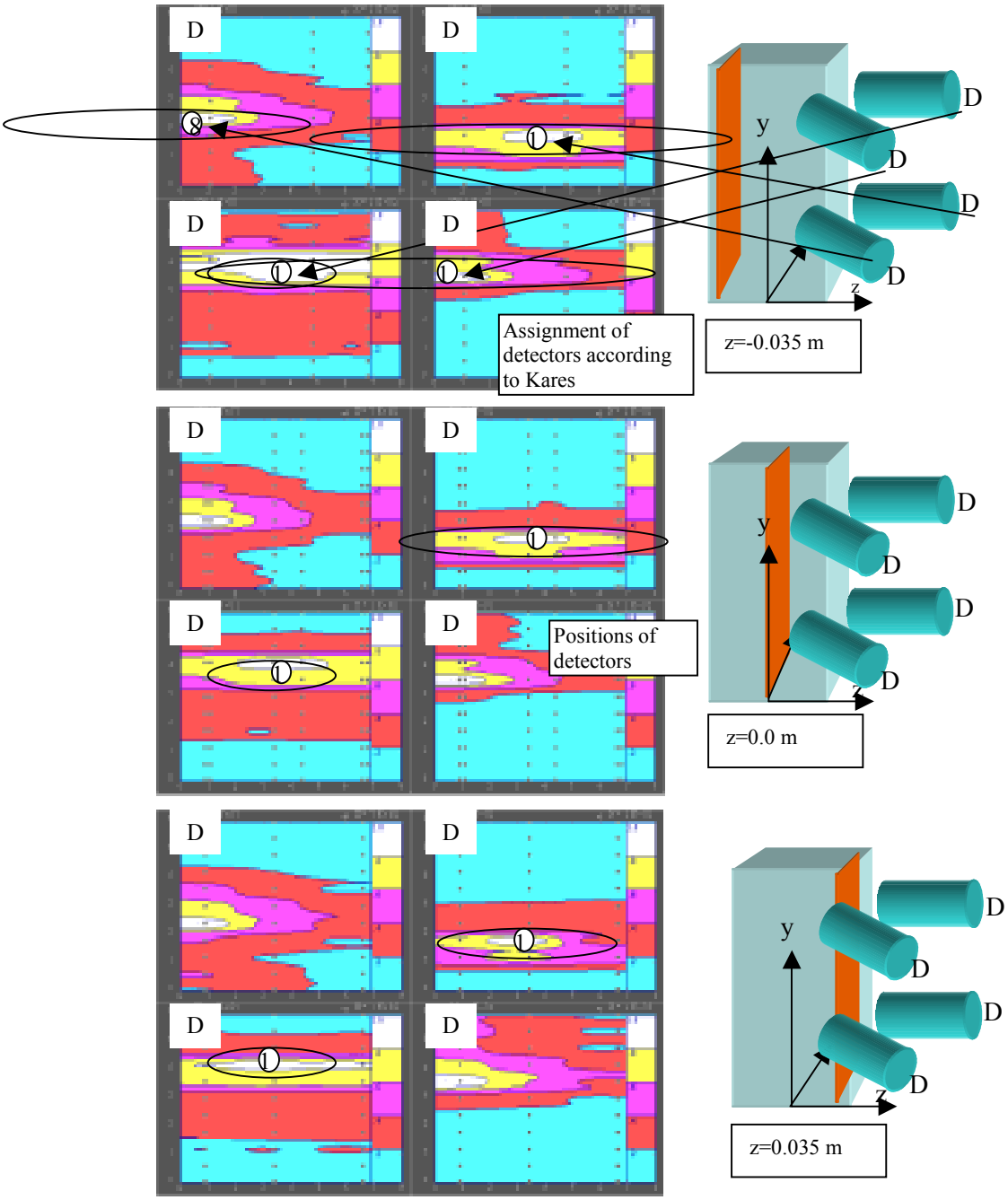

FIG. 8. Normalized count rate of collimated detectors at cross sections z=-0.035, 0, 0.035m m. Circles denotes positions of detectors (numbers within the circles are number of holes).

Evaluation of responses by Fluent

Verification of computational fluid dynamics (CFD) results by radiotracer methods will be demonstrated on the system for continuous direct ohmic heater (CDOH). The CFD method, which uses the commercial software Fluent is based on "control finite volume techniques" which solve so called transfer equations. These equations are essential for prediction of heat, mass and momentum flow. The application of Fluent demands setting up the complex grid or mesh representing the flow field. Mesh generation can be done by special pre-processor GAMBIT.

The procedure of verification of CFD after decision which software will be used (Fluent, CFX, Cosmos) follows several phases. When Fluent is used than for mesh construction commercial Software Gambit or MixSim may be used.

In pre-processing phase the decision has to be taken about:

- type of elements (tetra or hexahedron),
- the mesh density,
- boundary conditions.

Another decision has to be taken during CFD analysis (after using pre processor):

- additional declaration of the rest boundary conditions,
- choice of the model (laminar, turbulent e.g.) - (on the basis of experience, value of Re, or experiment),
- creation of the scripts (if the evaluation should be done "behind" (=files of the commands for proceedings of evaluation of flow, and for numerical simulation of tracer experiments)
- monitoring of tracer concentration at the outlet tube.

In so-called post-processing phase the conversion of outlet files (of type patran-neural as well as patran nodal) to neutral format files (NFF) should be done. And these files are used for numerical simulation of detector observation and for results comparison with real tracer experiments.

It is recommended to try to find *optimal positions* of side detectors. Optimal position can be estimated from the evaluation of spatial distribution of deviations between flow models obtained in different positions of the vessel. The spatial distribution of deviation between the laminar and turbulent flow is presented on the Fig.9.

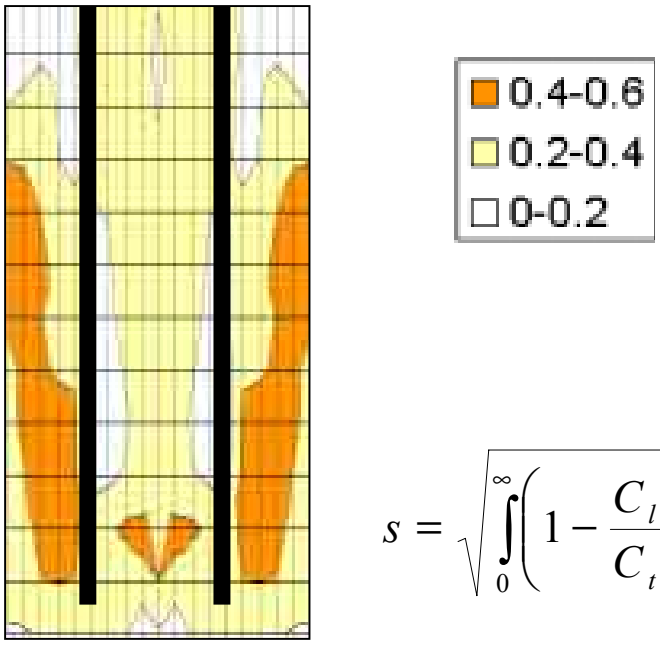

$$s = \sqrt{\int_0^{\infty} \left(1 - \frac{C_l}{C_t}\right)^2 dt}$$

FIG. 9. Distribution of deviations between models for laminar flow (l) and RNG k-ε (t) in the ohmic.

Tracer experiments with Tc-99m and with KCl

CFD numerical modeling and tracer tests were performed in the continuous direct ohmic heater (volume = 4.10^{-3} m^3). Conductivity with KCl and radiotracer (^{99m}Tc) were used simultaneously in the experiments without heating. The stimulus and the response of the system were detected with conductivity probes C1, 2. While local responses were obtained by collimated scintillation detectors D1, 2,3 and 4. Positions of probes and scintillation detectors are shown on the Fig.10.

Water flow was about 80 ml/s. Re number in the output – outlet tube was about Re = 3.10^3, while the Re calculated for lateral and central channels were $Re_l = 1.6 \cdot 10^3$ and $Re_C = 1.3 \cdot 10^3$. The results of CFD evaluation by Fluent presented as mean and variance of residence time distribution are presented in Table I together with tracer experimental values. Laminar and turbulent RNG k-ε models with high (HD) and low density (LD) of mesh size of hexagonal elements were used in numerical evaluation. Turbulent model with using HD seems to be more closed to reality.(Fig.11).

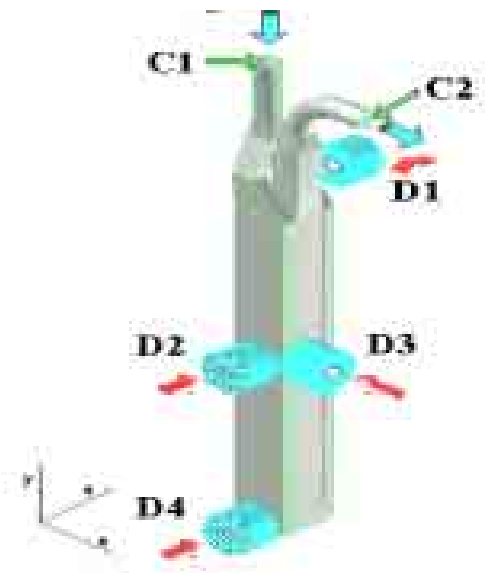

FIG. 10. Heater with conductivity probes and collimated scintillation detectors.

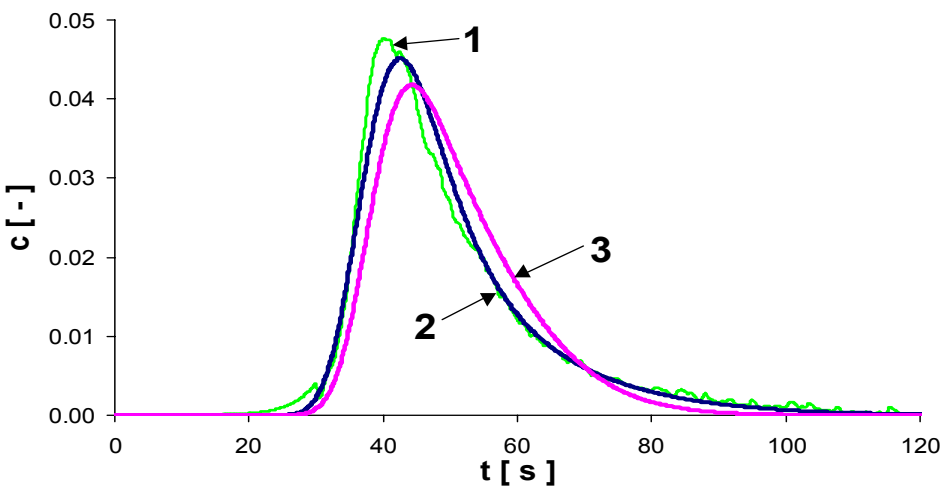

FIG. 11. Comparison of tracer RTD experiments (1&2) with RTD calculated by CFD models (3).

TABLE I. COMPARISON OF CFD AND RTD RESULTS

CFD - Models	Flow [ml/s]	Time step [s]	T_{mean} [s]	σ^2 [1]	$\Sigma\lvert Y_i - Y_{exp}\rvert / n$ [1/s]
Lam flow (LD)	80	1	50.74	0.04	0.0028
Lam flow (HD)		0.25	49.91	0.04	0.0021
RNG k -ε (LD)		1	49.42	0.088	0.0012
RNG k -ε (HD)		0.25	49.8	0.07	0.0008
Low Re flow (HD)		0.25	49.72	0.03	0.0038
Experiment	79.3	0.5	49.87	0.09	

Where LD - Low density (178 932 nodes, 160 560 elements)
HD - High density (834 432 nodes, 790 400 elements)

As an example of the local responses, the results obtained using ^{99m}Tc as a radiotracer are presented in Fig. 12, 13 and 14. The local responses were obtained using well focused collimated scintillation detectors D2 and D4. The focal distance was 85.10^{-3} m. The detector D3 had only one hole (with diameter 14.10^{-3} m). The vertical positions for PSR experiments are shown on the graphs. The difference between the models for laminar and turbulent flow is small, but better fitting gives the RNG k-ε model.

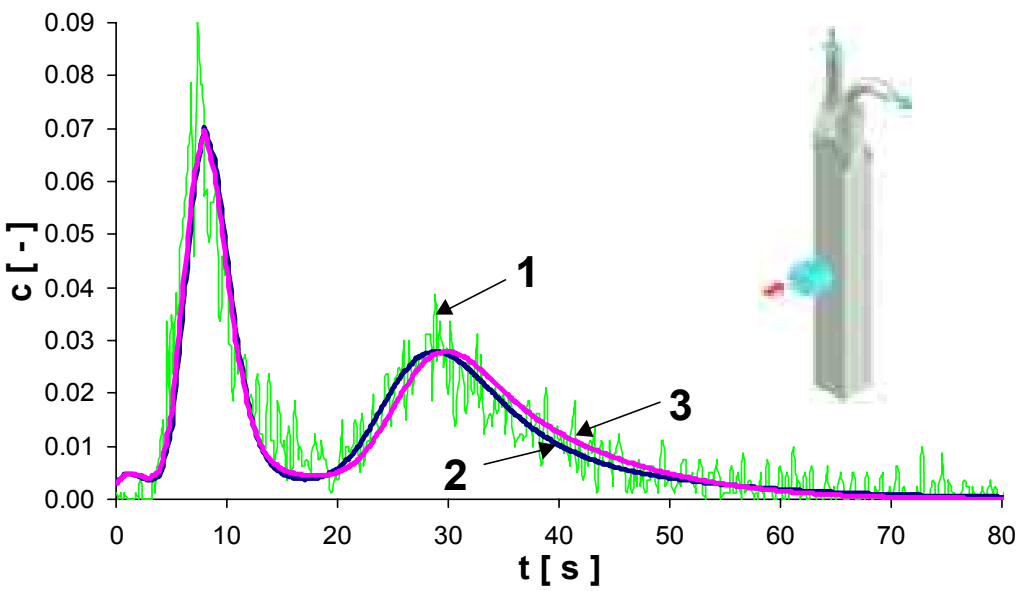

FIG. 12. Experimental response (1) observed by detector D2 and evaluated responses by RNG k-ε model (2) and laminar flow (3).

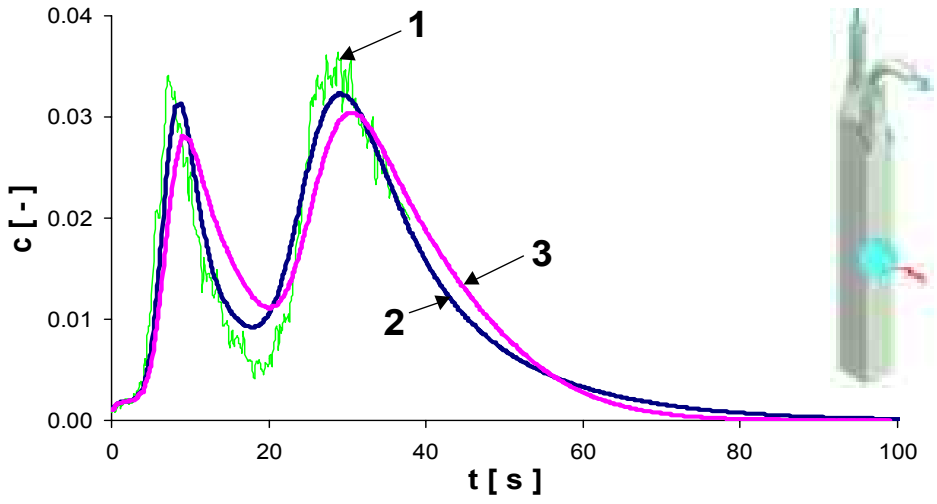

FIG. 13. Experimental response (1) observed by detector D3 and evaluated responses by RNG k-ε model (2) and laminar flow (3).

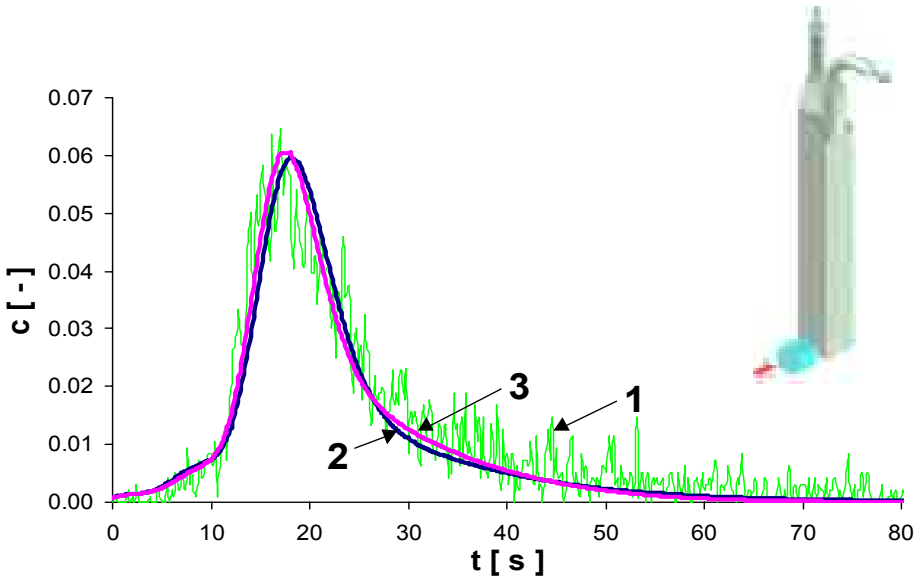

FIG. 14. Experimental response (1) observed by detector D4 and evaluated responses by RNG k-ε model (2) and laminar flow (3).

Time homogenisation simulation by CFD

Commercial software Fluent 6. (with a pre-processor MixSim for generating mesh) was used to simulate the homogenization of liquid in a mixed vessel with Rashton turbine. The numerical simulation of time homogenization by CFD (for different values of detected volume) was confronted with measurement of time homogenization with conductivity probe and with different radionuclides ^{198}Au, ^{82}Br and ^{24}Na. The tracer concentration measured in different positions of the vessel volume was affected by different energies of radiotracers.

Experiments in Mixed vessel

Measurement of time homogenisation was performed in the equipment shown on Fig. 15.

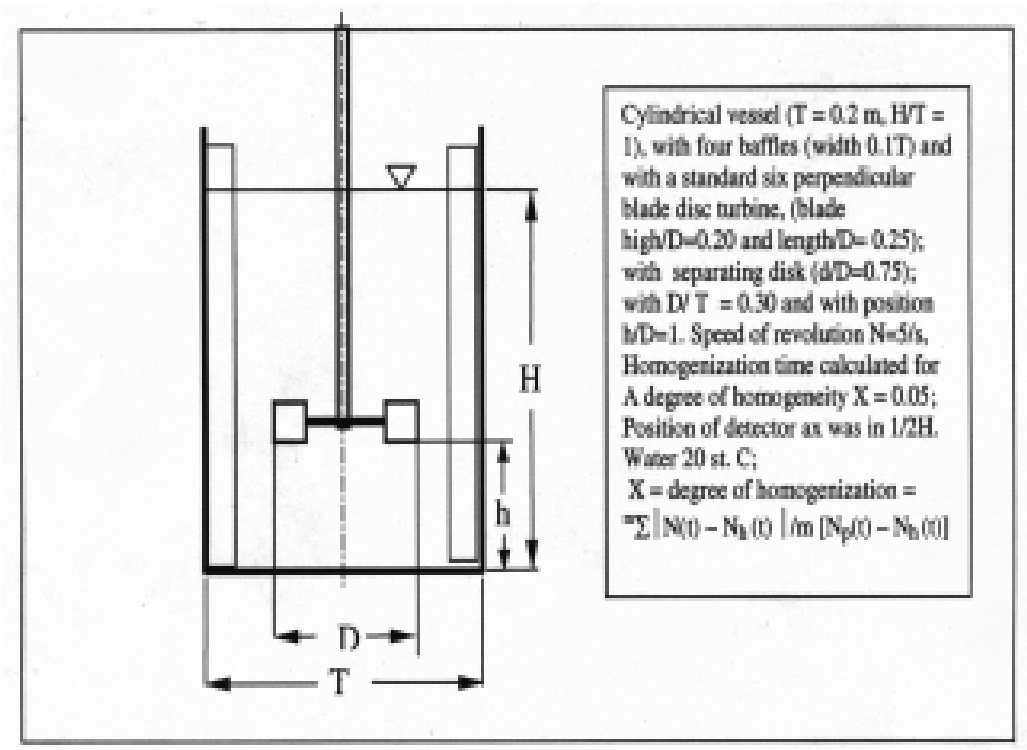

FIG. 15. Mixed vessel with Rushton turbine.

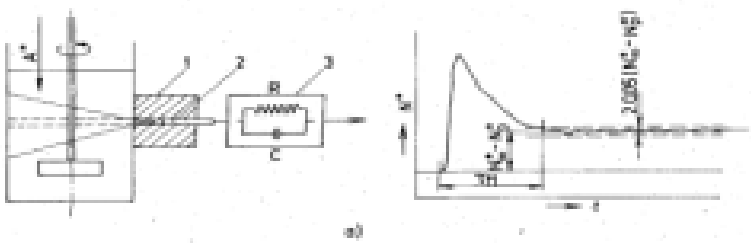

FIG. 4-9a Homogenization time measurement.
A- instantaneous tracer dosing;1 - lead shielding;*
2 - scintillation detector; 3 - rate meter.

FIG. 16. Homogenisation time measurement by tracers.

Evaluation of homogenization time is clearly visible in Fig. 16. The read off homogenization time will be probably shorter than homogenization time obtained by e.g. the conductivity method. The difference is caused by the fact that when measuring with radiotracers, the tracer concentration is observed in larger volume of the homogenized batch. To be able to consider the difference from this point of view, it is necessary to evaluate the measured volume or the observation scale.

When radiotracers are used, the detection probe is fixed outside the unit. The measured space is given not only by the shielding collimation opening and energetic properties of the tracer in the measured media, but also by the detector properties. The larger the collimation opening or closer to the wall the detector is fixed, the larger is the measured volume. The radiotracer with high radiation energy will be registered by the detector from a longer distance. Each elementary part of the detected volume, however, contributes in a different way to the total radiation recorded. Therefore it is clear that theoretical evaluation of the measured volume or observation scale is quite difficult.

CFD numerical simulation

Stirred tank typically consists of a baffled-tank and an impeller. From a numerical viewpoint, flows in mixing tanks are difficult to simulate because of the interaction of the rotating impeller with stationary baffles on the periphery of the tank. Special sliding mesh technique: Multiple Reference Frames MRF is used in this case.

In this method multiple grid frames are used where one frame is attached to the rotating impeller and the other remains stationary with the tank baffle. For the computation the program Fluent V4, V5 with a preprocessor MixSim 1.7 created by Fluent Inc for agitated vessels were used. For the density of the grid the number of the cells T per diameter of the vessel were defined. The calculation was performed for the vessel where tracer experiments were carried out. Total number of elements was 327 672. After the grid creation Fluent 6 was applied. MRF calculated radial and axial profiles of the velocity for given revolution speed. The CFD results were compared with the results from literature. The influence of the Schmidt number was taken account (Fig. 17).

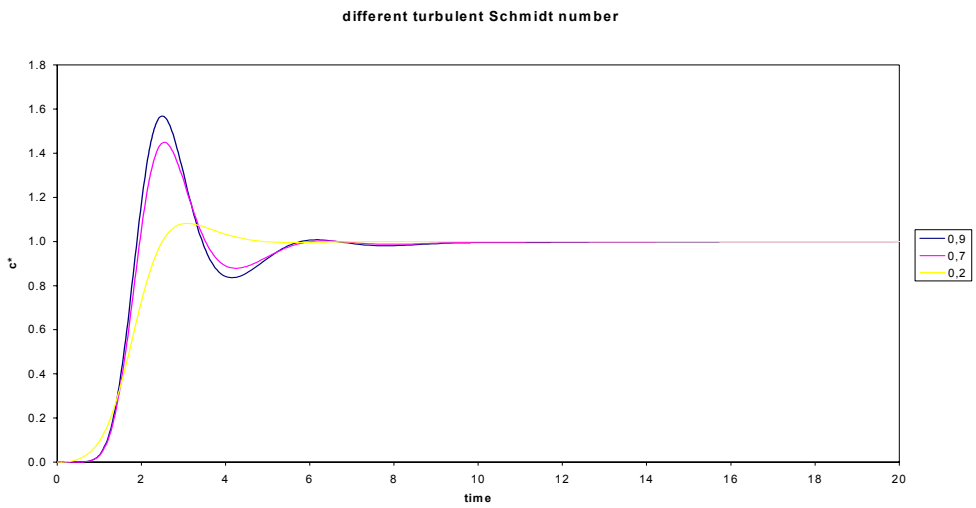

FIG. 17. The influence of Sc number on the simulation of the homogenisation.

The example of the evaluated velocity profiles for 5 rps is presented in the Fig. 18.

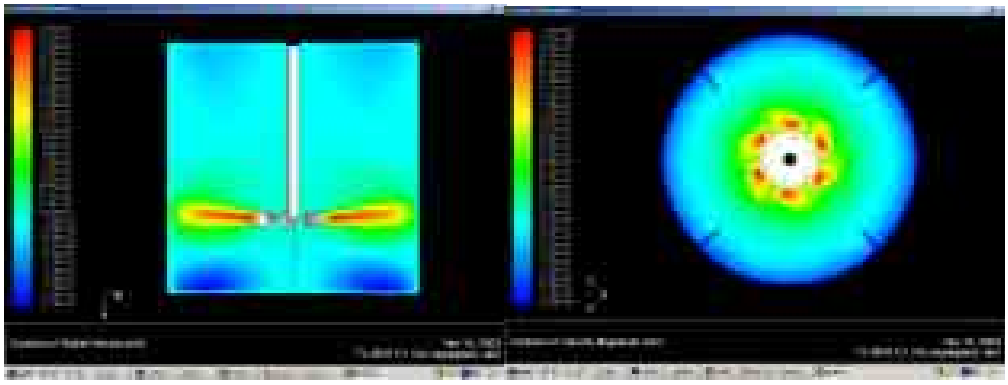

FIG. 18. Simulated velocity field for 5 rps.

The example of homogenization simulation by using detector algorithms and PSR methods for different radionuclides and direct evaluation for conductivity probe is presented in the Fig. 19.

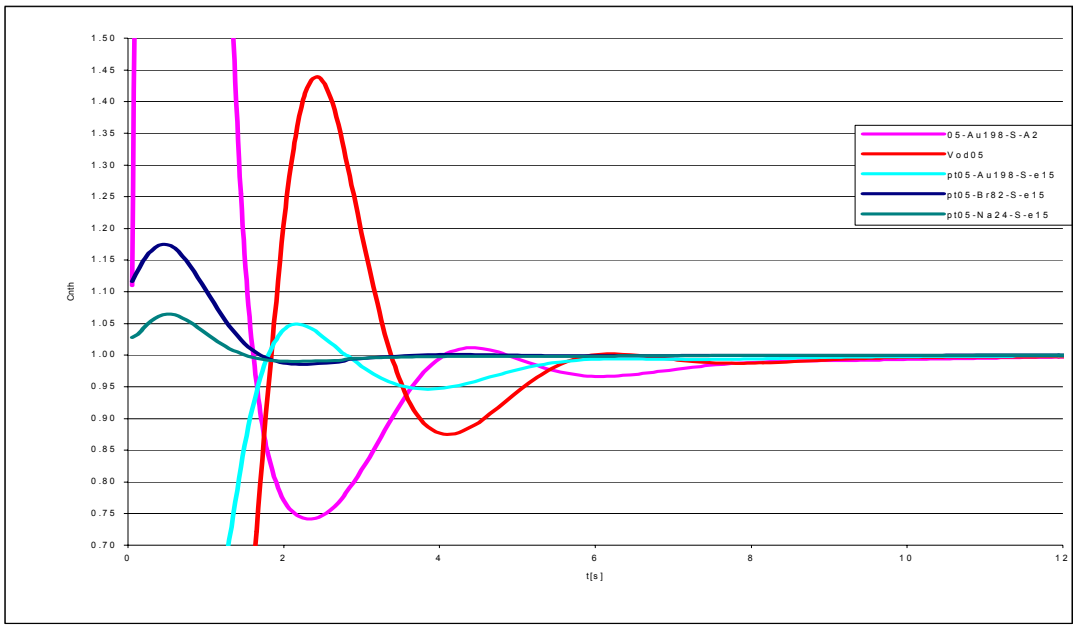

FIG. 19. Simulation of homogenisation measured with conductivity probe and with "central detector with different tracers ^{198}Au, ^{82}Br and ^{24}Na.

From the diagram it follows that longer time of homogenization is measured with conductivity probe (with small measured volume) and then with ^{198}Au, ^{82}Br and ^{24}Na. There is practically the same results for application of algorithm and RSR for ^{198}Au. This tendency was experimentally proved, however there are differences in the values of homogenization time.

Results obtained

- The way of verification of CFD results by RTD measurement was suggested and tested on direct ohmic heater with method of conductivity as well as with radiotracers ;
- The fluid velocity field and numerical RTD calculated by Fluent was received for simple operation conditions of direct ohmic heater (with full electrodes and without heating);
- The special software was prepared for evaluation of the responses in direct ohmic heater with perforated electrodes and acceptable results were obtained for so called cold as well heating conditions;
- The way of verification of CFD results on the basis of local responses (method which use detector algorithms and PSR) ware suggested and required software was prepared, tested and used for experiments evaluation;
- Suggested methods for verification CFD by using algorithm of detectors or PSR in the Ohmic Heat exchanger was used and proper CFD model was found;
- Method of CFD prediction for the time of homogenisation in the mixed vessel was used and results for verification by experiments with conductivity as well with different radiotracers were realised.
- The dependence of the time homogenisation on the detected volume can be predicted by CFD, and supposed tendency between time of homogenisation and measured volume was proved.

4. CONCLUSIONS

- The verification of CFD models by stimulus response method requires numerical simulation of experiment.
- Verification on the basis of RTD can be done easily by simulation of RTD experiment directly by using commercial software Fluent.
- Verification on the basis of measurement of local responses requires post processing of CFD results based either upon specific algorithms of collimated detectors
- The way for optimal configuration of “side” detectors was suggested in procedure for finding proper CFD model for the analysed system.

Both ways of CFD verifications ware tested by the tracer experiments on the model of the ohmic heater. For the proper choice of CFD model on the basis of measurement of local response is recommended to find optimal positions of “wall” detectors which can be found by the analysis of local responses by help of detector transfer function evaluated by algorithms of detector.

REFERENCES

[1] THYN, J., ZITNY, R., et al. "Analysis and diagnostics of Industrial Process by Radiotracers and Radioisotope Sealed Sources" Vol. 1 and Vol. 2, Czech Technical University, *(*CVUT), Prague 2002.

[2] ZITNY, R., THYN,J., "Verification of CFD prediction by Tracer Experiments", 14-th Intern. Conf. CHISA'2000, Prague, Czech Rep. 27–31 August 2000; Czech Society of Chemical Engineering.

[3] ZITNY, R., and THYN, J., "Parallel flow asymmetries due to non-uniform temperatures investigated by tracer techniques" Proceedings of 1st International Congress Tracers and Tracing Methods, Nancy , France, French Society of Chemical Engineering, 29–31 May 2001, 48–52.

[4] THYN, J., ZITNY, R., "Verification of flow model by radiotracer – the models of collimated detectors" (In Czech) , 48th CHISA Conference, Srni, 15–18.October 2001; Czech Society of Chemical Engineering.

[5] THYN, J., NOVY, M., HOUDEK, P., BORROTO PORTELA, G., and ZITNY, R. "Verification of CFD model by Stimulus Response method." 15-th Intern. Conf. CHISA'2002, Prague, Czech Rep., 26–30 August 2002; Czech Society of Chemical Engineering.

[6] TOLA,F., "Ecrin code Monte-Carlo", Report CEA/DTA/DAMRI/SAR/t40, 1996.

[7] TAYLOR,G., "Dispersion of soluble Main Solvent flowing slowly through a Tube"; Proc. Roy Soc. A, 219, (1953) 186–203.

TRACER EXPERIMENTAL TECHNIQUES FOR CFD MODEL VERIFICATION AND VALIDATION IN SUGAR CRYSTALLIZER

J. GRIFFITH[A], J. BORROTO[B], J. DOMINGUEZ[B],
M. DERIVET[A], J. CUESTA[A], P. FLORES[A],
D. FERNÁNDEZ[B], A. AMOR[B], B. FRANKLIN[B]
[a] Department of Nuclear Techniques
Cuban Institute of Sugar Researches, Havana, Cuba
[b] Department of Radiochemistry
Institute of Applied Technologies and Sciences, Havana, Cuba

Abstract

In the framework of the CRP improvement of the experimental design for RTD tests at a pilot crystallizer was performed. A new approach for RTD studies in non-Newtonian fluids for flow patterns characterization at the pilot crystallizer was carried out. Batch mixing process was tested and the homogenization time for massecuite fluid close to seven hours proved that the crystallizers with relative low residence time that the Cuban sugar industry is trying to develop will achieve low exhaustion efficiency with significant sugar losses. The flow simulation was carried out by CFD Flotran in ANSYS 5.4 package. The possibility of RTD prediction on the basis of numerical solution of transport equations for fluid dynamics in a more simplified geometry of the crystallizer and molasses as fluid using transient analysis of temperature pulse spreading is discussed. Finally, taking in account that in complex flow structure, the most general Stimulus Response Method (SRM) based in point source response (PSR) is more suitable for CFD verification than the ambiguous, in some cases, RTD function, the design and preparation of a multipurpose relative long live $^{99}Mo/^{99m}Tc$ point source device has been developed and special PC-program has been prepared for the interpolation of detector responses function.

1. INTRODUCTION

The overall objective of the research work was to introduce CFD simulation along with RTD medalling for investigation of processing operations in sugar industry. The research was developed in two directions:

- Development of basic researches on tracer methodologies for Newtonian viscous and non-Newtonian fluids in a pilot sugar crystallizer. These include RTD and batch macromixing studies of sugar fluids (molasses and masecuittes) in the crystallization.
- Verification of CFD flow simulation with radiotracer RTD and PSR experimental data

It is well known that the Stimulus Response Method (SRM) as a basis for the evaluation of RTD is one of the most important applications of tracer techniques. As it has been stated in the previous CRP, the RTD method is a well-established methodology with almost universal application in many industrial processes, with the main limitation that it is only applicable for linear process [1].

From the other hand, nevertheless that RTD systemic analysis can be used for verification and validation of CFD models, there is still a need to improve RTD formulation and modeling in complex processes. This is the case of sugar continuous crystallizer in which heat and mass transfer are needed in order to reach the proper exhaustion of the mother liquor. This operation is facilitated by the displacement of the massecuite fluid as a dispersed plug flow in the axial direction with complete mixing in the radial one [2].

The situation becomes still more complicated due the high viscosity of the massecuite and its behavior as a non-Newtonian fluid [3].

It has been pointed out that the current state of CFD does not allow the simultaneous prediction of turbulent flow for non-Newtonian fluids because this is at the forefront of numerical non-Newtonian rheology research.

The approach proposed by Griffith [4], the RTD curve normalization by the apparent outlet viscosity to smooth the fluctuations is a still arguable and needs further validation [5]. The only available information at our disposal, concerning the use of CFD for modeling a low-grade sugar crystallizer was the work performed by Sima and Harris [1], but they were forced to make a series of simplifications in order to achieve reliable results.

Taking in account this overall situation, the main objective, as the initial step of the work was to develop and optimize radiotracer experimental RTD technique for CFD model verification and validation at bench scale in a pilot crystallizer.

2. EXPERIMENTAL APPARATUS AND FLUIDS

Pilot crystallizer

A sketch of the pilot crystallizer and geometrical parameters of the mixing system investigated is shown in Figure 1. The unit was designed and constructed very close to the "Blanchard" type exhaustion crystallizer almost common in the majority of raw sugar factory in Cuba. It is a U horizontal half cylinder (*1200×350×270 mm*) divided in three compartments by two vertical baffles. The fluid passes from one compartment to other one by overflow. The impeller is composed by 30 curved blades along the shift (10 for each compartment) disposed with an angle 36° to avoid the formation of stagnant zones. In addition, it is equipped with a water jacket for temperature regulation.

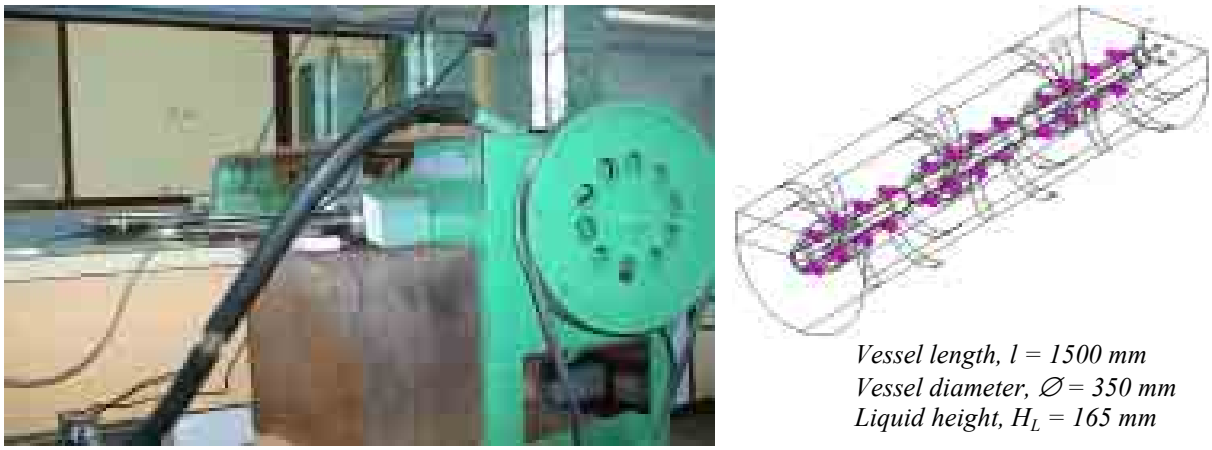

FIG. 1. View and geometrical parameters of the pilot crystallizer.

The baffles were designed also to have a space without agitation for the installation of the viscometer spindle, conductivity cell and other measuring devices. However, after some preliminary test conducted with water, sugar syrups and molasses, it was shown that the installed baffles were an obstacle for the free movement of some part of the fluid entering into the unit and provoking backmixing effect. Then, the initial design of the crystallizer was modified and the installed baffles were removed.

Fluids

Different fluids covering a wide range of viscosities ($1{,}002 < \mu < 3{,}4\times10^5$ mPa·s) were used in tracer tests and numerical simulations. The Newtonian fluids were water, mixture of glucose syrups with various water concentrations, and molasses B and C and the non-Newtonian fluids were mixture of molasses C with increasing content of sugar crystal, and molasses B with different proportions of 3% solution of Carboxyl Methyl Cellulose (CMC). The main rheological characteristics of the fluids are reported in Table I.

TABLE I. FLUID PARAMETERS

Fluids	Crystal content (%)	Brix (%)	Pol (%)	Purity (%)	Density (kg/m^3)	Flow index (n)	Consistency (mPa·s)
Newtonian fluids							
Water	–	–	–	–	998	0	1,002
Glucose syrup	–	69,5	–	–	1344	0,980	262
Molasses B	–	–	50,40	69,7	1316	0,958	918
Molasses C	–	89,5	33,0	36,9	1475	–	43952
Non-Newtonian fluids							
Massecuite I	14,9	88,3	43,0	48,7	1467	–	94889
Massecuite II	26,3	92,4	51,6	53,9	1496	–	112286
Massecuite III	29,9	92,8	56,3	61,1	1499	–	192856
Massecuite IV	42,4	93,1	61,3	65,8	1501	–	343721
Fluid A*	–	54,7	29,3	53,0	–	0,788	359
Fluid B**	–	57,9	32,8	56,0	–	0,845	593

* Molasses B + 3% solution Carboxyl Methyl Cellulose (4:1 w/w)
** Molasses B + 3% solution Carboxyl Methyl Cellulose (3:1 w/w)

The rheological characteristic of fluids were determined employing a programmable rheometer with a properly spindle (*Brookfield*, USA), meanwhile Brix (solid soluble content), Pol (sucrose content by polarization) and purity (ratio of Pol to Brix) were estimated by the standard conventional sugar analysis described elsewhere. Others specifics analysis such as the determination of reducing sugars (%), ash content (%), total polysaccharides (ppm) and starch (ppm) were performed to the molasses B and C following the procedure described in [6].

Tracers

Taking in account that there is not any nuclear installation for the production of short-lived radioisotopes in Cuba, among the commercial radioisotope generators available, two of them ^{99}Mo/^{99m}Tc and ^{113}Sn/^{113m}In were chosen for this work. The validation of the radiotracer tests was performed using in some cases the standard conductivity method with KCl and in others the sampling method.

Detection

Three collimated NaI(Tl) 1”×1” detectors coupled to ratemeters (*Miniken*, Australia) were used. Two of them were placed in fixed positions over the crystallizer or at its wall and the third at the outlet. Signals from each ratemeter were recorded continuously to a PC and the software D.T.S PRO was used for data treatment and modeling [7].

3. RTD STUDIES WITH NEWTONIAN AND NON-NEWTONIAN FLUIDS

Tracer tests with Newtonian fluids

Tracer tests were performed with molasses B as standard for the comparison with non-Newtonian fluids. Several attempts were done to insure the correct response of the outlet detector in order to achieve the real DTR function of the system.

About 1,85 GBq (5 mCi) of ^{113m}In (5 mL of the eluted solution) thoroughly mixed with 5 g of molasses B was suddenly injected at the unit inlet. The rotation speed of the agitation system was fixed to 0,314 rad/s (3 rpm) and the volumetric flow was situated at 3,5 L/min. Samples were periodically drawn out at the outlet of the crystallizer and measured at the APTEC system composed by a well-shielded scintillation NaI (Tl) 2”×2” detector coupled to a multichannel analyser.

In Figure 2, the RTD curves for the "on line" outlet detector D3 and the sampling method are shown. They are quite similar which demonstrated that the response of the outlet well-collimated shielded detector describes correctly the RTD function of the tested fluid within the crystallizer and therefore the pattern flux.

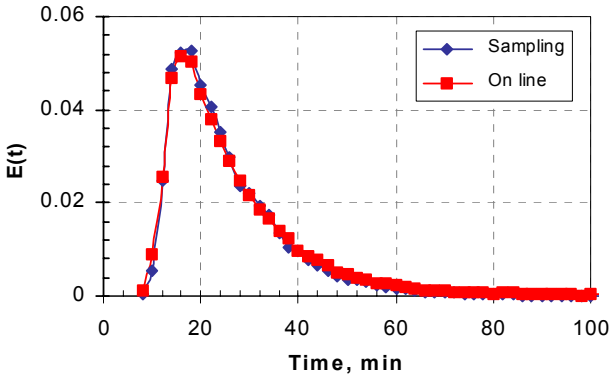

FIG. 2. Comparison of RTD curve by "on line" and sampling methods (molasses B).

The first attempts to fit the tracer response curve to a model of perfect mixing cells in series, as it was achieved early in the previous tests performed before the redesign of the crystallizer, did not succeed. The only way to fit the response curve to a model with a physical meaning was assuming a model of perfect mixing cells with backmixing (PMCB) within the crystallizer (Figure 3).

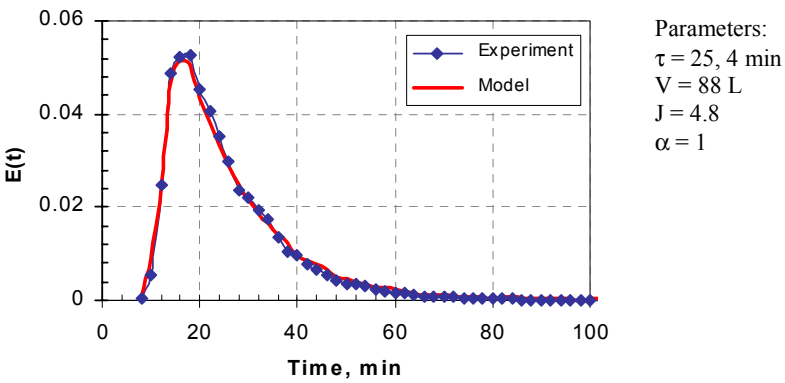

FIG. 3. Fitness of the experimental RTD curve of the Newtonian fluid (molasses B) to PMCB model.

There is really no contradiction between these results and those achieved early. It should be remembered that the response curve obtained at the outlet of the second baffle really described perfect mixing cells in series model due the overflow exit of the fluid. In the redesigned crystallizer measures are performed at the outlet of the unit where the fluid is forced to exit through a narrow gate and not by overflow. From our point of view, it seems logic that a part of the fluid has to recirculate or has to go to a backmixing process before leaving the crystallizer. The back flow rate ratio is high, and taking in account its influence on the number of cells achieved (near to five), we can predict that a good mixing process is taking place within the crystallizer.

Tracer tests with non-Newtonian fluids

Following the approach described in [8], different proportion of a 3% solution of Carboxyl Methyl Cellulose (CMC) was added to the molasses B in order to achieve a non-Newtonian fluid (flow

index less than 1). This procedure provoked the dilution of the original molasses B with the corresponding reduction of the apparent viscosity.

Under similar conditions (flow rate, rpm, and temperature) as mentioned above for pure molasses B a preliminary test was performed employing the Fluid A. In order to validate once more the response of the detector, samples were drawn periodically. Again the RTD curves obtained by both methods are quite similar, and the experimental response curve fits to PMCB model (Figure 4).

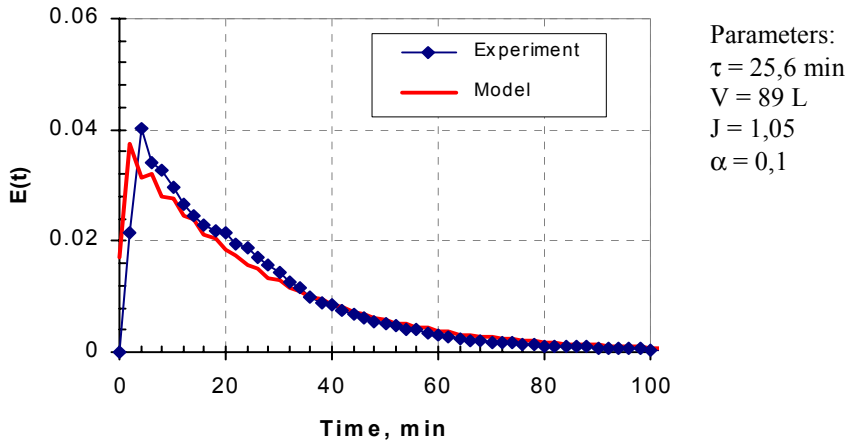

FIG. 4. Fitness of the experimental RTD curve of the non-Newtonian fluid (Fluid A) to PMCB model.

From the RTD analysis can be concluded that the pattern flux adjusts closely to a perfect mixer. This result, in a first approximation was unexpected, taking in account those described above for Newtonian fluids. The great difference between these two categories of fluid was not only in the value of the flow index, but also upon the consistency. For that it was decided to carry out another test with the Fluid B, with composition intermediate between the two extreme fluids (Figure 5).

Again the pattern flux is close to the PMCB model, but at the same time, the number of cells is lower than that obtained for the pure Newtonian molasses B. We should pay attention to the fact that the backflow rate ratio is relatively high ($\alpha = 0{,}8$), indicating that still a high mixing process is taking place in the system.

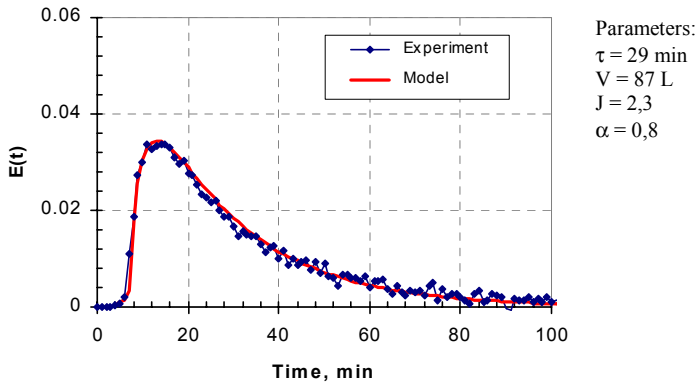

FIG. 5. Fitness of the experimental RTD curve of the non-Newtonian fluid (Fluid B) to PMCB model.

With the aim to clear up this phenomenon, the RTD curves for molasses B (n = 0,952), Fluid A (n = 0,788) and Fluid B (n = 0,845) are plotted in the same graphic for comparison (Figure 6).

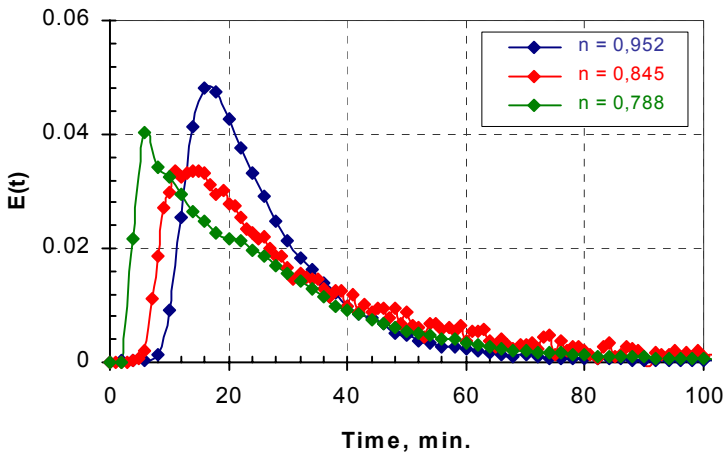

FIG. 6. Influence of flow index n upon the shape of the RTD curve.

These results indicate that with the diminishing of the flow index, and that is to say, when the fluid has more non-Newtonian character, the pattern flow comes more closer to a model that approaches a perfect mixing cells in series reaching nearly a perfect mixer (Figure 7).

In a first approximation it is not easy to give an explanation to this phenomenon, due that with the variation of the flow index also took place the reduction of the consistency and density of these fluids. For Newtonian fluids, changes in the consistency did not had any significant influence on the pattern fluxes achieved in those trials, but for non-Newtonian fluids we are not able for the moment to make the same conclusion. These results represent a new challenge for the CFD specialist in the search of a numerical approach to consider the flow behavior of non-Newtonian fluids.

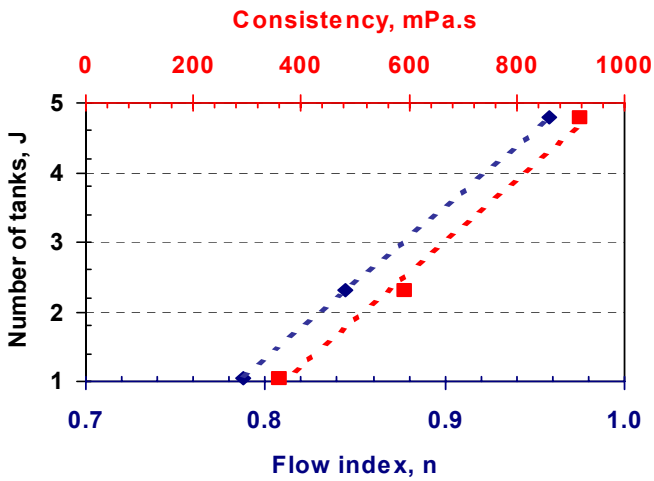

FIG. 7. Variation of the pattern fluxes with the flow index of the fluid.

4. BATCH MACROMIXING STUDIES WITH NON-NEWTONIAN FLUIDS.

In this part of work the attention was focused to the development of the radiotracer technique methodology, necessary to obtain reliable experimental data about the macromixing characteristic at a sugar pilot crystallizer.

Four artificial massecuites (Table 1) were prepared using molasses C as mother syrup. The following procedure was implemented: to the initial volume of molasses C, after each trial, certain calculated quantities of raw sugar with crystal size lower than 2 mm, was added in different position of the crystallizer. The mixture was stirred over the night (almost during 12 hours) and massecuites with increasing crystal content from 15 to 40% were obtained for mixing process experiment. The homogeneity in the preparation was tested, taking samples at different positions of the crystallizer and at different interval, that were after submitted to conventional sugar analysis for their characterization.

^{99m}Tc and ^{113m}In were used in all the tests by *"on line"* method. The detectors were placed in three positions along the axis of the crystallizer (Figure 8).

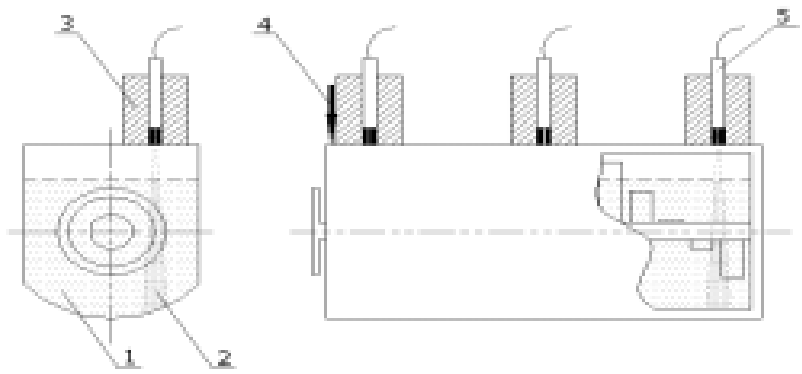

FIG. 8. Geometric arrangement of detectors: 1- fluid; 2- effective volume; 3- detector shielding;
4- injection point; and 5- detectors.

Two different types of collimators were employed for the optimization of the detection method: the so-called one-hole collimator (Figure 9) and multiple-holes collimator (Figure 10).

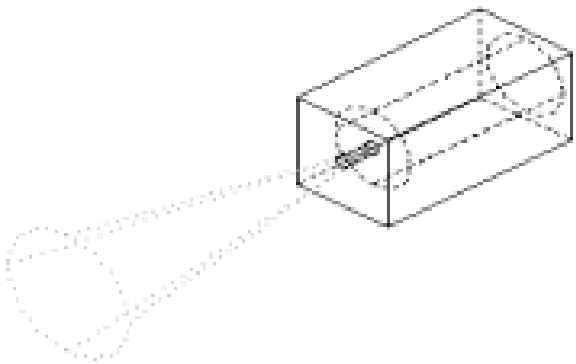

FIG. 9. One-hole collimator. Diameter: 3.6 mm. Effective volume: 4 L.

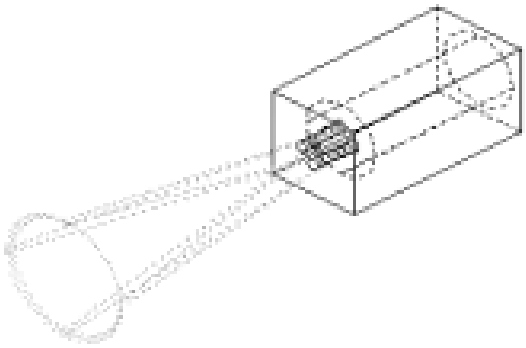

FIG. 10. Multiple-holes collimator: Effective diameter: 3.6 mm Inclination angle 10^0 Effective volume:10L.

The effective detection volume (V) was calculated through the equation $V = \xi \cdot d^2 \cdot h$. It was assumed that the probe only detects radiation coming from the fraction of the total volume delimited by the collimator visual field. For the one-hole collimator this fraction is calculated as the volume of a truncated cone [9].

Determination of homogenization time

Four series of experiments were performed for the determination of the homogenization times (t_{hom}). As criterion for the estimation of the homogenization time, a value of mixing index $I_m = \sigma^2(t)/\sigma^2(0) = e^{-\beta \cdot t} = 0{,}02$ was assumed. This value corresponds to 0,01% of the initial activity.

Figure 11 shows the plot of the normalized activity as a function of time for one-hole and multiple-hole collimators. In contrast with low viscous fluid, in this case, practically no oscillations of the normalized activity were observed. This result is not unexpected, the nature of the high viscous fluid attenuates these oscillations, that are a result of the effect that take place when, periodically, the tracer come closer and step faraway from the vision angle of the collimated detector during mixing.

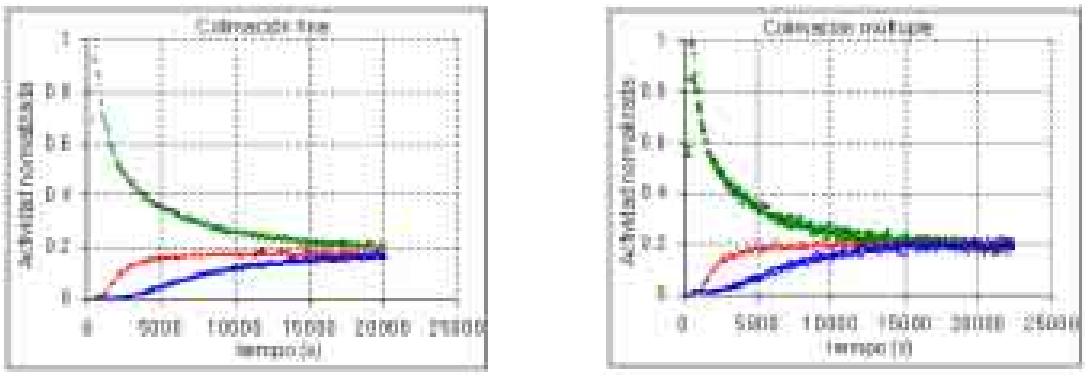

FIG. 11. Response curve of each detector after ^{99m}Tc injection: A one hole collimator,B multiple holes collimator, ▲ Detector 1 ■ Detector 2 ● Detector 3.

Table 2 resumes the results related to homogenization time, mixing rate number and Reynolds number for all the sugar fluids under study In order to establish the correspondent relationship with these parameters, values of apparent viscosity and crystal content are also reflected in this table.

TABLE II. MACROMIXING CHARACTERISTIC OF SUGAR FLUID AT DIFFERENT HOMOGENIZATION TIME

Fluids	Homogenization time t_{hom} (s)	Index rate number, N_{mez}	Crystal content (%)	Viscosity (mPa·s)
Molasses C	14400	720	0	43952
Massecuite I	18030	902	15,0	94889
Massecuite II	18720	936	26,3	112286
Massecuite III	20670	1034	29,9	192856
Massecuite IV	25530	1277	42,4	343721

From this table, could be concluded that the homogenization time (and the index number) increases with the crystal content increment. Similar results were reached by Bohacenko and Font [10] about the influence of crystal content in glucose massecuite during mixing in a pilot crystallizer. These results show that the crystal content that normally are encountered at massecuite C in the sugar industry (30 to 40%), the homogenization times are higher than the residence time at several industrial crystallizers [4]. This fact undoubtedly would have a negative influence in the "exhaustion" process of these massecuites and therefore more losses of sugar will be achieved.

5. CFD SIMULATION AND RTD PREDICTION

Because of the complexities of the problem, our first goals were becoming familiarized which the available CFD codes and achieving numerical calculations of the velocity fields for a substantially simplified configuration of the crystallizer (variant A): flow of Newtonian uncompressible fluid through the vessel of the unit without agitator. CFD Flotran developed in ANSYS 5.4 package was chosen to solve the Navier-Stokes equations in three dimensions.

First, the flow in the vessel of the crystallizer was simulated for a wide range of Reynolds number (from 5×10^4 to 10^6) with three-dimensional tetragonal grid. The influence of mesh size and shape was also investigated. Computed velocities were found to be in very good agreement with theoretical and experimental results. This gave us some confidence in the ability of the Flotran code to reproduce the hydrodynamics inside the vessel.

The next step was the incorporation of the geometry of the Blanchard agitator (variant B) to the computational domain to take into account the perturbation of the velocity field induced by the impellers. Others modeling options, available in the code as the *"Rotating Reference Frame"* were tested (Figure 12).

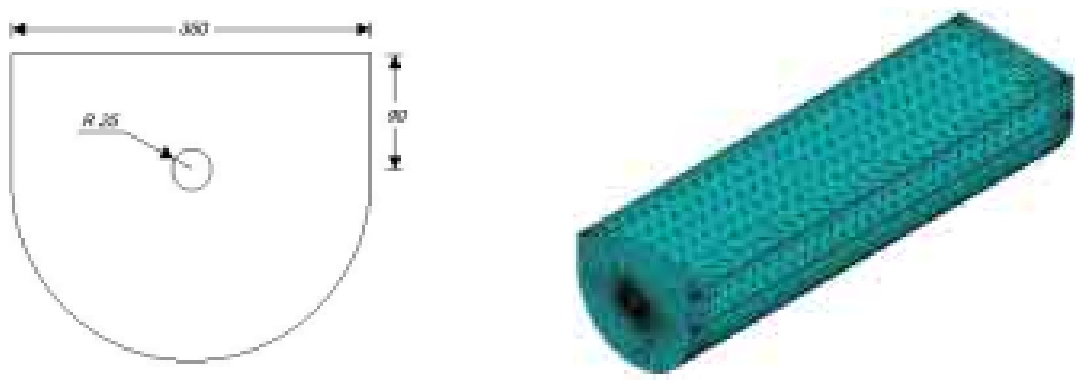

FIG. 12. Geometry and unstructured meshing used in the numerical calculations (variant B).

Again the flow field was computed by Flotran for a constant velocity of the fluid (u_B = 0,05 m/s) and the mean residence time τ = V/Q = 25,14 min. A fluid with a density ρ = 1475 kg/m^3 and viscosity μ = 47 Pa·s was used in the numerical experiments. The rotating velocity of the impellers was 0,314 rad/s (3 rpm). The numerical computations were done under the assumption of laminar and turbulent flow using the RNG k-ε model. The boundary conditions at the agitator and at the vessel walls were those derived assuming no-slip conditions. At the free surface, the boundary conditions were set assuming that there is no normal velocity and the normal gradients are zero for all variables. The results are presented in figures 13.

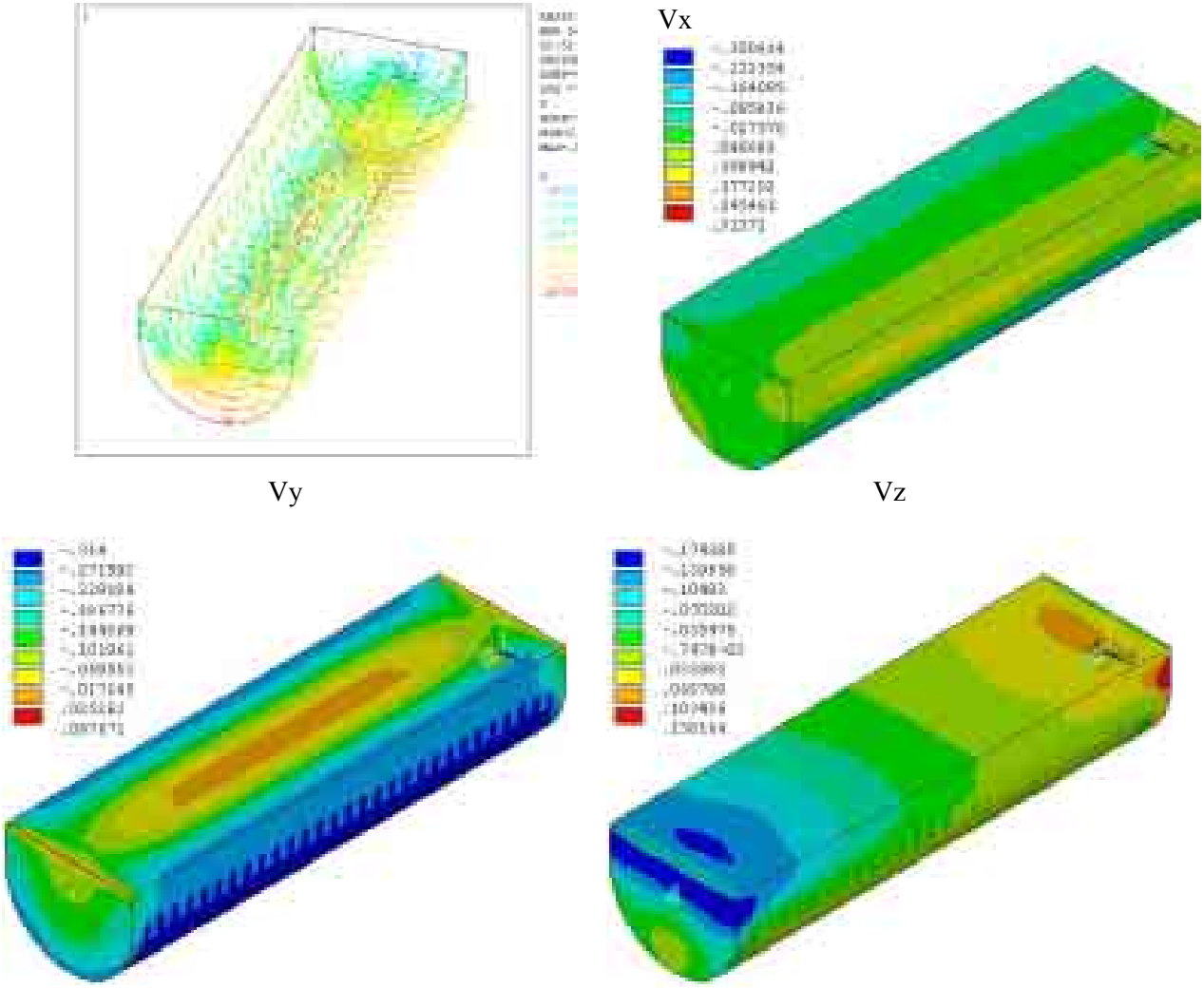

FIG. 13. Velocity vectors and contours of velocity magnitude in Vx, Vy and Vz.

There are several possibilities to predict RTD from velocity field. The standard procedure offered by FLOTRAN is based upon particles tracking. However this method can not be recommended because it is very difficult to avoid particles trapping in recirculating regions and the resulting integral RTD function is distorted appreciably especially for long times.

A much better, though more time spending procedure, is based upon modeling of transient temperature field, setting a short δ-Dirac pulse $(T = T_0\ \delta\,(x_0, y_0, z_0, t_0))$ at the inlet of the unit so that the mean calorimetric temperature monitored at the outlet can be considered impulse response E(t). In this case, the results of the RTD evaluation from temperature field are affected by molecular diffusion even when the walls of the unit are thermally isolated. For this purpose, a value of thermal

conductivity was fixed at 0,01 W/m·K and no variation of other fluid parameters as a function of temperature was assumed.

The progress of the simulation are presented in figure 14:

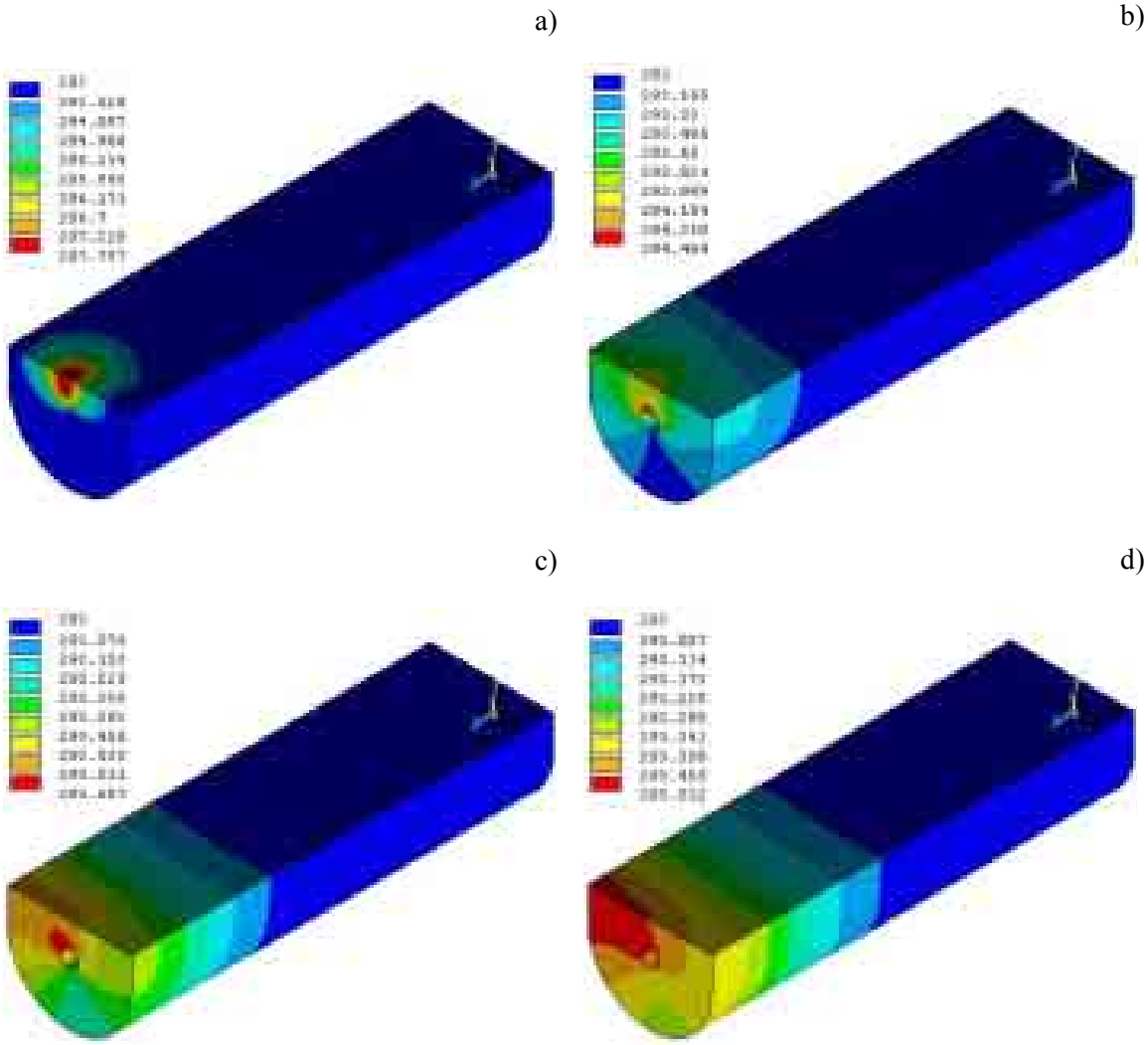

FIG. 14. Temperature distribution after: a) 1 min, b) 3 min, c) 7 min and d) 10 min.

The results of RTD evaluation by CFD for laminar and turbulent RNG k-ε models are show in Figure 15 and in Table III the parameters of the distribution: mean and variance of residence time.

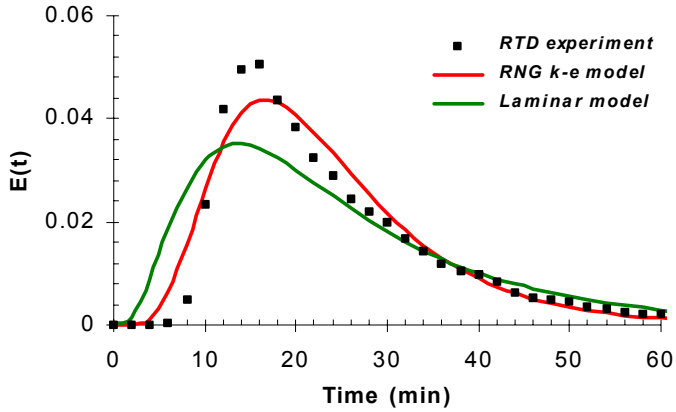

FIG. 15. Comparison of RTD from tracer experiment with ^{113m}In and RTD evaluated by model for laminar flow model and RNG k-ε turbulent model.

TABLE III. COMPARISON OF EXPERIMENTAL RTD WITH RTD CALCULATED BY CFD MODELS

CFD model	Flow rate, L/min	Time step, min	τ, min	σ^2	$\frac{\sum\lvert E_i - E_{exp}\rvert}{n}$
Laminar model	3,5	0,2	25,3	279,8	$2{,}58\times10^{-3}$
RNG k-ε model			23,5	139,1	$1{,}43\times10^{-3}$
Experiment	3,5	2	24,9	200,4	

The RTD calculated for a turbulent flow using the *k-ε* model seems to approach better to the reality; however, it still does not reach totally the experimental RTD. Then, other factors have to be taking in account during the simulation; however, these results demonstrate that the hydrodynamics of the crystallizer could be reproduced.

6. IMPROVEMENT OF POINT SOURCE RESPONSE (PSR) APPROACH

It has been demonstrated [11] that for complex flow structure, the most general Stimulus Response Method (SRM) based in Point Source Response (PSR) approach is more suitable for CFD verification than the ambiguous, in some cases, RTD function.

As a first step to improve this approach to the case of sugar crystallizer, preliminary tests in simple standard system were carried out in order to obtain data for preparing the spatial software for interpolation of detector responses and testing the algorithms suggested by the Czech team.

For this purpose an experiment in a rectangular glass vessel (*360×260×250 mm*) filled with water was conducted. Two one hole collimated NaI (Tl) detectors were placed at the walls of the vessel and a rack with 11×7 holes was used to allow the movement of the source through fixed positions in front of detectors (Figure 16) and Table IV.

FIG. 16. Installation for the PSR testing.

TABLE IV. POINT SOURCE RESPONSE TEST

Positions of detectors and collimation geometry

DETECTOR	Position			Collimation	
	X [mm]	Y [mm]	Z [mm]	∅ [mm]	d* [mm]
D1	0	120	130	10	10
D2	180	120	0	10	10

* focal length

Standard procedure for the preparation of ^{99m}Tc point source

^{99m}Tc is usually used for RTD measurement in crystallization and others sugar processes, but due its relatively short half life (6,02 h) is difficult to prepare an appropriate long in time point source for local response measurement. Taking in account this fact it was decided to use its parent isotope ^{99}Mo with a larger half-life (66 h).

As a result of the dynamic equilibrium between ^{99}Mo - ^{99}Tc the point source enlarge it useful utilization in more than 10 time. The scheme of point source is shown in Figure 17:

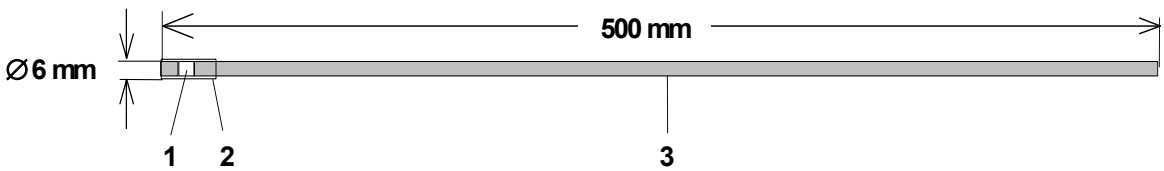

FIG. 17. Scheme of the point source: 1- ^{99}Mo adsorbed on alumina in equilibrium with ^{99m}Tc, 2- capsule of low-density polyethylene and 3- rod of plexiglas with scale.

The column of a ^{99}Mo/^{99m}Tc generator containing ^{99}Mo molibdate adsorbed on alumina (with a week of decay), is carefully removed. About 10 mg of the alumina was put in a vacuum micro-filtration unit with a 0,45 µm Millipore membrane, three time washed with 10 ml of deionized water to eliminate the residual eluting solution and dried under infrared lamp. A fraction of about 1mg of the alumina was carefully weighted in an analytical balance and put into the polyethylene capsule. The rod of plexiglas was then adjusted so that the alumina was confined in the lower volume inside the

capsule. The external surface of the source was washed with 0,1 mol/L EDTA and detergent solution 1:1 v/v and the hermetic was checked by immersion in water during 10 minutes (no count rate over background was obtained).

This point source has the following advantages:

- its half life is in one order of magnitude higher, then the errors introduced by the ^{99m}Tc decay are lower,
- the use of a solid matrix increase the hermetic of the source,
- the source could be renewed and used in multiple experiments.

Software for D(x,y,z) interpolation

To interpolate the responses *D(x,y,z)* obtained with the point source to the nodal points of the grid, Zitny and Thyn [2] have suggested to calculate distance $l_1, l_2, \ldots, l_8$ between the point *x,y,z* and the nodal points and to estimate the response *D* in *x,y,z* through the formula:

$$D(x,y,z) = \frac{\sum_{i=1}^{8} \frac{D_i}{l_i^m}}{\sum_{i=1}^{8} \frac{1}{l_i^m}}$$

where $D_1, D_2, \ldots, D_8$ are the responses at the nodal point of the finite element and the exponent *m* has been identified with the dimension of space (1, 2, or 3).

The algorithm for interpolation was programmed in DELPHI 5.5. The software architecture (Figure 18) allows the manual or automatic (from an Excel file) introduction of the response matrix at the nodal points of the finite element. The software calculates automatically the distance between the points and interpolate the response to any point of *x,y,z* co-ordinates.

FIG. 18. Window of the program.

As there are great differences between the density of measured point responses and density of mesh used in CFD simulation, the interpolation equation was tested for two different functions *c(x,y,z)* defined in the unit cube: normal Gaussian distribution and exponential decay (Figure 19).

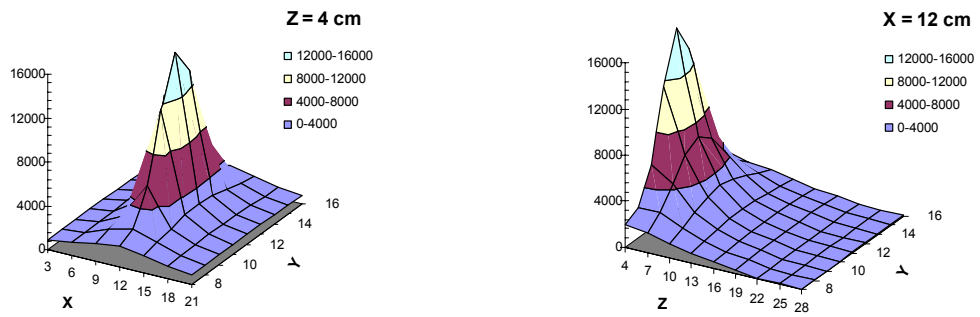

FIG. 19. Responses D(x,y) and D(y,z) of the detector D1. The response D(x,y) corresponds to a normal Gaussian distribution and the responses D(y,z) to an exponential decay.

It was shown that the optimum exponent *m* depends upon the form of function and on the number of nodal points (grid 3×3×1 cm gave smallest values of m, 1694 was maximum number of tested nodes). Most of *m* results were within the range 2 to 3. The relative error was acceptable, typically 2 to 5 percent when optimum *m* is selected for interpolation. Generally speaking, it is more reliable to use the higher values of exponent ($m = 3$), especially when the number of interpolation points is high.

Testing the PSR method in the pilot crystallizer

The second experiment was conducted in the crystallizer. Again two one-hole collimated NaI(Tl) detectors were placed at fixed positions in the lateral sides of the crystallizer filled with water and molasses B and the responses to the ^{99m}Tc point source were achieved (Figures 20 and 21).

The attenuation of radiation depends on the nature (density and chemical composition) of the fluid and materials. However in this case, although a significant difference in the count rates among the fluids was observed, after the normalization an acceptable similarity in the shape of D(x,y,z) responses is observed for both detectors. This fact may be explained because in this case the main type of γ photon interactions to be considered is the Compton effect. The effective atomic number ($\overline{Z/A}$) of the water and molasses are closer then the mass attenuation coefficient of both fluids must be similar too.

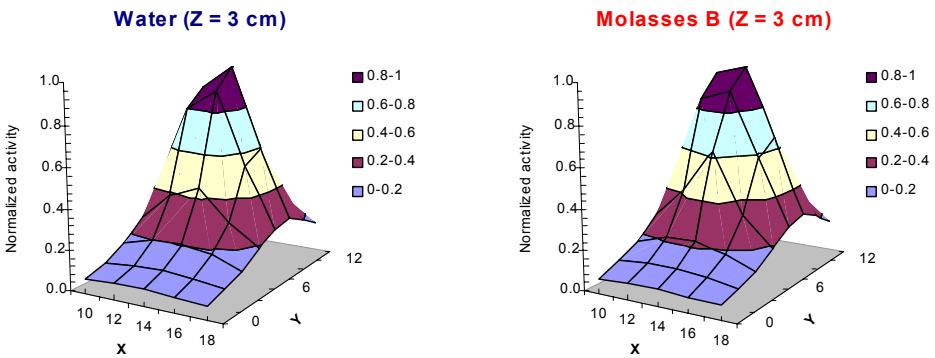

FIG. 20. Normalized responses D(x,y) of the detector D1 in the crystallizer.

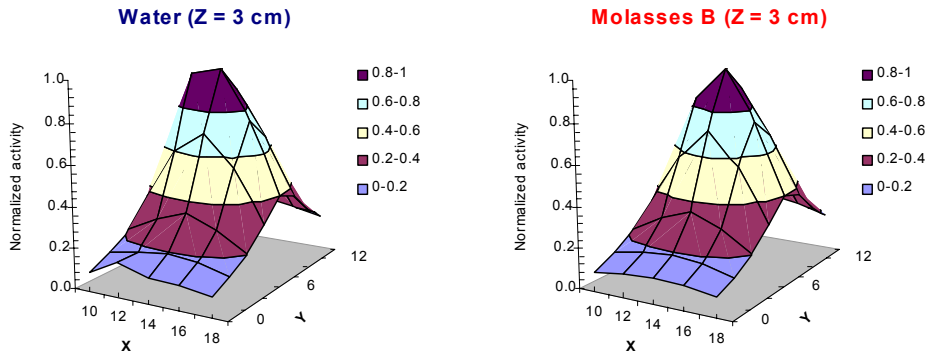

FIG. 21. Normalized responses D(x,y) of the detector D2 in the crystallizer.

Then, for the practice purposes is possible to use the normalized detector responses obtained with each fluid indistinctly.

7. CONCLUSIONS

The pattern flux of Newtonian fluids in Blanchard type exhaustion crystallizers fixes to a perfect mixing cells with backmixing model. However, with the decrease of the flow index (i.e. when the hydrodynamic behavior of the fluid is closer to non-Newtonian) there is markedly change on the RTD shape, the RTD fix better to a perfect mixing cell model ($J \rightarrow 1$ and $\alpha \rightarrow 0$). Nevertheless, further test should be carried out, to corroborate this statement taking in account that non-Newtonian tends to be the rule rather than the exception in the food industry. These results represent a new challenge for the CFD code specialist in the search of a numerical approach to consider the flow behavior of non-Newtonian fluids.

Concerning the batch macromixing studies it was found that the increment of the crystal content in the massecuites conduct to an increases of the homogenization time. Then, for the massecuite C normally encountered in sugar factory (with a crystal content from 30 to 40%) the homogenization time will be greater than the residence time of the operating crystallizers. Undoubtedly this fact would have a negative influence in the “exhaustion” process of these massecuites and therefore more losses of sugar will be achieved.

Finally, it was demonstrated that the verification of CFD models by stimulus-response requires numerical simulation of the experiment. The confirmation on the basis of RTD can be done "easily" by prediction of the RTD. The Flotran code in ANSYS 5.4 package, to the same as other commercial and popular codes (i.e, FLUENT, CASTEM2000, etc.), has demonstrated its ability to predict the RTD by means of the generation of a temperature impulse at the inlet of the system. However, confirmation on the basis of local responses requires post processing of CFD results based in detector point source responses which is a very time consuming practice.

Nevertheless, in the framework of this work, a new procedure for preparation of a ^{99m}Tc-point source based on the equilibrium with its parent radioisotope 99Mo was achieved. The use of a solid matrix and the possibility of renewing and using this source in multiple experiments simplify the task. In addition, a software for the interpolation of the D(x,y,z) responses using the algorithm suggested in this CRP was programmed

REFERENCES

[1] SIMA, M.A., HARRIS, J.A., Modelling of a low grade vertical cooling crystallizer using computational fluid dynamics, Proc. Aust. Soc. Sugar Cane Technol. 19 (1997) 448–455.

[2] THYN, J., ZITNY, R., "Stimulus response methods and computer fluid dynamics, our experiences and objectives", first Research Coordination Meeting of the CRP on "Integration of RTD tracing with CFD simulation for industrial process visualisation and optimisation", Technical Report, IAEA, Vienna, 7–11 May 2001.

[3] ZDZISLAW, J., JAN, D., CFD modelling of turbulent macromixing in stirred tanks. Effect of the probe size and number on mixing indices, in: European Symposium on Computer Aided Process Engineering, Bragge, May 24–27, 1998

[4] GRIFFITH, J., Formulation of flow model in low-grade massecuite fluids in sugar crystallization process, in: Tracer and Tracing Methods 79 (2001) 539–566.

[5] SHIUE, S.J., WONG, C.W. Studies on homogenization efficiency of various agitators in liquid blending, Can. J. Chem. Eng. 62 (1984) 602–609.

[6] MINAZ, Manual of analytical methods for quality control of sugar. Technical standard, Havana, 1995.

[7] Software “D.T.S. PRO v.4.2”, Instruction Manual, PROGEPI, Laboratory of chemical Engineering, Nancy, France, January 2000.

[8] MCBAIN, G.D, HARRIS, J.A, LEONG, Y.K, VIGH, S. Viscoelastic characterization of low-grade molasses by jet-swell measurements, Proc. Aust. Soc. Sugar Cane Technol. 22 (2000) 467–473.

[9] THÝN, J., Effect of the measured volume size on the homogenization time, J. Chem. Eng. 12 (1976) 211–217.

[10] BOHACENKO, I., FONT, I., Study of glucose massecuite mixing, Scientific paper of the Prague Institute of Chemical Technology E 50 Food, 1979.

[11] ZITNÝ, R., THÝN, J., Verification of CFD models by Stimulus Response Method, International Conference CHISA-2002, Prague, 28–31 August (2002), Czech Society of Chemical Engineering.

SIMULATION OF A RADIOTRACER EXPERIMENT BY FLOW AND DETECTION CHAIN MODELLING: A FIRST STEP TOWARDS BETTER INTERPRETATION

P. BERNE
DRT/DTEN/SAT,
CEA – Grenoble, France

Abstract

This document presents the work done by the French team in the framework of the IAEA Research Coordination Programme. A "thought experiment", consisting in an ideal γ-emitting tracer injection in laminar backward-facing step flow, was modelled. This included calculation of the flow and concentration fields by CFD, and calculation of detector response thanks to a Monte-Carlo code. The objective was twofold: show the influence of tracer energy on detector response in flow with a recirculation; set the foundations for (hopefully) better interpretation of data from a radioactive tracer experiment. The results are consistent with expectations. An attempt is made at determining the characteristics of the internal flow by exploiting the calculated tracer response curves with the usual tools for tracer data analysis. Limited success is achieved which shows the need for more work to reach the prescribed goal. A few proposals are made for improving the data treatment procedure.

1. INTRODUCTION

The concept of Residence Time Distribution (RTD) is a useful and well established one for the characterization of flow systems (Levenspiel [1], Villermaux [2], Schweich [3]). Among the various available tracers, labeling with gamma-emitting radionuclides offer several advantages (specificity, low detection limit, "see-through" capability) and the necessary tools for RTD measurement and analysis by radiotracer are now available (IAEA [4], Thyn et al. [5], [6]). Standard practice requires one detector at the inlet of the system and one at the outlet as shown on Fig. 1 top. For simple flow in the inlet and outlet channels of the system, usually one-dimensional pipe flow, the signals from the detectors are quite unambiguous. However, the system appears truly like a "black box", with the unhappy consequence that several different flow patterns may account for the same resulting RTD curve.

The radiotracer practitioner is therefore often tempted to locate a few more detectors on the system itself, in the hope of collecting useful information on the local age of the fluids (Thyn et al. [5]). And at this point he is apt to run into another sort of trouble: one feels that the signal from these detectors bears some relation with flow pattern and fluid velocity, but this relationship is often not a simple one, especially in the case of non-one-dimensional flow. This is all the more true since gamma ray measurement is not local, but rather volume-averaged with a complicated distance dependent weighting function. For example, how should the signal be interpreted if there is steep flow gradient, or even flow reversal, within the detection volume (see Fig. 1 bottom)? Obviously, the answer also depends on the properties of the tracer: a low energy tracer will mainly "see" the reverse flow, while at higher energy it may be possible to probe also into the main flow, as illustrated in Thyn et al. [5].

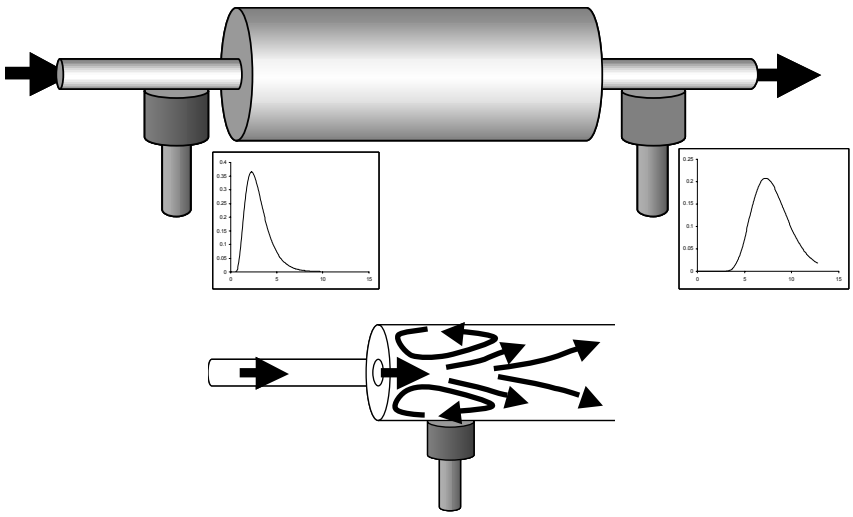

FIG. 1. *Two different situations in work with radiotracers Top: The classical configuration Bottom: A wall detector in complex flow.*

The objective of this work is to explore the relationship between the characteristics of flow and the measurements with radiotracers, using jointly Computational Fluid Dynamics (CFD) and detection chain modeling. The basic idea is to choose a reasonably complex flow configuration, simulate both the flow field and the development of the tracer plume with CFD, and couple the results with a model for the detector so as to predict the count rate as a function of time and detector position. The idea is not a novel one and has been expounded for instance by Linden et al. [7] for the interpretation of flow rate measurements in pipes by pulsed-neutron activation.

In this manner, we hope to obtain better understanding of the link between local flow conditions and signal from the tracer, and also on the influence of the parameters of the radiotracer experiment (mainly tracer energy, in the present work) on the measured tracer response. Referring to Fig. 2, this amounts to solving the "direct" problem (predict the output of a tracer experiment knowing the flow conditions). Lastly, we shall make an attempt at the more difficult "inverse" problem (see Fig. 2 again) by applying the usual tools for the analysis of tracer experiments to our synthetic data, further emulating Linden et al. in the treatment of their own flow problem.

• "Direct problem":

model flow field

model detection system

predict output from tracer experiment

• "Inverse problem":

determine flow field from results of tracer experiment

FIG. 2. "Direct" versus "inverse" problem.

2. METHODS

The basic relationship that will allow the calculation of count rate from a detector can be established in the following way: suppose a point source of unit activity is set at some point $M(x,y,z)$ within a system (Fig. 3).

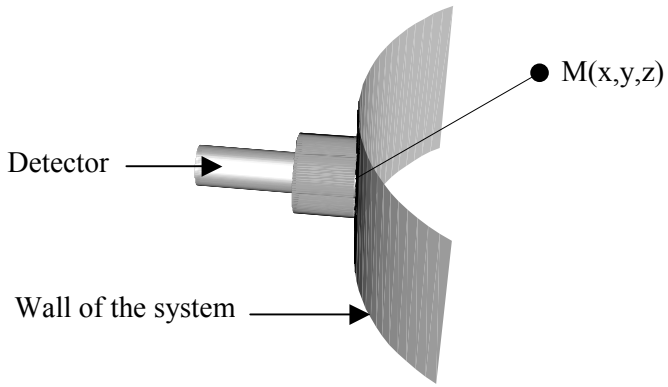

FIG. 3. Point source within the system.

Let $T(x,y,z)$ be the count rate generated in the detector by the source (in counts per second per Becquerel) when it is located at $M(x,y,z)$. The $T(x,y,z)$ functional is known as the "Point Source Response" (PSR - see for example Thyn and Zitny [8]). Some radioactive tracer with the same characteristics as the point source is now injected in the system, resulting in transient volumetric activity field $a(x,y,z,t)$ (in Becquerels per cubic metre). The instantaneous count rate, $\dot{n}(t)$, due to $a(x,y,z,t)$ is equal to the sum of the contributions from each point in space, weighted by functional $T(x,y,z)$:

$$\dot{n}(t) = \iiint a(x,y,z,t)T(x,y,z)dV \qquad (1)$$

This straightforward equation clearly delineates the steps towards predicting $\dot{n}(t)$:

- Solve the flow field and calculate $a(x,y,z,t)$
- Calculate $T(x,y,z)$
- Evaluate integral (1).

This technique has already been used by Thyn and Zitny [8] and applied to the verification of CFD results by radiotracer experiments in a complex system.

The very first stage obviously consists in selecting a case study. We want to select the simplest possible configuration that can yield multidimensional flow, a good candidate being the backward-facing step flow. Our case is inspired by the experimental work of Ruck and Makiola [9], who reported a well-documented study on air flow at large Reynolds number in a plane, with a 2D backward facing step, using two different types of particles as a tracers, as shown by Fig. 4.

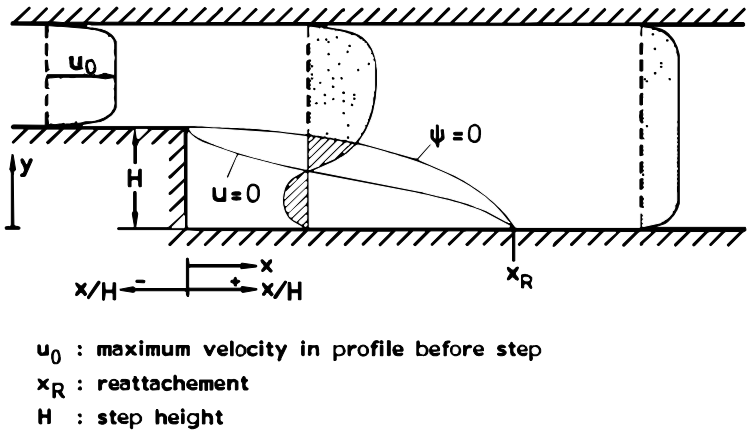

FIG. 4. Experimental configuration studied by Ruck and Makiola as described in their paper [9].

More precisely, we choose to keep the geometry from their work: a two-dimensional system with the same height for the inlet channel and the step. We also choose to solve the problem with non-dimensional quantities, therefore making the solution as "fluid-independent" as possible. The height of the step, H, is chosen as the unit length, the only remaining parameters being the Reynolds number and a non-dimensional diffusion coefficient, comparable to the inverse of the Schmidt number. These two quantities are defined by:

$$Re = \frac{UH}{\nu} \tag{2}$$

$$Sc = \frac{\nu}{D} \tag{3}$$

where U is the mean velocity at system inlet, ν the kinematic viscosity of the fluid and D the molecular diffusion coefficient of the tracer.

Two cases are investigated: a laminar case with a Reynolds number of 10^2 and a turbulent one with a Reynolds number of 10^5. The Schmidt number poses a specific problem in the sense that it does depend on the nature of the fluid and the tracer: typical values for a tracer in air and in water would be respectively 1 and 10^3. Even though we shall explicitly deal with water (see next section), we shall use a Schmidt number of 1, for three different reasons:

- First of all, the value of the Schmidt number is of little importance in the *turbulent* case, because turbulent diffusion is larger by several orders of magnitude than molecular diffusion, as shown in section 3.1.

- To make our point (tracer experiments in complex flows are difficult to interpret, data from tracers with different energies is useful), we need some amount of exchange between main flow and recirculation: in the opposite case, characteristic times will be quite different and the signals from both streams will be easy to separate. Choosing a Schmidt number of 1 allows to achieve that particular aim in the *laminar* case since it results in a dimensionless diffusion coefficient D equal to $1/Re$, hence 10^{-2} and a diffusion length (calculated as $\sqrt{Dt_{max}}$, where t_{max} is the dimensionless time needed for the tracer wave to disappear, about 100 as shown by Figure 9a) of 1, i.e. equal to the height of the step.

- Another (less honourable) consideration is the capability of the CFD code to handle high Schmidt numbers. This point is discussed further in the next section, additional details are also given in Appendix 1.

Choosing the value of viscosity ν and the value of H at some later stage will completely define the *dimensional* velocity and concentration fields.

The tools that we have adopted for this task are the CFD code *TRIO-VF*, a simple but effective finite volume programme (Villand [10]) and the Monte-Carlo software for radiation/matter interaction modelling *Inspect* (Tola [11]).

3. RESULTS

Flow field

The flow domain is shown on Fig. 5. Uniform unit velocity is imposed at the inlet, uniform zero pressure at the outlet. The length of the domain is large enough to allow development and reattachment of a recirculation.

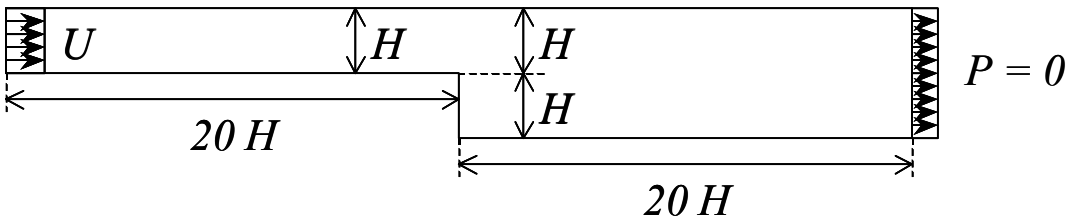

FIG. 5. Computational flow domain.

Once convergence of the flow calculation is attained, a uniform unit concentration is imposed at the inlet, for a duration of one time unit. The injected tracer is supposed to be passive, meaning that it does not affect the velocity field in the fluid.

The mesh comprises 1000 × 50 square mesh cells, 0.04 H by 0.04 H in dimensions in the laminar case. A coarser mesh (400 × 20 mesh cells, 0.1 H by 0.1 H in size) has been used in the turbulent one (it was found that instabilities appeared and could not be managed with the finer grid). The TRIO-VF code uses a finite volume formulation; flow and concentration fields are calculated with an explicit time scheme. A second-order scheme is used for concentration transport. In the turbulent case, the classical k-ε model is used.

With a Schmidt number of 1, the cell Péclet number (defined as $Pe = \frac{U\Delta x}{D}$, where Δx is the size of the mesh cells) is limited to 4, which results in negligible numerical diffusion. Numerical tests indicate that the second-order scheme could safely handle cell Péclet numbers up to 40, i.e. corresponding to a Schmidt number of 10 in our conditions. Beyond that value, numerical oscillations appear.

The resulting velocity fields are shown on Fig. 6a and 6b. In the laminar case, parabolic velocity profiles plausibly develop in the inlet and outlet channel. As expected, recirculation is visible downstream of the step. In the turbulent case, inlet and outlet velocity profiles are, correctly, predicted to be almost flat. The extension of the recirculation is larger than in the laminar case, though not quite as large as reported in experimental work ($6H$ in our computations instead of about $8H$ in experiments). No particular effort has been made to validate these results against experimental data: our objective being to have a reasonably realistic and detailed flow field if not an exact one.

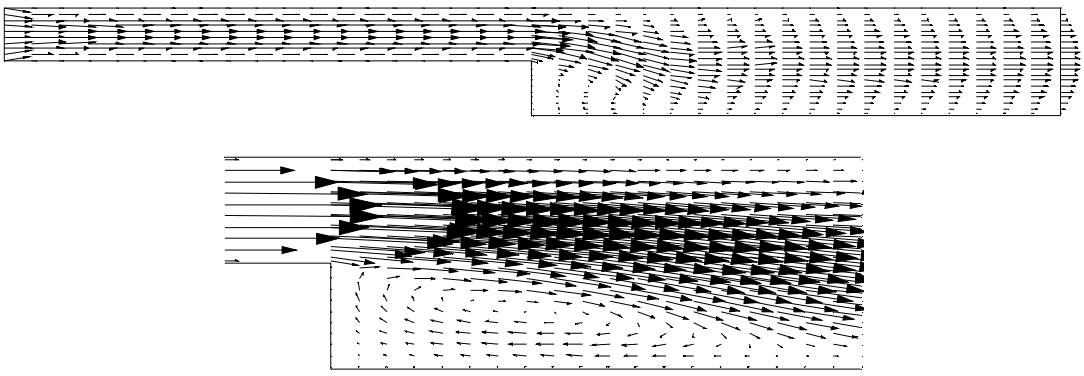

a)

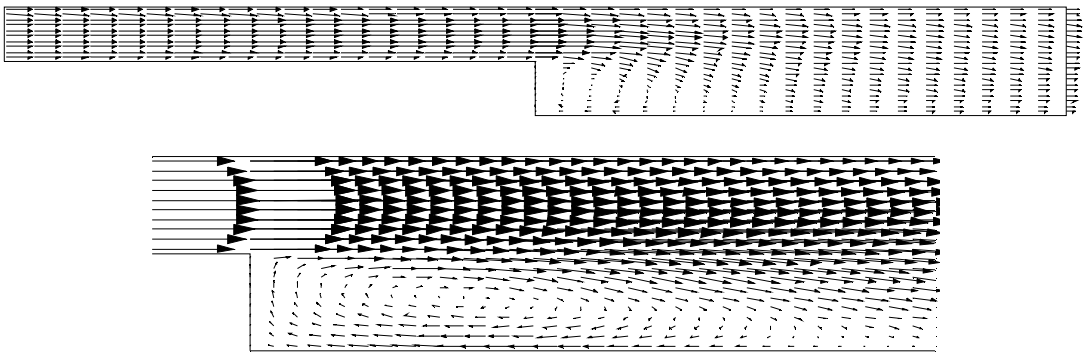

b)

FIG. 6. Flow field (a: laminar case – b: turbulent case).

The calculated field of turbulent diffusion coefficient, D_t, is shown on Fig. 7. D_t is always found to be at least ten times larger than the molecular kinematic viscosity and hence (since the Schmidt number has again been set to 1) than the molecular diffusion coefficient. In this case, molecular effects are indeed found to have no effect on the dispersion of tracer.

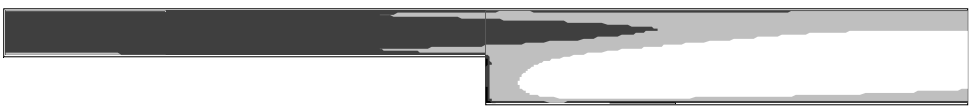

FIG. 7. Calculated turbulent diffusion coefficient
(Grey level code: black, $D_t > 10\nu$*, grey,* $D_t > 10^2\nu$*, white,* $D_t > 10^3\nu$*).*

The concentration fields (Fig. 8a and b) on the whole correspond to expectations: most of the tracer is entrained by the main flow, a small part of it being however "trapped" in the recirculation and released gradually.

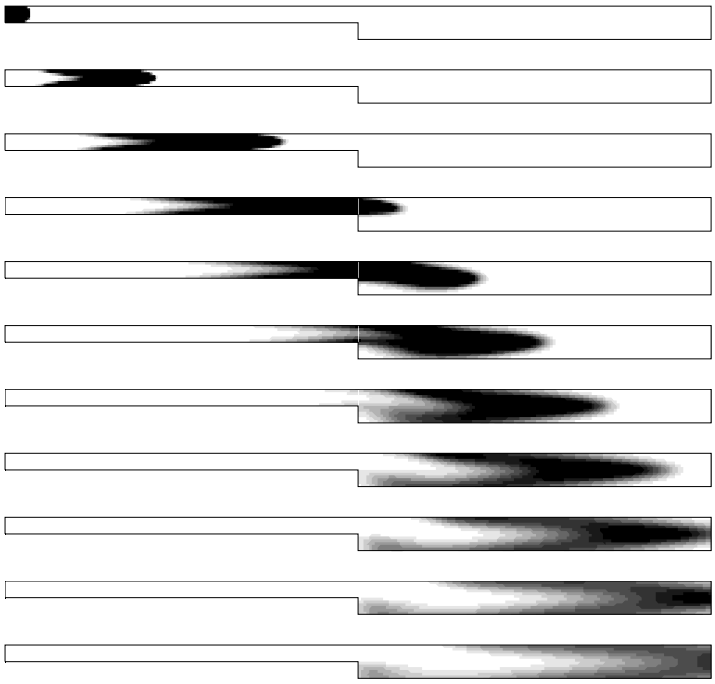

a)

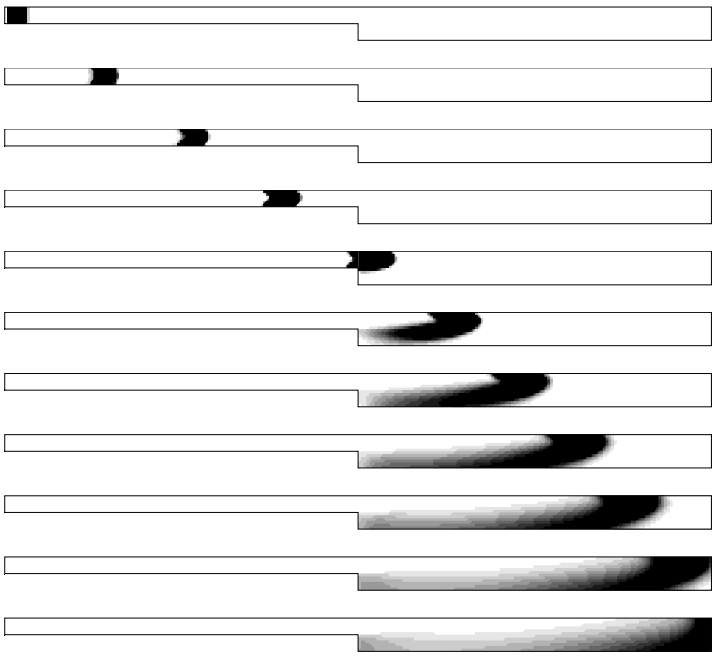

b)

FIG. 8. Concentrations fields (a: laminar case – b: turbulent case)
Non-dimensional time step: 5
Grey level code: White to black ➔ dimensionless concentration 0 to 0.05.

Comparison of concentration fields reveals that the tracer spot is more extended in the laminar regime than in the turbulent case, at least in the first stages of the experiment: one might therefore be tempted to draw the paradoxical conclusion that there is more diffusion in laminar than in turbulent flow.

As a matter of fact, it appears that the transport of tracer in the laminar regime is affected by the combination of the velocity profile and molecular diffusion. The parabolic shape of the velocity profile causes the bullet shape of the tracer spot, with an ever larger extension. In the turbulent case, the quasi perfect flatness of the velocity profile transports the tracer in a plug-like way, even though the diffusion coefficient is obviously much larger.

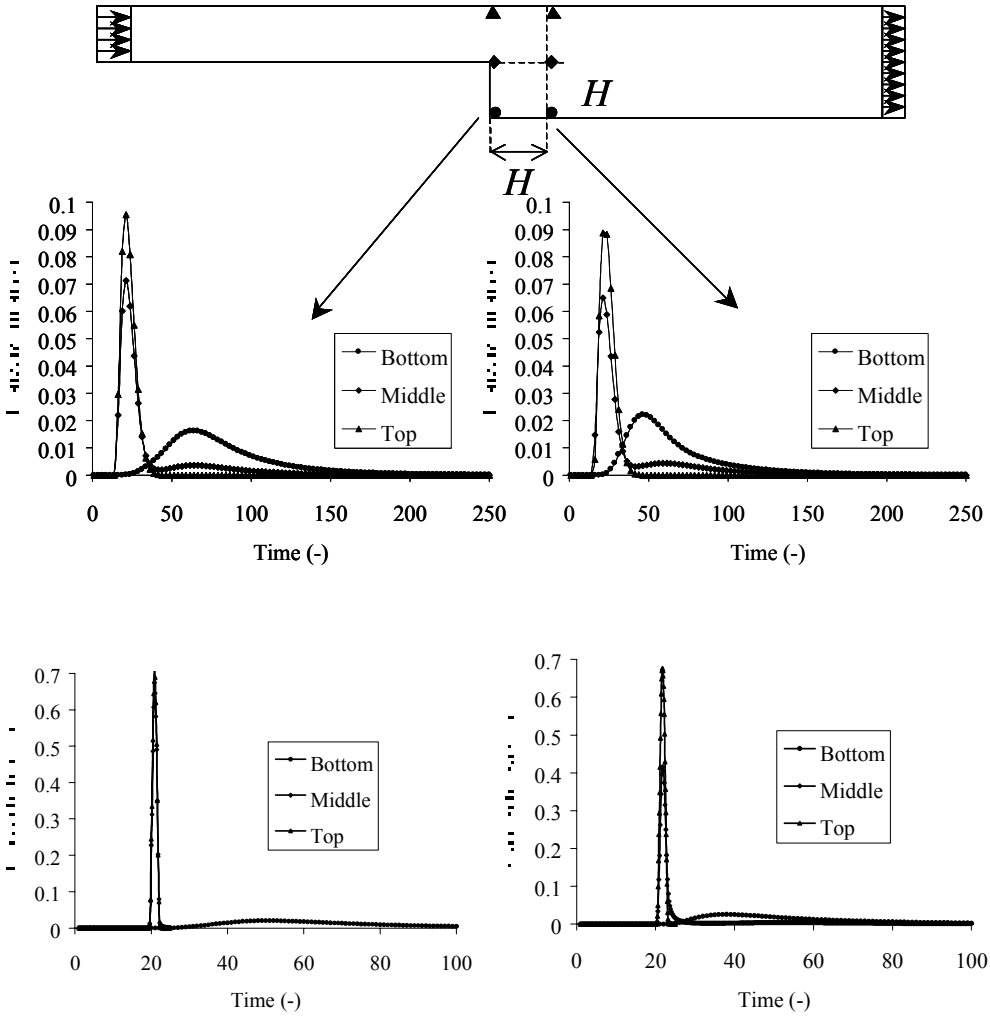

FIG. 9. Concentration histories at various points (a: laminar case – b: turbulent case).

The same effects are visible on Fig. 9a and b, which show concentration histories at various points downstream the flow enlargement. Basically, a peak is first seen at the top and middle positions. The recirculating flow creates a second, more diffuse peak at the middle positions, also visible at the bottom of the channel. In the turbulent flow regime, the first tracer peak is very sharp and practically identical at the top and middle positions, at a given distance from the step; these features are not to be found in the laminar case, once again the effect of the difference in the velocity profiles.

Detection chain

Since we want to emphasise the effects of tracer energy, and therefore attenuation, we shall attribute to the fluid the attenuation properties of water. We shall therefore be dealing with a "thought experiment" involving a hypothetic fluid with both high diffusion properties (like gas) and large attenuation of γ radiations (like water).

Three commonly used radiotracers for water covering a wide energy spectrum are ^{99m}Tc (140 keV) as $^{99m}TcO_4^-$, ^{113m}In (390 keV) as EDTA complex and ^{82}Br (up to 1.5 MeV) as $^{82}Br^-$. In order to guide our choice for the tracers and the dimensions of the flow system, we have plotted the attenuation of radiation from a point source of each of the radionuclides through a layer of water of thickness x in a perfectly collimated geometry:

$$\frac{I}{I_0} = \exp(-\mu x) \tag{4}$$

where μ is the linear attenuation coefficient (computed for the main photo peaks of each radiotracer using the tables by Hubbell [12]). The results are shown on Fig. 10.

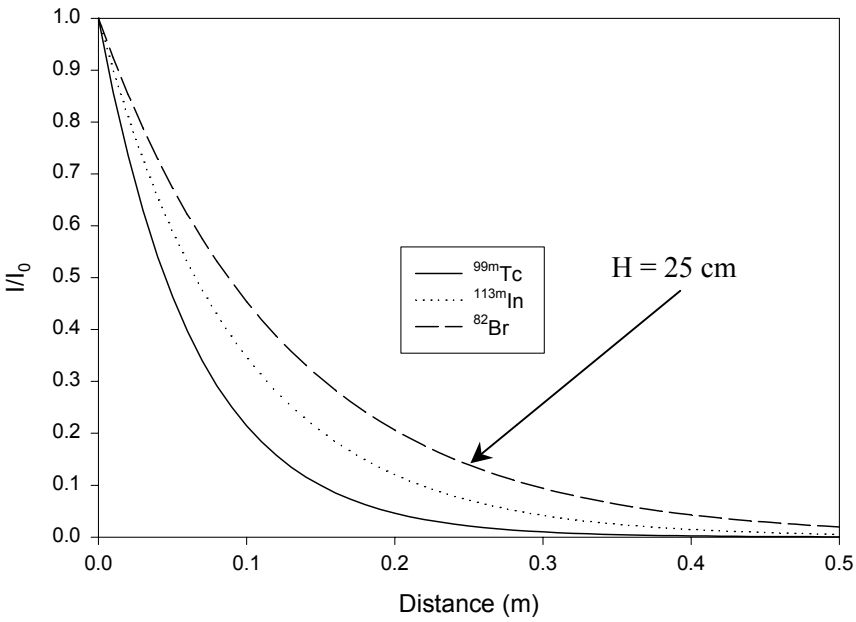

FIG. 10. Attenuation by a layer of water, for different radionuclides.

Considering that we seek the largest possible contrast between the high and low energy tracers, the best choice is ^{82}Br on the one hand and ^{99m}Tc on the other. It also appears that a 25 cm thick water layer generates an order-of-magnitude difference between ^{99m}Tc and ^{82}Br, while not totally extinguishing the ^{99m}Tc signal; the height of the step is therefore set to 25 cm.

Determining a value for H and assigning to the fluid the kinematic viscosity of water approximately 10^{-6} m^2/s) allows to calculate the *dimensional* values of the velocity U, the time scale τ and the molecular diffusion coefficient D:

$$U = \frac{\nu}{H} Re \tag{5}$$

$$\tau = \frac{H}{U} \tag{6}$$

$$D = \frac{\nu}{Sc} \tag{7}$$

all of which are summarised in Table I as a function of the Reynolds number.

TABLE V. DIMENSIONAL VALUES OF THE PARAMETERS

Re	U (m/s)	τ (s)	D (m^2/s)
10^2	4.10^{-4}	625	10^{-6}
10^5	4.10^{-1}	0.625	10^{-6}

The diffusion coefficient is too large by three orders of magnitude for the molecular diffusion of a substance in water. As discussed in Section 2, we believe that this inconsistency, though not pleasant to the mind, is of little importance in the aim we are pursuing here (the velocity scale hardly seems feasible in reality either).

The following step is to calculate function $T(x,y,z)$. As mentioned above, this is done with Monte-Carlo software *Inspect*, choosing the following configuration: NaI 1 inch by 1 inch scintillation crystal with 5 cm radius lead shielding and covered by a 1 mm thick steel window. The detector is located against the wall of the (virtual) flow rig, a 1 mm-thick steel sheet. A lower threshold of 30 keV is set; otherwise the whole of the energy spectrum is considered. The result is shown on Fig. 11, which maps the logarithm (base ten) of the count rates for ^{99m}Tc and ^{82}Br as a function of the position of a point source. The wiggles on the low count contours are due to poor count statistics (not too much of a problem since these regions will contribute little to the detector signal). The $T(x,y,z)$ function having polar symmetry, the corresponding plots need only be two-dimensional.

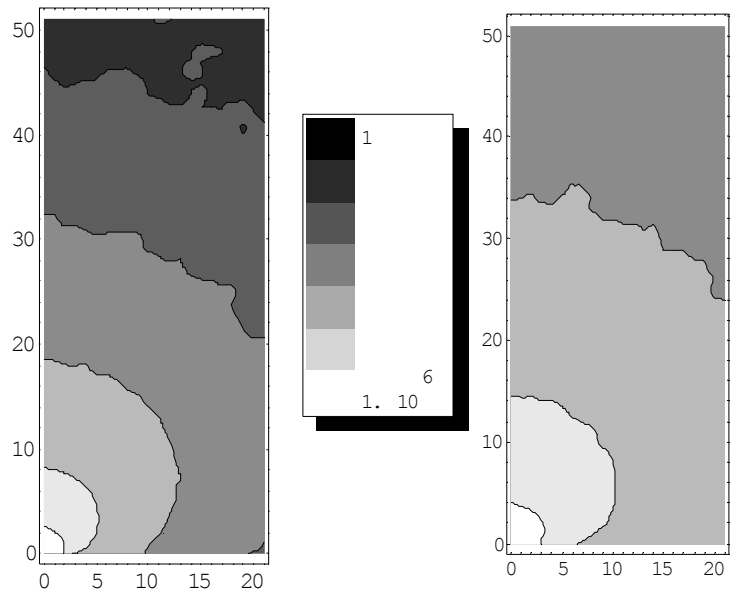

FIG. 11. T function for ^{99m}Tc (left) and ^{82}Br (right)
Detector is located at point (0,0) – Dimensions in cm
Grey level code: Black to white ➔ 1 to 10^6 counts/s/mCi (logarithmic scale).

Calculating count rates

Finally, the integral in equation (1) is evaluated in the following way: at each time step, the concentration field in the vicinity of the detector is extracted and converted into a volumetric activity field thanks to the following relation:

$$a(x,y,z,t) = \frac{A_0}{H^3} c(x,y,z,t) \tag{8}$$

where A_0 is total injected activity,

The product of activity A and function T is calculated over a tri-dimensional array of N points and the contribution of each point is summed to evaluate integral (1):

$$\dot{n}(t) = \sum_{i=1}^{N} A_i(t) T_i \tag{9}$$

This procedure is computationally quite simple but involves manipulation of large data files and a large number of computations. No effort has been made to optimise the number of points or the extension of the array over which the integral is evaluated.

This operation has been performed for both $^{99m}TcO_4^-$ and $^{82}Br^-$, three detector positions (H, $2H$ and $3H$ away from the step) in the laminar and turbulent regimes. Fig. 12 shows the position of the detectors, while Fig. 13 illustrates the results for ^{82}Br and ^{99m}Tc detection, respectively, at distance H and in the laminar case. Count rates are given in counts per second, for an injection of 1 mCi of tracer.

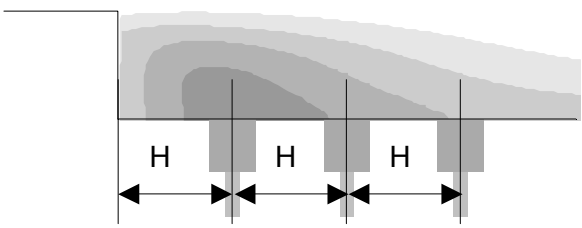

FIG. 13. Detector positions.

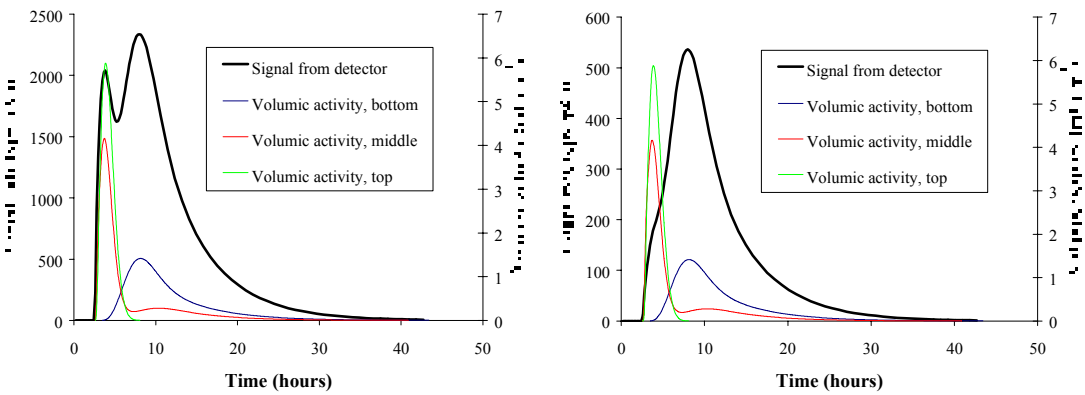

FIG. 13. Detector response and concentration histories
Laminar flow, detector at distance H
left: ^{82}Br *- right:* ^{99m}Tc.

Fig. 13 confirms that the detector is sensitive to all flow components (both main flow and recirculation) when ^{82}Br is used, much less so in the case of ^{99m}Tc (the signal mainly originates from the recirculation).

Fig. 14 compares the readings from all three detectors, for a given tracer and a given flow regime and highlights the same trends.

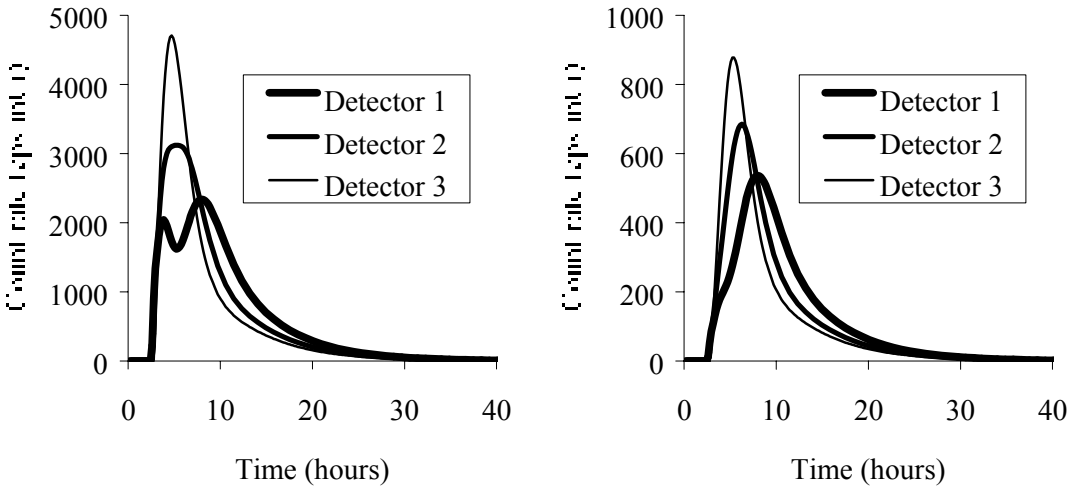

a)

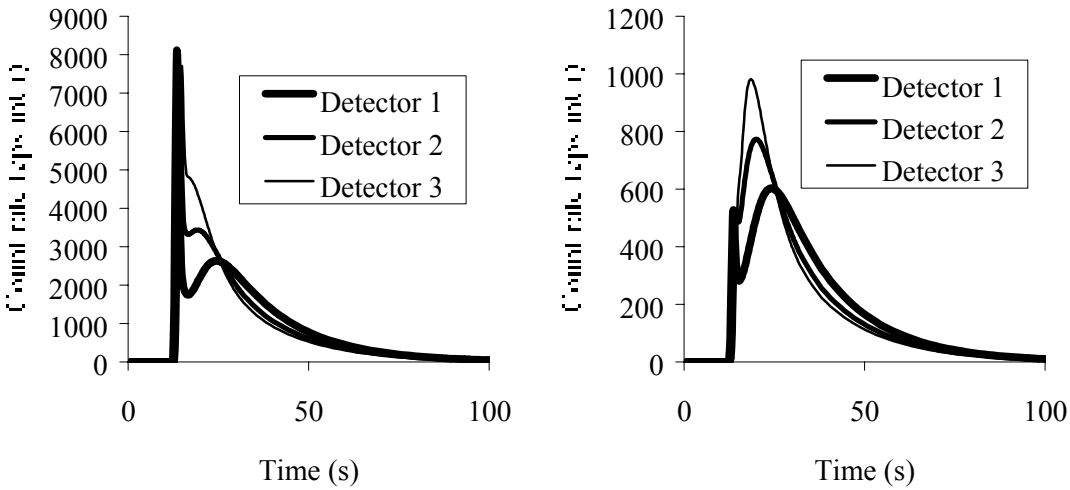

b)

FIG. 14. Detector responses, as a function of their position
a) Laminar regime – Left: ^{82}Br, right: ^{99m}Tc
b) Turbulent regime – Left: ^{82}Br, right: ^{99m}Tc.

4. AN ATTEMPT AT EXPLOITATION WITH THE CLASSICAL TOOLS FOR RTD ANALYSIS

We have been able to simulate the flow, the dispersion of a tracer and the response of the detectors, thus making clearer the link between the output from the detector and what it actually "sees". This is what we called the "direct" problem in the first section (cf Fig. 2).

Referring to the same notions, we shall now have a go at the "inverse" problem; we shall pretend to know the geometric characteristics of the experiment (both the dimensions of the flow rig and the positions of the detectors), the flow rate, the readings of the detectors in two different flow conditions (essentially the data on Fig. 14), but not the internal flow pattern. We shall then put in action the usual tools used by the tracer engineer to try to extract whatever information we can from these data.

Basically, exploitation of a radiotracer experiment involves (see for example Blet et al. [13]):

- Analysis of total counts,
- Shape and time analysis of the curves,
- Use of systemic models.

Note that we shall be spared the problems of preliminary data treatment, since we can assume our data background- and noise-free. Total counts collected by each detector are shown in Table II:

TABLE VI. TOTAL COUNTS FROM EACH DETECTOR

Flow regime	^{82}Br			^{99m}Tc		
	Detector 1	Detector 2	Detector 3	Detector 1	Detector 2	Detector 3
Laminar	$8.72.10^7$	$8.73.10^7$	$8.74.10^7$	$1.72.10^7$	$1.73.10^7$	$1.73.10^7$
Turbulent	$8.86.10^4$	$8.86.10^4$	$8.85.10^4$	$1.75.10^4$	$1.75.10^4$	$1.75.10^4$

For a particular flow regime and tracer, total counts at each position are identical (differences are less than 1 % and can plausibly be attributed to round off errors in the computation of integral (1)). This observation should not come as a surprise. Sandberg [14] demonstrated in his 1981 paper that the following equation:

$$\int_0^\infty c(t)dt = \frac{m}{Q} \tag{10}$$

where m is the mass of injected tracer (in our case: total injected activity) and Q the flow rate, held at all points in any *steady-state* flow with *zero concentration gradient* at the boundaries. In fact, it only means that tracer dwells a long time at those points where its concentration is low – not such a striking result. In our case, the fact that equation (10) is respected validates the calculation procedure, if nothing else. In real life, many facts will contribute to make equation (10) false: flow instabilities, inadequate boundary conditions, differences in detector settings.

Calculating the ratio of count rates in the laminar and turbulent regimes gives a value of about 10^3 for all tracers and all detectors. Taking advantage of the well known fact that count rates are inversely proportional to flow rate, also indicated by equation (10), this indicates a 1 to 10^3 flow rate ratio in the laminar and turbulent regimes, as indeed imposed in our calculations (cf. Table I). The latter result could in fact have been obtained with the results from only one tracer and one detector.

On the other hand, the value of having multiple detectors becomes clear if the analysis of the shape of tracer curves is attempted. Any complete set of curves from the three detectors suggests that the tracer flow is composed of two peaks moving in opposite directions, as illustrated by Fig. 15:

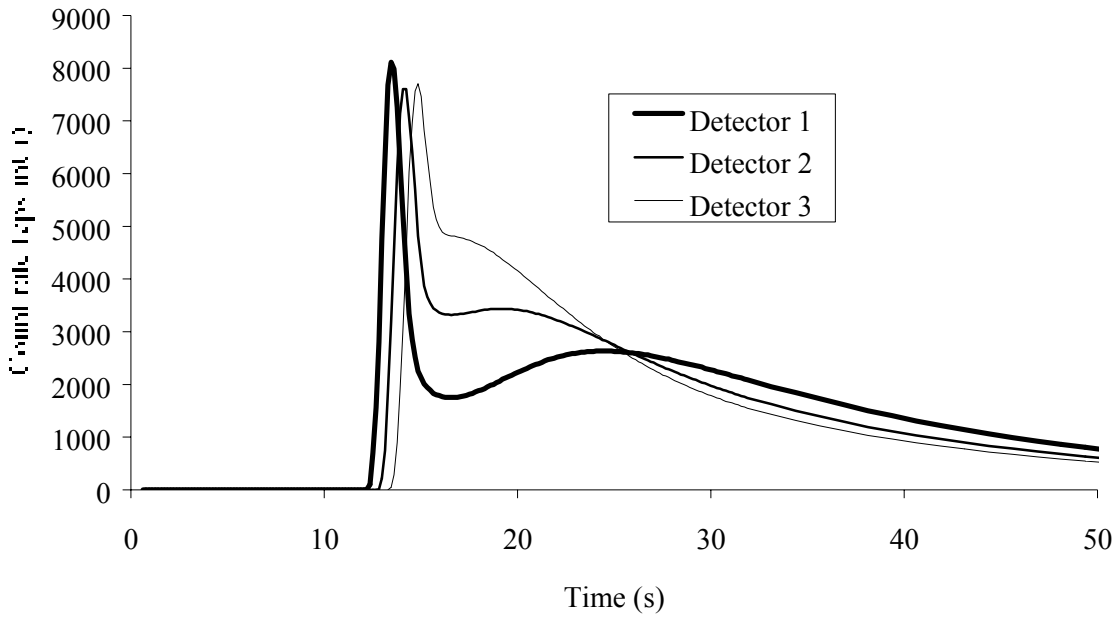

a)

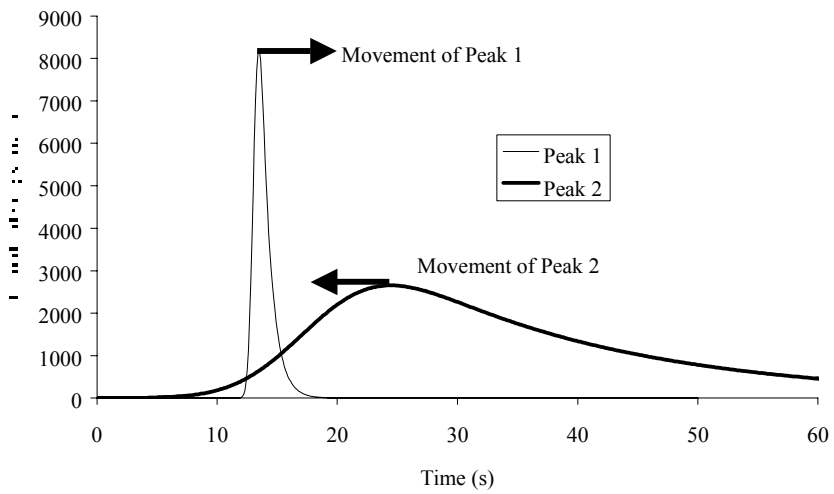

b)

FIG. 15. Tracing turbulent flow with ^{82}Br
a) Tracer curves b) Interpretation.

This is however clearest if data from ^{82}Br is available. Furthermore, comparing the height of the corresponding peaks with ^{82}Br and ^{99m}Tc allows to infer that the first peak is located further away from the detectors than the second one. This is however possible only if the tracers have been chosen to have very different attenuation coefficients under the flow conditions, a condition that is not always easy to fulfill.

No clear conclusion can be drawn if only detector 2 or detector 3 is available. For instance the shape illustrated by Fig. 16 can be obtained with any flow with some amount of dead volume and does in no way suggest the presence of recycling. Similarly, using only detector 1 can prompt the tracer engineer to consider the flow as the sum of two *parallel* streams – the information that the two streams actually flow in reverse directions can only be obtained if more detectors are available.

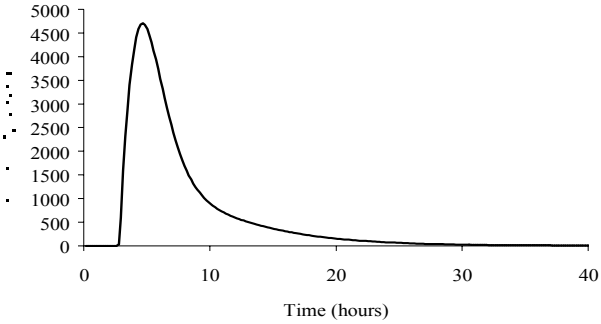

FIG. 16. Tracing laminar flow with ^{82}Br- Signal from detector 3.

The following step is to evaluate the velocity of the peaks by measuring their times of appearance in front of the detectors. Such a procedure requires that the peaks be well defined and will obviously not work in most cases. It is however possible to evaluate the velocity of the first peak with ^{82}Br in the turbulent case: 0.37 m/s between detectors 1 and 2, 0.32 m/s between detectors 2 and 3, a good enough order of magnitude considering that the inlet velocity is 0.4 m/s. The velocity of the second peak can be estimated under the same conditions, about 0.05 m/s between detectors 1 and 2. The latter value is not so bad, since the average velocity of the backward flow is in the 0.1 – 0.12 m/s range. In the laminar case, the peaks are distinct at detector 1 only, which forbids to use this method. An alternative is to measure the time lag between the tracer fronts. It works well enough with the upward front, giving a value of 6.10^{-4} m/s (maximum velocity in the inlet channel is actually 6.10^{-4} m/s). In reality, the fronts are so close together that the method could hardly be practical.

Lastly, modeling can be attempted using an "inlet" and an "outlet" signal and fitting a model to reproduce the latter. Obviously not all pairs of signals can be treated in this manner, failure being guaranteed in the case of the two-peaked ^{82}Br signals. The ^{99m}Tc signals show more promise: model adjustment will be attempted between detectors 2 and 1 and detectors 3 and 2, seen as the upstream and downstream detectors in the recirculation flow. Only the basic Mixers in Cascade (MC) model will be used; at best the results will be a transit time t and a number of mixing cells J; the former can be translated into an "average" velocity u, the latter being a measure of dispersion in the recirculation. The quality of fitting is reasonably good, as illustrated by Fig. 17 in a typical case.

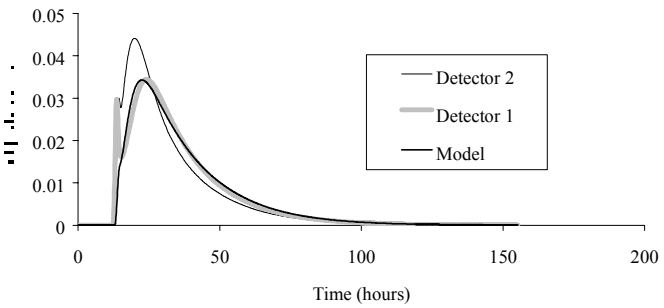

FIG. 17. Fitting the MC model: ^{99m}Tc, turbulent flow, detectors 2 and 1.

The final results are as shown on Table III.

TABLE VII. RESULTS FROM THE MC MODEL – ^{99m}TC

	"Inlet": det. 2 – "Outlet": det. 1		"Inlet": det. 3 – "Outlet": det. 2	
Laminar	t = 1.9 h u = 0.13 m/h	J = 0.75	t = 1.15 h u = 0.22 m/h	J = 0.38
Turbulent	t = 4.6 s u = 0.054 m/s	J = 0.32	t = 3.2 s u = 0.078 m/s	J = 0.1

The resulting velocities have the right order of magnitude. Comparison with the actual velocity profiles, shown on Fig. 18 a and b, indicates that they correspond to an average over the first ten centimeters of the flow rig – a quite plausible value considering the attenuation of the ^{99m}Tc radiation as illustrated on Fig. 10. The turbulent velocity profiles on Fig. 18 show little sign of coming close to zero near the walls. This is an effect of the finite volume calculation on a relatively coarse grid (velocity is only computed at the middle of the first cell – not at the wall), maybe also a consequence of the use of a wall function. Going back to Table III, the reason why calculated velocity decreases as we move towards the step is not clear. The values of J denote strong dispersion in the recirculation, even though the meaning of values as low as 0.1 is not clear.

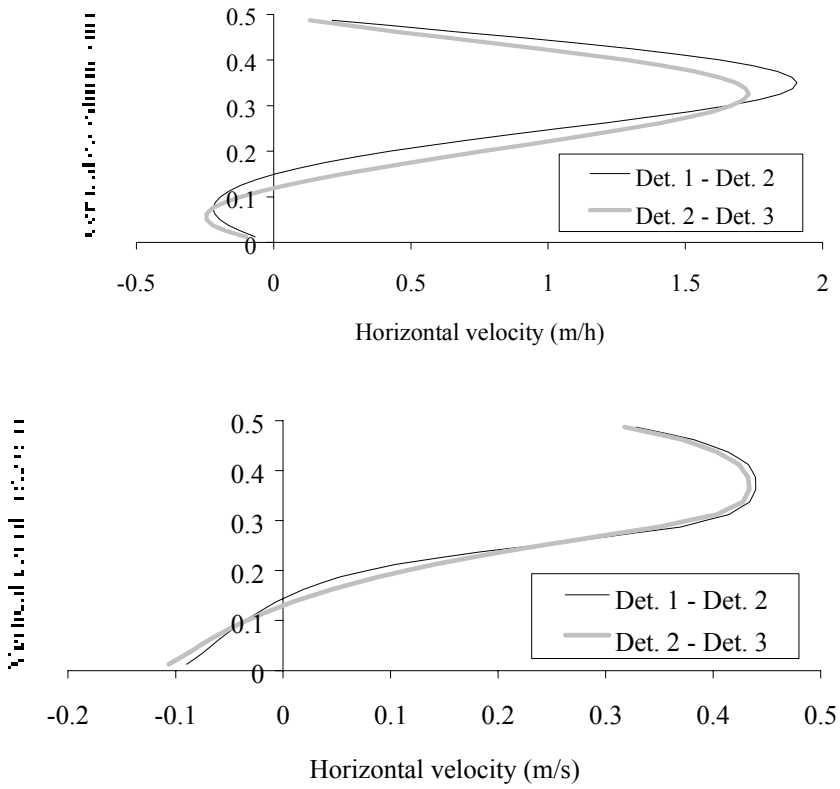

FIG. 18. Horizontal velocity profiles between detectors 1 and 2 and detectors 2 and 3 a) Laminar flow b) Turbulent flow.

On the whole, this attempt is at modeling considered as “moderately successful”. We now see two possibilities for improvement if work was to be continued on this problem. First of all, it would be interesting to test a less crude model, for example the one on Fig. 19 (drawn using the formalism of the *DTSPro* software). This model attempts to represent the recirculation, plus two groups of measurement stations (nodes 3 and 5 on the one hand; nodes 4 and 6 on the other hand) supposed to be located at the positions of respectively detector 1 and detector 2. The signals from these detectors should in fact be a weighted average of tracer curves at nodes 3 and 5/nodes 4 and 6, with different weights according to tracer energy. The optimized values of the parameters would provide information on the velocity and dispersion in each stream. With the large number of parameters involved (a total of 15 if we are not mistaken: 6 time constants, 6 numbers of cells, the ratio of the flow rates plus two weight factors), the optimization of such a system would however not be a simple matter.

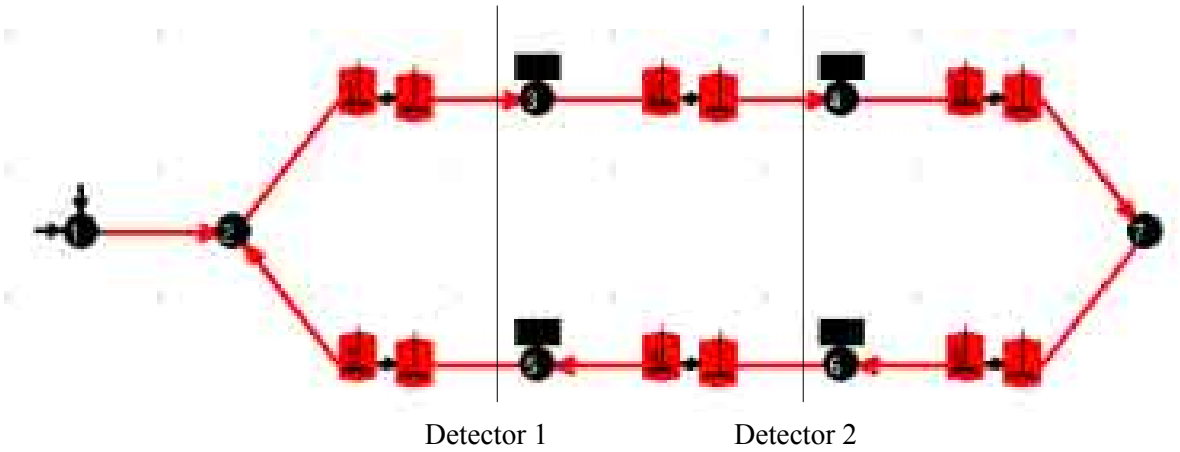

FIG. 19. A more complicated model.

Another procedure would be to use a simple decomposition of the signals at each of two successive detectors, say detectors 1 and 2, as a sum of two peaks:

$$\begin{aligned} s_1(t) &= p_1(t) + q_2(t) \\ s_2(t) &= q_1(t) + p_2(t) \end{aligned} \tag{11}$$

where p_1 and q_1 correspond to the first peak and p_2 and q_2 to the second one; the p peaks come before the q peaks. At this stage it is possible to try a decomposition like the one described by Vitart et al. [15], by selecting a mathematical shape for the peaks and using a multiparameter optimisation procedure. This method is however tedious and offers few guarantees regarding the uniqueness of the solution.

A slightly better approach, in our opinion, would be to introduce some modelling by assuming that the q peaks are the transformation of the p peaks by some adequate model the impulse response of which is h. In other words:

$$\begin{aligned} q_1(t) &= h_1(t) \otimes p_1(t) \\ q_2(t) &= h_2(t) \otimes p_2(t) \end{aligned} \tag{12}$$

where $\otimes$ stands for the convolution integral; or:

$$\begin{aligned} s_1(t) &= p_1(t) + h_2(t) \otimes p_2(t) \\ s_2(t) &= h_1(t) \otimes p_1(t) + p_2(t) \end{aligned} \tag{13}$$

The problem now consists in optimising the parameters in p_1, p_2, h_1, h_2 so that the best fit of $s_1(t)$ and $s_2(t)$ is simultaneously obtained. As a minimum, each peak can be represented by three parameters (for instance height, time and width) and each model by two (for example time and number of cells, in the case of the MC model). If s_1 and s_2 are area-normalised, two parameters can be eliminated, resulting in a total number of nine, which is probably manageable since two tracer curves are available as a target for the optimisation. Another advantage is that the order of appearance of the peaks is guaranteed by construction, which would not be the case with peak decomposition using just equation (10). The outputs are the parameters of models h_1 and h_2 which represent the time and dispersion characteristics of each stream. This methods requires development of a particular numerical procedure and has not been investigated further here.

5. CONCLUSIONS

The lessons that can be drawn from this work are in our opinion the following.

From a general point of view, we have verified that the signal created by a γ-emitting tracer in a non-one-dimensional flow does depend on the energy of the tracer. Observed trends correspond to expectations: a detector will probe deeper into the flow in the case of a high-energy tracer.

A consequence of this observation is that much caution should be exerted when interpreting such a signal with the usual tools of Residence Time Distribution analysis. To give an example from our test case, the practitioner may be tempted to interpret the ^{82}Br signals from one detector only as two or more plug flows in parallel. This choice, though quite attractive because summing up plug flows allows to reproduce any bizarre shape, would clearly be off the mark. Such an error can be avoided if signals from other detectors are also available. This point emphasizes the interest of having multiple detectors and, if possible, multiple tracers.

In the hope of getting closer to the ultimate goal of solving the “inverse problem”, we make the following suggestions for future work:

- Try to retrieve additional information from incident energy spectra. It can be expected that a low energy incident photon will result from more interactions with the fluid than a high energy one. Probabilities are that the low energy photon will have “traveled” some distance before reaching the detector while the high energy one has been emitted in the vicinity of the detector. Selecting appropriate high and low energy windows might therefore bring some information on the flow structures respectively close to and remote from the detector. This idea has been put forward by other participants in the Co-ordinated Research Programme and, in our opinion, bears much promise. It was unfortunately not possible to put it into practice during the present CRP.
- Develop specific treatment procedures for data from multiple detectors. This point has been briefly approached in the previous section but it clearly needs more thought and more work.

REFERENCES

[1] LEVENSPIEL, O., "Chemical reaction engineering", John Wiley and Sons, New York, 3rd Edition (1999).

[2] VILLERMAUX, J., "Chemical engineering — reactor design and operation", Tec & Doc Lavoisier, Paris (1985).

[3] SCHWEICH, D., "Chemical engineering", Tec & Doc, Paris (2001).

[4] IAEA, "Guidebook on radioisotope tracers in industry", Technical report series n° 316, International Atomic Energy Agency, Vienna (1990).

[5] THYN, J., ZITNY, R., KLUSON, J., CECHAK, T., "Analysis and diagnostic of industrial processes by radiotracers and radioisotope sealed sources", Vydavatelstvi CVUT, Prague (2000).

[6] THYN, J., ZITNY, R., "Analysis and diagnostic of industrial processes by radiotracers and radioisotope sealed sources", Volume II, Czech Technical University, Prague (2002).

[7] LINDEN, P., GROSSHÖG, G., PAZSIT, I., "Flowact, flow rate measurements in pipes with the pulsed-neutron activation method", Nuclear technology 124 (1998), 31–51.

[8] THYN, J., ZITNY, R., "Radiotracer applications for the analysis of complex flow structure in industrial apparatuses", Nuclear Instruments and Methods in Physics Research Section B: Beam Interactions with Materials and Atoms, **213** (2004) 339–347.

[9] RUCK, B., MAKIOLA, B., "Particle dispersion in a single-sided backward-facing step flow", Journal of Multiphase Flow 14 (6) (1988) 787–800.

[10] VILLAND, M., "TRIO-VF, Users manual — Version 8.7", Internal report CEA/STR/LMTL/96–49 (1996).

[11] TOLA, F., "Ecrin, Monte-Carlo code of simulation", Internal report CEA/DTA/DAMRI/SAR/96–111/T40 (1996).

[12] HUBBELL, J.H., "Photon mass attenuation and energy absorption coefficients from 1 keV to 20 MeV", International Journal of Applied Radiation and Isotopes 33 (1982) 1269–1290.

[13] BLET, V., BERNE, Ph., CHAUSSY, C., PERRIN, S., SCHWEICH, D., "Characterization of a packed column using radioactive tracers", Chem. Engng Sci. 54 (1999) 91–101.

[14] SANDBERG, M., "What is ventilation efficiency", Building and Environment 16 (2) (1981) 123–135.

[15] VITART, X., SANTOS-COTTIN, H., ROCHAS, J.L., MARGRITA, P., BERNE, Ph., BERNARD, J.R., CATROS, A., "Tracer studies on fluidised catalyst cracking plants: data analysis improvement", Proceedings of the NAARRI International Conference on Applications of Radioisotopes and Radiation technology in the 21st Century, (RAMAMOORTHY, N., ANANTAKRISHNAN, M., NANDAKUMAR, A.N., Eds) NAARRI (2001) 106–115.

[16] LEONARD, B.P., "Simple high-accuracy resolution program for convective modeling of discontinuities", International Journal for Numerical Methods in Fluids 8 (1988) 1291–1318.

Appendix
Calculated concentration fields for various values of the Schmidt number (in the laminar case)

The objective of this appendix is to illustrate the behaviour of our CFD code for increasing values of the Schmidt number. The flow domain, number and size of the mesh cells, Reynolds number, boundary conditions etc are kept the same as in the main text. Only the value of the molecular diffusion coefficient is decreased to obtain successive Schmidt numbers of 1 (the reference case), 10, 10^2 and 10^3, the latter corresponding to the case of water. The cell Péclet numbers increase from 4 to 4.10^3.

Even though the concentration balance is solved by a second order scheme (QUICK, first proposed by Leonard in 1988 [16]), it was expected that numerical diffusion would be predominant at such large cell Péclet numbers. In other words, our expectations were that the concentration field would not be greatly altered by increasing values of the Schmidt/Péclet numbers.

Such did not prove the case, as illustrated by the Fig. 1 to 4. For each value of the Schmidt number, they represent the concentration field at dimensionless times 1, 6, 11, 16, 21, 26, 31, 36, 41 and 46. The grey level code is white for zero concentration and black for a (dimensionless) concentration of 0.05 and more. They also represent the concentration histories at the top, middle and bottom levels, for positions right in front of the enlargement and 6 steps heights away from the latter.

Increasing the Schmidt number to 10 causes the tracer blob to become sharper and thinner, with a clearer effect on convection by the velocity profile; a dead zone also appears at the centre of the recirculation. The peaks at the middle and top levels in front of the step become wider, which is due to the tracer lingering in the very low velocity zones of the inlet channel. Also, the tracer subsides longer in the recirculation zone. Conversely, the peaks at a distance of $6H$ are sharper, due to the lesser extent of the tracer front. All these observations indicate that the code is reacting well, at least qualitatively, to the decrease of molecular diffusion.

The same trends become even more marked at a Schmidt number of 10^2. However, the concentration histories at some distance from the step show signs of instabilities. Closer scrutiny of the concentration field reveals that the tracer moves in sharp, isolated blobs. This effect gets worse at a Schmidt number of 10^3, the “blob-like” nature of the tracer field becoming ever more apparent as also visible on the concentration histories in front of the step (at $6H$ they consist mainly of noise and are not shown here).

On the whole: the QUICK scheme performs better than expected. It gives numerically and physically sound results for $Sc = 10$ (though no quantitative comparison could be made with other more accurate numerical methods) and still exhibits the right trends at higher values even if it generates strong instabilities.

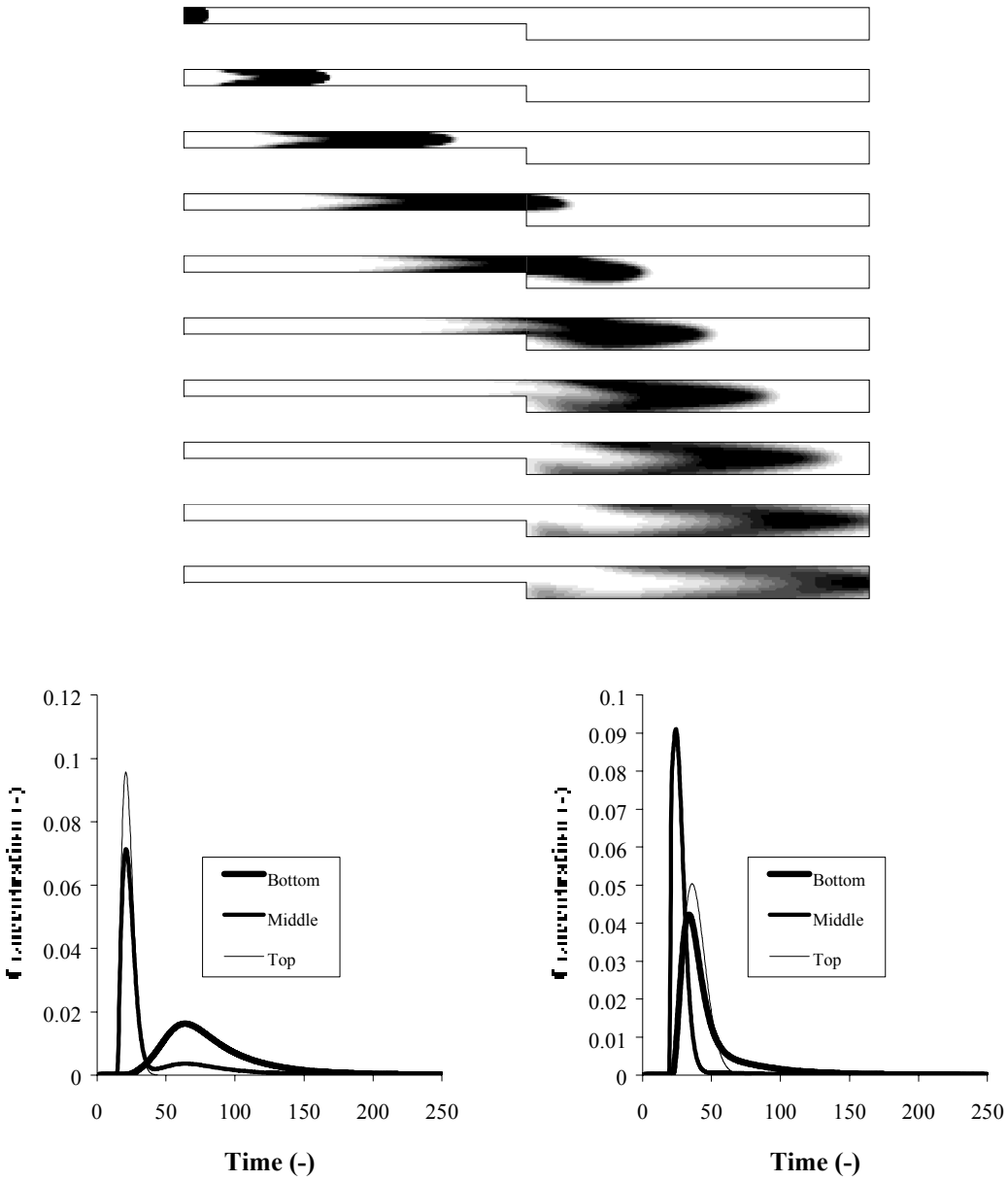

FIG. 1. Sc = 1 – Concentration field and concentration histories at 0 and 6H.

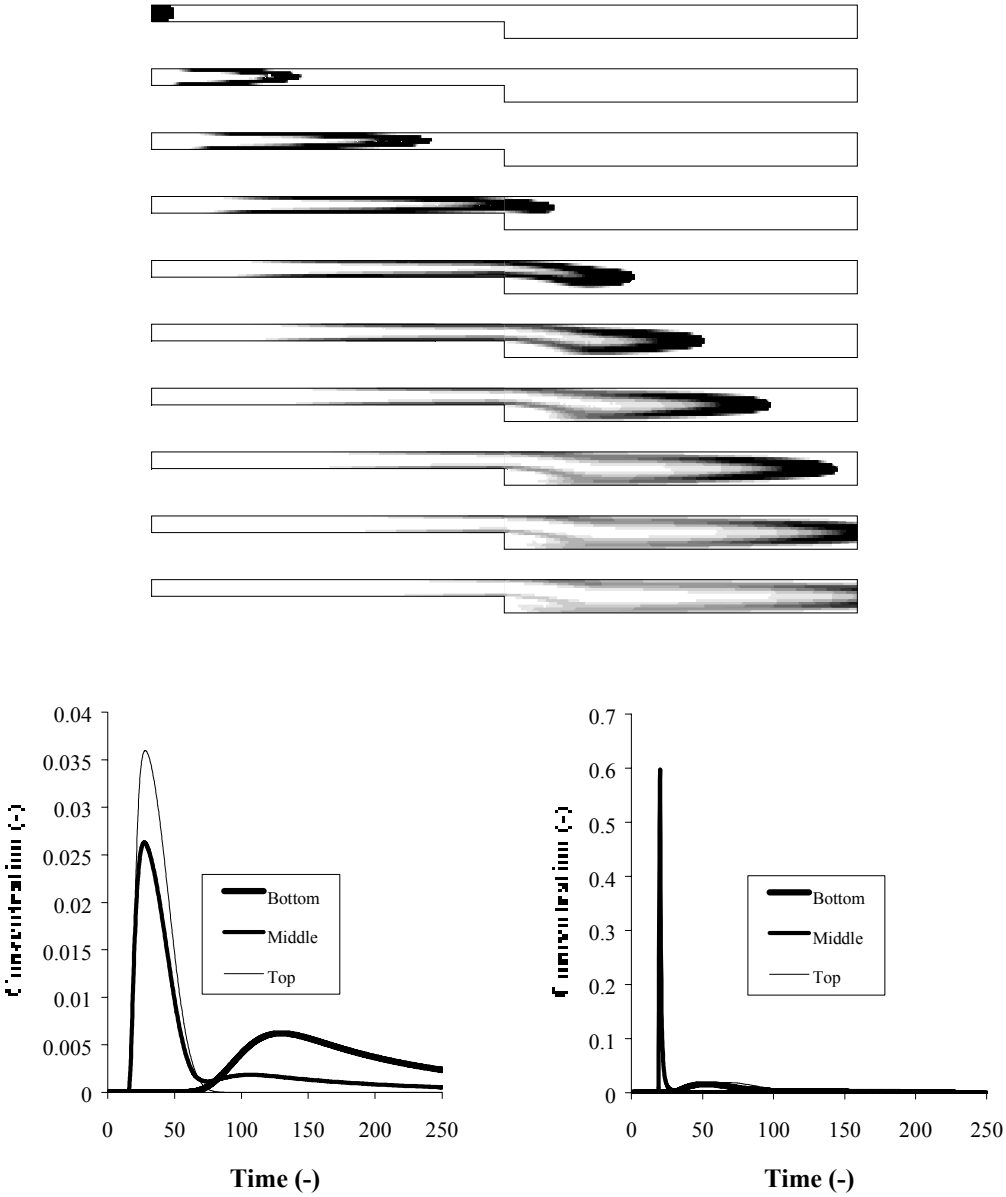

FIG. 2. Sc = 10 – Concentration field and concentration histories at 0 and 6H.

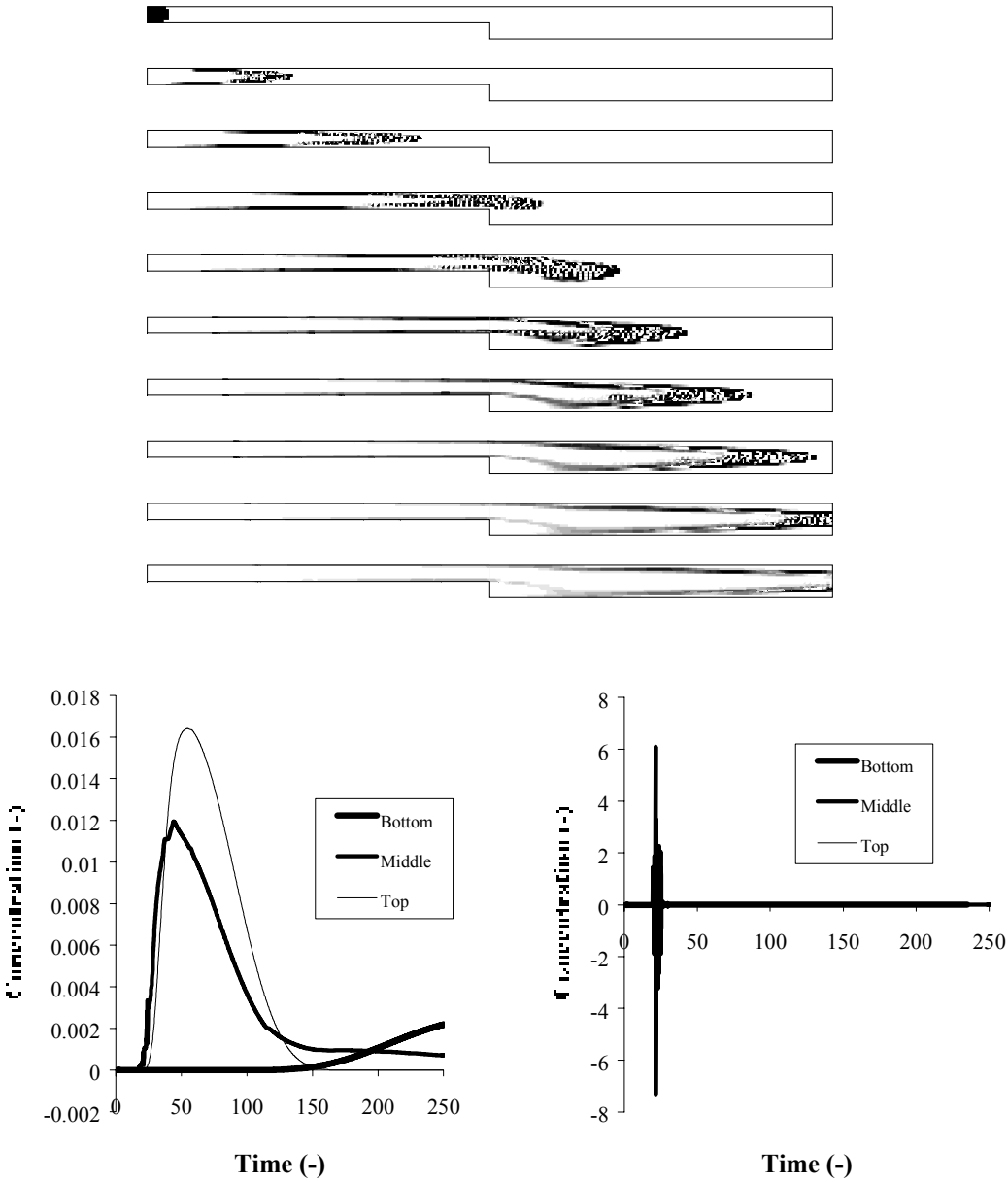

FIG. 3. Sc = 10^2 – Concentration field and concentration histories at 0 and 6H.

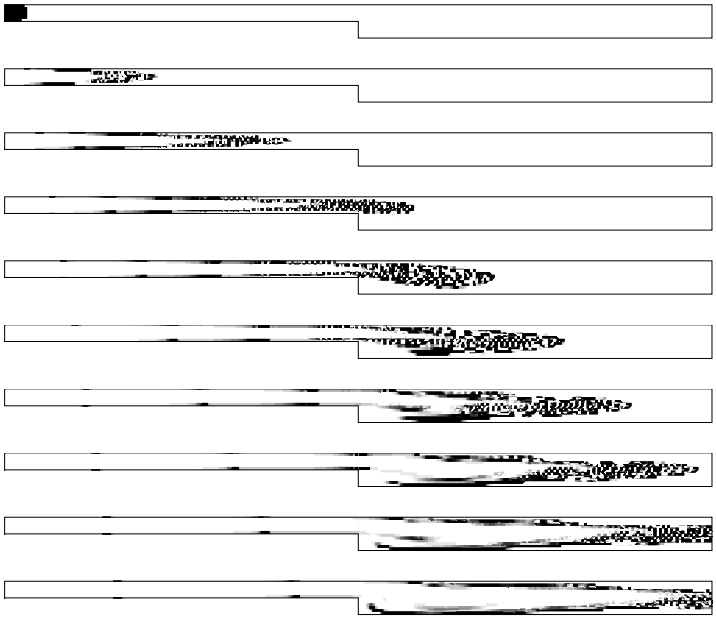

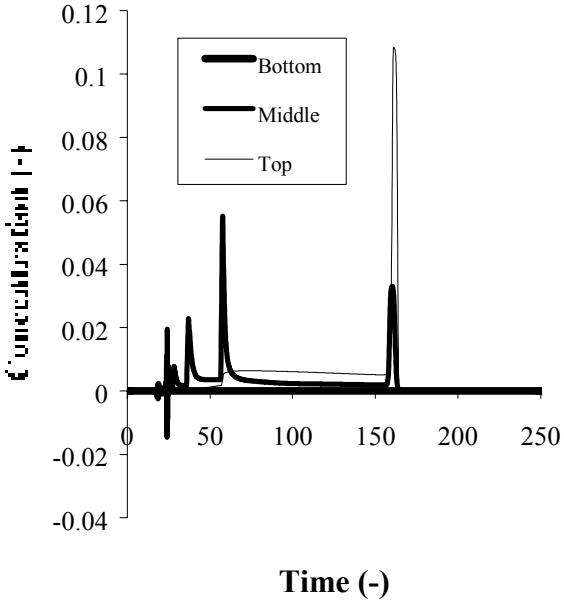

FIG. 4. Sc = 103 – Concentration field and concentration histories in front of the step.

INVESTIGATION OF TRANSPORT BEHAVIOUR OF SELECTED ORGANIC COMPOUNDS IN ELECTROCHEMICAL REMEDIATION OF CONTAMINATED SOILS

T. JENTSCH
Fraunhofer-Institute for Nondestructive Testing (IZFP),
Branch Lab for Acoustic Diagnosis and Quality Assurance,
Dresden, Germany

Abstract

Lab scale experiments were planned and executed to determine the necessity of contaminant transport and its operation in different electrical fields. The investigations were carried out with bromophenol labelled with the radionuclide ^{82}Br. ^{82}Br is a typical radioactive label and emits gamma radiation with energies in a wide range. The main gamma lines, i.e. those with the highest intensities, can be measured at 776 keV (83%), at 554 keV (72%) and at 619 keV (40%). A special procedure for the synthesis of labelled bromophenol from phenol and irradiated ammonium bromide in a single step was developed. Semi-automatically operating lab equipment was designed to investigate the transport behaviour of the labelled compounds in four soil samples simultaneously and independently from each other. Particularly, the influence of several soil compositions and different electrical field conditions was investigated. Reference experiments were executed with inorganic ammonium bromide as well as without the influence of an electrical field. The experimental results for remediation of the investigated soils have shown that a transport of the contaminants to the electrodes is necessary in each case.

1. INTRODUCTION

The objective of the research was to determine the necessity of organic contaminant transport and its operation at an electrochemical remediation of soils.

Several methods for soil remediation are known, but a lot of them can only be applied ex-situ. An ex-situ application causes a costly excavation and transport of large quantities to remove only small contaminant quantities from the soil. Some remediation methods are also applicable in-situ, e.g. leaching or washing procedures. But the applicability of these methods is only limited to hydraulically permeable soils: due to the restricted hydraulic permeability washing and leaching procedures are inapplicable for cohesive soils like clays or others. Particularly these kinds of soils promise to be a large market for electrochemical remediation procedures.

For the removing of *heavy metals* from soils in-situ electrochemical procedures are already successfully applied for the last few years, e.g. [1]. The causes for the clean up success are the well known electrokinetically enhanced transport mechanisms electroosmosis (water movement), electromigration (movement of ions and polar molecules) and electrophoresis (movement of charged solid particles) [2].

For the observed and verified decontamination results of *organic polluted soils* by electrochemical methods the physical/chemical reasons are controversially discussed in literature. Whereas many authors emanate from the necessity of an electrokinetically provoked transport of the contaminants towards the electrodes, e.g. [3], some authors feel confident that an electrochemical remediation can occur on the spot without any contact to the electrodes [4]. A special theory to describe this phenomenon by so called microconductors is given in [5].

Therefore, one objective of the lab scale experiments described in this paper was to determine the necessity of contaminant transport towards the electrodes. Another aim was to determine the influence of different soil compositions and of diverse kinds of electrical fields on the transport behavior of a selected organic compound.

2. MATERIALS AND METHODS

Experimental set-up

Figure 1 shows a photograph of the experimental set-up for the transport behaviour investigations of labelled contaminants within electrical fields.

The four containers were positioned in a special metal frame fixed on the carriage of a spindle drive linear unit electric powered by a stepping motor. A special programmable controller allowed toggle motions of the carriage with velocities in a range between 0.1 and 2000 µm/s (= 0.36 mm/h … 7.2 m/h) below four slot collimated (width: 10 mm) and well shielded NaI(Tl)-scintillation detectors.

Radioactive decay of the tracer results in a decreasing count rate during the long term experiment. To ensure a nearly uniform statistical error of all measuring results this fact can be only compensated by increasing the data logging intervals. The relationships between carriage velocities, data logging intervals and time needed for one scan realized for the transport behaviour investigations is presented in Table I.

FIG. 1. Photograph of the experimental set-up for the transport behaviour investigations of labelled contaminants within electrical fields.

TABLE VIII. RELATIONSHIPS BETWEEN CARRIAGE VELOCITIES, DATA LOGGING INTERVALS AND TIME NEEDED FOR ONE SCAN AT THE EXPERIMENTAL SETUP FOR THE TRANSPORT BEHAVIOUR INVESTIGATIONS

Carriage velocity of the spindle drive linear unit [cm/h]	Data logging interval [seconds]	Time needed for one scan (500 mm) [hours]
60	6	0,83
30	12	1,67
18	20	2,78
6	60	8,33
3	120	16,67
1,8	200	27,78

The only synchronisation of stepping motor and data logging system is the simultaneous start of both components. Whereas the carriage toggles without any interruption, a time offset of about 380 microseconds occurs between two data logging intervals. Since the position of the labelled contaminant shall be calculated from the countrate-time-curves, this time offset has to be taken into account at the evaluation algorithm.

Therefore, before starting the experiments with radioactively labelled contaminants in different soils the experimental set-up and the evaluation algorithm were tested by means of four sealed sources (^{137}Cs) positioned in the middle of each empty glass container. In this way, a really immobile contaminant could be simulated. For the test, the carriage was toggled ten times with a velocity of 60 cm/h and the data were logged in time intervals of 6 seconds (see Table I).

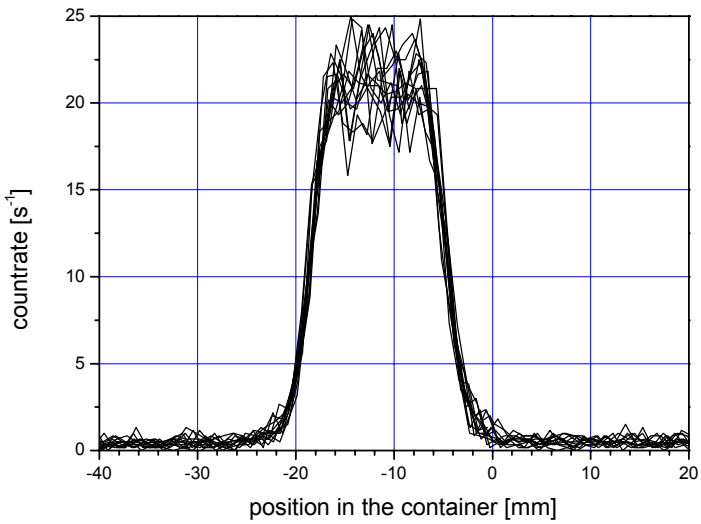

FIG. 2. Countrate measured in one of the four containers during a test of the experimental set-up carried out with a sealed calibration source (^{137}Cs), diagrammed as a function of the calculated position in the container

Results presented in Fig.2 show correctly no movement of the immobile sealed source in the container. Due to the sufficient detector shielding the countrate in container zones without any radiation source is in a typical range of background radiation.

Synthesis for labelling bromophenol

Halogenated aromatic hydrocarbons are representative of organic soil contaminants. Since the nuclide ^{82}Br is a suitable radiotracer a brominated aromatic hydrocarbon should be applied for the investigations. Because of other good properties, e.g. relatively low vapour pressure, bromophenol was chosen as model substance.

The labelling procedure was developed as a synthesis from phenol and irradiated ammonium bromide containing ^{82}Br in a single step. The procedure described below can be used for the synthesis of 40 mg radioactively labelled bromophenol which is necessary for one experimental run (simultaneously investigation of four containers).

Stock solutions of following concentrations are required:

- phenol in tetrachloromethane: 0.080 mol/,
- potassium bromide in ultrapure water: 0.033 mol/l,
- potassium bromate in ultrapure water: 0.042 mol/l.

To 7.26 ml of the phenol stock solution, 4.75 ml diluted hydrochloric acid (3%) and catalytic amounts of iron powder were added under stirring and cooling (about 0 °C, ice water bath in a round-bottomed flask (50 ml)). The content of the ampoule with the irradiated ammonium bromide (2.7 mg) has to be dissolved in 9.4 ml potassium bromide stock solution. After addition of 5.7 ml potassium bromate stock solution to the potassium bromide solution the mixture has to be added to the content of the round-bottomed flask. After about 10 minutes intensively stirring the organic phase has to be separated and given into a taper flask. For removing water soluble byproducts organic phase has to be washed two times by means of about 5 ml ultrapure water. In a final step the organic solvent tetrachloromethane has to be removed at 20 °C and reduced pressure of 40 mbar in a rotary evaporator. The labelled bromophenol remains in the distilling flask.

Soil sample preparation

A soil mass of about 410 g is necessary to completely fill each glass container. For the transport investigations only a narrow region of the container with a width of about 1 cm was provide for soil spiked with radioactively labelled contaminant. To avoid a contaminant transport caused by diffusion processes the remaining regions were filled with soil containing the non-labelled contaminant with the same concentration.

Inactive soil sample preparation

1600 g dried soil were mixed with 1.6 g bromophenol (800 mg 2-bromophenol and 800 mg 4-bromophenol) which was dissolved in about 230 ml methanol. After mixing the methanol was removed from the soil by evaporation in a fume hood under ambient conditions during a period of about 24 hours. For increasing the conductivity, immediately before filling into the containers the soil was mixed with 160 ml 0.2 m soda solution.

Radioactive soil sample preparation

About 6 ml methanol were given into the distilling flask containing the synthesis product (labelled bromophenol) before 40 g dried soil were added. After obviously mixing of all components the solvent was evaporated at 20 °C and reduced pressure of 40 mbar. Concluding the dry labelled soil was mixed with 4 ml 0.2 m soda solution.

Soil filling into the containers

At first, a mass of about 400 g non-labelled soil was filled in each container. To keep free the space for the labelled soil a special facility was used (*Fig. 3*). This facility also served as a funnel to fill in the soil containing the radioactively labelled contaminant.

FIG. 3. Photograph of a glass container before filling labelled soil (on the left hand side the electrolyte reservoir is visible).

Experimental design

The experiments were carried out with bromophenol in two kinds of soil: in sandy and in sandy with a clay fraction of 2%. For check and comparison, the first experimental series was executed with ammonium bromide in sandy soil. The concentrations of ammonium bromide and bromophenol in the soil were adjusted to 67.5 mg/kg and 1000 mg/kg, respectively. The concentration of the electrolyte (soda solution), which was used for increasing the conductivity in the soil amounted 100 ml/kg. All data are referred to dry soil. The electrolyte was also used for filling the reservoir to compensate the lack of ions in the soil near the anode. Due to the generation of hydronium ions at the anode by water

electrolysis, the pH-value of the electrolyte decreases. Therefore, the electrolyte was exchanged periodically (generally once a day).

Because of the radioactive tracer decay the duration of an experimental series could not be longer than 8 to 10 days. To ensure a nearly uniform statistical error of all measuring results the data logging interval had to be increased from time to time. As mentioned above, the carriage velocity of the spindle drive linear unit was changed at the same time (see Table I). The precise date for these changes was specified operationally in dependence on the ongoing measured values. Generally, the changes were done after one or two days.

3. RESULTS AND DISCUSSION

Transport investigations

Ammonium bromide in sandy soil

Figure 4 shows exemplary the results of an experiment with ammonium bromide in sandy soil fed with two ways rectified alternating voltage. As all following diagrams the presented results base on already nuclear physically corrected countrates. That means that the fraction of background radiation is subtracted and the radioactive decay is taken into account by referring the measured countrates to a defined date (here: the start time of the experiment).

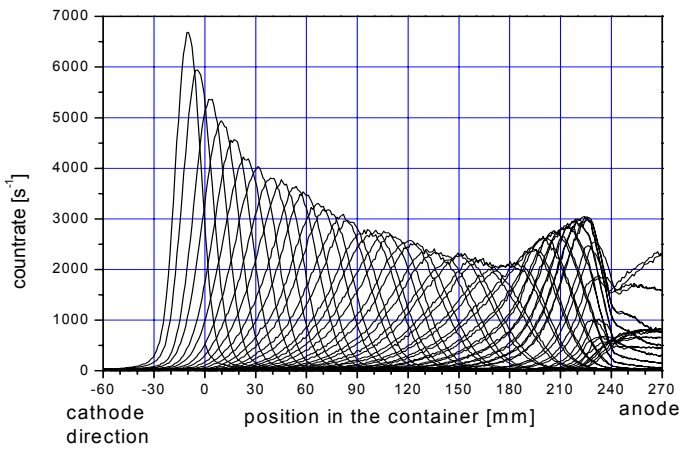

FIG. 4. Ammonium bromide in sandy soil: Measured and nuclear physically corrected countrates in dependence on the calculated position in the container fed with two ways rectified alternating voltage.

Figure 4 clearly displays a transport of the labelled bromide ions towards the anode. In spite of the radioactive tracer decay is already taken into account the maximum intensity of the countrate decreases during the experiment before it increases again near the anode reservoir. The decrease results probably from the axial dispersion during the transport process (the area under each curve is nearly the same). The increase near the anode reservoir is caused by the tailback due to the resistance of the cellulose acetate membrane. The position between about 240 mm and 270 mm represents a part of the anode reservoir. It is obviously that the membrane is permeable for the labelled ions. The change of the electrolyte in the reservoir is visible, too.

The first labelled bromide ions reach the anode reservoir one and a half day after start of the experiment. No significant influence of the investigated voltages was observed. The ion transport occurs uniformly during the first unaffected period of the experiment. From the data represented in Figure 5 a migration velocity of 6.4 mm/h could be calculated for all investigated voltages.

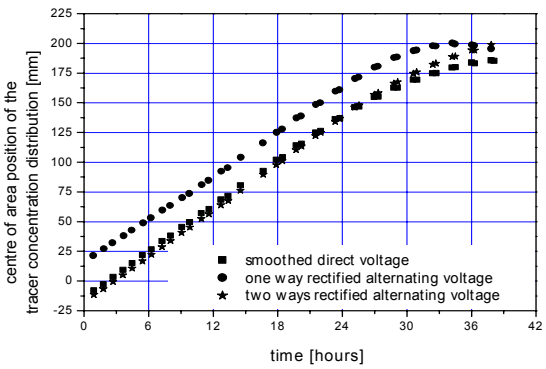

FIG. 5. Ammonium bromide in sandy soil: Time dependent displacement of the position of the tracer concentration distribution centre of area for the investigated kinds of voltage (path-time diagram)

Figure 6 shows exemplary the results of one reference experiment without voltage feed. No directed transport could be found although a light dispersion is observable.

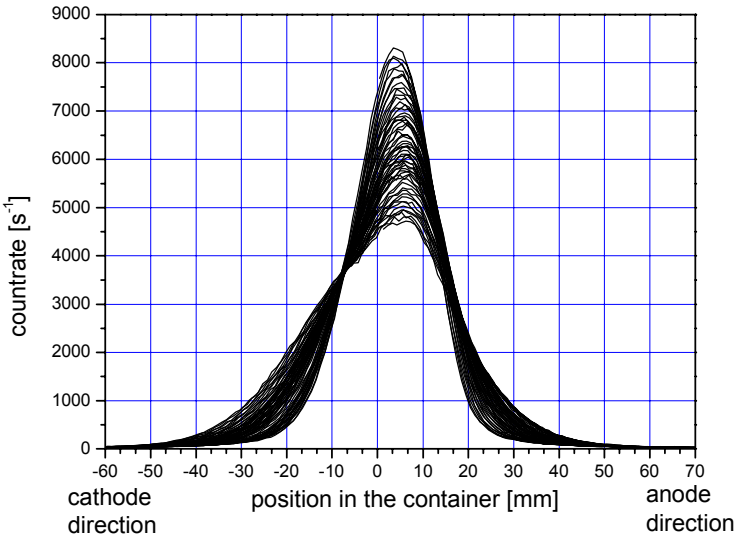

FIG. 6. Ammonium bromide in sandy soil: Measured and nuclear physically corrected countrates in dependence on the calculated position in the container without voltage feed.

Bromophenol in sandy soil

In sandy soils, the labelled bromophenol always moved towards the anode direction independently on the kind of voltage. Figure 7 shows exemplary the results of an experiment fed with smoothed direct voltage.

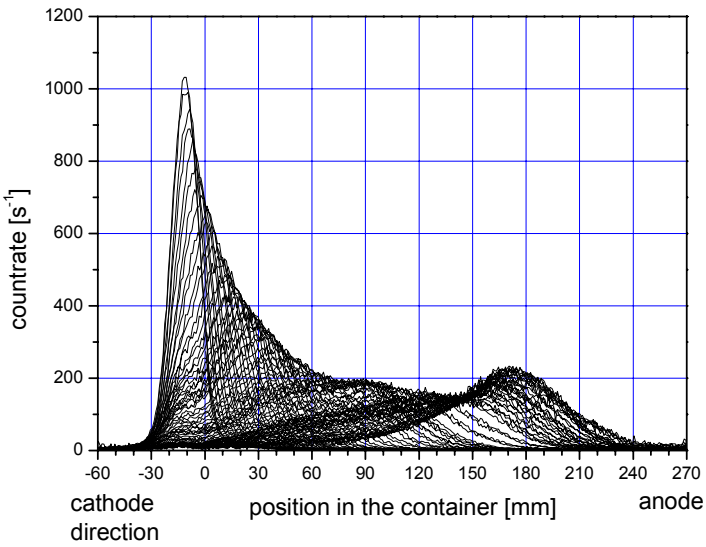

FIG. 7. Bromophenol in sandy soil: Measured and nuclear physically corrected countrates in dependence on the calculated position in the container fed with smoothed direct voltage.

Similar to the experiments with ammonium bromide in sandy soils the maximum intensity of the countrate decreases during the experiment before it increases again near the anode reservoir. The reasons for this behavior are assumed to be the same as in the case of ammonium bromide transport behavior: The decrease results probably from the axial dispersion during the transport process while the increase near the anode reservoir is caused by the tailback due to the resistance of the cellulose acetate membrane. Admittedly, the tailback occurs here in a larger distance from the anode reservoir than at the experiments with ammonium bromide. It is assumed that the resistance of the membrane is bigger for bromophenolate ions than for bromide ions. Since the entire soil is contaminated with bromophenol - and not only the labeled region - the tailback of the unlabelled ions influences the transport behavior of the labeled ions coming from the center of the container.

From Figure 8 it is visible that the maximum velocities of the bromophenolate ions in sandy soil are only a fourth to a fifth part of them of the bromide ions. As already found as a result of the experiments with ammonium bromide, the influence of the kind of voltage on the transport behavior of bromophenolate ions in sandy soil is not significant, too.

Explanation of the curve offsets in Figure 8 after an experimental duration of about 72 hours:

The offset is caused by the reduction of the toggle distance of the carriage. After 72 hours, there were no doubts that the ion transport occurs towards the anode direction. To spare time for the data logging the region near the cathode was no longer scanned. Although the measuring values from this region are only in the dimension of the background radiation the position of the center of the logged tracer concentration distribution relocates towards positions towards the anode direction. Since the ion transport velocities are calculated from the rise of the curves the offset does not influence the results.

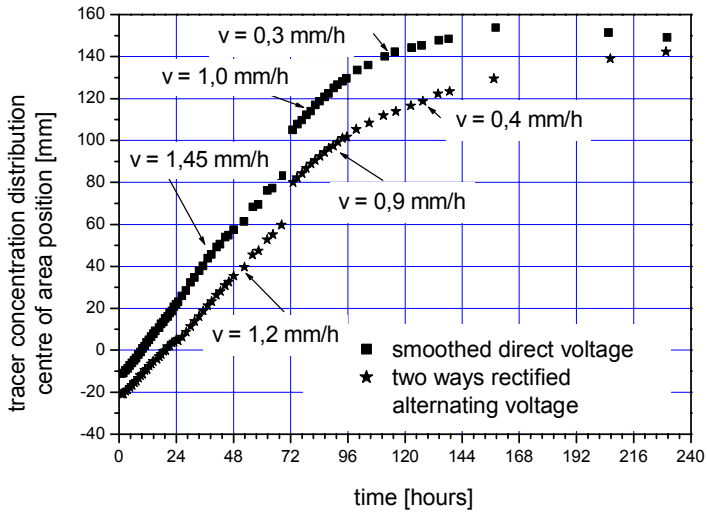

FIG. 8. Bromophenol in sandy soil: Time dependent displacement of the position of the tracer concentration distribution centre of area for the investigated kinds of voltage (path-time diagram).

Bromophenol in sandy soil with clay fraction

Figure 9 shows exemplary the results of an experiment with bromophenol in sandy soil with a clay fraction of 2% fed with two ways rectified alternating voltage. Independently on the kind of voltage the labelled substance moved towards the cathode direction. Only during the second experimental day the ion transport direction has changed towards the anode direction.

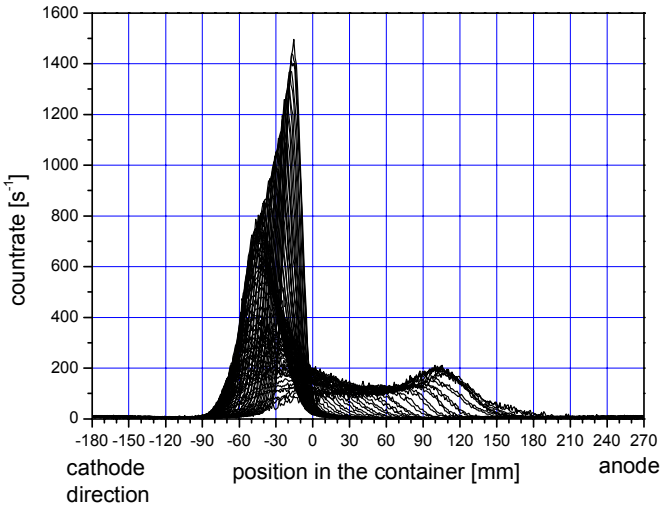

FIG. 9. Bromophenol in sandy soil with clay fraction: Measured and nuclear physically corrected countrates in dependence on the calculated position in the container fed with two ways rectified alternating voltage.

4. CONCLUSIONS

The results of the experiments have clearly confirmed that a contact and thus a transport to an electrode are necessary for an electrochemical degradation. Although the so called microconductors should be available in clay containing soils (e.g. iron minerals as red ox systems) degradation products only could be found after the contaminant had contact to an electrode

The experiments have shown that radiotracer experiments are favorably suited for lab experiments to determine the transport direction and velocity of labeled contaminants. The competitive influence of different electrokinetical transport phenomena like electroosmosis and electromigration could be made observably.

Only negligible influence of the kind of voltage could be found during the experiments. Therefore, only simple producible and thus cheap kinds of voltages are sufficiently for real electrochemical remediation applications. Lab experiments with radioactively labeled contaminants are a suitable method to get useful information about the transport direction and velocity in the run-up of a commercial electrochemical remediation application.

REFERENCES

[1] CLARK, R.L., KIMMEL, S., LAGEMANN, R., SMEDLEY, S., “Elektrokinetic remediation of soils, sludge and groundwater”, Proc. Am. Power Conf. 58 (1) (1996) 347.

[2] ACAR, Y.B., ALSHAWABKEH, A.N., “Principles of electrochemical remediation”, Environ. Sci. Technol. 27 (1993), 2638.

[3] TAKAYAMA, L.R., HUANG, C.P., “In situ removal of phenols from contaminated soil by electroosmosis process” Hazard. Ind. Wastes 27 (1997) 39.

[4] RAHNER, D., LUDWIG, G., ROEHRS, J., “Electrochemically induced reactions in soils — a new approach to the in-situ remediation of contaminated soils? Part 1: The microconductor principle” Electrochimica Acta 47 (2002) 1395–1403.

[5] HOFMANN, J., “Investigation of electrochemical processes for soil remediation”, Internal Research Report, INC Leipzig, 26.08.2002.

VALIDATION OF CFD MODELS AND INTEGRATION OF CFD-RTD METHODS FOR INDUSTRIAL PROCESS VISUALIZATION AND OPTIMIZATION

H.J. PANT
Isotope Applications Division, Bhabha Atomic Research Centre, Mumbai, India
A. PATWARDHAN
University Institute of Chemical Technology, Mumbai, India
A.K. MAHENDRA
Machine Dynamics Division, Bhabha Atomic Research Centre, Mumbai, India
V.V.RANADE
National Chemical Laboratory, Pune, India

Abstract

The main objectives of research project were: (i) Validation of the CFD models developed for different industrial systems by comparing the process parameters such as mean residence time, residence time distribution, mixing time etc. measured by radiotracer techniques and predicted by CFD simulations. (ii) Integration of experimentally measured results with that of results predicted by conventional flow modeling and CFD simulations to understand the complete flow behavior of the investigated system. The integration of the three different results will provide complete solution to process engineers for design of new chemical reactors and design modification, troubleshooting and optimizing the performance of full-scale industrial systems. Radiotracer experiments were carried out for measurement of mixing time and residence time distributions in different batch and continuous industrial systems, respectively. The measured results were treated and analysed using conventional modeling approach. Computational fluid dynamic (CFD) models were developed for the systems under investigations and validated. The validated CFD models were used to predict the flow behavior of the systems at conditions used in the experiments. The experimental results were integrated with that of the results of conventional modeling and CFD simulations to visualize the flow. The results of the research could help to promote the application of radiotracer techniques for flow visualization and validation of CFD models. The Indian Process Industry will be enormously benefited by this new approach in near future.

1. INTRODUCTION

The main objectives of the research were:

- To promote and harness the potential of radiotracer techniques to validate CFD codes/models developed by experts for different industrial process systems.
- Compare and integrate the results of RTD tracing and results predicted by validated CFD models for design of new reactors, design modification and optimization, flow visualization, troubleshooting and subsequently to enhance performance of industrial reactors and process equipment.

All industrial chemical processes are designed to transform cheaper raw materials to high value products. Process equipments are designed to: (1) bring the raw materials into intimate contact (to allow physical or chemical transformation to occur), (2) provide appropriate environment for adequate time to favor the desired transformation and (3) allow removal of products. A process engineer has to establish a relationship between process hardware and operating protocol and process performance.

The major questions facing a process engineer can be grouped into three classes:

- What transformations are expected to occur?
- How fast these changes will occur?
- What is the best way to carry out these transformations?

For addressing the first two questions, knowledge and expertise of thermodynamics, chemistry, catalysis, reaction kinetics and classical reaction engineering is required. Most of the models and tools falling in this category, however, make use of drastic simplifications while treating the process fluid

dynamics. These models rarely attempt to rigorously relate the fluid dynamics with reactor hardware and operating protocol.

The third question is addressed by designing and fabricating equipment (reactor) to carryout the required transformations with maximum possible efficiency. The desired hydrodynamics of the phases involved in the transformation is a key to the success of the process and equipment. Therefore, it essential to investigate the flow dynamics at the design stage itself by performing experiments in pilot scale reactors and optimize their design and performance. It is also quite often required to investigate the flow dynamics of full scale industrial reactors as a number of malfunctions could occur during the course of their operation which tends to reduce the process efficiency as well as deteriorate the product quality.

Mixing time, mean residence time and residence time distribution are important parameters used to characterize the performance of chemical process equipments. Radiotracer techniques are widely used to measure process parameters such as flow rate, mixing time, residence time distribution of process material in chemical engineering systems in various industries because of their certain advantages such as high detection sensitivity, "*in-situ*" detection, availability of wide range of suitable tracer compounds for various applications and utility in harsh industrial environment [1,2,3]. The conventional approach to analyse the flow performance of a chemical reactor is to measure these parameters experimentally and model the obtained results using suitable models [4,5,6,7]. This approach of flow modeling relies either on experimental investigations or on making drastic simplifications of the flow problem to allow analytical solutions. However, the this approach provides global information about the flow dynamics and does not give any information about the local information about mixing pattern inside the system, which is one of the most desired information to predict the behavior or performance of a system as a reactor

Although governing equations of fluid mechanics and many key ideas in numerical solution of partial differential equations were established more than a century ago, these were of little use before the advent of digital computers. The revolution in the ability of computers to store the data and to perform algebraic operations has greatly accelerated development of numerical techniques for solution of equations of fluid mechanics. This has led to the birth of a specialized discipline called computational fluid dynamics (CFD). The drawbacks of conventional approach as mentioned above are overcome by simulating the flow dynamics using CFD models [8].

CFD simulations allow detailed analysis of industrial flow processes, at an earlier stage in the design cycle, for less money, with lower risk and in less time than experimental testing. Indeed, these advantages of CFD are conditional on being able to solve the fluid dynamic equations accurately, which is extremely difficult for most engineering flows. It must be remembered that numerical simulations will always be approximate. There can be various reasons for differences between computed results and 'reality'. Errors may arise from each part of the process used to generate results: approximations in the fluid dynamic equations, inadequate accuracy of input data, approximations the numerical techniques, computational constraints, interpretation of results and so on.

2. MIXING TIMES: RADIOTRACER MEASUREMENTS AND CFD SIMULATIONS

Rectangular Bubble Column Reactor

Bubble column is one of widely used process equipment used to carry multi-phase reactions/operations. Mixing and transport processes are key issues in design of bubble columns, especially for processes involving multiple reactions where selectivity to desired product is important. Under such circumstances, the local fluid mixing often decides the performance of reactor. The gas-liquid flows in bubble columns are known to be intrinsically unsteady. The local flow field and turbulence governs the fluid mixing and are interrelated in a complex way with the design and operating parameters. Hence, it is important to understand fluid mixing and develop experimentally validated models to predict the mixing time accurately.

Recently, we have attempted quantitative characterization of dynamics of gas-liquid flow in 2-D rectangular bubble column and found a good agreement between experimentally measured and numerically predicted plume oscillation period [9,10]. Buwa and Ranade have studied the sensitivity of operating parameters (gas velocity), design parameters (sparger configuration,H/D ratio) and liquid physical properties (viscosity), numerically and experimentally.

In the present work, mixing times have been measured using radiotracer technique at different operating and design parameters [12]. Effect of superficial gas velocity, height to diameter (H/D) ratio, sparger configuration and liquid phase physical properties is studied. The mixing time predicted using CFD simulations is compared with experiments wherever possible. A rectangular bubble column (20cm width x 100 cm height x 5 cm depth) was used for experimental measurements (Fig.1). Experiments were carried at different superficial gas velocities in the range of 0.1 to 1.0 cm/s and at different H/D ratios (of 1.125, 2.25 and 4.5).

Air and water were used in the experiments unless otherwise mentioned. Multiple hole sparger (8 holes) and sintered disc sparger was used to study the effect of sparger configuration on the mixing time [9].

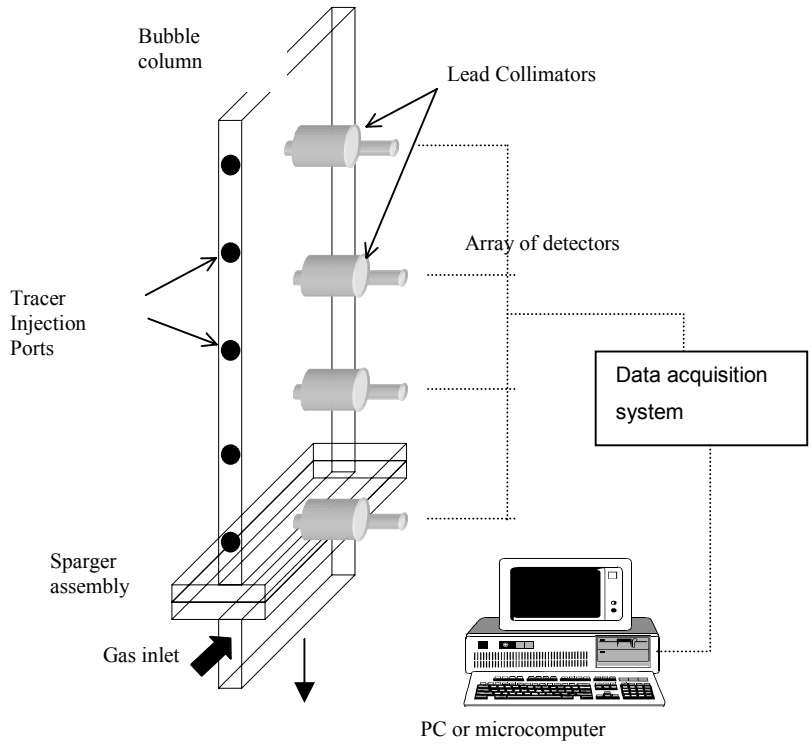

FIG. 1. Experimental set-up for mixing time measurements.

The sensitivity of mixing time to physical properties of liquid phase was studied by adding 0.25% BuOH. The radioactive tracer measurements are carried out using ^{99m}Tc (gamma energy=140 keV, half life: 6 h) as a tracer. The tracer concentration was recorded at different spatial positions in the columns as shown in Fig.1. Collimated NaI (Tl) scintillation detectors were used to measure the tracer concentration at different locations as shown in Fig. 1. Tracer was injected through various ports provided along the height of column.

The processed data is shown in Fig. 2 (b). Mixing time was calculated as time required for tracer concentration to reach within ± 10% of final tracer concentration. The average mixing time was obtained by averaging of all mixing times measured from different detectors locations

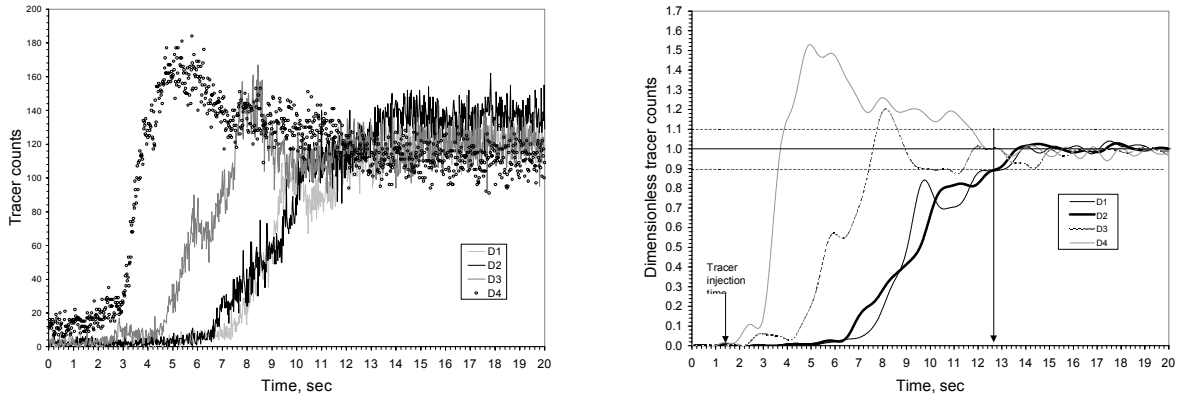

(a) b)

FIG. 2. Typical tracer concentration curves (a) Raw curves (b) Treated curves.

Two-fluid Eulerian-Eulerian model described by Buwa and Ranade (2001a) [9] was used to simulate dispersed gas-liquid flow in bubble columns. Mass conservation equation in a general form (after Reynolds averaging) can be written as:

$$\frac{\partial}{\partial t}\left(\rho_k \alpha_k\right)+\frac{\partial}{\partial x_j}\left(\rho_k \alpha_k V_{ki}\right)=\frac{\partial}{\partial x_j}\left(\frac{\Gamma_k}{\sigma_k}\frac{\partial \alpha_k}{\partial x_j}\right)+S_k \qquad (1)$$

where ρ_k is density, α_k is volume fraction, V_{ki} is mean velocity in i direction of phase k (L or G). α_k is effective momentum diffusivity and Γ_k is turbulent Schmidt number for phase k. S_k is a mass source for phase k. Liquid is represented as a continuous phase in a computational model. Since, there is no mass source for the liquid phase (no mass transfer between gas and liquid phase) and for single group (only one dispersed phase), the source, S_k, appearing in the mass conservation equation can be set to zero. Momentum conservation equation for each phase (Reynolds averaging) can be written as:

$$\frac{\partial}{\partial t}\left(\rho_k \alpha_k V_{ki}\right)+\frac{\partial}{\partial x_j}\left(\rho_k \alpha_k V_{ki} V_{kj}\right)=-\alpha_k \frac{\partial P}{\partial x_i}+\rho_k \alpha_k g_i+F_{ki}+\frac{\partial}{\partial x_j}\left(\alpha_k \mu_{effk}\left(\frac{\partial V_{ki}}{\partial x_j}+\frac{\partial V_{kj}}{\partial x_j}\right)\right)-\frac{2}{3}\frac{\partial}{\partial x_i}\left(\alpha_k \mu_{effk}\frac{\partial V_{km}}{\partial x_m}\right) \qquad (2)$$

where P is a pressure shared by all the phases and F_{ki} represents all the inter-phase momentum exchange terms. μ_{effk} is an effective viscosity of phase k. The standard k-ε model of turbulence appears to perform satisfactory. In the present work, we have, therefore, used standard k-ε model to estimate effective viscosity of liquid phase. Buwa and Ranade (2001a) have discussed the turbulence model, closure models and inter-phase coupling terms in detail and will be not discussed here.

The computational model described above was solved using commercial flow simulation software FLUENT 4.5 (1997) [14]. QUICK discretization scheme with SUPERBEE limiter functions was used for the numerical solution of model equations [14].

A typical mixing simulation, a pulse of tracer is injected in the reactor (which is achieved patching a known mass fraction of tracer over a known volume). The mass fraction of the tracer is recorded at several points in the reactor. Buwa and Ranade (2001b)[10] have discussed various approaches used for mixing simulations [12]. In the present, the mixing time is calculated by solving flow and species equations simultaneously. In the mixing simulations, the mixing time is estimated as the time required for 90% of reactor volume to reach ± 20% of final tracer concentration.

Mixing in bubble columns is essentially controlled by the dynamics of gas-liquid flow within such columns. Experiments and CFD simulations were carried out to understand dynamics of gas-liquid flows in 2D bubbles columns. Buwa and Ranade (2001a, 2001b)[10, 11] have discussed the modeling approach and simulated results in detail. A sample of the simulated flow in the experimental bubble column at two values of gas velocity is shown in Fig. 3. The simulated flow field was then used to predict the mixing occurring within the bubble column. For the mixing simulations, it was assumed that tracer concentration does not affect viscosity and flow field.

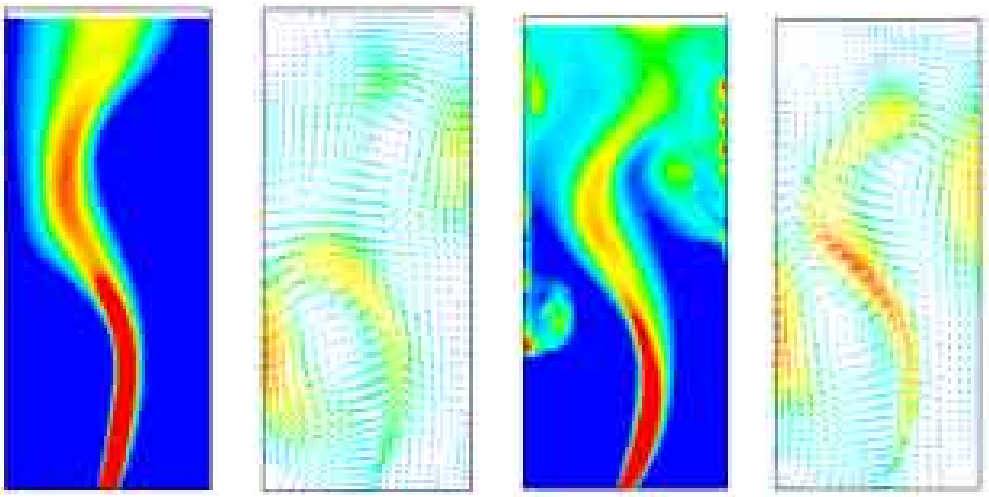

Gas superficial velocity of 0.17 m/s *Gas superficial velocity of 0.73 m/s*

FIG. 3. Typical flow field (contours of gas volume fraction and vector plot).

The mixing time was estimated using several different definitions proposed by Ranade *et al.*(1991) [15]. In experimental measurements, the average mixing time was obtained from the average of mixing time calculated from each detector. However, the detector aperture through which the tracer concentration is monitored was of the diameter 3.5 cm. Hence, the tracer concentration measured will be representative of the reactor volume around the center of the detector aperture. Therefore, it may not be appropriate to compare the mixing time obtained from CFD simulations which is based tracer history recorded at several points in the reactor (which corresponds to point measurement against the volume averaged measurement done in experiments). Therefore, in CFD simulations, the mixing time calculated based on time required to achieve certain degree of homogeneity over all the reactor volume.

The comparison of mixing time obtained using CFD simulations and experimental measurements are shown in Fig. 4 (a) and (b) for H/D ratio of 4.5 and 2.25, respectively. It can be seen that CFD models used in the present work can capture the sensitivity of mixing time to superficial gas

velocity and H/D ratio. The quantitative agreement is yet not satisfactory. This is possibly because of the sensitivity of mixing time to the criteria used to define mixing time and also because of apparent difficulties in correlating the mixing time definitions used for CFD simulations and experiments. Work is in progress to evolve general methodologies for rational estimation of mixing time. Meanwhile, the radioactive tracer technique also needs to be improved by using small aperture detectors.

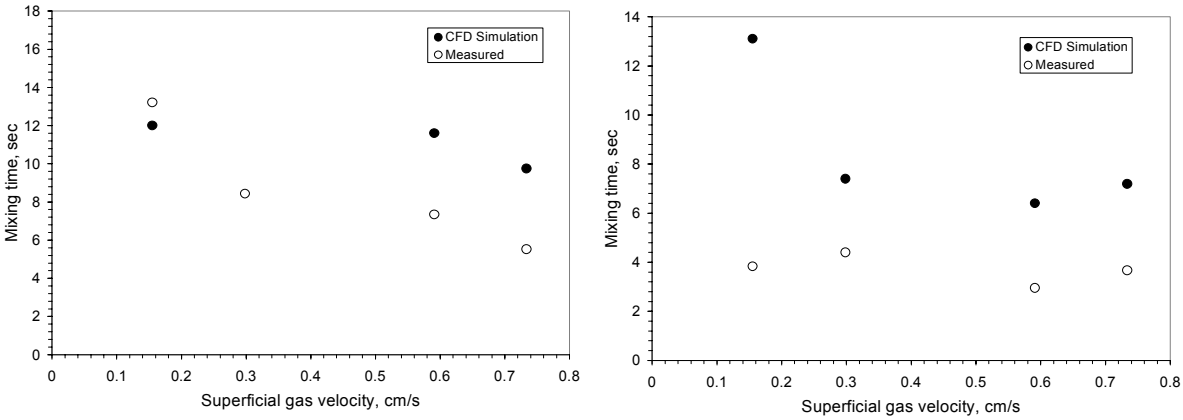

(a) H/D=4.5 (b) H/D=2.25

FIG. 4. Comparison of mixing time predicted using CFD models and radiotracer measurements.

Liquid phase mixing in rectangular bubble columns was studied using CFD simulations and radioactive tracer measurements. The CFD model was found to capture the sensitivity of mixing time to superficial gas velocity and H/D ratio. The mixing time definitions used for evaluating mixing time in CFD simulations and experiments needs to be studied rigorously to obtain a quantitative agreement. In addition, the role of lift forces on dynamics and therefore on mixing should be critically evaluated especially by considering taller columns. The present work was quite useful to understand the intricacies of radioactive tracer measurements in bubble columns and the correspondence between what is seen by the detectors and by the CFD model. The rigorously validated CFD models with radioactive tracer techniques can be extended to study liquid phase mixing in industrial bubble columns.

Jet Mixer

In chemical process industry, stirred vessels are frequently employed to carry out homogeneous as well as heterogeneous reactions, either in a batch or continuous mode. The function that an impeller has to perform in a stirred reactor range from simple homogenization, to the very complex: gas dispersion, solid suspension, heat transfer, or any combination of the above. It may also happen that the operation of the stirred reactor is controlled by the rate of chemical reaction (homogeneous or heterogeneous) taking place in it. If the jet mixer is operated in a batch manner, then the mixing process can be characterized by “mixing time”, whereas in a continuous system the mixing process can be characterized by “residence time distribution”. Thus as a starting point it was thought desirable to carry out mixing time studies [15,16,17] in jet mixers experimentally (using radiotracers) as well as numerically (using computational fluid dynamics, CFD).

Experiments for mixing time measurements were carried out in a 0.5 m diameter tank filled to height equal to tank diameter. Tap water was used as the working fluid. The details of the experimental set-up are depicted in Fig. 5. ^{113m}In (Half-life: 1.65 hours, gamma energy: 392 keV) was selected as a tracer. A series of experiments was carried out and about 10 mCi activity was used in each run. The tracer was instantaneously injected into the tank and its concentration was recorded at three different axial locations using collimated scintillation detectors (D1, D2, D3) as shown in Fig. 5.

Two typical measured tracer concentration curves recorded as a function of time are shown in Fig. 6a and 6b. Experiments were carried out at different jet velocities (flow rates) and different positions of the jet in the tank.

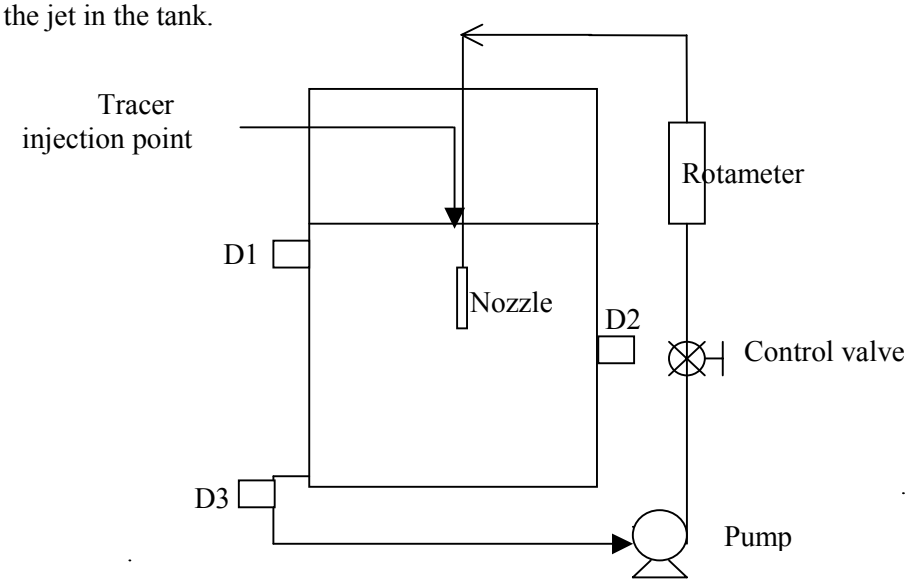

FIG. 5. Schematic diagram of experimental setup for mixing time measurements in jet mixer(D1, D2, D3: Radiation detectors.

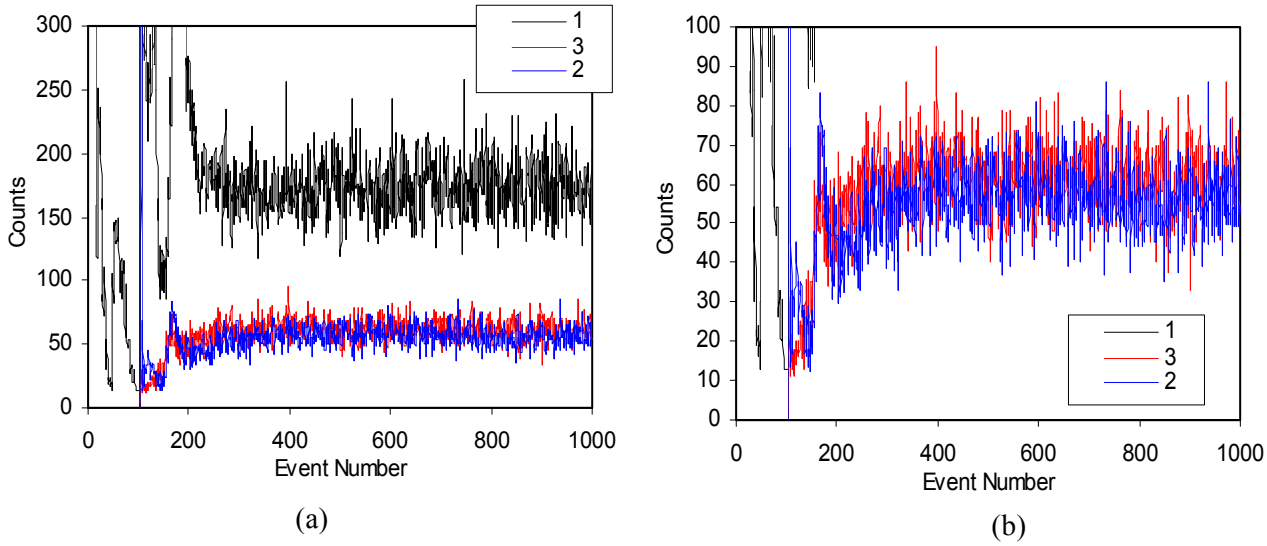

FIG. 6. Typical measured tracer concentration curves (1:D1, 2: D2, 3: D3).

The CFD model enables the solution of Reynolds transport equations together with a turbulence model to close the set of equations. In the present work, a standard 'k-ε' model was employed to close the Reynolds transport equations. The transport equations in all the three directions and the 'k' and 'ε' equations were written in a generalized form as:

$$\frac{1}{r}\frac{\partial}{\partial r}(rV_r\phi)+\frac{1}{r}\frac{\partial}{\partial \theta}(V_\theta\phi)+\frac{\partial}{\partial z}(V_z\phi)=\frac{1}{r}\frac{\partial}{\partial r}\left(r\Gamma_{eff}\frac{\partial\phi}{\partial r}\right)+\frac{1}{r}\frac{\partial}{\partial \theta}\left(\frac{\Gamma_{eff}}{r}\frac{\partial\phi}{\partial \theta}\right)+\frac{\partial}{\partial z}\left(\Gamma_{eff}\frac{\partial\phi}{\partial z}\right)+S_\phi \qquad (3)$$

where, ϕ stands for a generalized transport variable. For the three equations of motion, it stands for V_r, V_θ, and V_z. For the 'k-ε' model it stands for 'k' and 'ε' respectively. Γ_{eff} represents eddy diffusivity plus molecular diffusivity.

The solution of the above set of equations results into the prediction of mean velocity and turbulence levels throughout the tank. This can then be used to solve the conservation equation for an inert tracer, which was written as:

$$\frac{\partial C}{\partial t}+\frac{1}{r}\frac{\partial}{\partial r}\left(rV_rC\right)+\frac{1}{r}\frac{\partial}{\partial \theta}\left(V_\theta C\right)+\frac{\partial}{\partial z}\left(V_zC\right)=\frac{1}{r}\frac{\partial}{\partial r}\left(\Gamma_{eff}r\frac{\partial C}{\partial r}\right)+\frac{1}{r}\frac{\partial}{\partial \theta}\left(\Gamma_{eff}\frac{\partial C}{r\partial \theta}\right)+\frac{\partial}{\partial z}\left(\Gamma_{eff}\frac{\partial C}{\partial z}\right)+S_C \quad (4)$$

The concentration profiles can be obtained by the solution of equation (2) with the help of predicted mean velocity field and eddy diffusivity levels. The mean velocity field determines the convective transport of mass and eddy diffusivity determines the dispersive transport of mass. The concentration profiles can then be used for the estimation of the mixing time.

The above equations were discretized by control volume formulation on a staggered grid arrangement. Power law scheme was used for discretization. SIMPLER algorithm [14] was used to obtain the velocity, pressure and turbulence fields. The discretized equations were solved by TDMA algorithm. The jet entry into the tank was simulated by specifying the number of grids occupied by the nozzle. At the location of the nozzle, the jet velocity was resolved in the three directions, r, θ, and z, and was specified as a boundary condition. The equations were solved till the normalized mass residue fell below 0.005. The conservation equation for the inert tracer (Equation 2) was solved by implicit method. The time step was chosen to be very small initially, when the concentration gradients are very large. The initial dimensionless time step was 0.0025 and later on it was slowly increased to 0.25. The simulation results were found to be independent of the time step. With this time step, the solution for say 30 s of mixing simulation required about 2500 time steps. The addition of tracer pulse was simulated by specifying a very high value of concentration at the corresponding grid points. This acted as the initial condition for the solution of equation (2).

Initially, studies were carried out to investigate the effect of grid size. For this purpose, three simulations were carried out with 125,000 nodes, 216,000 nodes, and 343,000 nodes. The solutions took around 24 hrs, 40 hrs, and 65 hrs respectively on a P-III PC. It was observed that the concentration profiles predicted by simulations with 125,000 and 216,000 nodes differed substantially. However, the change from 216,000 to 343,000 was found to be very slight. Thus, for all future studies 216,000 (60 x 60x 60) nodes were employed. This is the largest grid size ever employed for the jet mixing simulations; in fact, many of the stirred tank simulations also use a much smaller number of grid points. This was necessary to resolve the jet and its spread within the tank.

The predicted detector response from the CFD simulations is compared with the experimental measurements (for location 3) in Fig. 7. The black line indicates the measured values and the red line indicates the predicted values. It can be seen clearly that the CFD simulations predict the trend correctly, but there is a clear mismatch between the predictions and experimental measurements. From this figure it is clear that the CFD model needs to be refined further and also tested for other configurations of jet mixers. However, in order to do this, further experimentation is also needed. These experiments would serve as a validation for the CFD simulations. Additional experiments could have been carried out with radiotracers; however, the logistics of using radiotracers were not very convenient, especially, since the experiments were going to be used only for validation of CFD models. Thus, additional experiments were carried out with using sodium chloride solution as a tracer. The tracer input location was kept the same as that for radiotracer experiments (near the top liquid

surface). The conductivity of the solution in the tank was monitored with the help of conductivity probes [16,17,18].

Fig. 8a shows the comparison of experimental measurements of conductivity with the CFD simulations. These experiments and CFD modeling were carried out with the nozzle coming in from the sidewall, and at an angle of 45 degrees. It can be seen that, the predicted start of the concentration profile is earlier than that observed experimentally.

However, the peak value in the concentration profile is well predicted. At large value of time, the predicted concentration profile approaches the experimental curve. Therefore, the final mixing time predictions are reasonably good. These observations hint to the fact that the CFD simulations under predict the extent of turbulent dispersion. That is, the predicted values of the eddy diffusivity would be lower that that observed experimentally. This would be due to an under-prediction of the turbulent kinetic energy or over-prediction of the turbulent energy dissipation rate. This result also shows that the CFD model needs to be improved further. The likely reason for this could be the non-validity of the standard 'k-ε' model used in this work. In order to test this hypothesis, several sets of simulations were carried out by changing the value of the parameters in the 'k-ε' model. The 'k-ε' model contains three fitted parameters, namely, C_μ, C_1 and C_2. These values were changed and the sensitivity of model predictions was first tested. Finally, best set of values and predictions arising out of them are shown in Fig. 8b. It can be seen that this improves the predictions considerably.

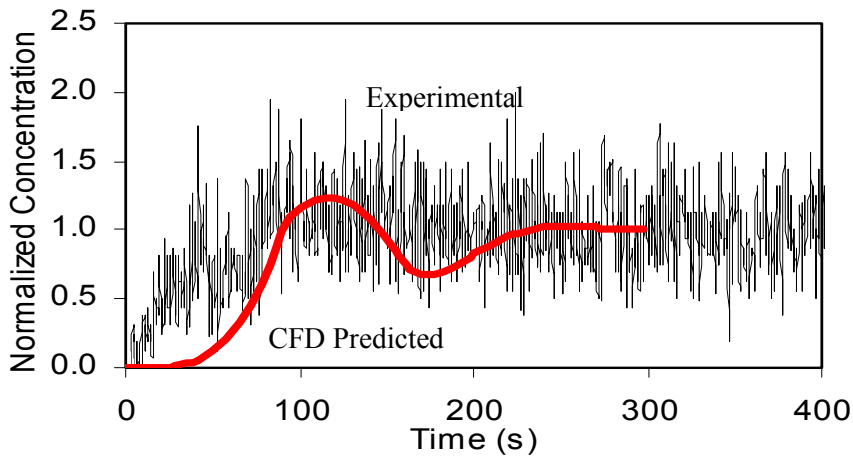

FIG. 7. Measured and predicted tracer concentration curves (radioactive).

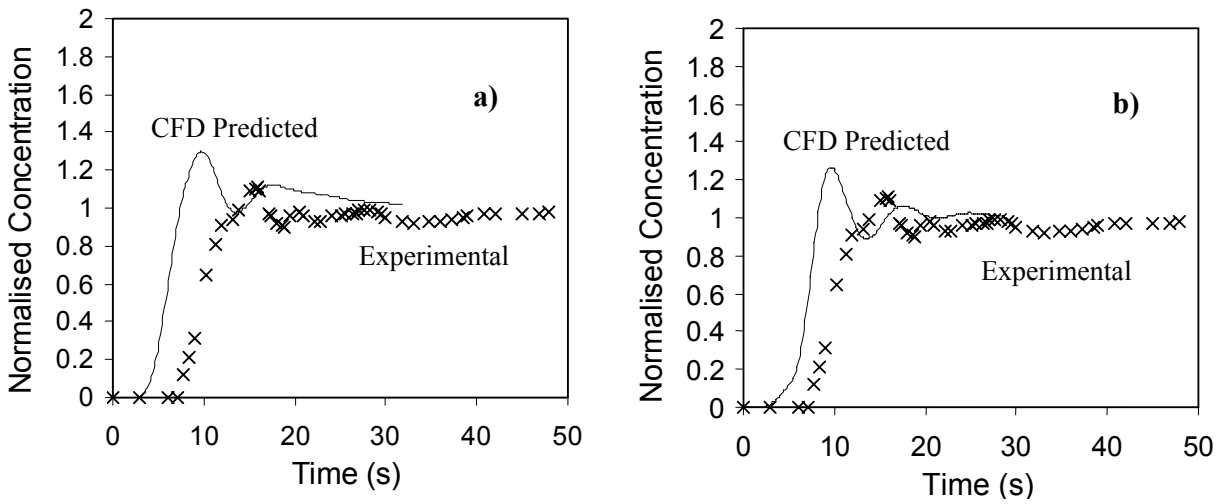

FIG. 8. Measured and predicted tracer concentration curves (chemical tracer).

Sludge Hygienization Research Irradiator (SHRI)

Irradiation of sludge is aimed at reducing the microbial load. Each element of liquid sludge should receive the appropriate minimum required dose while undergoing the irradiation process.

Liquid sludge irradiators may operate in batch or continuous mode. Radiotracer study in a liquid sludge hygienization research irradiator (SHRI) was performed. Details of the considered irradiator are shown in Fig. 9. The sludge in the irradiator is kept under constant circulation using an external circulation via a pump. Obviously the flow rate through the external circulation loop controls the fluid dynamics and mixing within the irradiator. Intuitively it can be said that higher the flow rate, better will be the mixing. However, higher flow rate requires higher energy consumption. In order to optimize the irradiator, it is essential to identify an optimum circulation flow rate, which will minimize the energy consumption without jeopardizing the mixing within the irradiator.

FIG. 9. Schematic of irradiator and source assembly.

Flow rate through the external loop is a gross parameter characterizing a mixing within irradiator. Local mixing and therefore the dosage received by the sludge will depend on the underlying fluid dynamics. In order to get some information about the underlying fluid dynamics, Pant *et al.* (2001) [19] have carried out a series of radiotracer studies. These experiments were carried out at three

different flow rates. Experimental technique was validated by comparing the values of flow rate obtained from the tracer response data with those from the flow meter. Typical experimentally observed tracer response curve is shown in Fig. 9 for the case with flow rate of 1 m^3/hr. The experimental data was interpreted using different compartmental models based on tanks-in-series and plug flow components with or without dead volume. Fig. 10 also shows model predictions in the form of smoother line. It can be seen that a proposed compartmental model leads to reasonable predictions of the residence time distribution. The fitted value of the dead volume obtained for the model for the considered case was about 7 %.

The types of model used by Pant et al. (2001) [19] are useful to simulate overall tracer response. However, these models are not able to provide any information about the local mixing. Applicability of these types of models is also restricted to the range of parameters studies in the experimental program. Extrapolation to different range is rather risky.

Computational fluid dynamics models, on the other hand, may provide detailed information about the local flow and mixing. The validated models may be used to extrapolate the experimental data. In this work, therefore, a CFD based model of flow and mixing in SHRI was developed.

A sludge used in SHRI may typically contain solids up to 1.5 %. However, the density of solids is not very different from water. Viscosity of the sludge is also almost same as that of water. Therefore, a pseudo-homogeneous model with effective viscosity and density is adequate to understand flow and mixing within SHRI. It is not necessary to treat the solids and liquid phases separately by invoking two-fluid model.

Standard Navier-Stokes equations may be used by considering sludge as constant density and viscosity fluid. Under the typical operating conditions, the flow is turbulent. It is necessary to use an appropriate turbulence model to represent additional turbulent stresses. Recently, Ranade, (2001)8 has discussed the guidelines for selecting turbulence models for simulating industrial flow processes in detail. Following those guidelines, a standard two-equation model, k–model was used in the present work.

It is necessary to first model the geometry and generates a suitable grid before solving the governing model equations. A commercial grid generation tool called GAMBIT14 was used to model the geometry and to generate the grid. During the course of normal operation, SHRI vessel is not completely filled with sludge. In the computational model, solution domain was considered only up to the operating liquid level. The incoming flow was assumed to be distributed evenly over the cross section of SHRI vessel. Constant velocity inlet boundary condition was used at the top surface. In order to reduce the computational load, tubes containing radioactive source were modeled as square bars. Computational grid used in the present work is shown in Fig. 11a. Preliminary numerical experiments using Commercial CFD solver, FLUENT 4.5 (1997)14 were carried out to ensure the adequacy of the generated grid.

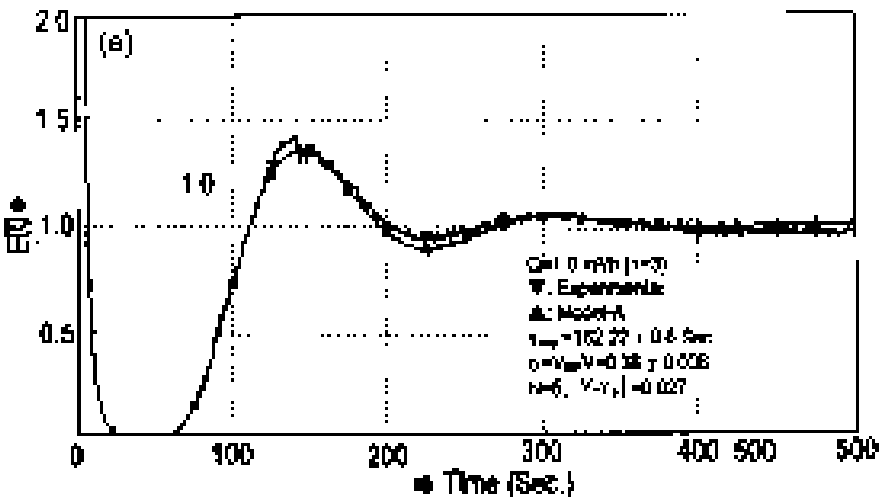

FIG. 10. Typical tracer response curve (Pant et al. 2001).

The flow results obtained from the CFD model were then used to carry out simulations of tracer response experiments. It was assumed that addition of a tracer does not affect the underlying flow field. Therefore, while simulating mass balance equation for the tracer mass fraction, the momentum equations were not solved. A square pulse of a tracer was introduced in the computational model for the duration of 0.5 s. It must be noted that since the SHRI is a closed system, the tracer mass fraction out going from SHRI re-enters SHRI after the delay time of the process piping outside SHRI. In the present work, such a delay time was neglected since it was much smaller than the mean residence time. Equivalence of mass fractions of entering and outgoing fluids was mapped on to FLUENT [14] using the 'user defined subroutine'.

Simulations were then carried out to understand local and overall mixing in SHRI under different circulation flow rate. Typical results in the form of contours of mass fraction of tracer are shown in Fig 11b.

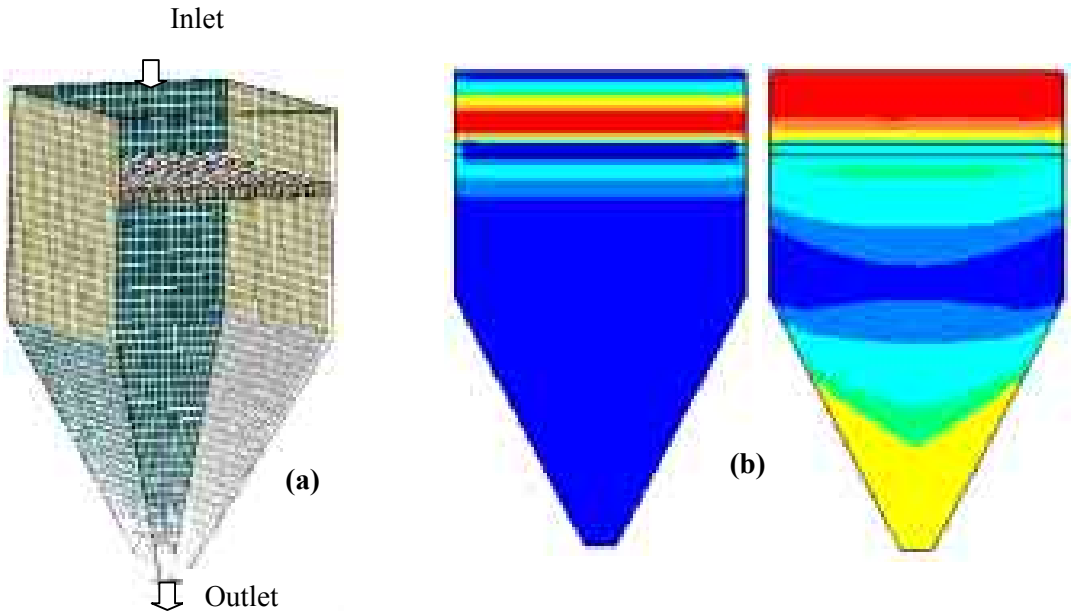

FIG. 11. a. Solution domain and computational grid; b. Predicted flow field (contours of velocity magnitude and turbulent viscosity).

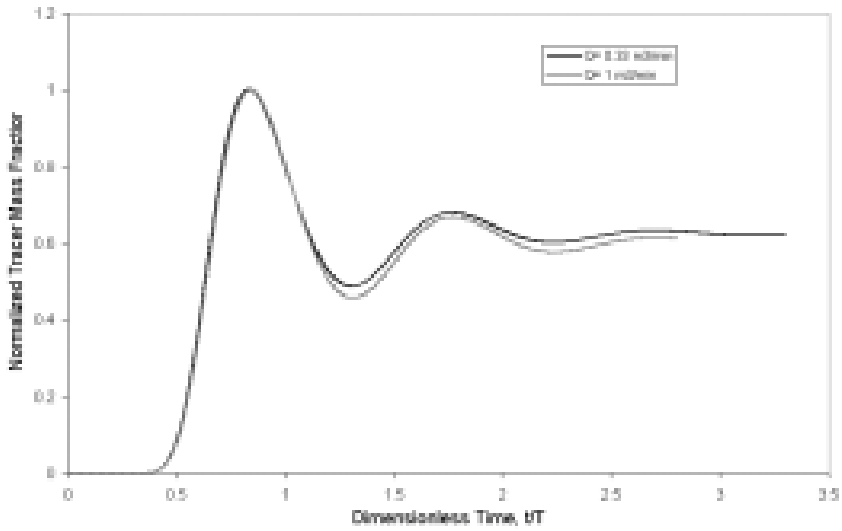

FIG. 12. Normalized tracer distribution curves predicted by CFD model.

Simulations indicate that about three circulations through the reactor lead to reasonable mixing within the contents of the vessel. This result agrees with the tracer response studies (Fig.9). CFD simulations were also used to calculate variation of tracer mass fraction in the outlet with time. The predicted variation can then be compared with the experimental tracer response studies. Typical predicted C-curve from the CFD model for the case of 1 m^3/hr and 0.33 m^3/h are shown in Fig. 12. It must be noted that since the duration of the tracer pulse was kept constant for both the simulations, actual tracer amounts injected into SHRI vessel were different for the two cases. In order to bring the predicted responses on uniform basis, the predicted values were normalized using the maximum tracer concentration observed during the mixing simulations. The normalized tracer concentration response was plotted against the dimensionless time normalized by residence time. It can be seen that normalized tracer responses for the two values of circulation flow rate are almost same.

Comparison of Fig. 10 and Fig.12 indicate that the tracer response curves predicted by CFD model agree quite well with the experimental data. For the case of circulation flow rate of 1 m^3/hr, CFD model predicts the average circulation time based on consecutive peaks observed in the predicted results as 174 s. Considering the actual mean residence time based on the volume of the solution domain and flow rate, the results indicate the dead volume of about 7.8% which agrees quite well with the value reported by Pant *et al.* (2001)[19] using a compartment model.

CFD model and predicted results can be used to track the history of each fluid element within SHRI vessel. Since the dosage received by the fluid element is a function of distance from the source, effective dosage received by any fluid element may be calculated by integrating the received dosage over a trajectory of a fluid element till it leaves the SHRI vessel. Such a tool will allow reactor engineering to optimize the location of inlet and outlet entry nozzles as well as location and configuration of radioactive source tubes. CFD model may also be used to evaluate newer modes of operation like a reverse flow SHRI. Trajectories of solid particles may also be simulated within the CFD framework in order to examine possible accumulation of solids in the regions of low velocity (dead volume). The present work and the results obtained therein open up several possibilities for performance enhancement of SHRI.

Flow and mixing in a sludge hygienization research irradiator (SHRI) was modeled using computational fluid dynamics. Standard k-ε model was used to simulate turbulent flow within SHRI. Fluid dynamics of SHRI was simulated at different flow rates through the external circulation loop. Residence time within the external loop was assumed to be negligible compared to the residence time in the SHRI vessel. Simulated tracer response curves agree quite well with the experimental tracer curved measured by Pant *et al.* (2001)[19]. CFD model and predicted results can be used to track the

history of each fluid element within SHRI vessel. Since the dosage received by the fluid element is a function of distance from the source, effective dosage received by any fluid element may be calculated by integrating the received dosage over a trajectory of a fluid element till it leaves the SHRI vessel. Such a tool will allow reactor engineering to optimize the location of inlet and outlet entry nozzles as well as location and configuration of radioactive source tubes.

3. RESIDENCE TIME DISTRIBUTIONS: RADIOTRACER MEASUREMENTS AND CFD SIMULATIONS

Continuously operating chemical process systems (reactors) are designed to have either plug flow or mixed flow conditions. But real systems never follow the ideal flow behavior. If the deviation from the ideal flow behavior is considerable then it has a direct effect on the process conditions (efficiency) and ultimately on the product quality. The problems of non-ideal flow are intimately tied to those of scale-up. Often the uncontrolled factors in scale-up are the magnitudes of the non-ideality of flow. Ignoring these factors may lead to gross errors in design. The formation of stagnant regions, channeling or short-circuiting causes the non-ideal flow in process equipment.

If we know precisely what is happening within the reactor, that is complete velocity distribution map for the fluid, then we are able to predict the exact behavior of a reactor. Though fine in principle, the complexities present along with flow made it difficult to used this approach. The second approach developed by earlier workers (design engineers) is less ambitious and easy. They have measured the distribution of residence time of flowing fluid. It is evident that element of fluids taking different routes through the reactor may require different lengths of time to pass through the reactor. The distribution of these times for the stream of fluid leaving the reactor is called the residence time distribution (RTD) of fluid. This information is used to identify malfunctioning and to estimate the degree of deviation from the ideal flow behavior [6]. The residence time distribution is determined easily and directly by a widely used method, stimulus response experiment.

The RTD study is unsuccessful to provide the detail information about the hydrodynamics present within reactor. Hence, in order to improve the performance of the reactor the entire flow field within the reactor must be known. The recent development in turbulence models and computational resources facilitate design engineers to use the computational fluid dynamic based models to know complete velocity distribution map of the fluid in reactor.

Pilot-Scale Continuously Stirred Tank Reactors

A continuously stirred tank reactor (CSTR) is considered to be the one in which there is uniform concentration throughout the reactor and the entire contents are well mixed. The flow behavior in a stirred vessel is quite complex. Any channeling or bypassing occurring in the flow or existence of dead zones is indicated in the RTD curve. The residence time distribution studies in stirred tanks provide a good insight into the flow behavior of stirred tanks.

A radiotracer study was carried out to measure the residence time distribution of fluid (water) in a pilot-scale CSTR with an objective to characterize the mixing and flow behavior of the reactor; and to validate a developed CFD model. The schematic diagram of the CSTR and experimental set-up is shown in Fig. 13a. The reactor consists of a flat bottom acrylic cylindrical tank of 30 cm internal diameter and a pitched blade turbine type agitator of 10 cm diameter. The speed of the agitator is controlled by a motor coupled with a variable speed drive. The agitator produces downward flow. Tap water was used as a process fluid and the liquid height in the tank was kept equal to the diameter of the tank.

RTD measurements were carried out at two different flow rates (3 liter/min. and 16 liter/min.) and four different agitator speeds (50,100, 200 and 400 RPM). Bromine-82 as ammonium bromide was used as a tracer and about 10-20 MBq (200-500 μCi) activity was used in each run. The tracer was instantaneously injected into the tank from top using a syringe and monitored at the outlet of the tank using a collimated scintillation detector as shown in Fig. 13a.

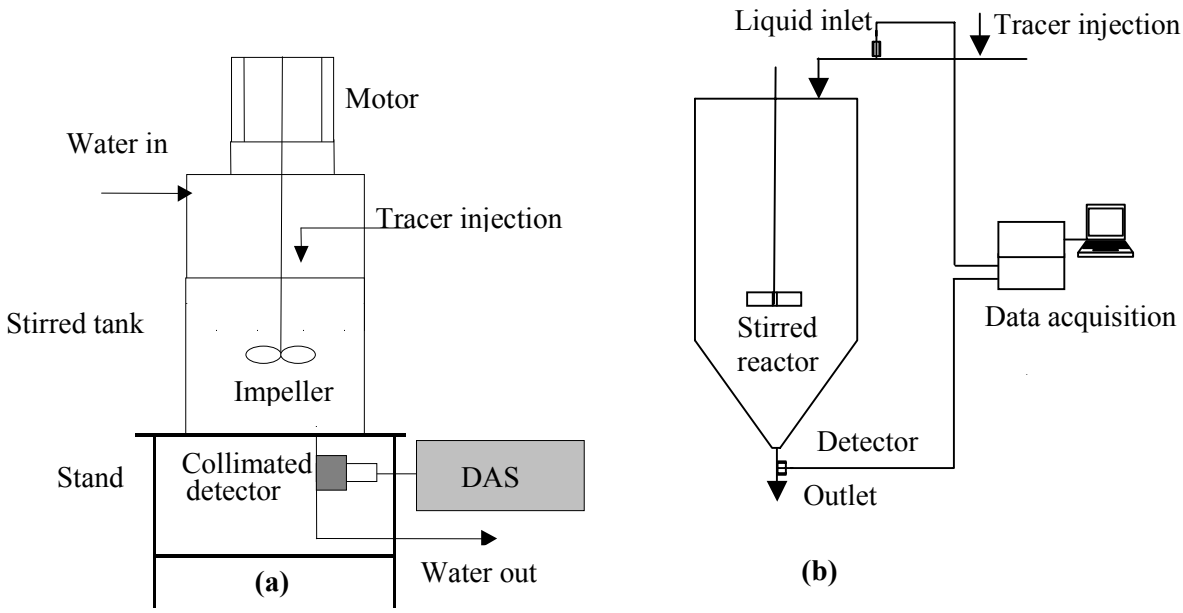

FIG. 13. Schematic diagrams of pilot-scale CSTRs and experimental set-up for RTD measurements.

The measured tracer concentration curves were treated and analysed using a standard RTD analysis software [7]. As a conventional approach to characterize the flow behavior of the reactor, simple analytical tanks-in-series model was used to simulate the experimentally measured RTD curves and the results are given in Table 1. A typical plot of measured and tanks-in simulated RTD curves is shown in Fig.14**.** It is observed that the value of the model parameter i.e. tank number (N) is slightly less than one indicating bypassing of a small fraction of the fluid from the reactor without proper mixing. However, no attempt was made to quantify the bypassed fraction in the present work. Poor agreement was observed between theoretical (τ_{Theo}) and experimentally determined mean residence times (τ_{Exp}), which may be due to bypassing.

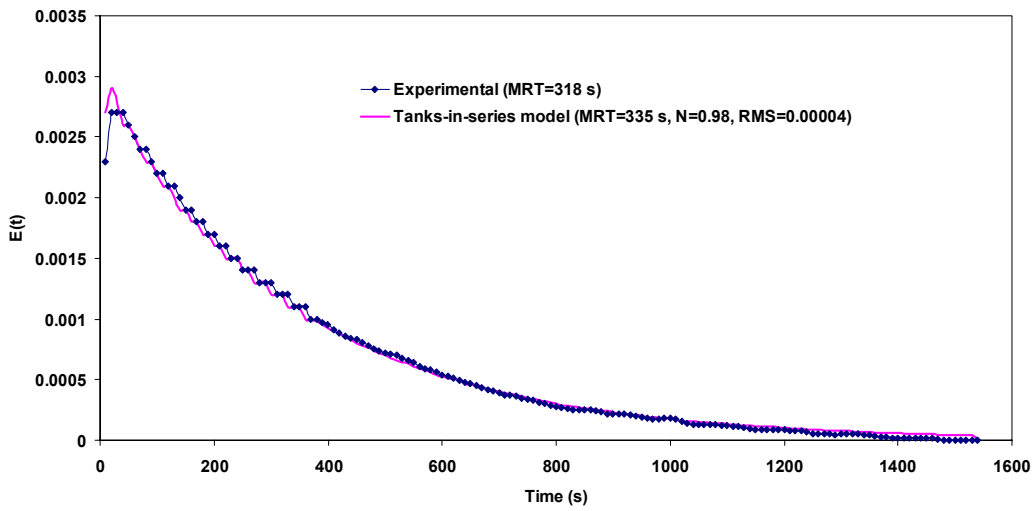

FIG. 14. Comparison of experimental and model tanks-in-series with backmixing model simulated RTDs (Flow rate= 3 lpm, Impeller speed=400 rpm).

A CFD model Patwardhan (2001) [20] was developed and used to characterize the hydrodynamics and predict the RTD of the fluid in the reactor. In order to validate the developed CFD model and visualize the flow in the reactor, the CFD predicted and experimentally measured RTD curves were compared. Two representative plots showing comparisons of CFD and experimentally measured RTDs are shown in Fig. 15, Fig. 16 and Fig. 17. Fairly good agreement is observed between the two RTD curves at 3 lit/min. flow rate and 400 rpm agitator speeds (Fig. 17). However, the agreement is rather poor at other flow rates and agitator speeds (Fig. 15 and Fig. 16). In most of the CFD predictions, high intensity of tracer concentration is observed in the beginning of the RTD curves, which indicates bypassing of trace. However, the bypassing is absent in experimentally measured RTDs. The experiments and CFD simulations were repeated, but similar results were obtained. The mean residence times were also determined from the CFD predicted RTD curves and are given in Table 1. The agreement is not good between experimentally (τ_{Exp}) measured and CFD predicted mean residence times (τ_{CFD}), probably due to bypassing shown in CFD predictions.

The poor agreement between measured RTD and predicted by CFD indicated that the CFD models is not suitable for prediction of flow behavior of the investigated CSTR and could not be considered as validated. Therefore the CFD models needs to be revised/improved before it is used for flow behavior prediction.

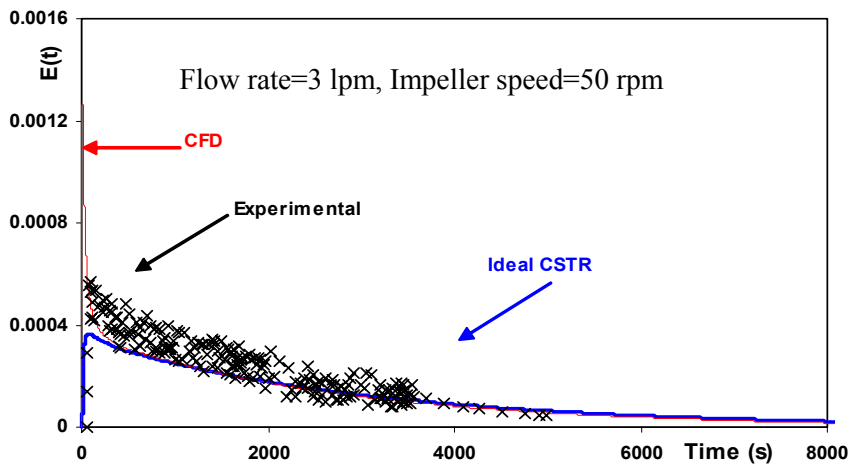

FIG. 15. Experimental and CFD predicted RTD curves.

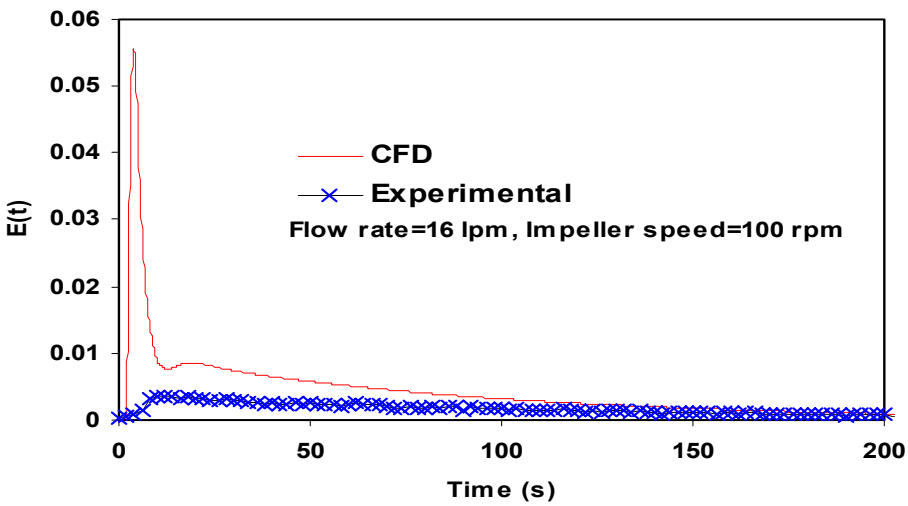

FIG. 16. Experimental and CFD predicted RTD curve.

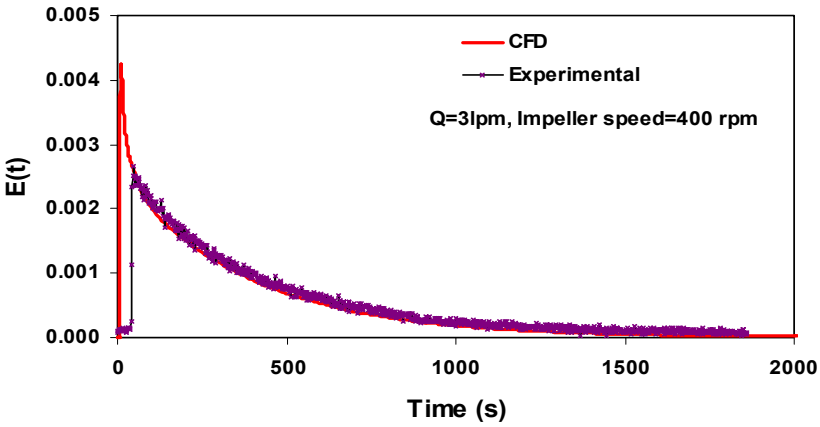

FIG. 17. Experimental and CFD predicted RTD curves.

TABLE I. RESULTS OF THE RTD STUDY IN A PILOT SCALE CSTR.

Sr. No.	Flow rate (lpm)	Speed (RPM)	τ_{Theo} (s)	τ_{Exp} (s)	τ_{CFD} (s)	Tanks-in-series model		
						τ_{Model} (s)	No. of Tanks	RMS
1	3	50	420	409	337	429	0.97	0.00008
2	3	100	420	310	-	333	0.96	0.00011
3	3	400	420	326	368	348	0.96	0.00007
4	3	800	420	326	-	354	0.88	0.00019
5	16	50	78.8	127	-	121	0.95	0.00021
6	16	100	78.8	87	74.3	99	0.89	0.00047
7	16	200	78.8	111	-	112	0.89	0.00026
8	16	400	78.8	95	-	100	0.95	0.00014
9	16	800	78.8	96	-	99	0.91	0.00032

Another radiotracer study was carried out to measure the RTD of process fluid (water) in a bigger scale, unbaffled continuous stirred reactor of 60 cm diameter having conical bottom and equipped with 4-blade paddle impeller using radiotracer technique[21]. Reactor diameter was 600 mm and the height of the process fluid was also maintained to be 600 mm during the experiments. A 4-blade paddle impeller of 176 mm diameter with standard dimensions fitted on a shaft of 34 mm diameter was located at a height of 260 mm (impeller bottom clearance) from the bottom of reactor. A D.C. motor with speed regulator was used to rotate the impeller. Schematic of the experimental set-up used in the present work is shown in Fig. 13b. ^{99m}Tc as sodium pertechnatate was used as a radiotracer

and about 20 MBq activity was used in each test. The tracer was instantaneously injected into the feed pipe and monitored at the inlet and outlet of the reactor using collimated NaI(Tl) scintillation detectors connected to a data acquisition system. The experiments were carried out for two liquid flow rates (5 lpm and 10 lpm) and for three impeller speeds (100, 200 and 300 RPM).

The recorded RTD data were treated and analysed and mean residence times were determined. The RTD curves were simulated using Tanks-in-series with backmixing model and model parameters (backmixing ratio, f; number of tanks, N and mean residence time were obtained. A representative plot showing comparison of experimental and model simulated curves is shown in Fig. 18. The comparison shows good agreement between experimental and model predicted results. The predicted residence time using tank in series model was 973 seconds.

Fig. 19a and Fig. 19b shows the solution domain and velocity field distribution within the stirred reactor respectively. The face average outlet concentration of tracer was written in an output file for each time step. Fig. 20 shows the CFD predicted RTD curve at the outlet of reactor. The mean residence time predicted by CFD based model was 770 seconds, which does not agrees well with the experimentally determined value (980 s).

In order to evaluate the potential of CFD tools, the flow within the continuous stirred reactor was solved by a multiple reference approach using a commercial CFD solver FLUENT (1997) [14]. The solution domain, to solve the flow, was constructed in preprocessor GAMBIT [14]. The solution domain contains about hundred thousand cells. Preliminary simulations indicated that the constructed computational grid was adequate for the purpose of simulation of bulk flow and mixing.

Standard k-ε turbulent model was used and respective flow equations were solved with appropriate boundary conditions after the flow was completely developed. The injection of tracer was considered as an impulse and was represented by an impulse of width equal to one second. The tracer transport equation was solved more than three times of experimentally measured mean residence time.

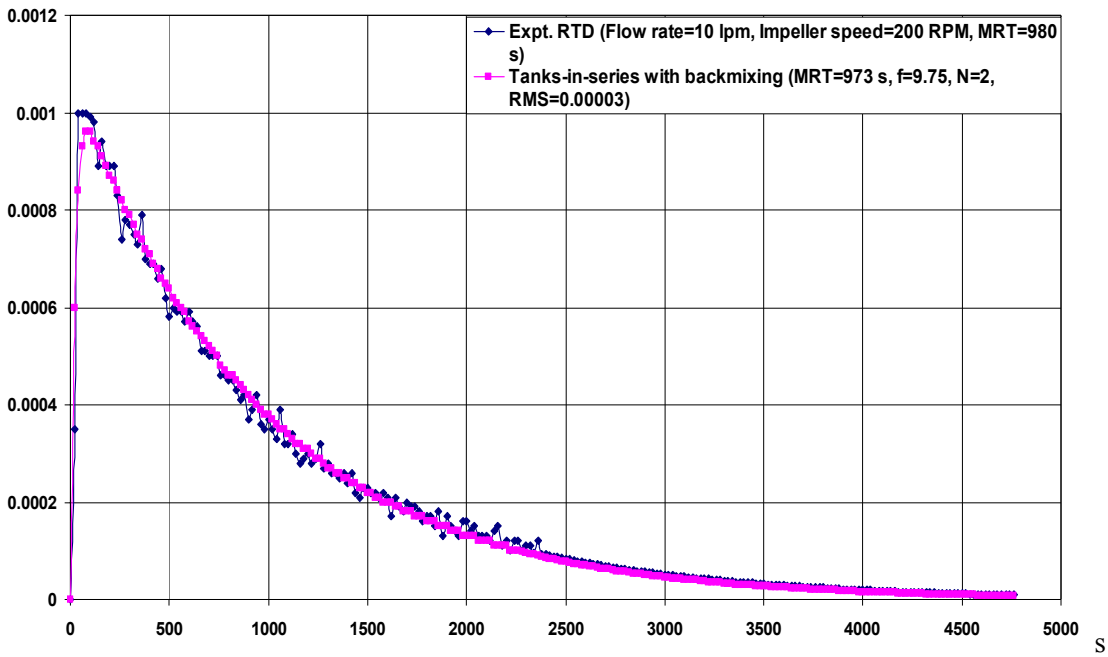

FIG. 18. Comparison of experimental and tanks-in-series with backmixing model simulated residence time distribution curves.

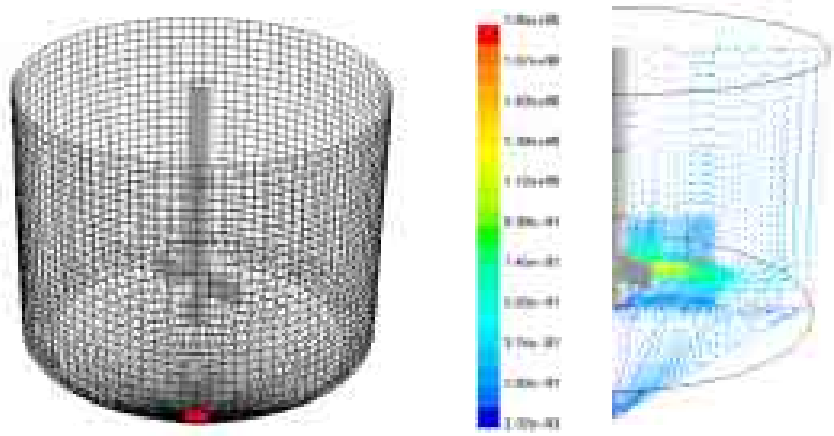

(a) Computational grid *(b) Velocity vectors*

FIG. 19. CFD grid and generated velocity vectors.

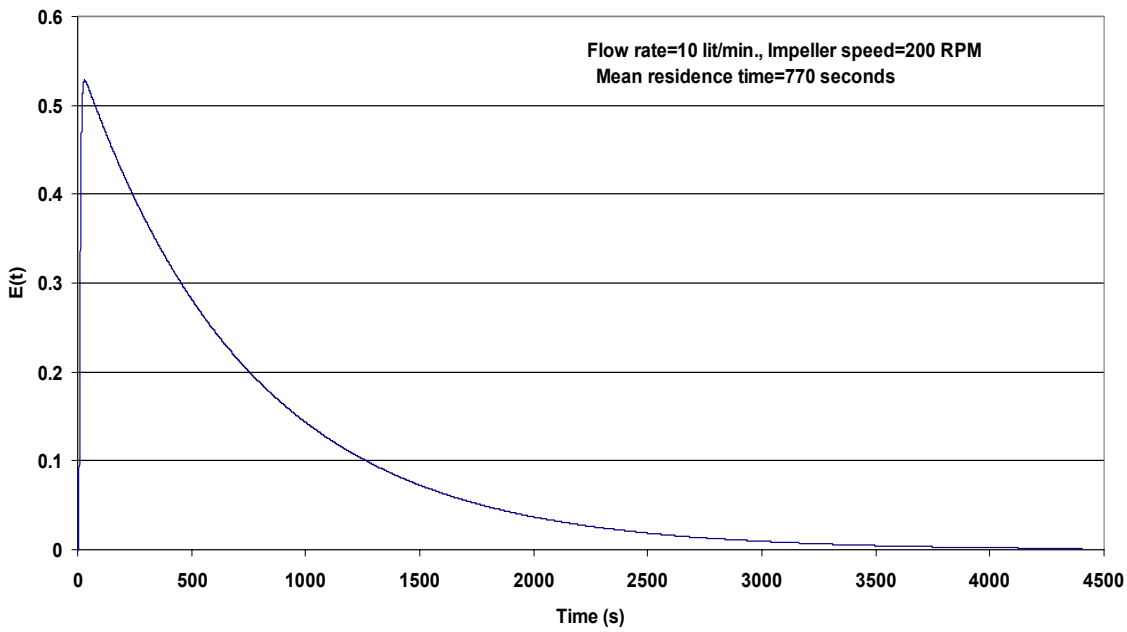

FIG. 20. CFD model simulated RTD curves

Experimentally measured RTD of liquid phase in CSTR was described by a tank in series model with two well-mixed tanks connected in series and a dead volume. The model fits very well with the experimental curve for given model parameters.

A CFD based model was developed and CFD simulated RTDs were compared with the experimental results. The CFD predicted mean residence time, 770 seconds, was not in agreement with the experimentally measured residence time. The results indicate that the CFD model needs to be improved and revalidated in order to obtain more accurate and satisfactory results.

Mixer-Settler

Liquid-liquid extraction (LLE) is a key operation in hydrometallurgical recovery of copper, zinc, uranium *etc*. from ore leach solutions. Among various equipments being practiced for LLE,

mixer settler systems are preferred choice because of their certain advantages, such as ease of handling of large liquid volume at high flow rates, operating flexibility, easy scale-up and adequate combination of agitation with sufficiently long residence time. In a pump-mix mixer settler, the mixer is designed such that the interstate pumping is taken care of by the mixer impeller, resulting in capital saving and prevention of emulsions due to centrifugal pump. Shenoy *et al.* (1997) [22] and Pant (2000) [23] and earlier carried out radiotracer investigations in a pilot-scale mixer and characterized the general hydrodynamic behavior of the mixer. Based on the results of the studies, a semi-industrial scale mixer settler was designed and it was desired characterize the mixing by conventional RTD analysis approach [22, 23]. In addition to this, it was also desired to develop a CFD model, validate it and use the same for performance prediction of the mixers. The results of CFD modeling and RTD analysis will enable process engineer to develop an industrial scale mixer-settler system.

In the present study, liquid residence time distributions were measured in two pump-mix mixers, connected in series, at different combination of parameters like impeller diameter, impeller clearance, speed and flow rate, using radiotracer technique. All the experiments were carried out on single-phase fluid i.e. water.

The schematic diagram of the mixer-settler system and the experimental set-up is shown in Fig. 21. Each mixer is a cylindrical tank of 700 mm diameter (D), 700 mm and 0.269 m^3 volume. The mixers had fluid inlet at the bottom and discharge from top. Two top shrouded turbine type impellers are of sizes 350 mm (0.5D) and 280 mm (0.4D) were used in the present study. A variable speed drive was used to control the speed of the impeller. A series of experiments were carried out to measure liquid RTDs at different operating conditions such as impeller speed flow rate and impeller clearance for both the impellers. Bromine-82 as ammonium bromide was used as a tracer and about 1.0 mCi (37 MBq) activity was used in each run. The tracer was instantaneously injected as an impulse at the inlet of the first mixer and monitored at inlet and outlet of both the mixers using a collimated NaI (Tl) scintillation detector, coupled to a computer controlled data acquisition system (DAS).

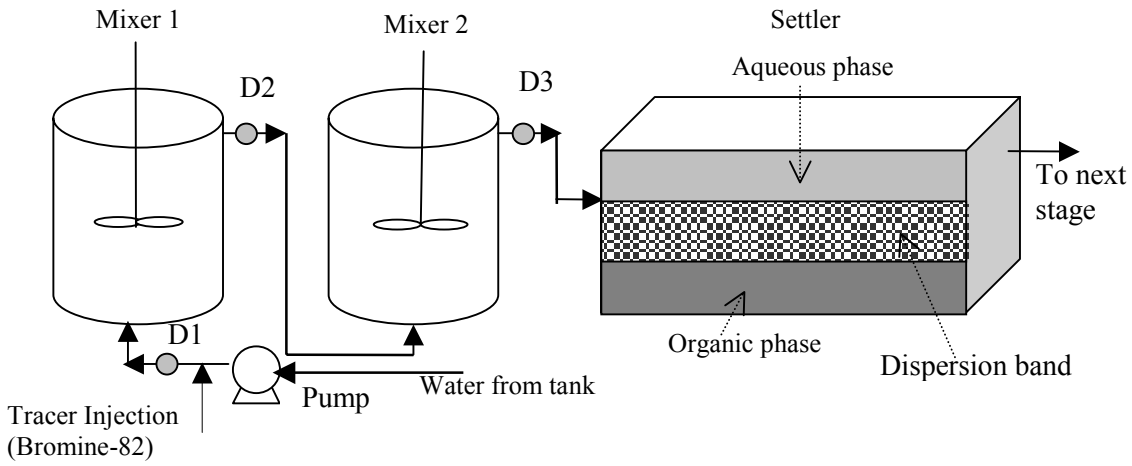

FIG. 21. The schematic diagram of the mixer-settler system and the experimental set-up.

The data recorded RTDs were treated and analysed using standard RTD analysis software [7]. Two representative RTD curves monitored at the outlet of the two mixers are shown in Fig. 22. From the treated RTD curves, mean residence times were determined. It is observed that the MRT values determined from the measured curves are much higher than the theoretical mean residence times. The reasons for this discrepancy were investigated and it was concluded that improper calibration of the flow meter installed in the flow line was responsible for this discrepancy. Therefore, it was decided to check the calibration with the supplier of the flow meter. The RTD curves were simulated simple tank-in-series model and model parameters such as mean residence times and tank numbers (N) were estimated and are shown in Table 2 and Table 3. Poor agreement is observed between experimentally determined MRTs and model predicted MRTs. The causes of this discrepancy are being investigated. The plots showing the comparison of experimentally measured and model simulated RTDs at the outlet of mixer 1 and mixer 2 is shown in Fig. 23 and Fig. 24, respectively.

Two representative plots showing comparison of CFD simulated and measured RTDs at the outlet of both the mixers are shown in Fig. 25 and Fig. 26. The mean residence time values predicted by CFD simulations are slightly lower than the experimentally measured values. Fairly good agreement is observed between experimentally measured and CFD simulated RTD curves. However, the preliminary results have been quite encouraging and at this stage it could be concluded that the CFD model is valid for flow visualization in mixers, however this needs to be confirmed by comparing CFD simulations at different operating and process conditions to that of the experimentally measured RTDs. Detailed CFD simulations for flow analysis of mixers are in progress.

TABLE II. EXPERIMENTAL CONDITIONS AND RESULTS OF THE RTD STUDY IN MIXER 1

Run No.	Experimental Conditions						Results of Analysis Mixer 1			
	Flow rate (m^3/h)	*Speed* (RPM)	*d/D*	*C/D*	*d* (mm)	τ_{Theo} (s)	τ_{Exp} (s)	*Tank-in-series model*		
								$\tau_{Model\ (s)}$	*N*	*RMS*
1	2	164	0.5	0.5	350	484	779	809	1.04	0.00004
2	2	164	0.5	0.5	350	484	635	689	0.99	0.00008
3	2	164	0.5	0.5	350	484	735	755	1.00	0.00002
4	4	164	0.5	0.5	350	484	348	374	1.00	0.00012
5	4	164	0.5	0.3	350	484	392	412	0.96	0.00017
6	2	164	0.5	0.3	350	484	1558	1645	1.00	0.00003
7	4	163.5	0.3	0.3	280	242	330	355	1.00	0.00007
8	4	205	0.3	0.5	280	242	416	464	0.92	0.00018

TABLE III. EXPERIMENTAL CONDITIONS AND RESULTS OF THE RTD STUDY IN MIXER 1 & 2

Run No.	Experimental Conditions						Results of Analysis Mixer 1 +Mixer 2			
	Flow rate (m^3/h)	*Speed* (RPM)	*d/D*	*C/D*	*d* (mm)	τ_{Theo} (s)	τ_{Exp} (s)	*Tank-in-series model*		
								$\tau_{Model\ (s)}$	*N*	*RMS*
1	2	164	0.5	0.5	350	968	1156	1137	2.00	0.00002
*2	2	164	0.5	0.5	350	968	1521	1397	1.66	0.00002
3	2	164	0.5	0.5	350	968	1183	1136	1.80	0.00002
4	4	164	0.5	0.5	350	968	491	493	2.14	0.00005
5	4	164	0.5	0.3	350	968	563	554	2.00	0.00008
6	2	164	0.5	0.3	350	968	2499	1995	2.00	0.00003
7	4	163.5	0.3	0.3	280	484	600	579	2.00	0.00007
8	4	205	0.3	0.5	280	484	699	663	1.76	0.00004

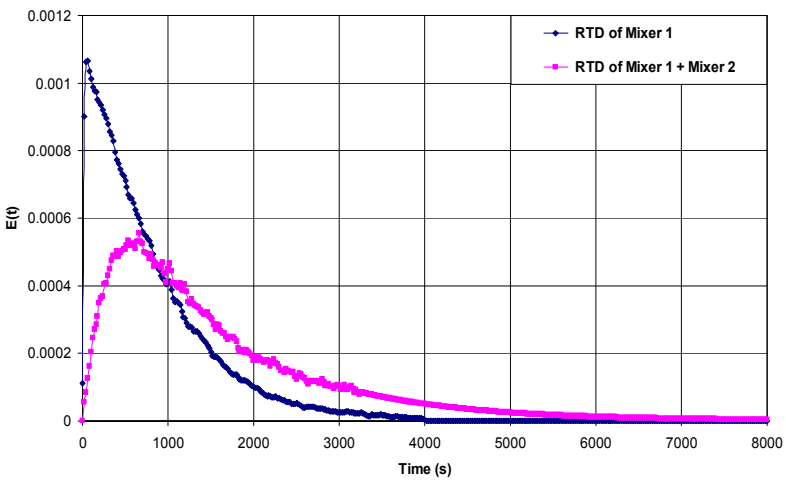

FIG. 22. Typical RTD curves recorded at the inlet and outlet of the mixers.

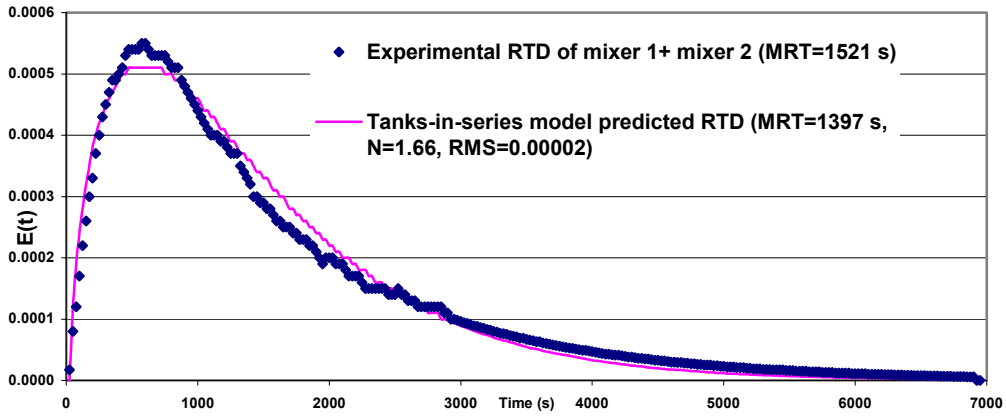

FIG. 23. Comparison of experimental and model simulated RTDs at the outlet of mixer 1 (Flow rate=2 m3/h, Impeller speed=164 rpm, d=350 mm d/D=0.5, C/d=0.5, d=350 mm).

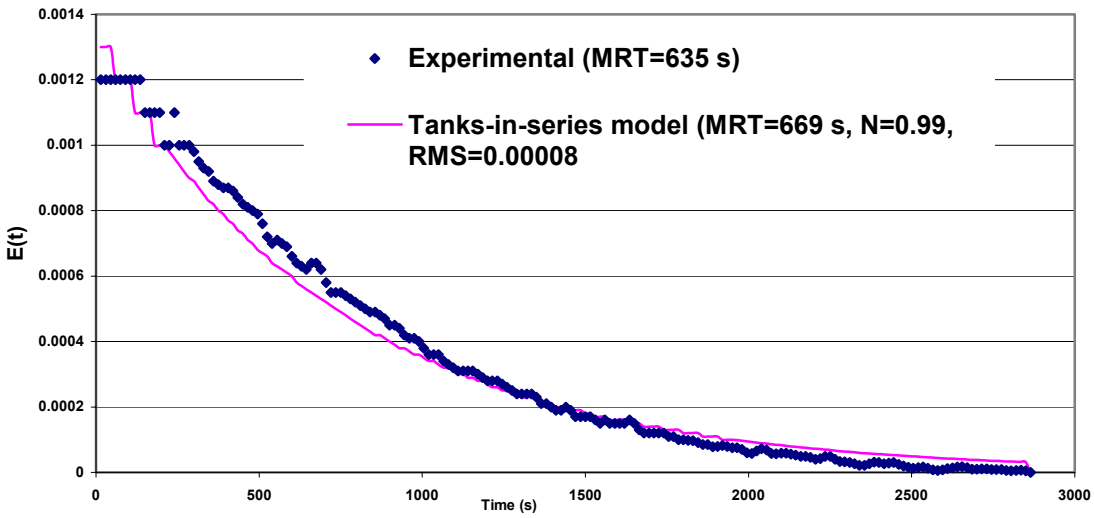

FIG. 24. Comparison of experimental and model simulated RTDs at the outlet of mixer 2 (Flow rate=2 m^3/h, Impeller speed=164 rpm, d=350 mm d/D=0.5, C/d=0.5, d=350 mm).

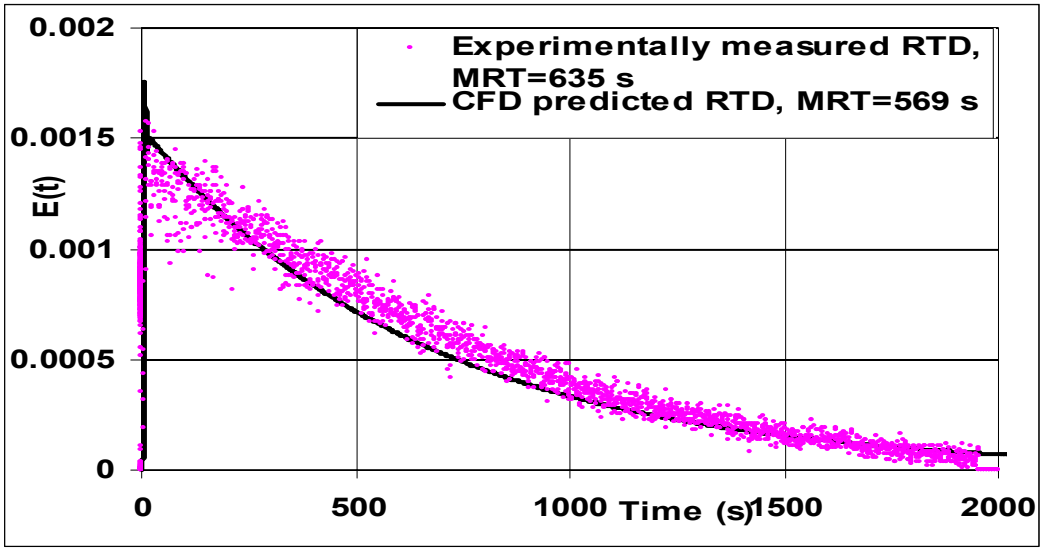

FIG. 25. Comparison of experimentally measured and CFD predicted RTDs at the outlet of mixer 1 (Flow rate=2 m^3/h, Impeller speed=164 RPM, d/D=0.5, C/D=0.5, d_{im}=350mm).

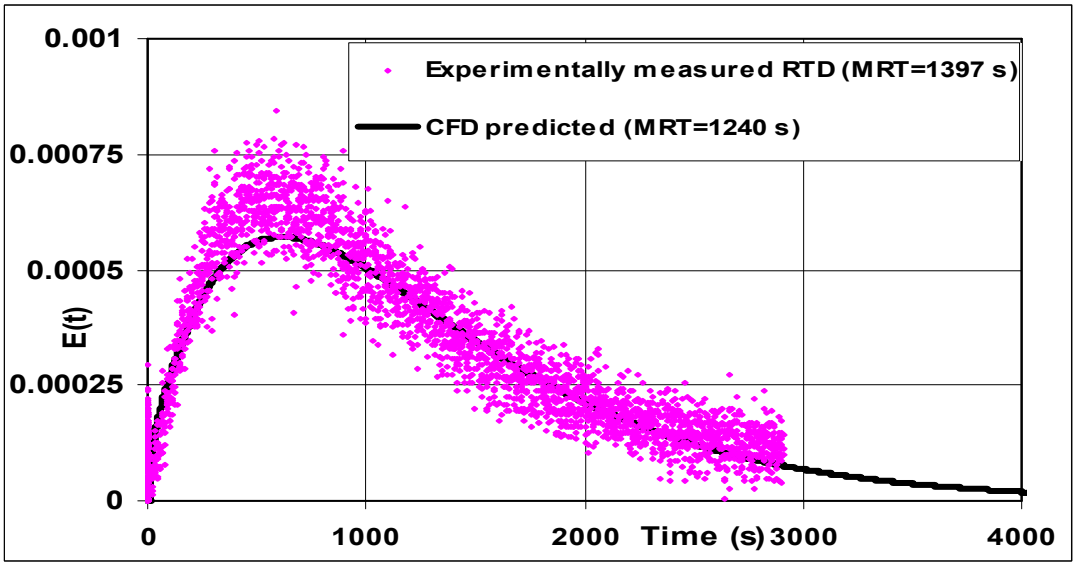

FIG. 26. Comparison of experimentally measured and CFD predicted RTDs at the outlet of mixer 2 (Flow rate=2 m^3/h, Impeller speed=164 RPM, d/D=0.5, C/D=0.5, d_{imp}=350mm).

Oxidation Reactor

For the production of PTA, paraxylene is oxidized by air in the oxidation reactor (a centrally stirred vessel) in the presence of acetic acid and catalyst. Mixture of organic phase (paraxylene) and aqueous phase (acetic acid+water) is introduced into the oxidation reactor in the lower portion from feed drum. Air is introduced into the reactor at 180-200^0 C. As the reaction of oxidation is exothermic, temperature in the reactor rises above 210° C. Oxidation results in the formation of some solid component which leaves the system along with liquid through an outlet pipe similar to the inlet pipe but at the upper portion of the reactor. Outlet material travels through crystallizers in which solids is further crystallized and is taken out for drying and liquid is recycled to the feed drum. Most of the material going into the vapor phase is condensed and fed back to the reactor. The schematic diagram of the reactor is given in Fig. 25.

The measured tracer concentration at the outlet of the reactor was simulated using a tank-in-series with backmixing model and model parameters i.e. backmix ratio, number of tanks and mean residence times were obtained. The results obtained in one of the study are shown in Table IV. The results of radiotracer investigation confirmed poor mixing of the reactants as the values of the backmix ratio were quite low. For good mixing, the values of backmix ratio have to be of the order of a few thousands. The experiments were repeated after changing the position of the feed and other modifications, but similar results were obtained.

The CFD simulations were carried out for a few experimental conditions. One of the plots showing the experimentally measured and CFD simulated RTD at identical experimental conditions are plot in Fig. 26. The mean residence time (τ_{CFD}) predicted by CFD simulation was 1835 seconds.

However, the mean residence time determined from experimentally measured curve was 2431 seconds. It could be observed that CFD simulated RTD matches fairly well with the experimentally measured RTD. This led to the conclusion that the developed CFD model with some improvement can be used for prediction detailed hydrodynamic behavior of the reactor. The combination of RTD measured with radiotracers with CFD predictions could reveal the global as well as the localized flow behavior of the oxidation reactor. Based on the results, necessary modifications to improve the design of the impeller were suggested to achieve the desired degree of mixing in the reactor.

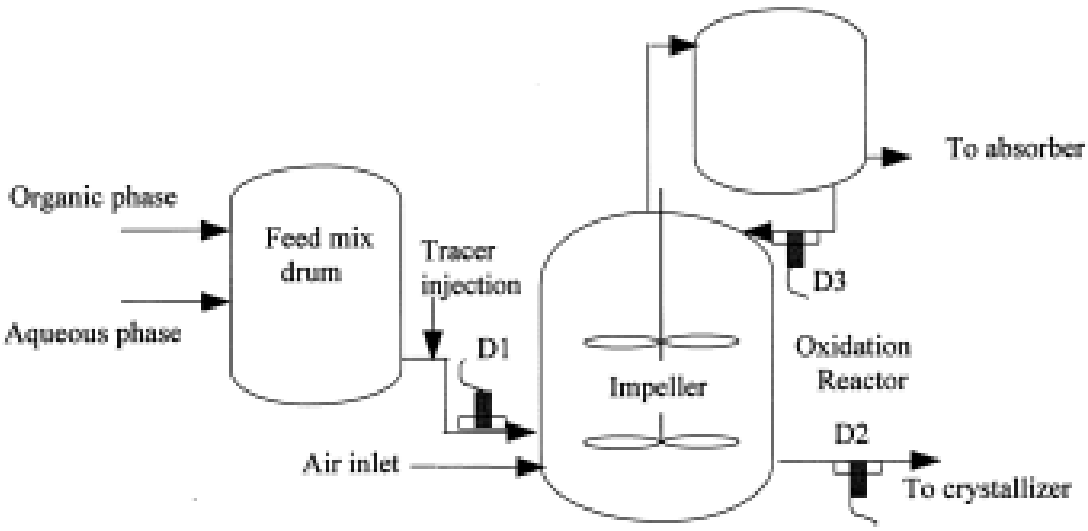

FIG. 27. Schematic diagram of the reactor and experimental setup (D1, D2, D3: scintillation detectors).

TABLE IV. PARAMETERS OBTAINED FROM SIMULATION OF THE MODEL

S.No	Radiotracer	$\tau_{Exp.\ (s)}$	Recirculation ratio (f)	$\tau_{Model\ (s)}$	Number of stirred tanks (N)
1	^{24}Na as Na_2CO_3	2431	40	2400	2
2	^{82}Br as dbbp	2172	9	1600	2
3	^{82}Br as dbbp	2139	8.4	1700	2
4	^{24}Na as Na_2CO_3	2160	17	1935	2
5	^{24}Na as Na_2CO_3	1928	38	1800	2
6	^{24}Na as Na_2CO_3	2281	312	2503	2
7	^{24}Na as Na_2CO_3	2316	233	2048	2
8	^{82}Br as dbbp	2200	17	1823	2

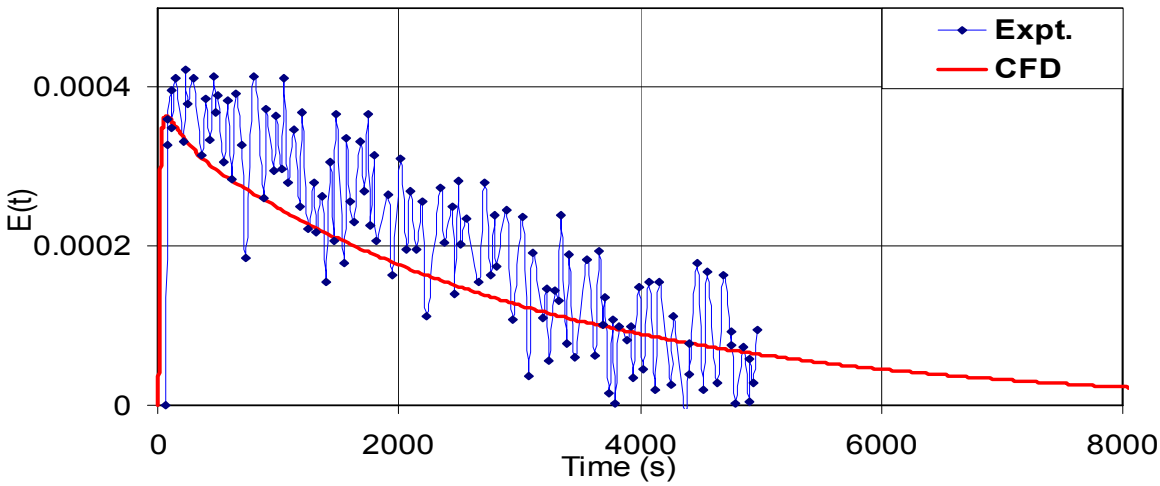

FIG. 28. Comparison of experimentally measured and CFD predicted RTDs.

4. CONCLUSIONS

Computational fluid dynamics based modeling offer powerful tools to understand complex industrial flow processes. Coupled with reaction engineering models, the CFD models offer unique tools to enhance performance of reactors and process equipment. CFD is a tool for experts, to be used in awareness of current limitations, dangers and assumptions. When developing modeling approaches to particular classes of problems, experimental validation is necessary. Thus, before applying CFD models for performance enhancement, it is essential to validate these models either directly or indirectly. Most of the laboratory measurement techniques are not applicable for carrying out measurements in industrial equipment.

Radioactive tracers offer unique capabilities to provide the necessary experimental data to validate CFD models. Radiotracer investigations have been carried out for mixing time and residence time distributions in different industrial process systems. The measured data were treated and simulated using flow models. The computational fluid dynamic models were also developed for these systems and validated using radiotracer techniques. The validated CFD models were used to predict the flow behavior at different conditions. The experimentally measured data were integrated with the results of the conventional modeling and CFD simulations to visualize the flow within the investigated system.

From the studies reported in this paper, it can be concluded that CFD modeling shows lot of promise for predicting the residence time distribution. Worldwide, CFD models are still in a developmental stage, primarily because of the complexity of fluid mechanics even in seemingly simple geometries. The physics of turbulent flow in closed systems still needs to be understood further so that proper turbulence models can be developed.

The work carried out has opened new possibilities to visualize the flow, to optimize the design and process and troubleshooting in industrial process systems. There is tremendous potential to synergistically harness potential of radioactive tracer techniques and CFD models to enhance performance of industrial reactors and process equipment.

REFERENCES

[1] INTERNATIONAL ATOMIC ENERGY AGENCY, Guidebook on Radiotracers in Industry, Technical Report Series No. 316, IAEA, Vienna, (1990) 374 pp.

[2] CHARLTON, J. S., (Eds.), “Radioisotope Tracer Techniques for Problem Solving in Industrial Plants”, Leonard Hill (1986), 320p.

[3] PANT, H. J., KUNDU, A., NIGAM, K. D. P., “Radiotracer applications in chemical process industry, Reviews in Chemical Engineering, Vol. 17, (2001), pp.165–252.

[4] THYN J., ZITNY, R., JAROSLAV, K. and CECHAK, T., “Analysis and diagnostics of Industrial Processes by Radiotracers and Radioisotope Sealed Sources”, Vol.1 Vydavatlstvi CVUT, Prague (2000), pp 329.

[5] THYN J., ZITNY, R., Analysis and diagnostics of Industrial Processes by Radiotracers and Radioisotope Sealed Sources [II], CTU Faculty of Mechanical Engineering, Department of Process Engineering, Prague (2002), pp. 249.

[6] LEVENSPIEL O, “Chemical Reaction Engineering”, John Wiley & Sons, (1972) pp.253–08

[7] INTERNATIONAL ATOMIC ENERGY AGENCY, “Residence time distribution software analysis user’s manual”, Computer Manual Series No. 11, IAEA, Vienna, Austria, (1996) pp. 218.

[8] RANADE, V.V. “Computational Fluid Dynamics for Chemical Reactor Engineering”, Academic Press, London (2001).

[9] BUWA V. V., RANADE, V. V.,“Mixing in 2-D bubble columns: Role of dynamics of gas liquid flows”, National Chemical Laboratory, Internal report (2001c).

[10] BUWA, V.V., PANT, H.J., RANADE, V.V., "Mixing in 2-D bubble columns: Experiments and CFD simulations", Proceeding of the NAARRI International Conference (NIC-2001) on Applications of Radioisotopes and Radiation Technology in the 21st Century at Mumbai, India, December (2001), pp. 169–174
[11] SUNTHANKAR, A. A., RANADE, V. V. Dynamics of gas-liquid flow, National Chemical Laboratory, Internal project report (1997).
[12] FLUENT 4.5, Fluent Users manual, Vol. 4, Fluent Inc., USA (1997).
[13] RANADE, V. V., BOURNE, J. R. and JOSHI, J. B. "Fluid mechanics and blending in agitated tanks", Chem. Eng. Sci., 46, (1991). Pp. 1883–1893.
[14] PATWARDHAN A. W., "CFD Modeling of Jet Mixed Tanks", Chem. Eng. Sci. (2002)
[15] PATWARDHAN A. W., GAIKWAD S.G., "Mixing in Tanks Agitated by Jets", Chem. Eng. Res. Des. (2003)
[16] PANT, H.J., THYN, J., BHATT, B.C., "Radioisotope tracer study in a sludge hygienization research irradiator", Applied Radiation and Isotope, 54, (2001), 1–10.
[17] PATWARDHAN, A. W., "Prediction of residence time distributions in stirred reactors", Ind. Eng. Chem. Res. 40, (2001), 5686–5695
[18] KOHOPKAR, A., PANT, H.J., RANADE, V.V., "Residence time distribution study in continuous stirred tank reactor", Proceeding of the NAARRI International Conference on Applications of Radioisotopes and Radiation Technology in the 21st Century (NIC-2001), Mumbai, (2001), 205–209.
[19] SHENOY, K.T. GHOSH, S.K. and KENI, V.S., "Hydrodynamic Studies in a Mixer Settler System. Advances in Chemical Engineering in Nuclear and Process Industries, Bhabha Atomic Research Centre, Trombay, Bombay, India (1994).
[20] PANT, H.J., Chapter 4 of the Ph.D thesis entitled "Studies on Process Dynamics of Industrial Process Systems Using Nuclear Techniques", Ph.D Thesis, University of Mumbai, Mumbai, India (2001)
[21] SHENOY, K.T., PANT, H.J., GHOSH, S.K., NAVADA, S.V., "Residence time distribution study in a pump-mix mixer of mixer-settler system", Proc. Symp.on Advances in Chemical Engineering-97 (Eds. B. Bhattacharjee, B.M. Misra, V.K.Tangri, M.S.Krishan, S.K.Ghosh, S.K.Malhotra), BARC, Mumbai, India, pp. 9–17 (1997).

RADIOTRACER ASSISTED VISUALIZATION AND CFD MODELLING OF MULTIPHASE FLUID FLOW IN POROUS MEDIA

T. BJØRNSTAD, A. HAUGAN, C. CHATZICHRISTOS,
J. SAGEN, Ø. DUGSTAD
Institute of Energy Technology (IFE),
Kjeller, N
Nuclear Chemistry Group, Department of Chemistry,
University of Oslo, Oslo, N

Abstract

The intension of the present project has been to study some basic phenomena of fluid flow in porous media for enhanced oil recovery purposes. One goal has been to study the use of both passive water tracers and water/oil partitioning tracers in a heterogeneous reservoir to measure remaining oil saturation. These studies have been carried out by targeted laboratory experiments utilizing radioactive tracers and nuclear detection techniques. Conventional core flooding experiments have been conducted to qualify tracers for this purpose. Water has been labelled with tritiated water (HTO), $^{131}I^-$ and $^{57}Co(CN)_6^{3-}$. Two partitioning radiotracers have been qualified at simulated reservoir conditions (reservoir-like rock, pH, temperature and pressure). They will here be named Part1 and Part2. Construction and fabrication of a mini-reservoir has been implemented in which tracers can be injected in injection wells, move in the pore space through the reservoir rock and then be produced in production wells. In sequential experiments this reservoir has been prepared to full water saturation, to full oil saturation at residual water saturation and to residual oil saturation after water flooding. The movement of tracers and the space differential fluid saturations in the reservoir has been recorded by gamma camera detection and by sampling of produced fluids in the various production wells followed by detection by gamma spectroscopy or liquid scintillation counting.

1. INTRODUCTION

Oil components are generated in source rocks and migrate through fractures and fissures into traps in porous rocks. These traps will, with time, be filled with oil. This process takes place over tens of millions of years. The oil traps represent the oil reservoirs as we know them today.

Oil is produced in the first stage by so-called primary production, which simply is the use of the internal pressure in the reservoir to expel the oil from the porous reservoir rock and out through production wells. As the pressure decreases, secondary production methods are necessary. Secondary production may include water injection. This serves two purposes: One is to keep up the pressure in the reservoir and the other is to provide a driving or sweeping mechanism by pushing the oil forward to the production wells. Obviously, secondary production requires specific injection wells.

The production process will leave oil behind. This remaining oil can be regarded to be of two kinds, - one is the oil left behind in the swept volumes in smaller droplets, the other is that larger volumes have been bypassed (not swept) by the injected water.

In average, on a world scale, only 30-35% of the oil in place has been produced after secondary production. If conditions allow, it is possible to continue with another production phase called tertiary production. This includes for instance large-volume injection of different chemicals like alkaline solutions, surfactants, polymers etc. This type of operation is expensive. Therefore, before embarking upon such a program, one has to make probable that the extra oil gained can at least pay for the extra expenses.

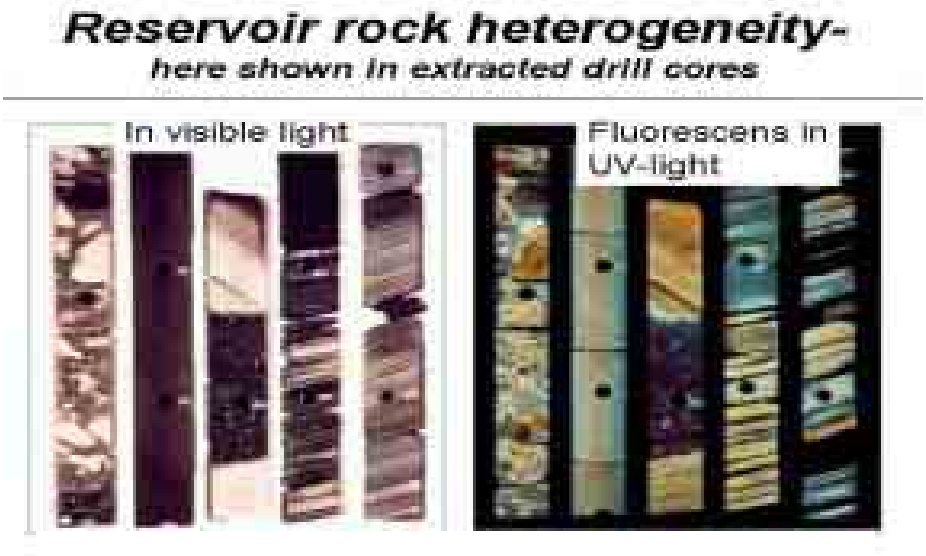

FIG. 1. Cores of heterogeneous and stratified reservoir rock

A key to optimized oil production is a good knowledge of the internal structure of the reservoir. Reservoir rock is stratified (Fig.1), and most often the reservoirs composed of those rocks are fractured and heterogeneous and compartmentalized with no or little communications between the compartments. Besides the production history of reservoir fluids (water, oil, gas), the only technology, which can give information on fluid flow conditions in the reservoir is tracer technology. By this method, various substances, tracers, are injected in small amounts along with the injection water in the injection wells. Each well is labeled differently. By detecting the various tracers in surrounding production wells, indispensable information can be gained of the fluid flow and other reservoir properties [1,3]). Such properties are for instance zones of high permeability, barriers to flow, volumes which are swept (efficiency of water injection) and, by using so-called oil/water partitioning tracers it is in principle possible to get an idea about the amount of oil left behind (remaining oil saturation).

2. PURPOSE OF THE PROJECT

The purpose of the present project is to study some basic phenomena of fluid flow in porous media by laboratory experiments utilizing radioactive tracers and nuclear detection techniques. This includes construction and fabrication of a mini-reservoir in which we can inject tracers in injection wells and produce in production wells. The tracer production curves so generated can be compared with residence time distribution (RTD) curves, but does in principle not satisfy fully the requirements of the definition of RTD. For simplicity however, the tracer production curve is hereafter called the RTD-curve. The purpose is further to examine how well experiments can be simulated by CFD modeling, here represented with application of one of the major finite difference reservoir simulators in combination with an in-house made advanced tracer simulation module.

Basic concepts

Fluid flow conditions are studies by so-called *passive tracers* (sometimes incorrectly called ideal tracers, [3]-[5]). A passive tracer is supposed to follow the water phase exactly without any other interactions with surrounding media than those of the water molecule itself. Structures in the RTD-curve of a passive tracer contain information about reservoir heterogeneities and flow volumes.

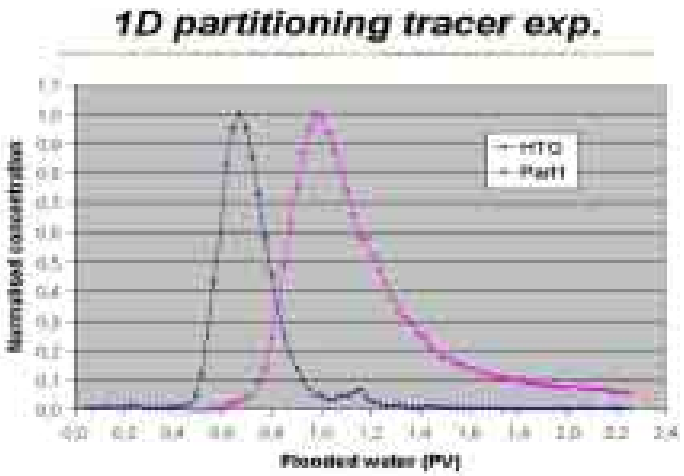

FIG. 2. RTD-curves of passive (HTO) and partitioning tracer.

Remaining (or residual) oil saturation in a reservoir may conceptually be measured by the use of a mixture of passive and partitioning tracers. A passive tracer will exclusively follow the water path while the partitioning tracer will partition into the stagnant oil phase according to its partition coefficient. The result is that the RTD-curve for the partitioning tracer will be produced later as measured by its first moment. This curve also shows a larger dispersion than the RTD-curve for the passive tracer (Fig.2). The difference between equal landmarks of the two curves (most often used is the first moment) is a measure of the water-contactable oil saturation in the flooded volume.

From the measured retention volumes V_R^1 and V_R^2 and the previously measured corresponding partition coefficients K_1 and K_2, the residual oil saturation S_o may be calculated in a one-dimensional (1-D) system by the Eqn.1:

$$S_o = \frac{V_R^2 - V_R^1}{V_R^1 \cdot (K_2 - 1) - V_R^2 \cdot (K_1 - 1)} \qquad \text{(Eqn.1)}$$

This method has already been tried implemented in field operations (see [6]-[7] and references therein), but a number of questions remain to be answered before it can be fully understood and trusted.

Experimental arrangements

1D experiments to study the basics of the behavior of partitioning tracers for measurement of non-movable residual oil is carried in flow-rigs similar to the one outlined in Fig.3.

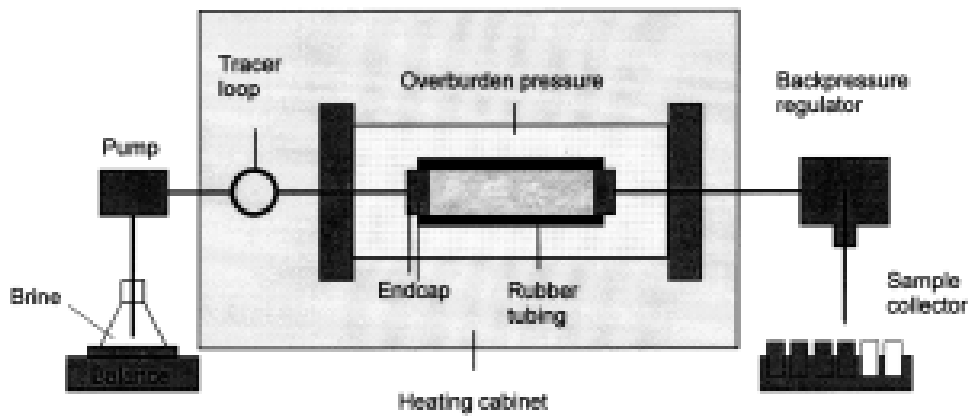

FIG. 3. 1D flow rig for tracer examinations at simulated reservoir conditions.

A cylindrical core (various dimensions, but typically 1 inch diameter and 3 inch long) of reservoir-like material is incorporated in a rubber (neoprene, viton) tube with end-caps in both ends. The core arrangement is fitted with thin steel tubing (typically 1/16 inch ID) to the endcaps and incorporated into a high-pressure steel housing. The flow-rig thus created may be positioned in a heating cabinet. In this way, experiments at simulated reservoir conditions (temperature 70-150 °C, pressure about 300 bar) may be carried out if needed.

It has been demonstrated in previous work that residual oil saturation in 1D flow systems, S_o (amount of available pore space occupied by oil), can be reliably derived from Eqn.2 by measuring the retention volume V_R (flooded volume to the first moment of the RTD curve) with partitioning tracers if the pore volume V_p (total volume available for fluid saturation) is known and the partition coefficient K is determined by other means. Reversely, if the oil saturation is known, the K-values may be determined with the same technology with the same equation.

$$S_o = \frac{V_R - V_P}{V_P \cdot (K - 1)} \qquad \text{(Eqn.2)}$$

The question is how the flow behaves in a 2D reservoir without and with oil saturation, and whether partitioning tracers may be used to monitor S_o in 2D systems. We foresee that the simple relation of Eqn.1 cannot be used in 2D, but a more complex modeling has to be applied with the principles of oil/water partitioning built into a common reservoir simulator. For these experiments a 2D laboratory model of consolidated sandstone has been constructed.

If the injection water is labeled with a suitable gamma-emitting radiotracer, the distribution of that tracer inside the reservoir rock could then be imaged. Considering the reservoir as a 2D system and provided the tracer is a passive water tracer, the area activity distribution is a measure of the 2D porosity distribution. Hereafter this setup is called the homogeneous mini-reservoir.

A modification of the reservoir rock was then done by introducing a major heterogeneity into the reservoir. This was achieved by creating a cavity through the whole thickness of the reservoir and fill the cavity with epoxy. Hereafter, this experimental setup is called the *heterogeneous mini-reservoir* or *the 2-D reservoir*.

Some information on the radiotracers used in these experiments are given in Table I. Unfortunately, not all information on the partitioning tracers can be disclosed at this stage.

TABLE I. RADIOACTIVE TRACERS USED IN THE 2-D EXPERIMENTS

As conservative (passive) water tracers:

- Tritiated water, HTO E_β = 18 keV, $T_{1/2}$ = 12.32 y
- $^{60}Co(CN)_6^{3-}$, E_γ = 122 and 136 keV, $T_{1/2}$ = 270 d
- ^{131}I, E_γ = 364 keV, $T_{1/2}$ = 8 d

As oil/water partitioning tracers:

- Part1, ^{14}C-labelled, E_β = 159 keV, $T_{1/2}$ = 5730 y
- Part1, non radioactive, K = 0.265
- Part2, ^{14}C-labelled, E_β = 159 keV, $T_{1/2}$ = 5730 y
- Part2, non-radioactive, K = 1.05

Experiments and corresponding results with the homogeneous mini-reservoir

Experiments were carried out under ambient conditions (room temperature and atmospheric pres-sure). The reservoir was evacuated by a vacuum pump, and brine traced with $^{57}Co(CN)_6^{3-}$ sucked into it through the center well E. This tracer has previously been qualified as a near-passive tracer for water flooding under existing experimental conditions. Brine traced with $^{57}Co(CN)_6^{3-}$ was then flooded between all the pairs of wells, until air was produced at the production wells. The gamma camera was then used to image the porosity distribution of the reservoir. Results are shown in Fig.4.

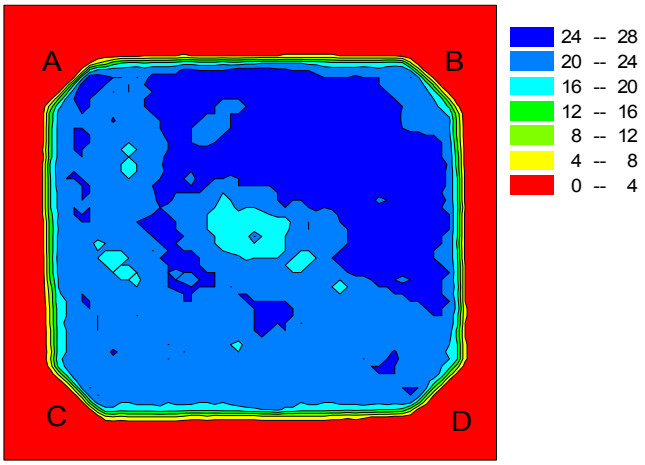

FIG. 4. The porosity distribution, proportional to the activity distribution, (given in %) of the homogeneous mini reservoir.

Experiments with this simple reservoir showed that it constituted a feasible experimental setup, and that the gamma camera was well suited to record activity distribution and, accordingly, the porosity distribution.

Experiments and corresponding results with the heterogeneous mini-reservoir

The reservoir was evacuated by a vacuum pump, and brine traced with $^{57}Co(CN)_6^{3-}$ sucked into it like for the homogeneous reservoir. Also here, brine traced with $^{57}Co(CN)_6^{3-}$ was then flooded between all the pairs of wells, until air was produced at the production wells. The gamma camera was then used to image the porosity distribution of the reservoir. Results are shown in Fig. 5.

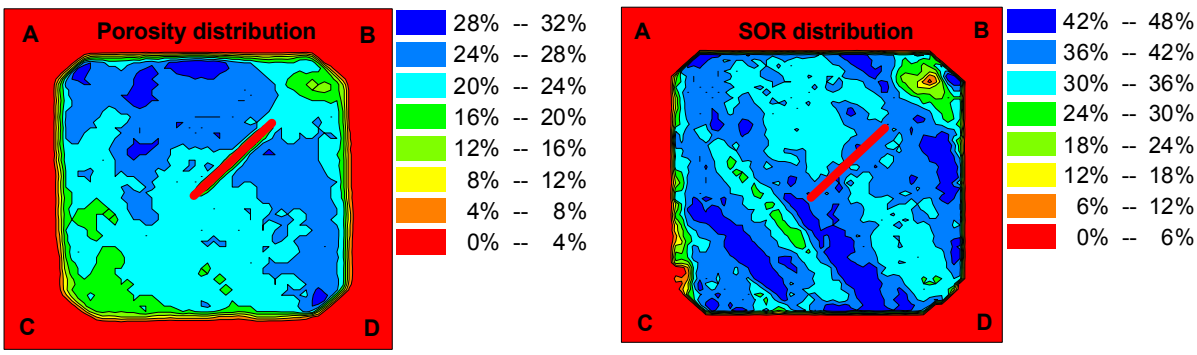

FIG. 5. Tracer and porosity distribution

Brine traced with $^{57}Co(CN)_6^{3-}$ and dead crude oil from a North Sea oil field were then successfully flooded between well pairs until residual oil saturation was obtained. Images of the residual oil distribution and the water distribution are given in Figure 5.

In all the flooding experiments with the heterogeneous mini reservoir at residual oil saturation, the mobile phase (brine) was pumped through the reservoir by the use of an HPLC pump. For the experiments reported here, well A was used as injection well and well D used as the production well. The effluent was collected in small consecutive samples by the use of a sample changer. The samples were successively counted with a combination of gamma-ray spectrometry for gamma emitters and liquid scintillation counting for pure beta emitters. The tracer production curves constructed on the basis of these measurements represent the RTD-results in the experiments.

Three types of experiment were performed with the heterogeneous mini-reservoir:

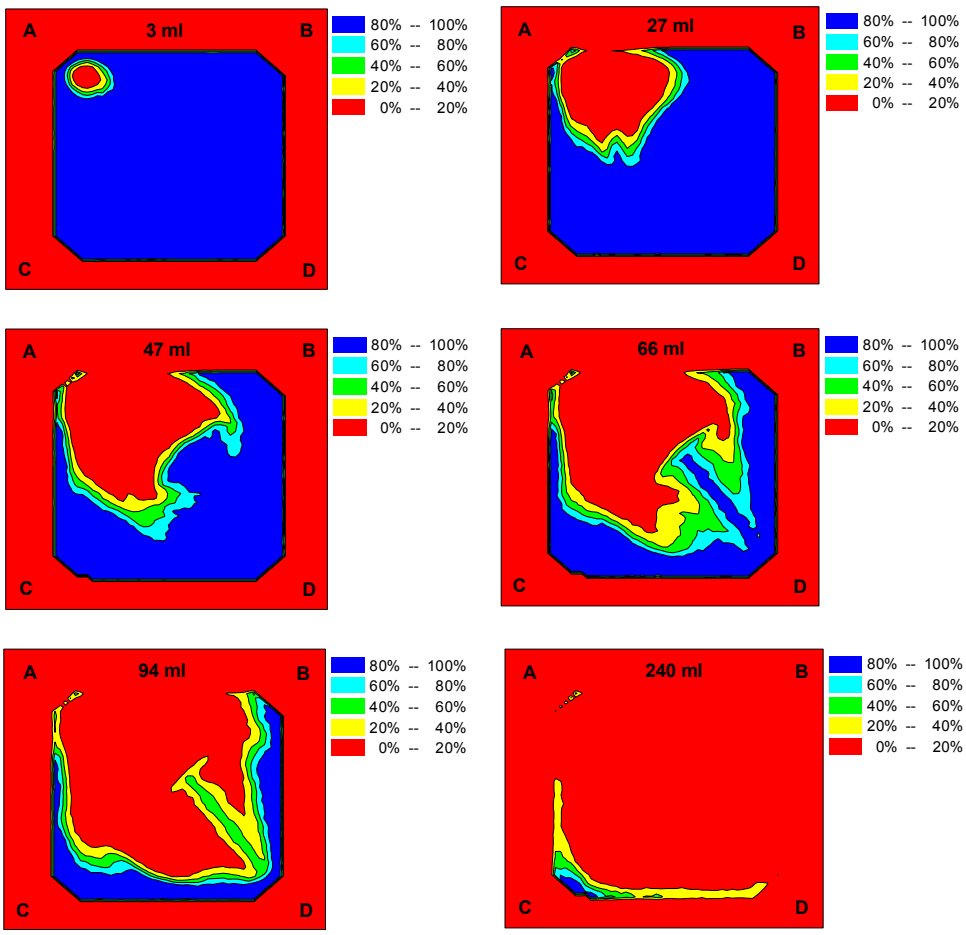

FIG. 6. Replacement of radioactive brine inside the "heterogeneous mini reservoir" by continuously pumping non-radioactive brine into well A and produce brine from well D. The pixel values show how much of the "original" radioactive formation water remains. The flow rate was 0.04 ml/min and each image was measured for 25 min. The non-radioactive brine injected into the "reservoir" is indicated on the images.

To visualize the flow pattern of the brine, non-radioactive brine (without $^{57}Co(CN)_6^{3-}$) was pumped into well A, replacing the radioactive brine (with $^{57}Co(CN)_6^{3-}$) originally inside the "reservoir". Well D was used as production well. The effluent were analysed for $^{57}Co(CN)_6^{3-}$ by gamma-ray detection with the use of a NaI detector. The production curve is shown in Fig. 7. The

gamma camera continuously measured the tracer distribution. Selected images with time show the replacement as illustrated in Fig.6.

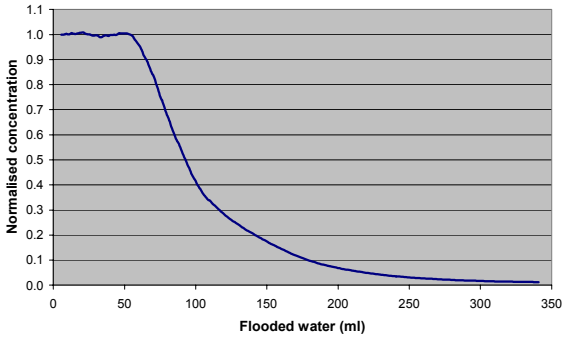

FIG. 7. Production curve from well D of radioactive brine originally inside the "reservoir" when non-radioactive brine is continuously injected into well A.

When all the radioactive water was replaced, a tracer pulse with $^{131}I^{-}$ was injected in well A and produced in well D to further visualize the flow pattern. The collimator of the gamma camera is designed for 140 keV (^{99m}Tc), while the gamma-ray energy of ^{131}I is 364 keV. The resolution of the images is therefore not optimal. The images are shown in Fig.8, while the production curve (analysed with liquid scintillation counting) from well D is shown in Fig.9.

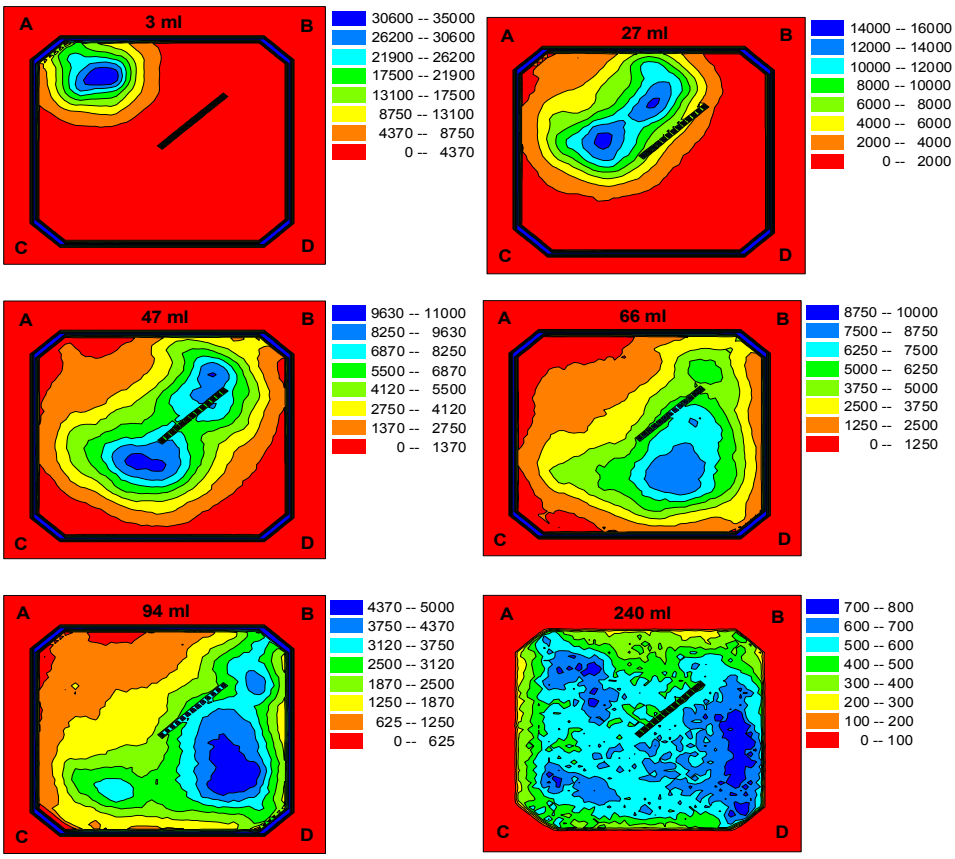

FIG. 8. Images of a ^{131}I pulse injected in well A and produced in well D. The flooded amount of brine is indicated on the images.

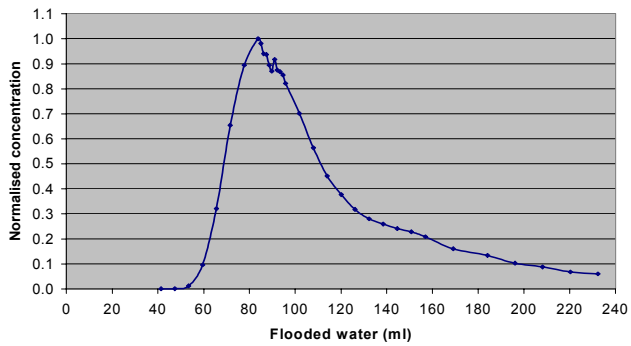

FIG. 9. Production curve of a ^{131}I pulse injected in well A and produced in well D.

Two flooding experiments injecting a tracer pulse that have been performed with the heterogeneous mini reservoir are reported here. The mobile phase was brine with $^{57}Co(CN)_6^{3-}$ at the same concentration as the water already inside the "reservoir". The tracers used in the first experiment were HTO and Part1 (see Table 1) and in the second experiment HTO and Part 2. In both experiments the volume of the tracer pulse was 250 µl, and the flow rate was 0.04 ml/min.

0.4 ml samples were continuously collected at the outlet. These samples were analysed for HTO (^3H), Part 1 and Part 2 by liquid scintillation counting. The results are shown together in Fig.10 where the curves are the raw date normalized on their height (maximum value) only. The presence of ^{57}Co in the mobile phase introduced "noise" to the production curves due to its contribution to the liquid scintillation counting.

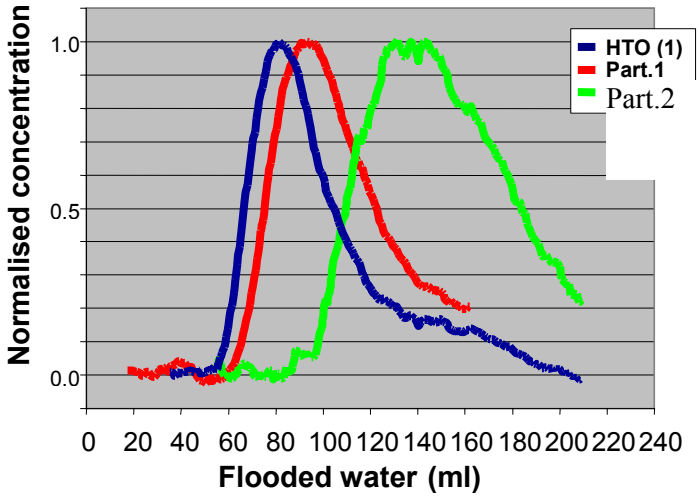

FIG. 10. Production curves from pulse injection of two flooding experiments with the "heterogeneous mini reservoir". Well A was used as injection well, and well D as production well. The results are corrected for dead volumes in the experimental equipment.

3. SIMULATION OF PARTITIONING TRACERS IN 2-D

The simulation of the partitioning tracers (Part1 and Part2) flow in the 2-D core slab was carried out using the ITRC Tracer Module developed at IFE ([8]-[10]), coupled to STARS reservoir simulator from Computer Modeling Group (CMG) in Calgary.

The slab was divided in 141 x 147 grid blocks. The porosity and the residual oil saturation (Fig.11) were inserted in the model directly from the slab measurements. The injection and the production rates are set at 0.04 ml/min.

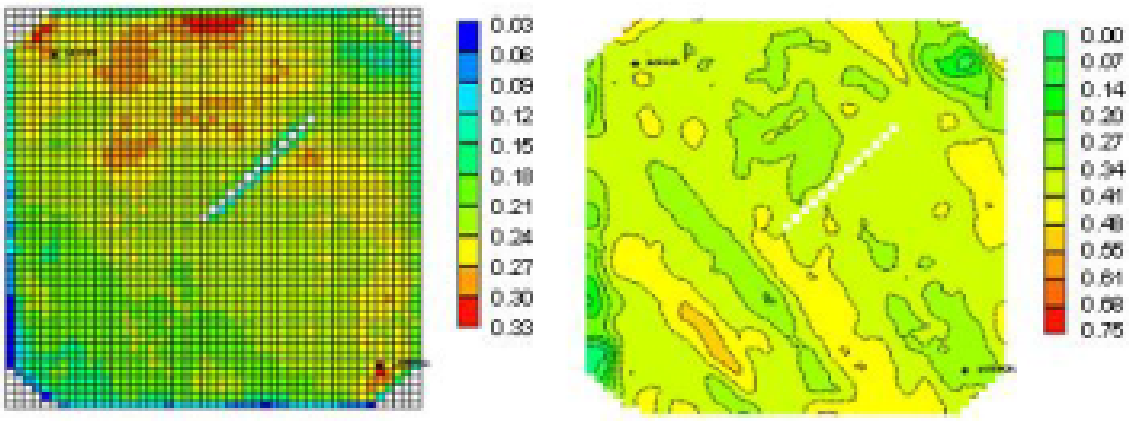

FIG. 11. Input values for reservoir model-ling: Porosity distribution. Oil saturation distribution.

First the work focused on the reservoir model representing the core slab as accurately as possible. In order to evaluate this representation, simulation of the displacement of radioactive water by non-radioactive water was carried out. Fig.12 shows the comparison of the simulated with the experimental production profile of the displaced water.

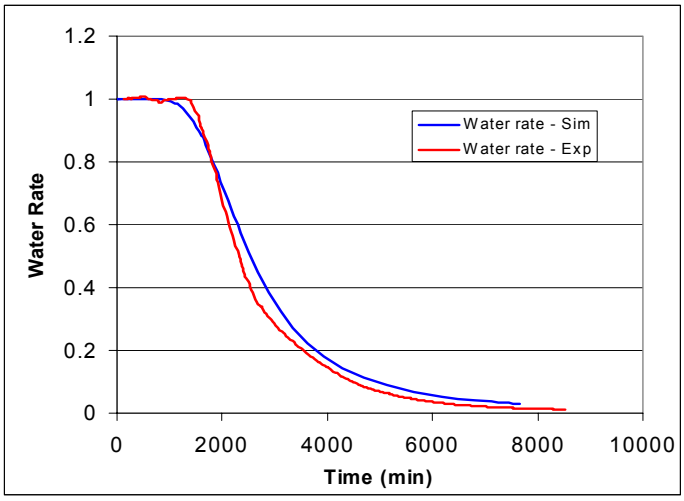

FIG. 12. Comparison of the production profile of the displaced water with the simulated profile with the reservoir simulator.

In addition, a comparison of the concentration of the radioactive water in the porous medium at consecutive time intervals is illustrated in Fig.13.

Finally, the flow of the tracers is simulated using partitioning coefficients 0.265 for the Part 1 and 1.05 for the Part 2. The results are presented in Figures 14, 15 and 16 and compared with the experimental results.

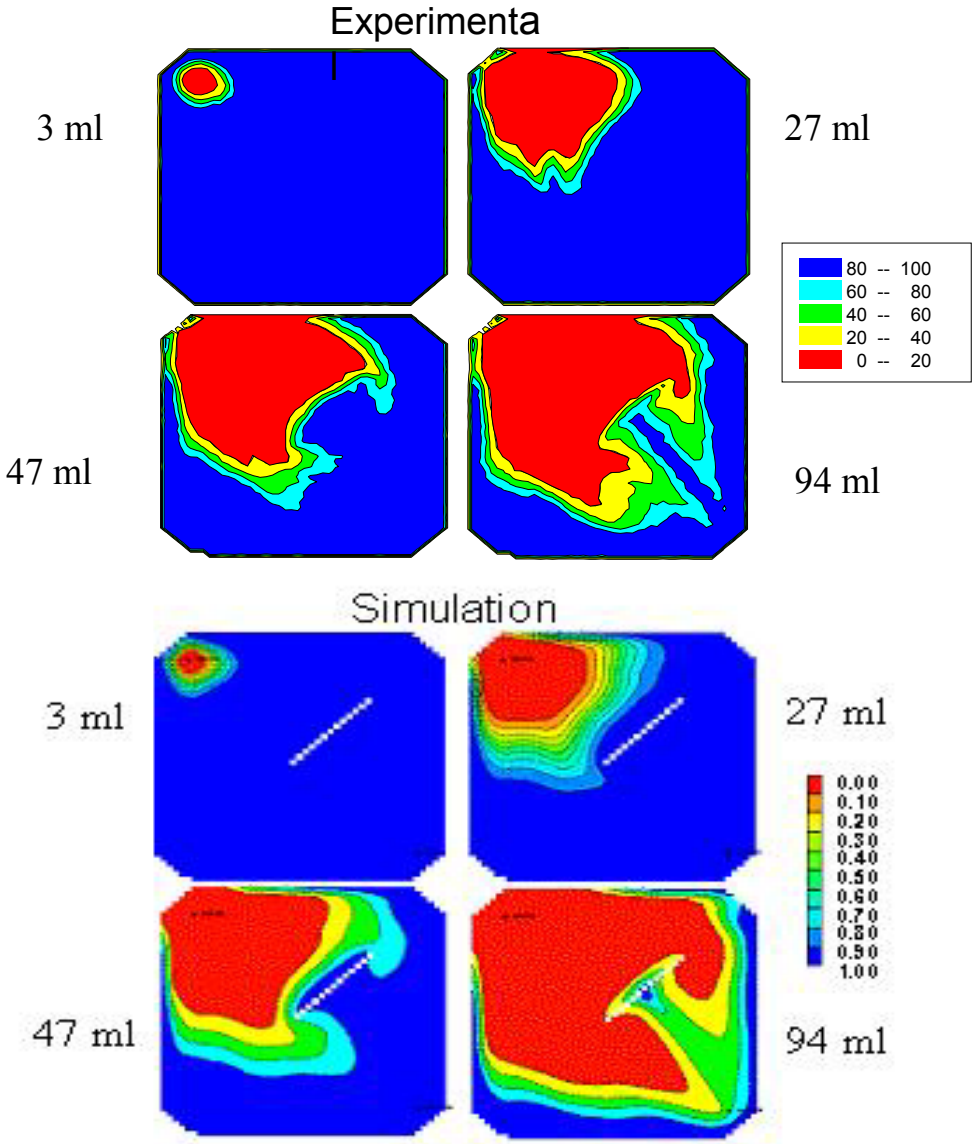

FIG. 13. Concentration of radioactive water expelled by non/radioactive water in the mini/reservoir as a function of injected water volume indicated in the fig. The upper 4 frames are the experiments while the lower 4 frames are from simulations.

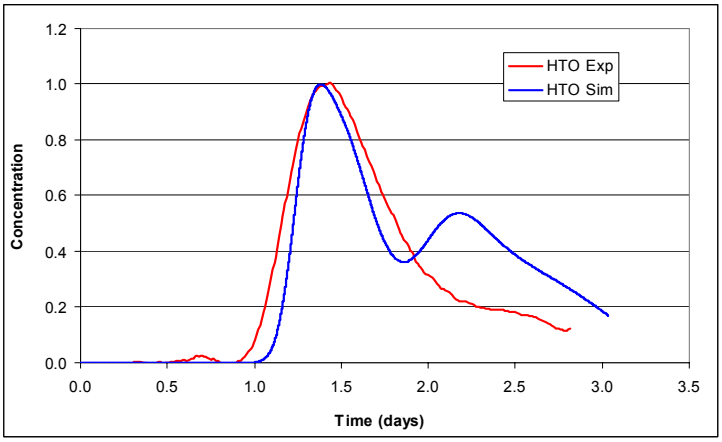

FIG. 14. Comparison of experimental production profile (using HTO) for the heterogeneous reservoir and the simulated one without physical dispersion option switched on.

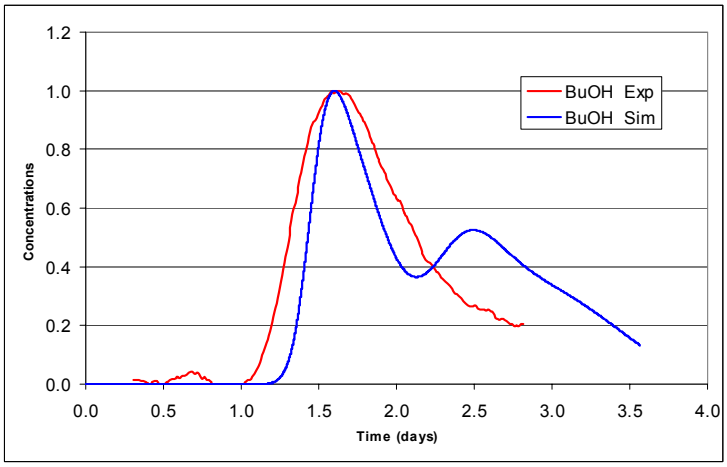

FIG. 15. Comparison of experimental production profile of partitioning tracer Part1 for heterogeneous reservoir and simulated one without physical dispersion option switched on.

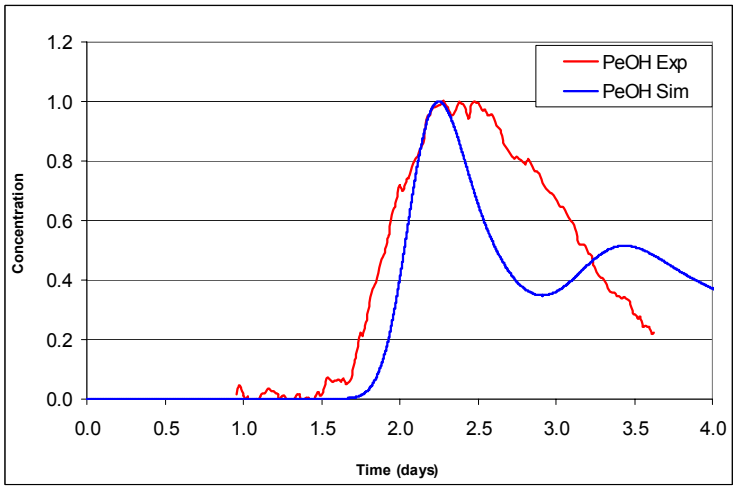

FIG. 16. Comparison of experimental production profile of partitioning tracer Part2 for heterogeneous reservoir and simulated one without physical dispersion option switched on.

The simulations are in reasonable agreement with the experiments with the two flow paths being easily distinguishable. The simulations focus mainly on the first peak (main flow path). It should be mentioned that the simulations have higher resolution due to the absence of physical dispersion in the calculations. Physical dispersion has been included in the ITRC-SIM simulator, and simulations will be repeated with this option switched on at a later stage.

4. CONCLUSIONS

Passive radioactive water tracers suitable for application in laboratory experiments with the use of both non-intrusive detection techniques based on gamma radiation and on sampling followed by liquid scintillation counting have been qualified in core flooding experiments.

Two water/oil partitioning tracers, Part1 and Part2, have been qualified for use in laboratory as well as full field experiments to measure water contactable residual (or even remaining) oil saturation in porous reservoir rock.

A 2-D mini reservoir has been constructed and successfully applied in basic studies of the partitioning tracer concept for determination of space distributed oil saturation in porous reservoir rock.

A numerical tool has been developed and evaluated, involving both microscopic and macroscopic models and taking into account the fundamental properties of the tracers, capable of simulating with high accuracy the flow of passive and partitioning tracers.

Movement of passive water tracers in the 2-D mini reservoir has been simulated with the ITRC-SIM tracer module coupled to the STARS reservoir simulator. Agreements between experiments and simulations are not perfect but reasonably good.

The partition coefficients of Part1 and Part2 obtained from numerical modeling of 1-D flow experiments on cores with known residual oil saturation have been used to simulate the tracer flow in the 2-D slab case using the ITRC-SIM tracer module coupled to the STARS reservoir simulator. Agreement between experiments and simulations are reasonable although there is obviously room for improvements.

It was estimated that the alcohols have high enough mass transfer coefficient to be able to reach equilibrium between water and oil at any “normal” flow condition.

It is concluded that the macroscopic flow (core scale) of the partitioning tracers is influenced mainly by the following parameters:

- Partition coefficient
- Mass transfer coefficient
- Interaction with the rock
- Rock heterogeneity
- Molecular diffusion and dispersion.

Results from the present work support the potential of the passive tracer/partitioning tracer concept for measurement of remaining oil saturation in swept zones between wells in oil reservoirs and encourage further studies to qualify the method for field implementation.

REFERENCES

[1] LICHTENBERGER, G.J., "Field Applications of Interwell Tracers for Reservoir Characterization of Enhanced Oil Recovery Pilot Areas",Technical Paper SPE-21652, 1991

[2] ZEMEL, B., "Tracers in the Oil Field" (book), Developments in Petroleum Science, 43, Elsevier Science, Amsterdam, 1995

[3] BJORNSTAD, T., MAGGIO, G.E., BARRY, B.J., "Tracers in oilfields and geothermal fields", in "Guidebook on Radiotracer Applications in Industrial Processing, Oil & Geothermal Reservoirs", IAEA Technical Report Series No. 423, IAEA, Vienna, May 2004.

[4] BJØRNSTAD, T., "Selection of Tracers for Oil and Gas Reservoir Evaluation", Technical Research Report IFE/KR/E-91/009, 1991, 43 pp.

[5] BJØRNSTAD, T., DUGSTAD, Ø., GALDIGA, C., SAGEN, J., "Interwell Tracer Technology in Oil Reservoirs: State-of-the-Art", in Proc. of the "First International Congress on Tracers and Tracing Methods", 29–31 May 2001, Nancy, France, French Society of Chemical Engineering.

[6] ALLISON, S.B., POPE, G.A., SEPEHRNOORI, K., "Analysis of Field Tracers for Reservoir Description", J. Petrol. Sci. Eng., 5, (1991) 173–186

[7] TANG, J.S., "Partitioning Tracers and In-Situ Fluid-Saturation Measurements", Formation evaluation 10 (1), (1995) 33–39.

[8] JOHANSEN T., ANTONSEN B., SAGEN J., HIDLE S., "A Theory of Multicomponent Chromatography for Tracers in Two Phase Flow", Proceedings from "The Fifth European Symposium on Improved Oil Recovery", Budapest, April 1989.

[9] SAGEN, J., CVETKOVIC, B., BRENDSDAL, E., HALVORSEN, G., YOU, Y.L., BJØRNSTAD, T.: "Reservoir Chemical-Thermal Simulation with Tracers", Internal Technical Paper SPE-36921, 1996.

[10] CHATZICHRISTOS, C., DUGSTAD, Ø., HAUGAN, A., SAGEN, J., MÜLLER, J., "Application of Partitioning Tracers for Remaining Oil Saturation Estimation: An Experimental and Numerical Study", Internal Technical Paper SPE-59369, April 2000.

COMBINING CFD SIMULATION WITH EXPERIMENTAL RTD FUNCTION FOR HYDROCYCLONE SEPARATOR STUDIES

Z. STEGOWSKI, E. NOWAK E, L. FURMAN
University of Mining & Metallurgy,
Krakow, Poland.

Abstract

The first part of this report presents radiotracer experimental Residence Time Distribution (RTD) functions for hydrocyclone separators, their analysis and macro modelling. The second part of the report presents the Computational Fluid Dynamics (CFD) simulation for the hydrocyclone. Combining the experimental data and the CFD simulation results allows understanding the fundamental principles of the flow and solids' separation in hydrocyclone. The experimental data help choosing the proper parameters for CFD simulation and from the other side the CFD results allow better analysis and macro modelling of the experimental data. Radiotracer methods have been used for industrial experiments. For CFD simulation the FLUENT software has been applied.

1. INTRODUCTION

The Copper Industry is one of the largest companies in Poland. This industry includes mining, concentration and foundry processes. Thirty million tons of copper ore are processed per year. In the concentration process the copper ores that contain about 1%–2% of copper are benefiting for concentration material which includes 20% of copper. The concentration process includes three steps: comminution, beneficiation and dewatering processes (Figure 1). For optimization and the automatic control of this process the knowledge of the proper, accurate flow parameters of each operation (milling, classification, flotation etc.) is necessary. One of the more efficient methods applied to investigations of industrial flow processes is the radiotracer method. In Polish Copper Industry this method has been used for more than 20 years [1]. At present, as electronics, computers, data storage and data analysis software are highly developed, this method is much more powerful than at the start [2]. Also, combining the CFD methods for flow processes simulations should significantly develop the industrial processes recognition, control and optimization.

2. THE PRINCIPLE OF TRACER METHODOLOGY AND RTD ANALYSIS

The principle of tracer methodology

The principle of the tracer measurement consists in a common impulse-response method. The radiotracer is injected at the inlet of a system and the concentration-time curve is recorded at the outlet. In the case the tracer is not instantaneously injected the concentration-time curves both at the input $C_i(t)$ and the output $C_o(t)$ should be recorded.

For the closed-closed system, that is the system with the internal mixing and plug flows (no mixing at all) when the tracer is pulse injected, the residence time distribution function E(t) is obtained after normalization of C(t). The definition of E(t) is the basis of the flow description proposed by Danckverts.

Residence time distribution, as defined above, may be applied only to constant flow / constant volume systems. This implies the necessity of ensuring that the tracer does not influence/disturb the flow and that the tracer behavior simulates that of the flowing media.

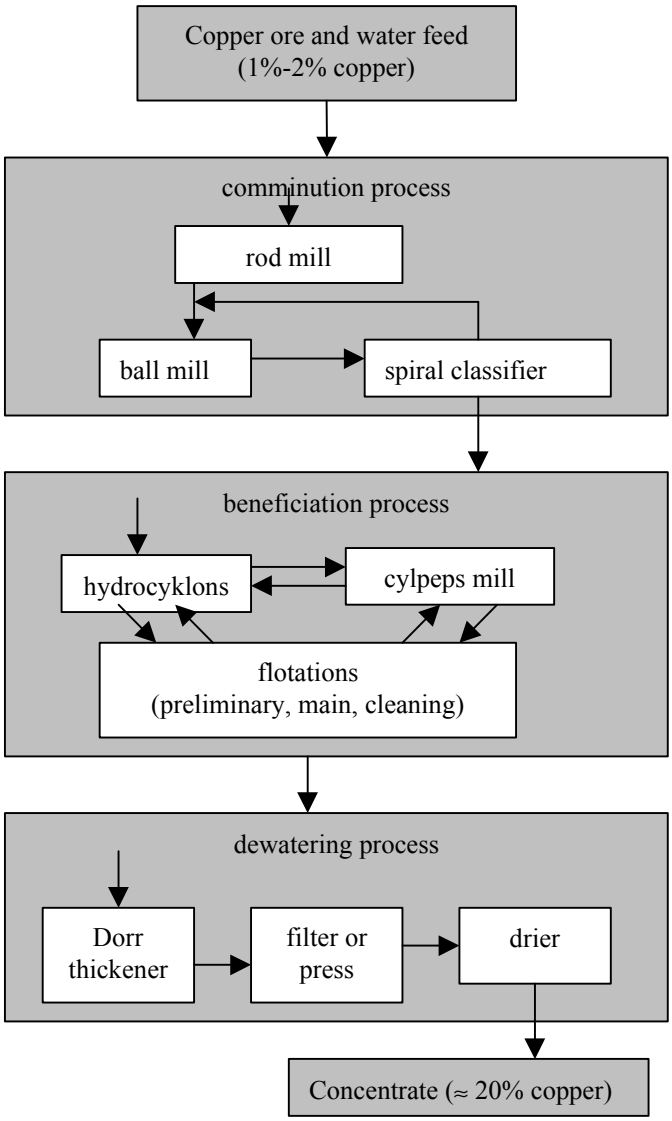

FIG. 1. General schema of the copper ore concentration process.

If the $C_i(t)$ is not a Dirac function (not a perfect impulse injection of the tracer) the Danckverts description is not applicable. In such a case the transfer function in time domain g(t) may be utilized.

After normalization, in order to obtain:

$$\int_0^\infty C_i(t)dt = \int_0^\infty C_o(t)dt$$

the relation between $C_{we}(t)$, $C_{wy}(t)$ and g(t) expresses the convolution integral (Duchamel's integral):

$$C_o(t) = \int_0^t C_i(\tau) g(t-\tau) d\tau$$

Theoretical work of Kreft and Zuber [4] show that E(t) and g(t) functions are not identical in general, and depend on how the tracer concentration is measured. The radiotracer methodology distinguishes between the residence and flux concentrations. In practice, usually in industrial processes, dealing with closed-closed systems E(t) = g(t).

Evaluation of Residence Time Distribution Function

Residence time distribution function E(t) (or RTD), the result of tracer measurements, is the basis for the flow description of the selected material in a system.

The moments' method is the fundamental method of estimating the distribution's parameters [7]

The following notation will be further used:

$$\tau = \int_0^\infty tE(t)dt$$

$$\sigma^2 = \int_0^\infty (t-\tau)^2 E(t)dt$$

where:

- τ (MRT) – mean residence time calculated from E(t) curve,
- σ (SD) – standard deviation of E(t) (RTD),

Fig.2. presents the RTD E(t) function; mean residence time (MRT) and its standard deviation (SD).

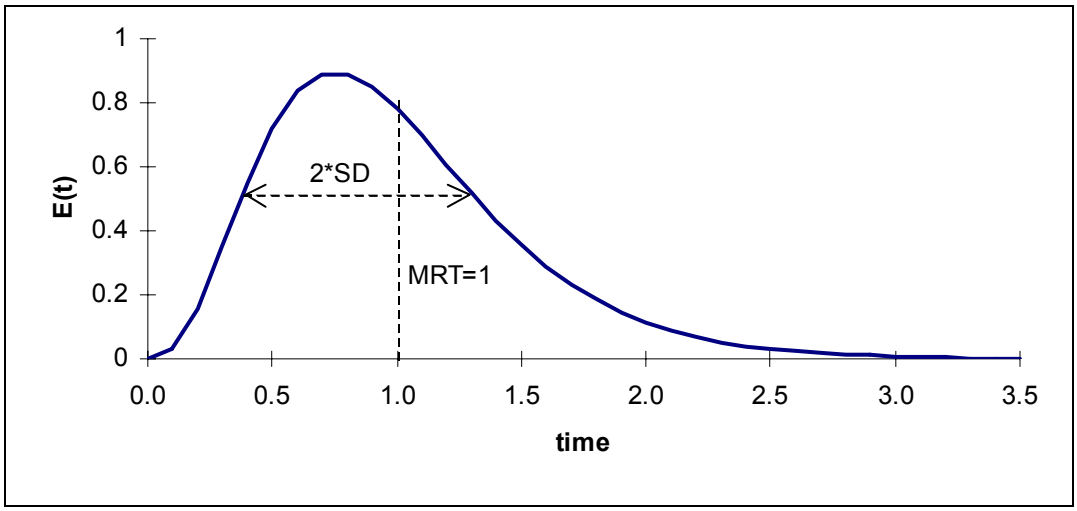

FIG. 2. The exemplary E(t) function with MRT and SD parameters.

MRT and SD have the following physical interpretation in relation to flow systems:

- MRT (mean residence time) is directly related to flow rate and the effective flow volume of the system
- SD (standard deviation of MRT) characterizes the mixing rate of the given medium in the system. In case of lack of mixing (plug flow) SD equals zero. The higher mixing rate, the grater value of SD. For perfect mixing system E(t) is the exponential function.

Flow System Modelling by DTS Software

The experimental radiotracer's data needs the proper analysis. One of the more advanced software is the French DTS package for flow process modeling [8]. This is the object oriented programming software working in Windows Systems. The software can simulate the response to any input of the complex network. Eight different elementary reactors can be chosen that are based on perfect mixer and dispersion models [9]. The parameters can be optimized by comparison of experimental data with the response of the model.

Processes with multiple inlets or outlets can be modeled by convolution and optimization procedures. Local measurements may be validated through the possibility to simulate the local response within the model and to optimize the corresponding parameters. This use of the well-known elementary "bricks" permits us to work directly in the Laplace domain where we know, in particular, that the convolution product is transformed into a simple product of the functions. For example three basic models and their parameters are presented in Table I.

TABLE II. RTD SIMPLE MODELS.

Model's name	Model's symbol	Parameters
Plug flow		T — flow time
Perfect mixers in series	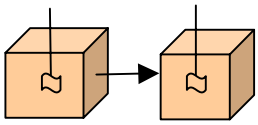	τ — total mean residence time I — number of perfect mixers
Perfect mixers in series with exchange zones	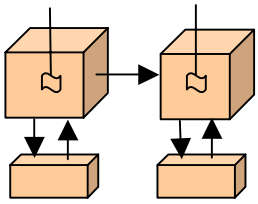	τ — mean residence time for mixers I — number of perfect mixers τ_m — mean residence time for exchange zones K — ratio between exchange zones volume and mixers volume

Radiotracer used for RTD analysis

A radiotracer emitting γ-radiation is injected (as a pulse function) to the system at the inlet. The scintillation probe, mounted at the outlet, detects gamma radiation intensity as a function of time. The counting rate is directly proportional to the concentration of the radiotracer and provides the RTD. Natural copper in ore contains two stable copper isotopes ^{63}Cu and ^{65}Cu. Due to the thermal neutron activation in a nuclear reactor the radioactive isotope ^{64}Cu is obtained from isotope ^{63}Cu. This copper isotope is the perfect tracer for copper ore processing study. The half-life of ^{64}Cu is 12.7 hours. It emits a positron, which immediately annihilates with an electron. Two electromagnetic quanta, each having energies of 511 keV, are emitted in this process.

3. SEPARATION PROCESS IN A HYDROCYCLONE

A hydrocyclone is a device where the grain material classification proceeds in the field of the centrifugal force action. The centrifugal forces are generated by a flowing liquid on spiral trajectory in a motionless vessel. This spiral flow is generated by tangential enter of the suspended solids with proper velocity. Differences in grain sizes and specific gravity make possible to separate the grains in the hydrocyclone. Inside the hydrocyclone two opposite rotating streams are formed. Coarse grains rotate closer to hydrocyclone wall and flow down to underflow. Fine grains rotate inside and flow up to overflow (Fig. 3).

Radiotracer tests were performed in a hydrocyclone employed inside the beneficiation process [11]. In this case it was not possible to make the pulse injection of the radiotracer and the scintillation probes were placed in three different positions: inlet, underflow outlet and overflow outlet (Fig. 4).

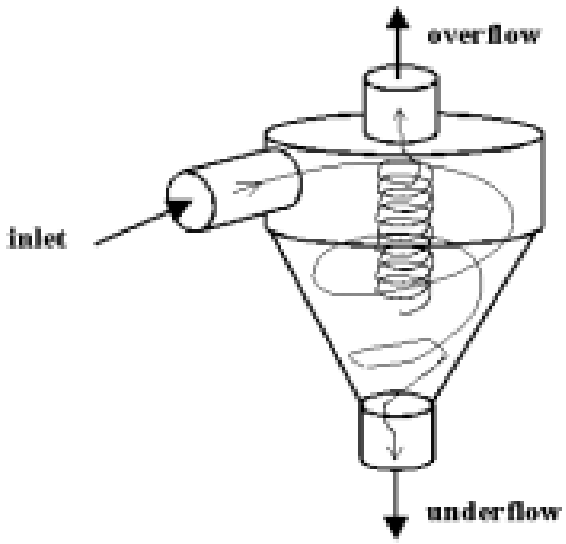

FIG. 3. Scheme of the hydrocyclone.

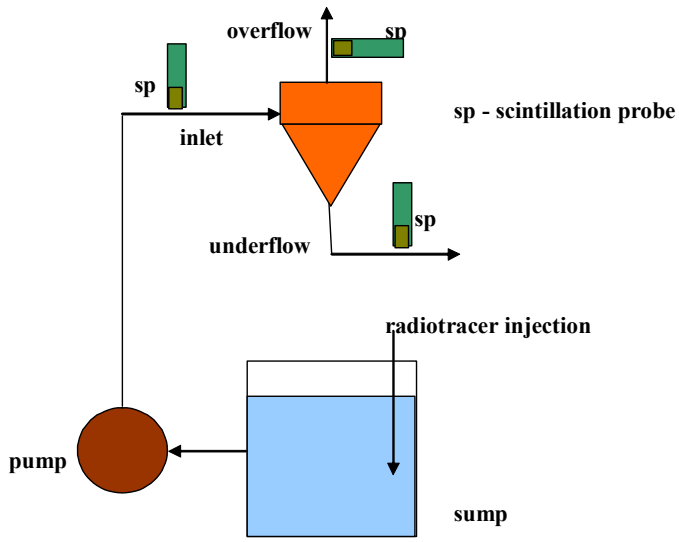

FIG. 4. Scheme of the radiotracer experiment.

Radiotracer tests have been conducted by injection of different grain sizes. Some experimental data are shown in Fig. 5, 6 and 7.

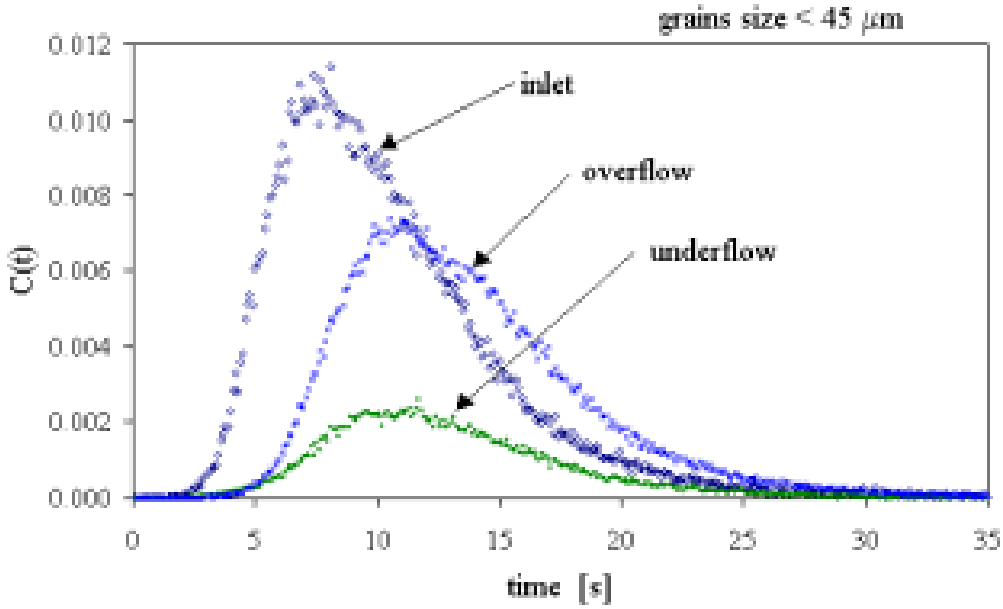

FIG. 5. The experimental data; the grain sizes <45 μm have been radiotraced.

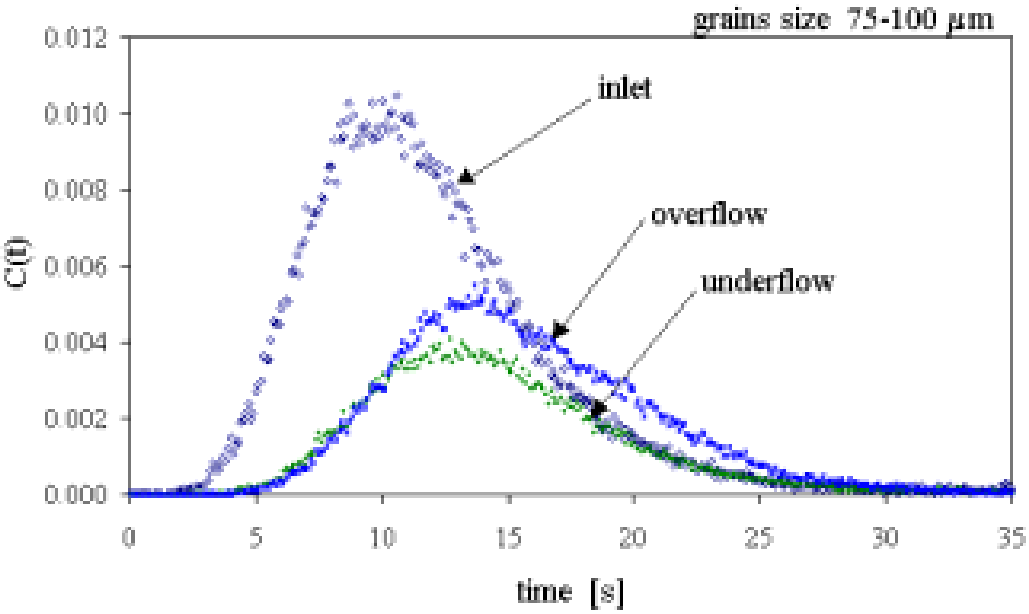

FIG. 6. The experimental data; the grain sizes 75-100 μm have been radiotraced.

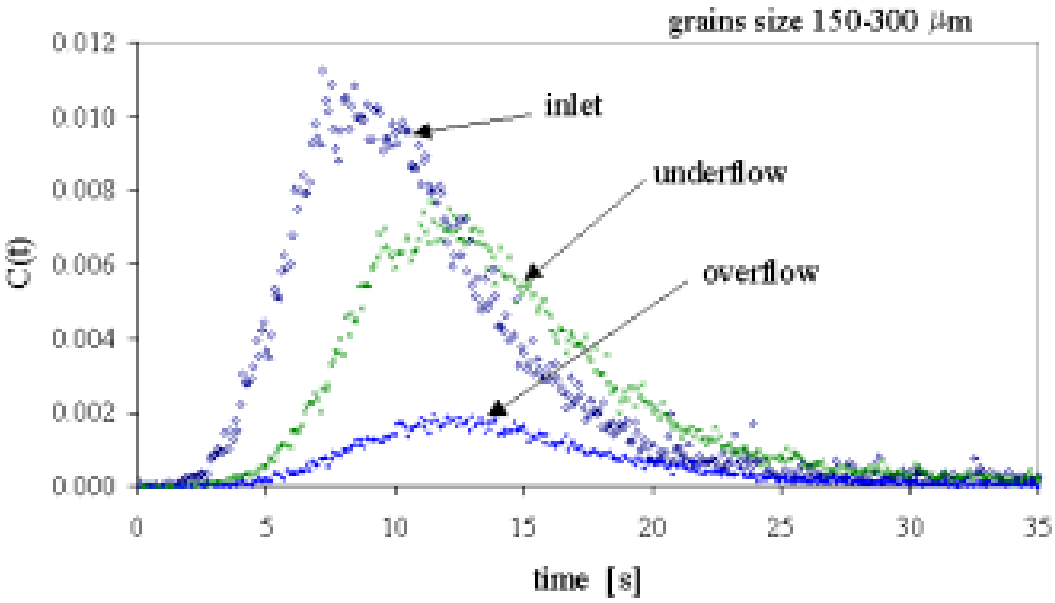

FIG. 7. The experimental data; the grain sizes 150-300 μm have been radiotraced.

Analysis of this data has been performed by the moments method and modeling by DTS software. Fig. 8 shows the simple model for hydrocyclone used for modeling by DTS software. Fig.9 shows how experimental data fits the model.

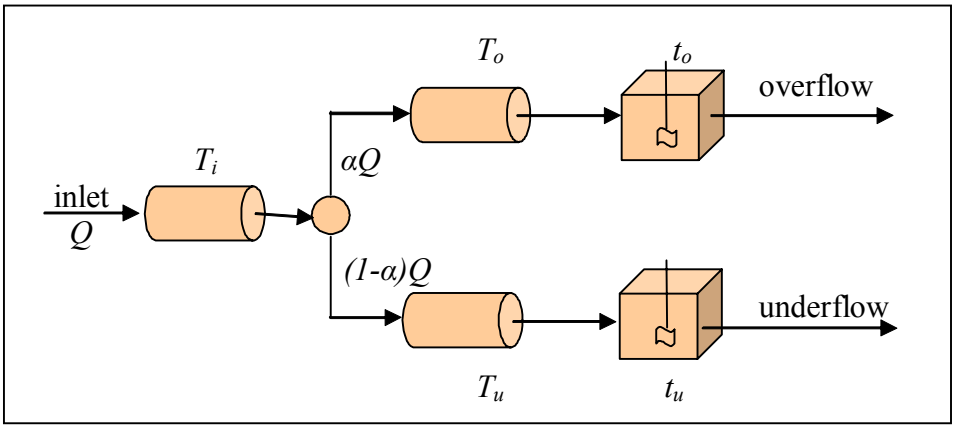

FIG. 8. Model for hydrocyclone Q *- flow rate,* α *- part of grains flowing to overflow.*

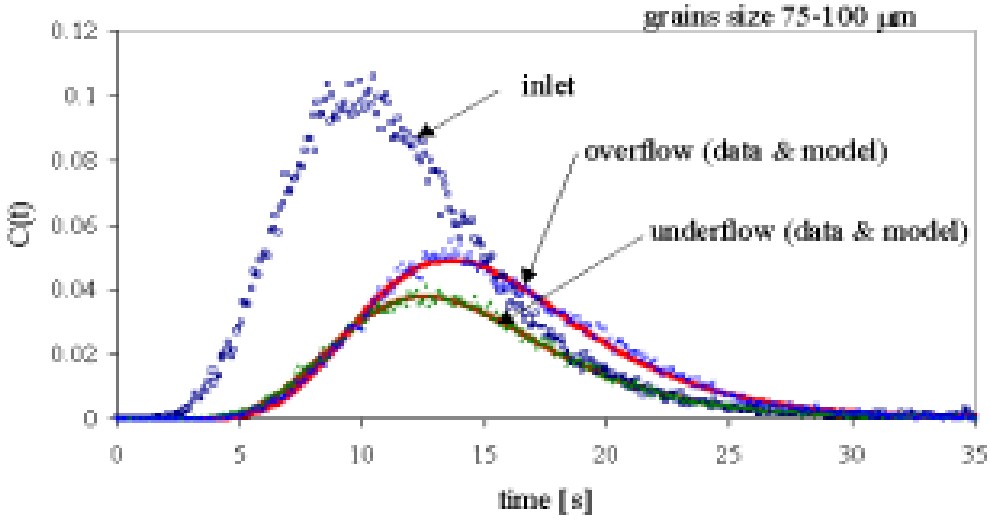

FIG. 9. The experimental data with models obtained by RTD software.

4. CFD SIMULATION

For CFD simulation the commercial software GAMBIT and FLUENT have been used. GAMBIT was used for hydrocyclone geometry and mesh preparation (Fig.10). The FLUENT software has been used for flow simulation. At the first step, the modeling of one-phase flow (water), in the hydrocyclone, has been done. At the second, solid particles' flow in hydrocyclone was simulated. For water flow simulation the turbulent model k-ε has been used. For solid particles flow simulation the turbulent dispersion model has been used.

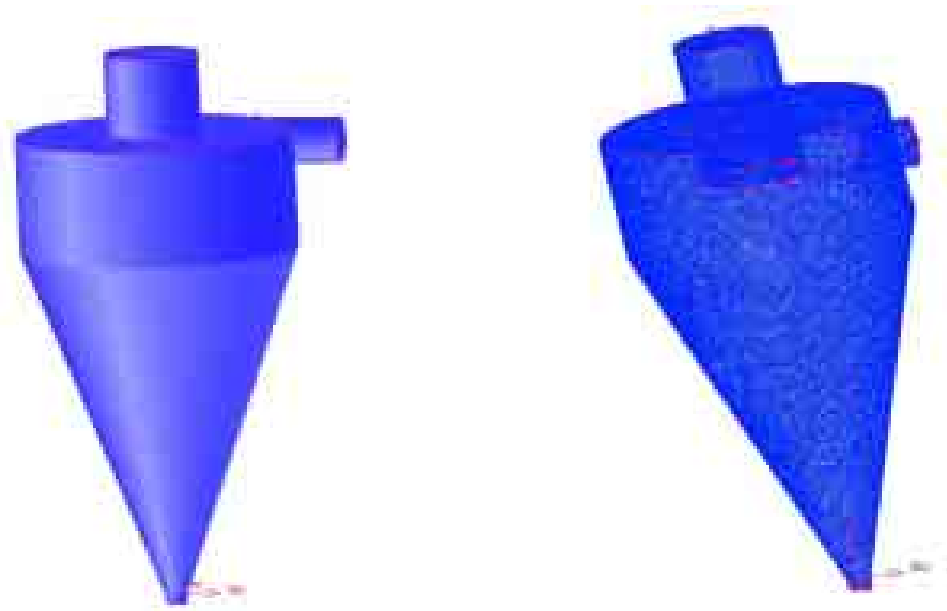

FIG. 10. Hydrocyclone geometry and the mesh prepared by GAMBIT software.

Fig. 11 to 22 shows the results for water flow CFD simulation. Fig. 23 to 28 presents the solid particles flow CFD simulations.

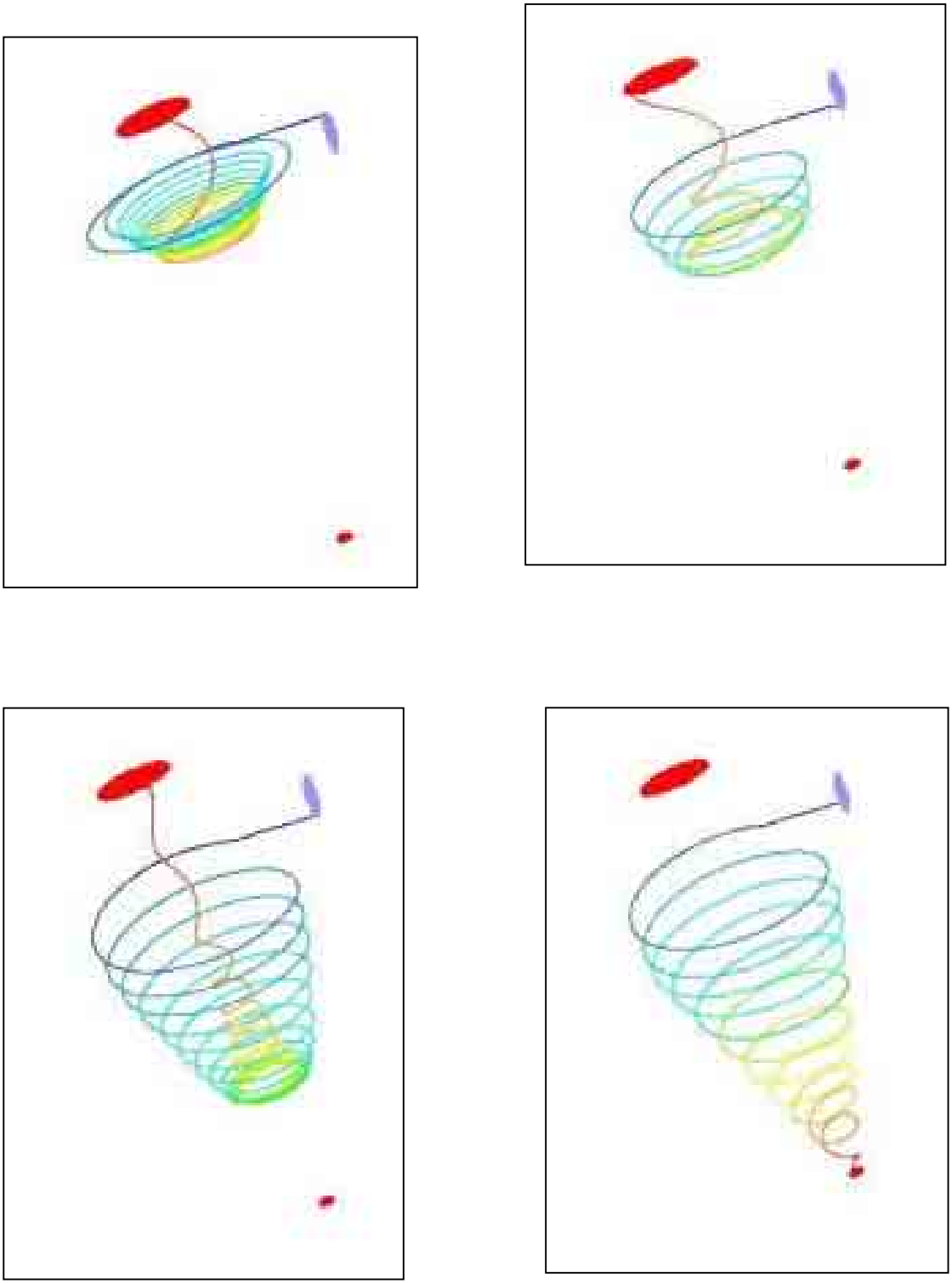

FIG. 11. Examples of the flow path line.

FIG. 12. All path lines flowing from the inlet.

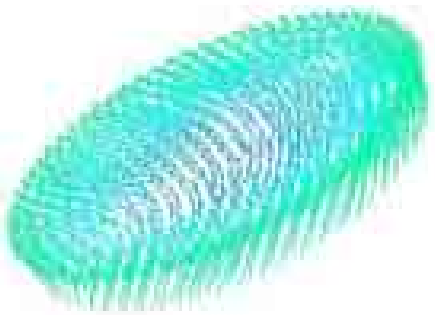

FIG. 13. Velocity vectors on overflow.

FIG. 14. All path lines flowing from a horizontal cross section.

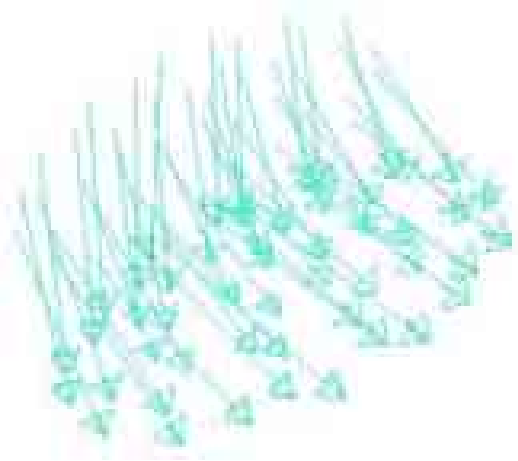

FIG. 15. Velocity vectors on underflow.

FIG. 16. Velocity vertical vectors on horizontal cross sections.

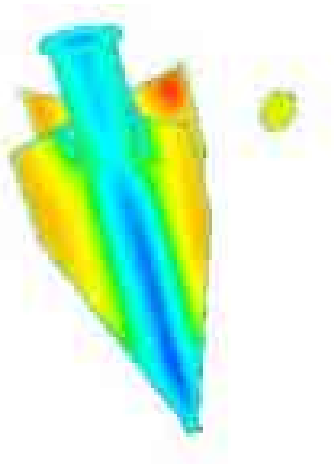

FIG. 17. Velocity contours on vertical cross sections.

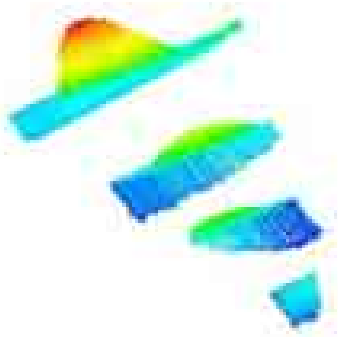

FIG. 18. Velocity vertical vectors on horizontal cross sections.

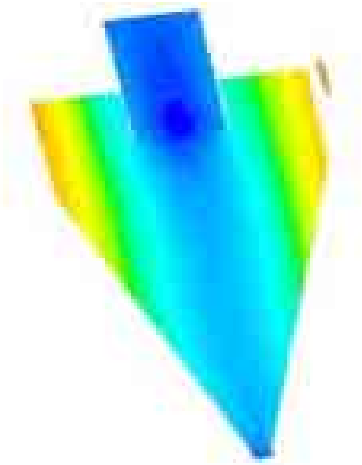

FIG. 19. Contours of static pressure on vertical cross section.

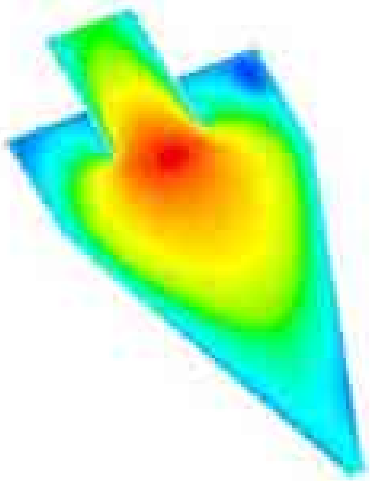

FIG. 20. Contours of turbulence intensity on vertical cross section.

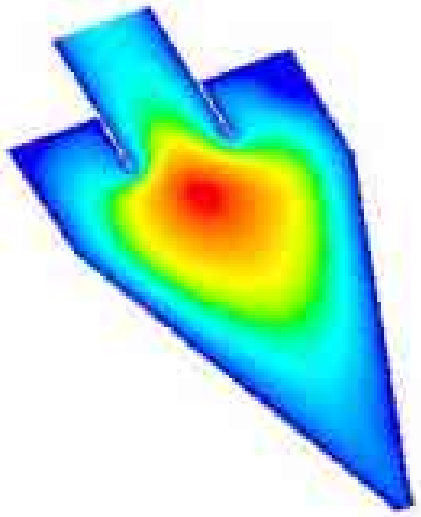

FIG. 21. Contours of turbulent viscosity on vertical cross section.

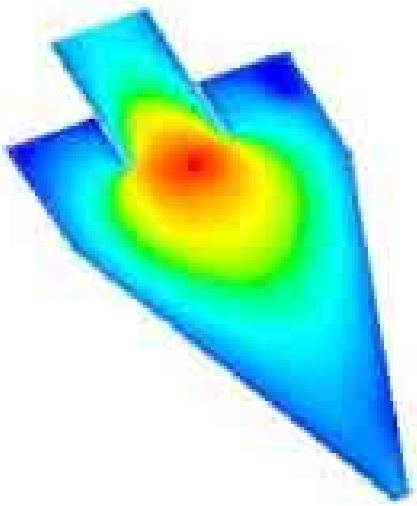

FIG. 22. Contours of turbulent kinetic energy on vertical cross section.

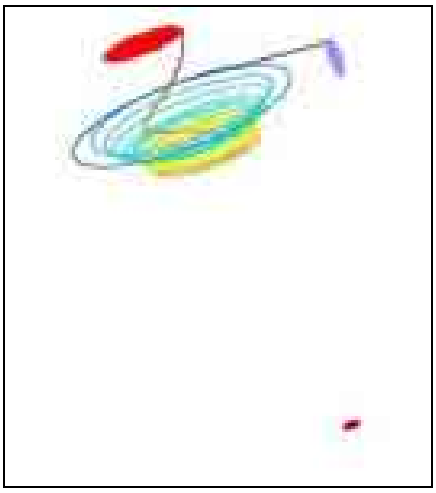

FIG. 23. Particle d=5 μm trace.

FIG. 24. Particle d=300 μm trace.

FIG. 25. Particle d=80 μm trace.

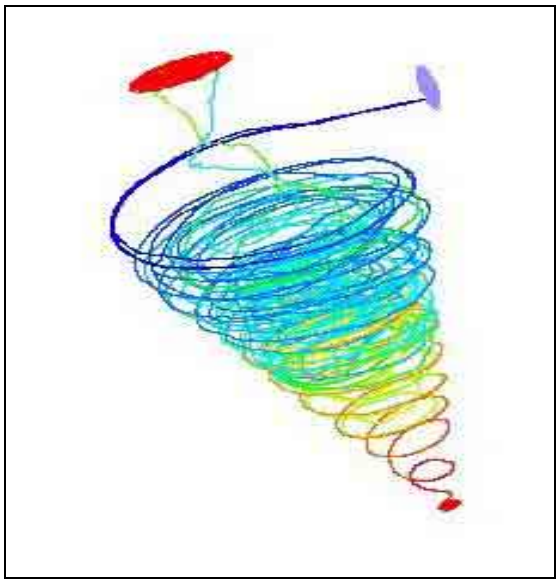

FIG. 26. Three Particle(d=5 µm) traces for high turbulent dispersion.

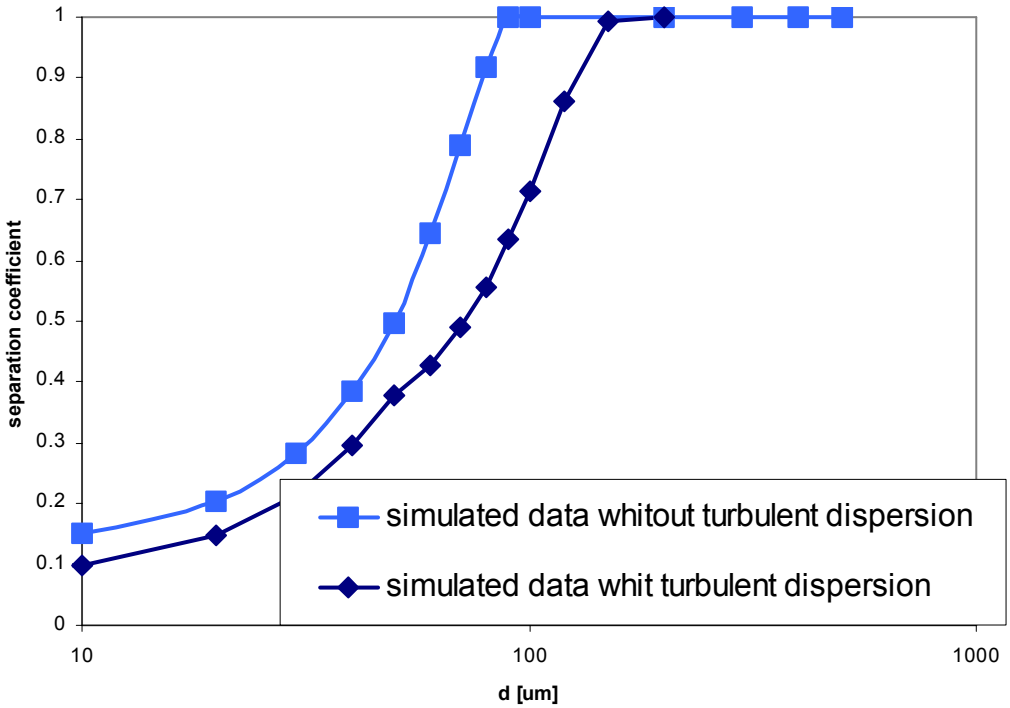

FIG. 27. Simulated separation curves without and with turbulent dispersion.

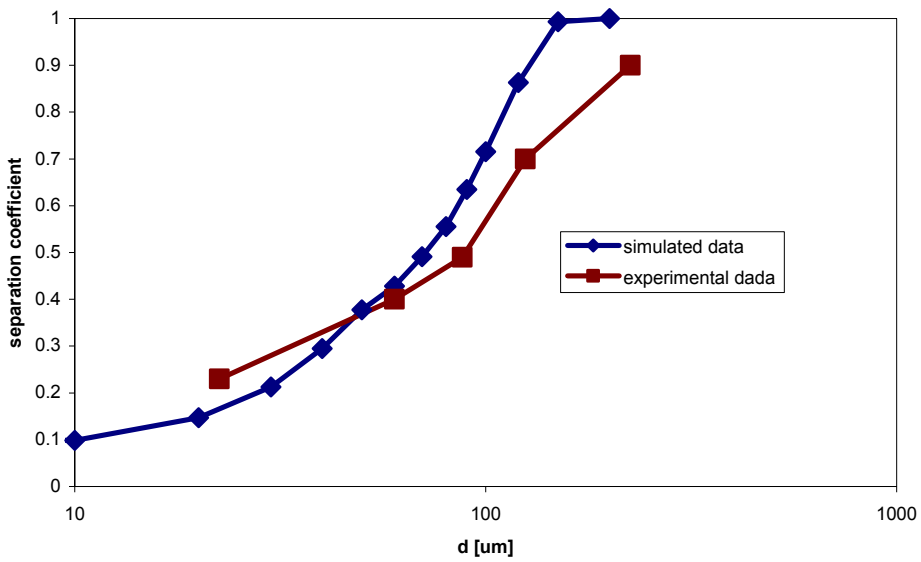

FIG. 28. Simulated and experimental separation curve.

Finally it was possible to simulate the separation curve and RTD function for solid particles. In Fig. 27 the simulated separation curves without and with turbulent dispersion of solid grains are shown. In Fig. 28 the simulated and experimental separation curves are shown. In Fig. 29 the simulated and experimental Mean Residence Times (MRT) on overflow are shown as a function of grain sizes. In Fig. 30 the simulated RTD function and RTD function calculated from experimental data are shown.

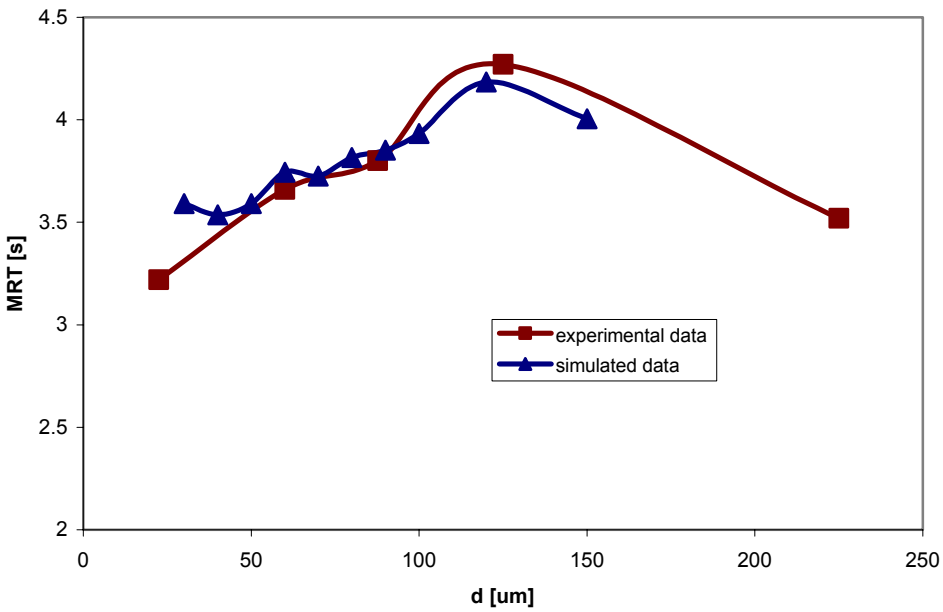

FIG. 29. CFD Simulated and experimental Mean Residence Times (MRT) on overflow as a function of grain sizes.

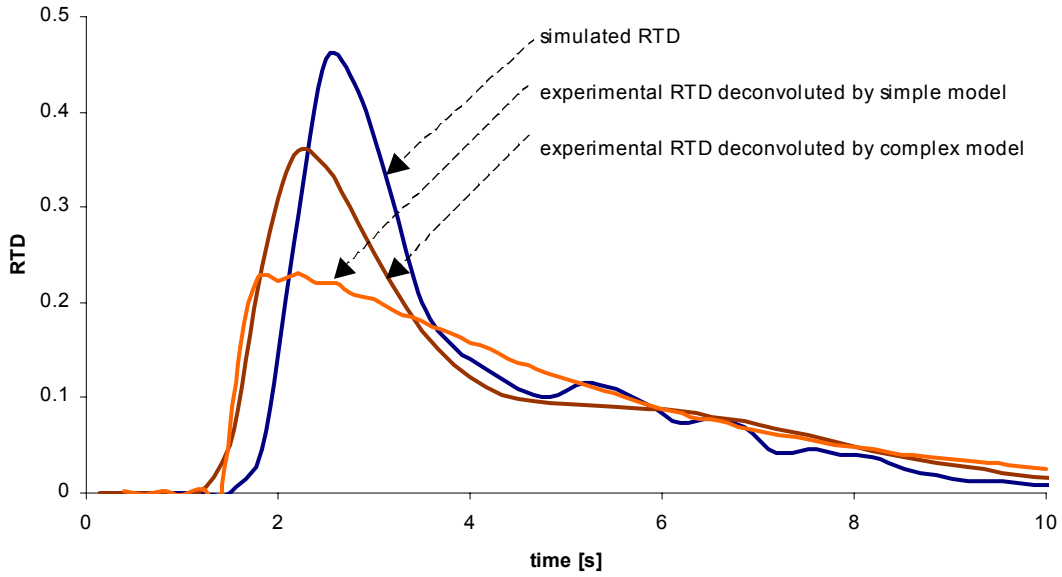

FIG. 30. CFD Simulated and experimental RTD on overflow for grain size d=22.5 µm.

5. CONCLUSION

The radiotracer experiments in copper enrichment hydrocyclones provide major hydrodynamics parameters for understanding better the separation process. RTD results in the hydrocyclone help the analysis and macro modeling of the system.

The CFD simulations of water and solid particles flows provide additional information about the flow map inside the hydrocyclone. At the first step of the CFD simulations, the modeling of one-phase flow (water) in the hydrocyclone has been done. At the second step the flow of solid particles in the hydrocyclone has been simulated. The preliminary CFD simulation results were in agreement with the RTD experimental data. Both of them are important for description of the solid particles' separation in the hydrocyclones. The hydrocyclone separators study by combining the radiotracer RTD experiments and CFD simulation is just an example of the significant possibility of utilization the CFD simulations and RTD experiments for the industrial processes evaluation, control and optimization. The research work proofed that the CFD simulation of hydrocyclones is possible and the methodology applied was correct. The simulation of the homogeneous matter (water + solids) and the solid grains separation under real industrial condition will be performing soon.

REFERENCES

[1] PETRYKA L., FURMAN L., PRZEWLOCKI K., STEGOWSKI Z. (1993), *Radioisotope Investigation of Copper Ore Dressing Processes*, Nuclear Geophysics,, vol. 7 no. 2, pp. 313.

[2] FURMAN, L.; PETRYKA, L.; STEGOWSKI, Z.; WIERZBICKI, A., (2003), *Data acquisition and processing in radiotracer experiments*, Nuclear Instruments and Methods in Physics Research Section B: Vol: 211, Issue: 3, pp. 436–442.

[3] DANCKVERTS P.V. (1953), *Continuous flow systems, Distribution of Residence Times*, Chemical Engineering Science, 2, 1, 1–13.

[4] KREFT A., ZUBER A., (1978), *On the Physical Meaning of the Dispersion Equation and Its Solution for Different Boundary Condition*. Chem. Engng. Sci. 43, 1471.

[5] THYN J., ZITNY R., KLUSON J., CECHAK T., (2000), *Analysis and Diagnostics of Industrial Process by Radiotracers and Radioisotope Sealed Sources*, Czech Technical University, Prague.

[6] FURMAN L., (2002) *Z-Transform and Adaptive Signal Processing in Analysis of Tracer Data*, The Canadian Journal of Chemical Engineering, June 2002, Vol. 80, No. 3, 472–477.

[7] STEGOWSKI Z. (1993), *Accuracy of Residence Time Distribution Function Parameters*, Nuclear Geophysics, vol. 7 no. 2, p. 335.

[8] LECLERC J-P., DETREZ C., BERNARD A. AND SCHWEICH D. (1995) RTD software helping fluid modeling *in reactors,* Revue de l'Institut Français du Pétrole, 50, 5, 641–656.

[9] LEVENSPIEL O. (1999) Chemical Reaction Engineering, 3 ed., John Wiley & Sons, New York.

[10] PRZEWLOCKI K., PETRYKA L., STEGOWSKI Z. (1990) *Radiotracer Identification of the Copper Ore Beneficiation Process*, Isotopenpraxis,, vol. 26, n°9, pp. 439–444.

[11] STEGOWSKI Z. AND LECLERC J-P. (2002), *Determination of the solid separation and residence time distributions in an industrial hydrocyclone using radioisotope tracer experiments*, International Journal of Mineral Processing vol. 66, pp. 67–77.

[12] POPE B. S. (2000), *Turbulent Flow*, Cambridge University Press.

[13] SALAS M.D., HEFNER J.N., SAKELL L. (1999), *Modelling Complex Turbulent Flows*, Kluwert Academic Publishers.

[14] WILKES J.O. (1999), *Fluid Mechanics for Chemical Engineers*, Prentice Hall PTR, New Jersey.

APPLICATION OF RADIOTRACER TECHNOLOGY AND CFD FOR DIAGNOSIS OF WASTEWATER TREATMENT PLANT

J.H. JIN, S.H. JUNG, J.B. KIM
Korea Atomic Energy Research Institute,
Yuseong, Daejon, Republic of Korea
D.S. JANG, H.S. KIM, M.S. SHIN
Department of Environmental Engineering,
Chungnam National University, Daejon, Republic of Korea

Abstract

The radionuclides ^{113m}In-EDTA and $^{131}I^-$ were used as tracers for large-scale unit and it was observed that $^{131}I^-$ shows more stable detection results rather than ^{113m}In-EDTA. In spite of its short half-life, ^{113m}In also has many advantages that it emits appropriate gamma energyas tracer and can be easily produced from a portable radionulide generator in the field. CFD simulation from two-dimensional model produced the concentration-time (RTD) curves that are very much similar with radiotracer data and they were compared with each other for evaluating the flow pattern qualitatively and quantitatively. The simulated RTD profiles are generally in a good agreement with the experimental RTD curves at the upstream and the middle-stream sections but a great difference was observed at the area of discharge weirs. The CFD simulation program developed from the radiotracer RTD validation method shows the potential role for the design and determination of optimal operating condition of a clarifier. But the quantitative evaluation of 3-D configuration of the weir will be one of the major research topics by the development of 3-D CFD model in near future.

1. INTRODUCTION

The objective of this study was to develop and elaborate radiotracer experimental techniques for validation of CFD model of a clarifier in wastewater treatment plant.

Separation of suspended particles from wastewater by gravitational force is the most common and extensively applied treatment process in wastewater treatment plants. The performance improvement of a clarifier has been one of the important topics of numerous theoretical and experimental studies because the investment for settling tanks in wastewater treatment plants is as high as about 30% of the total investment (Stamou, 1994). In recent year the standard of effluent quality is getting more and more stringent for the protection of environment in every country.

The efficiency of clarifier depends on the characteristics of the solids (particle size, density, settling velocity, and concentration), the flow field (inlet flow velocity, flow rate, turbulence intensity), and the geometrical dimension of clarifier. Especially the determination of the flow field in the secondary clarifiers and thereby physical solution is not easy problem due to the strong buoyancy effect of density variation by the concentration of solids.

Computational fluid dynamic (CFD) model was developed for a rectangular clarifier of WWTP. Using this model, the flow pattern was investigated in terms of hydrodynamic characteristics and suspended solid loading, which causes the density waterfall phenomenon in the inlet zone. Most numerical models presented in open literature have been mainly restricted to primary clarifiers with discrete particle suspension at relatively low concentrations operating in a neutral density environment.

The CFD model developed is able to predict the behavior of the sediment induced density currents in rectangular final clarifier. Residence time distribution (RTD) of radiotracer was also calculated from the CFD model and then compared with the experimental results to validate the model developed with RTD profiles as a protocol for mutual comparison between CFD and RTD results.

In short, the objective of this study was to develop a reliable computer program to predict the flow patterns and to obtain a sound understanding for a full-scale final clarifier. It will be a viable tool to assist in the design and determination of optimal operating condition of a final clarifier.

2. THE CFD MODEL FOR RECTANGULAR CLARIFIER AND ITS SOLUTION

The flow patterns for density-stratified fluids in a settling clarifier are usually quite different from those with uniform density under the same external and boundary conditions. The relative importance of inertial and gravity forces in the settling tank can be characterized in terms of the initial momentum and buoyancy flux defined by the inlet densimetric Froude number, F.

$$F = \left[u_0^{\,2} / \frac{gH_{in}(\rho - \rho_r)}{\rho_r} \right]^{1/2} \tag{1}$$

in which ρ_r = the reference density (clean water). The value of ρ is the local density of mixture; u_0 = influent velocity; and H_{in}= depth of influent stream.

The local fluid density is related to the local values of sediment concentration given by

$$\rho = \rho_r + C(1 - S_S^{-1}) \tag{2}$$

where C = solid concentration and SS = the specific gravity of the solid particles.

A numerical model consists of a set of conservation equations for continuity and momentum, turbulence kinetic energy k, dissipation of turbulence energy ε and solid concentration. They can be expressed as in a governing equation

Governing equation

$$\frac{\partial(\rho\phi)}{\partial t} + \frac{\partial}{\partial x_j}(\rho \vec{u_j}\phi) = \frac{\partial}{\partial x_j}(\Gamma_\phi \frac{\partial \phi}{\partial x_j}) + S_\phi \tag{3}$$

U-momentum equation

$$\frac{\partial u}{\partial t} + u\frac{\partial u}{\partial x} + v\frac{\partial u}{\partial y} = -\frac{1}{\rho}\frac{\partial p}{\partial x} + \frac{\partial}{\partial x}(\nu_t \frac{\partial u}{\partial x}) + \frac{\partial}{\partial y}(\nu_t \frac{\partial u}{\partial y}) + S_u \tag{4}$$

V-momentum equation

$$\frac{\partial v}{\partial t} + u\frac{\partial v}{\partial x} + v\frac{\partial v}{\partial y} = -\frac{1}{\rho}\frac{\partial p}{\partial y} + \frac{\partial}{\partial x}(\nu_t \frac{\partial v}{\partial x}) + \frac{\partial}{\partial y}(\nu_t \frac{\partial v}{\partial y}) + g\frac{\rho - \rho_r}{\rho} + S_v \tag{5}$$

where $S_u = \frac{\partial}{\partial x}(\nu_t \frac{\partial u}{\partial x}) + \frac{\partial}{\partial y}(\nu_t \frac{\partial v}{\partial x})$ and $S_v = \frac{\partial}{\partial x}(\nu_t \frac{\partial u}{\partial y}) + \frac{\partial}{\partial y}(\nu_t \frac{\partial v}{\partial y})$ (6)

SS concentration equation

$$\frac{\partial C}{\partial t}+u\frac{\partial C_i}{\partial x}+v\frac{\partial C_i}{\partial y}=\frac{\partial}{\partial x}(\nu_{sx}\frac{\partial C_i}{\partial x})+\frac{\partial}{\partial y}(\nu_{sy}\frac{\partial C_i}{\partial y}+V_sC_i) \quad (7)$$

where φ denotes general dependent variables expressed as a physical quantity per unit mass.

Further, u, v, ρ, $\Gamma\ \phi$ and $S\phi$ stand for x, y velocity components, density, diffusion coefficient and source term corresponding to φ, respectively. Eqn (7) is a convection and diffusion equation for the suspended solid particles where Vs is the settling velocity .

The main feature of the density–induced flow field in final clarifier is known to be strongly affected by solid distribution and removal rate (DeVantier and Larock, 1987; Lyn et al., 1992). The settling velocity of a particle contained in a disperse suspension, as specially found in final clarifier, is also dependent on both its individual characteristics (size, density, shape, etc.) and interactions with other particles. In low concentration, the effect of particle interaction is not significant and thus each particle settles as a separate entity while in high concentration, inter-particle force hinders the settling process of the particle, which settles as a unit, with decreasing mass velocity as the concentration increases (Vesilind, 1968; Takacs et al., 1991).

Therefore modeling the settling properties of SS is one of the significant processes in the development of solid transport models of a final clarifier.

A number of empirical formulas have been proposed to describe the relationship between solid concentration and solid settling velocity. For low SS concentration, settling velocity may be calculated with a discrete settling model. The settling velocity of particle is dependent on its size, which develop that larger particles show up higher settling velocities.

Discrete settling model

$$V_s = 0.35+1.77D_i \quad (8)$$

where: D_i = 0.05~1.4mm (Vesilind, 1968; Takacs et al., 1991).

Since solid concentration in a final clarifier typically varies from relatively high values of the inlet suspension to low values of the clarified effluent, a specific discrete settling model cannot be applied consistently to the entire volume of the clarifier.

Therefore, in recent years, Takacs et al.(1991) proposed a monodisperse settling model in which the average settling velocity V_s of the settleable fraction of SS is given by the sum of two exponential terms:

Monodisperse settling model

$$V_S = V_0[e^{-K(C-C_{\min})} - e^{-K_1(C-C_{\min})}] \quad (9)$$

where V_o = Stokes velocity (settling velocity of single particle in clear water)

K = an empirical coefficient for rapidly settling flocks

C_{min} = the concentration of non-settling flocks

K_1 = a settling exponent for the poorly settling particles

The first term in Eqn. (9) reflects the settling velocity of the large particles, whereas the second term is a velocity correction factor to account for the smaller, slowly settling particles.

For low concentration, Eqn. (9) is more sensitive to k_1 and it gives increasing values of V_s as the concentration increases, whereas for high concentration it reduces to Vesilind's equation [Mazzolani *et al.*, 1998]. The regions of low and high solid concentrations are separated by the point where V_s reaches a maximum value.

The application of two distinct settling models in the numerical analysis of a final clarifier produces somewhat different results of SS concentration and removal rate but the main features of the hydrodynamics show a qualitatively similar trend.

The eddy viscosity, ν_t is calculated from the k-ε turbulence model which relates ν_t to the turbulence kinetic energy of k and the turbulence dissipation rate ε. The formula is:

$$\nu_t = C_\mu \frac{k^2}{\varepsilon} \tag{10}$$

The distribution of k and ε is calculated from the following semi-empirical transport equations.

$$\frac{\partial k}{\partial t} + u\frac{\partial k}{\partial x} + v\frac{\partial k}{\partial y} = \frac{\partial}{\partial x}\left(\frac{\nu_t}{\sigma_k}\frac{\partial k}{\partial x}\right) + \frac{\partial}{\partial y}\left(\frac{\nu_t}{\sigma_k}\frac{\partial k}{\partial y}\right) + P - \varepsilon \tag{11}$$

$$\frac{\partial \varepsilon}{\partial t} + u\frac{\partial \varepsilon}{\partial x} + v\frac{\partial \varepsilon}{\partial y} = \frac{\partial}{\partial x}\left(\frac{\nu_t}{\sigma_\varepsilon}\frac{\partial \varepsilon}{\partial x}\right) + \frac{\partial}{\partial y}\left(\frac{\nu_t}{\sigma_\varepsilon}\frac{\partial \varepsilon}{\partial y}\right) + C_1\frac{\varepsilon}{k}P - C_2\frac{\varepsilon^2}{k} \tag{12}$$

in which P is the production of turbulent energy by the mean velocity gradients as

$$G_{k1} = \mu_t\left[2\left(\frac{\partial \bar{u}}{\partial x}\right)^2 + 2\left(\frac{\partial \bar{v}}{\partial y}\right)^2 + \left(\frac{\partial \bar{u}}{\partial y} + \frac{\partial \bar{v}}{\partial x}\right)^2\right] \tag{13}$$

The k- ε model constants, C_1, C_2 and C_μ as well as turbulent Prandtl numbers for k and ε, σ_k and σ_ε are selected as the conventional standard values of 1.42, 1.68, 0.09, 0.9 and 0.9, respectively.

Boundary conditions for u, v, k, ε and C_i are minutely presented in a previous work [H.S.,Kim et al, 2003] and are briefly mentioned for completeness. A uniform parallel inlet flow is assumed with specified values of k and $\varepsilon = C_\mu^{3/4}(k^{3/2}/l_m)$.

The inlet SS loading is assumed to be in a well mixed state with dimensionless concentration unit. The outlet boundary values are computed from near outlet grid points by satisfying the overall mass continuity. Near wall velocities parallel to the wall are calculated using the local logarithm law. Near wall k and ε can be calculated from the assumption of local equilibrium condition. The clarifier bottom is treated as a perfect absorbing boundary where particles may not be resuspended by the fluid flow.

A control volume-based finite difference method by Partankar is used for the discretization of the general 2-D governing equation together with the SIMPLEC (Semi-Implicit Method for Pressure Linked Equations Consistent) algorithm for the pressure-linked momentum equation.

Eqn (14) shows the general discretized form for the above governing Eqn (3).

$$a_p\phi_p = a_E\phi_E + a_W\phi_W + a_N\phi_N + a_S\phi_S + b \tag{14}$$

where a_E, a_W, a_N, a_S, and a_P are coefficients of east, west, north, south and main grid nodes.

Eqn (14) is solved iteratively due to the nonlinear feature of the implicit equation with the use of line-by-line TDMA. Steady state solution is obtained starting from initially guessed value. The flow

and solid transport equation coupled in the densimetric source term are simultaneously calculated in every iterative process.

3. RADIOTRACER EXPERIMENTS

RTD profiles with ^{113m}In-EDTA as a tracer

The radiolabelled tracer, ^{113m}In-EDTA, was injected at the outlet of aeration tank, which is located ahead of the clarifier. EDTA is a complex compound, which is considered as a good tracer of water. It flows along with water in the clarifier.

Figure 1 shows the positions of 12 radiation detectors in the clarifier that is 52m long and 7.5m wide. Figure 2 presents the result of radiotracer experiment from which the break-through time and maximum concentration time at each detector was calculated and summarized in table I.

According to the order each detector records the radiotracer, it was observed that a circulating flow is present behind the baffle. The fast flow flowing at the bottom was simulated as axial dispersion model without consideration of water dispersion and change of mass balance. In spite of this simplification, the simulation curve fits quite well to the experimental result as shown in figure 3.

As a radionuclide, ^{113m}In has many advantages such as low gamma energy and short half-life, and especially the availability from the portable generator. But compared with the mean residence time of the clarifier (>3hrs.), the half-life of ^{113m}In (99.5min) is relatively short. The radiation measurement error was gradually getting increased since the middle of the experiment. It is strongly recommended to use other radionuclides whose half-lifes are comparable with flow transit time to guaranty a better accuracy.

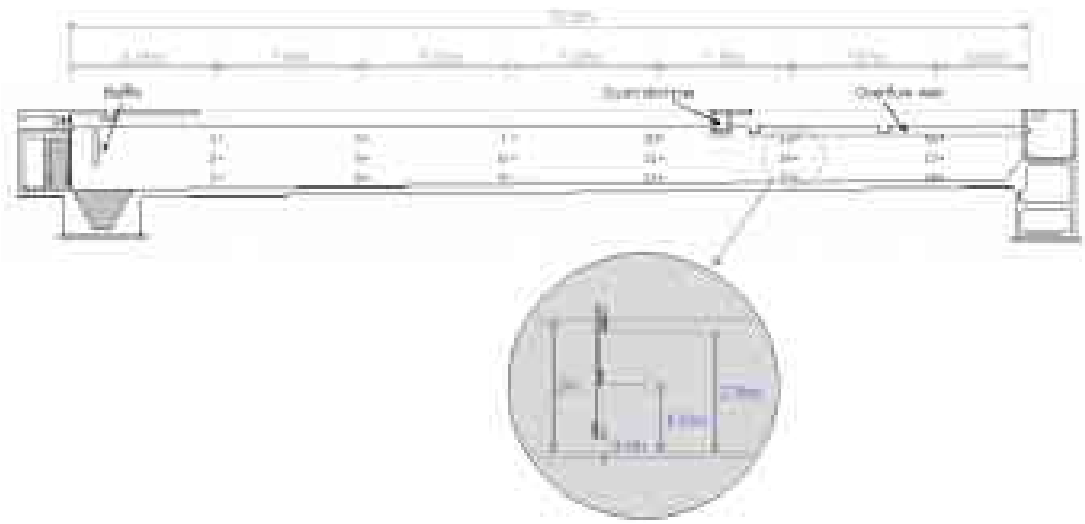

FIG. 1. The clarifier for RTD study and the position of detectors.

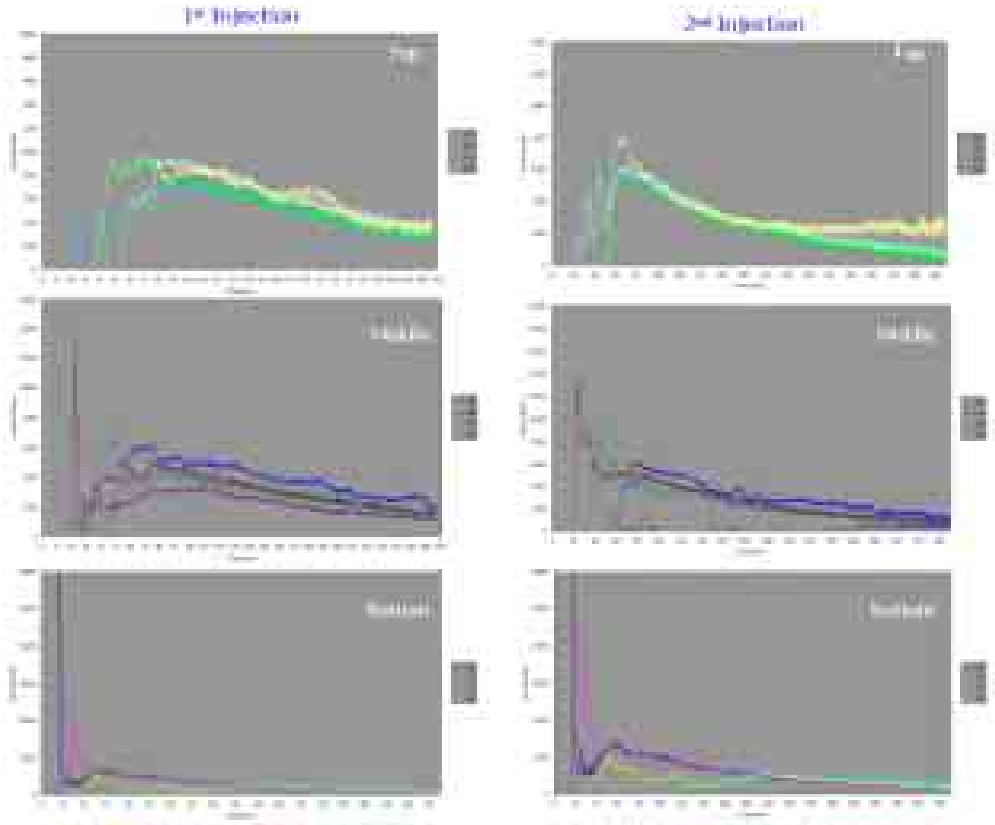

FIG. 2. Evolution of radiotracer concentration at the position of each detector.

TABLE III. THE BREAK-THROUGH TIME AND THE MAXIMUM CONCENTRATION TIME OF CLARIFIER.

Position		C1	C2	C3	C4
Break-through time (sec)	top	110	930	1010	3090
	middle	110	490	690	1670
	bottom	60	310	590	1970
Maximum concentration time (sec)	top	600	1740	2370	3620
	middle	180	1550	1570	3000
	bottom	80	410	870	2380

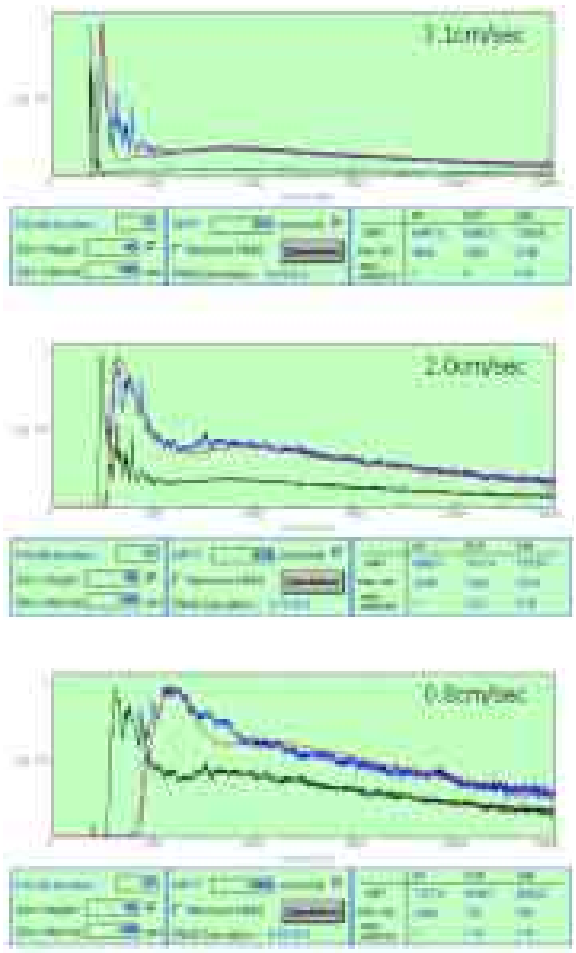

FIG. 3. The result of RTD analysis using axial dispersion model.

RTD Profiles with 131I- as a Tracer

In the previous experiment, the Residence Time Distribution was measured by making use of ^{113m}In-EDTA as a tracer and the results were supplied to CFD modeler in order to help them to figure out the method to compare the RTD data with the CFD simulation. The radionuclide, ^{113m}In, extracted from a Sn/In portable generator is pretty much available but its half-life (99.5min) was not enough to measure RTD of the clarifier which has over 3 hours as MRT.

^{131}I ($T_{1/2}$= 8.04days) is routinely produced from HANARO, the research reactor in KAERI, in order to supply to domestic hospitals for medical purpose. It may have too long half-life for this application but it is very advantageous. ^{131}I in anionic form (in NaI solution) is very good and stable tracer of water, and easy to handle due to relatively low gamma energy. The tracer detection was performed at the same position as in the first experiment of using ^{113m}In-EDTA and the results are plotted in figure 4.

For quantitative analysis, the break-through time and the maximum concentration time was calculated from the radiotracer results and compared with those from CFD simulation. The flow behavior can also be studied by comparing the pattern of RTD curves at detection positions.

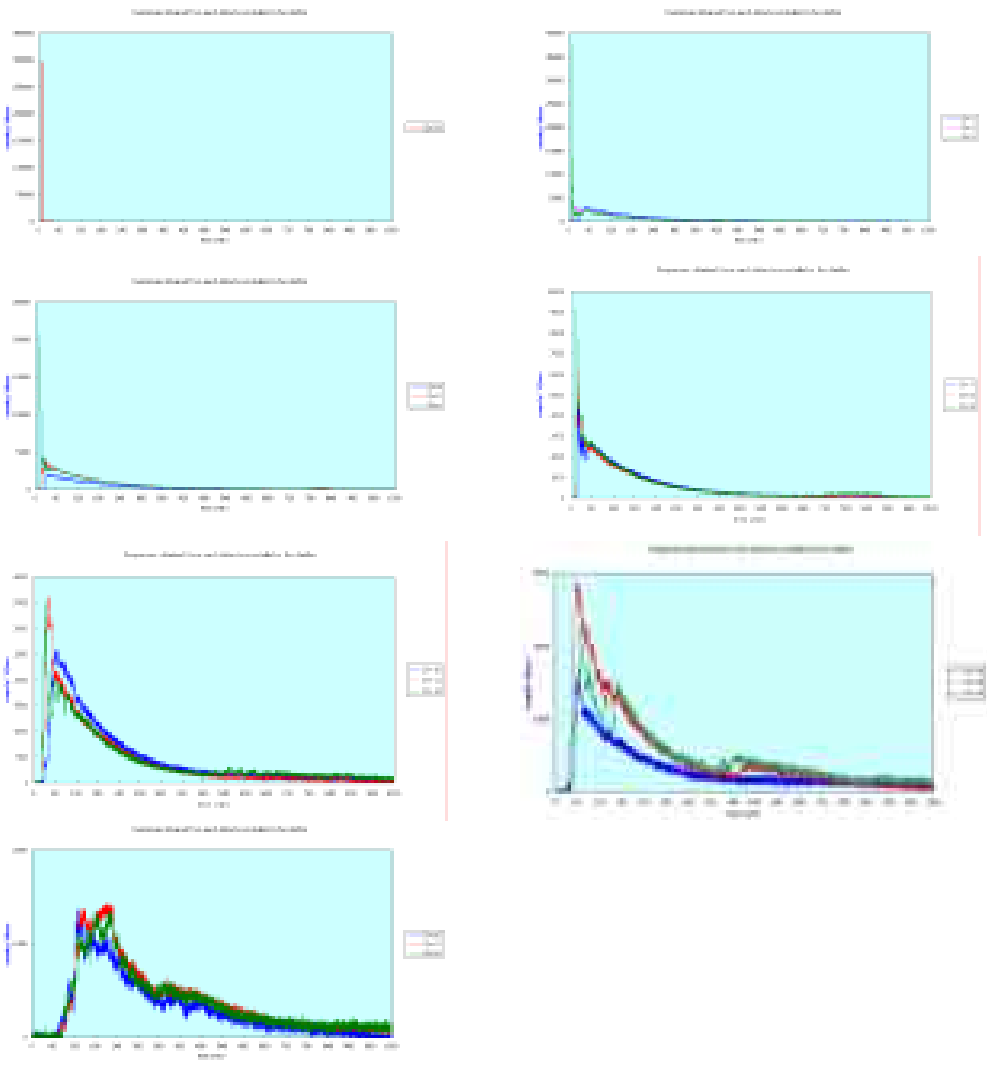

FIG. 4. The responses at each detectors installed inside the clarifier.

In the latest radiotracer experiment, the radiation detectors were installed close to the longitudinal central streamline to measure the flow pattern that is representative for the overall flow and can be directly compared with the CFD simulation results. The depth of each detector was adjusted so that the continuously circulating scrapper collecting sludge on the bottom didn't make disturbance to the detectors during the experiment.

The positions of detectors are shown in figure 5 and the experimental results will be used for the 3-dimensional CFD model validation of the future study.

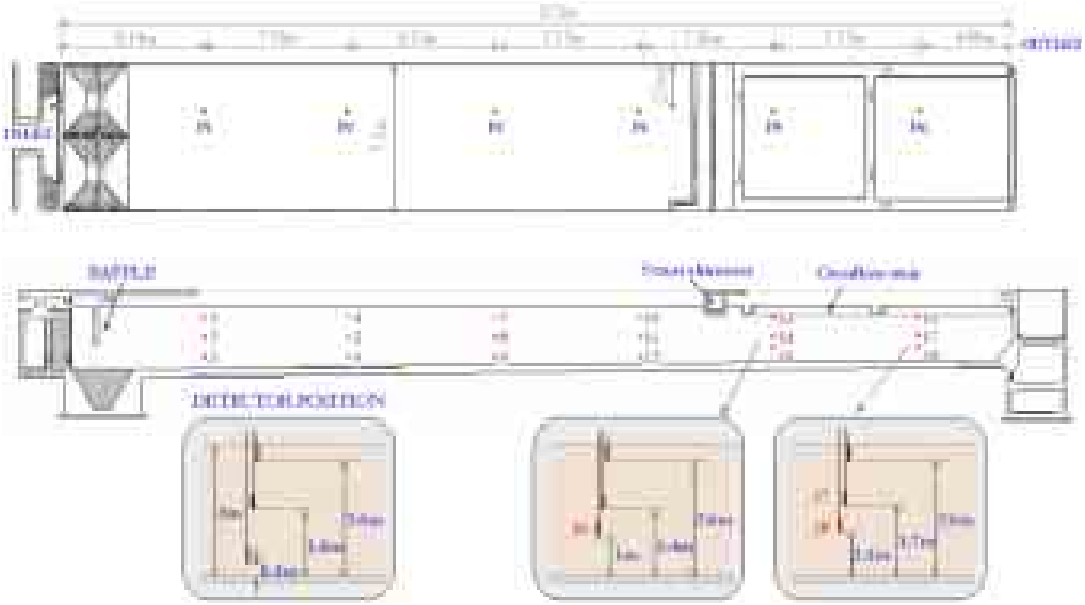

FIG. 5. Radiotracer detection points located near the longitudinal central streamline.

4. CALCULATION RESULTS AND DISCUSSIONS

Density Effect

The flow field is affected by the hydraulic characteristics and SS concentration. Fig. 6 and 7 show the density effect caused by the SS inlet loading. As shown in figure 6 the influent flow for neutral density situations is deflected strongly downward after impinging on the reaction baffle. The downward current impinges on the tank bottom below the reaction baffle and then goes upward right behind the baffle and forms two visible recirculation zones. In neutral density condition, uniform flow occurs except the neighborhood of baffle, which is not the real phenomenon in a final clarifier.

Considering the density effect as shown in figure 7, the horizontal inlet jet does not reach and strike the flow-control baffle, but plunges toward the tank bottom as a density waterfall due to the low densimetric Froude number. The inlet concentration of C0 is 1300ppm. Under the submerged lip of the baffle, a strong counter flow re-entered the inlet zone to provide for the entrainment of fluid by the density waterfall. And then the flow forms a forward bottom current on the settling zone and goes upward on the withdrawal zone. The strength of the bottom density current, the upward flow in the withdrawal zone, and the recirculation are getting increased with a decreasing inlet velocity and higher SS inlet loading (low Froude number). Therefore, the calculation result shows that SS inlet loading affects significantly on the flow pattern in the clarifier.

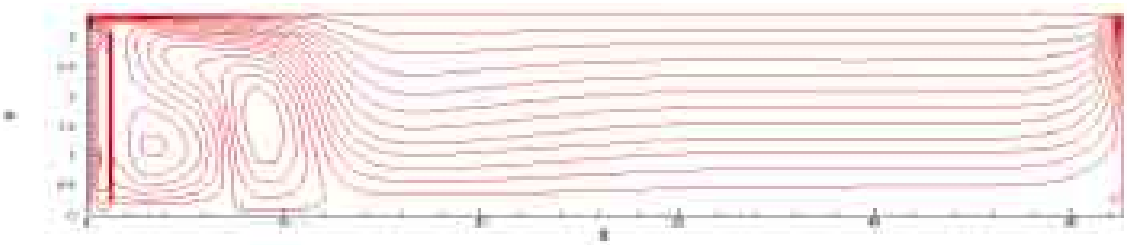

FIG. 6. Predicted streamline contour plot for neutral density situation (Uin=3cm/sec,Cin=0ppm).

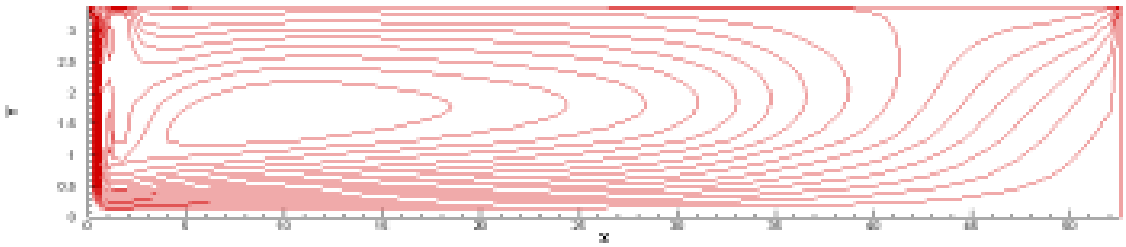

FIG. 7. Predicted streamline contour plot with the inclusion of SS density effect (Uin=3cm/sec, Cin=1300ppm).

As shown in figure 8, the solid distribution in the inlet zone is nearly uniform except for a shallow bottom layer. A significant dilution occurs below the baffle lip, which is called a local entrainment zone. The contour line of 650mg/l enters even in the inlet zone because of dilution by the entrainment. If the distance between inlet and baffle increases more, the effect of entrainment compensation flow will become more significant. There is an abrupt change in the solids distribution downstream of the baffle due to deflection of influent solids by reaction baffle and the downward flow of the surface return current in this region. The minimum solid concentration region appears in the water surface layers, where downward flow current increases the downward flux. However, in the withdrawal region, solid contours are shifted upward due to the upward current in this region. The upward velocities counteract the settling velocity of the particles; the fine particles in the upper layers are most sensitive to the upward flow velocities.

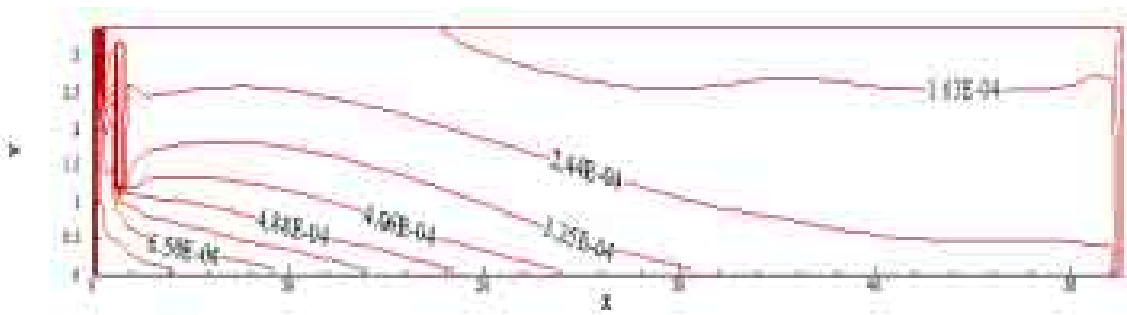

FIG. 8. Suspended solid distribution (Uin=3cm/sec, Cin=1300ppm).

Effect of Outlet Configuration

Vertical outlets on the water surface are modelled to describe accurately the effluent top weirs instead of horizontal end outlet. Figure 9 also includes a distribution port in which the fluid divide uniformly and flow into the final clarifier. Some of return flow goes outward through top outlets and others form circulating flow in the settling zone as shown in figure 9(a). Return flow and upward flow are not clearly divided like Fig. 7, which enlarge the settling zone so that SS have many chances to settle down and then the removal efficiency reaches over 96%.

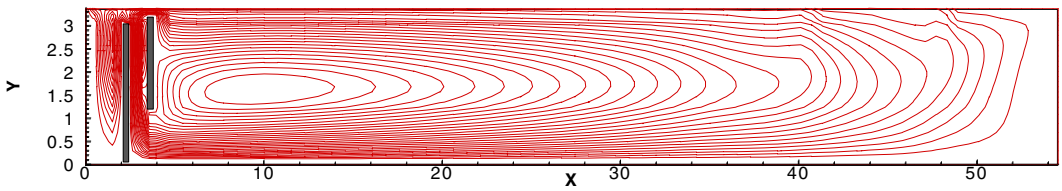

(a) Streamline contour (Uin=0.23cm/sec, Cin=900ppm)

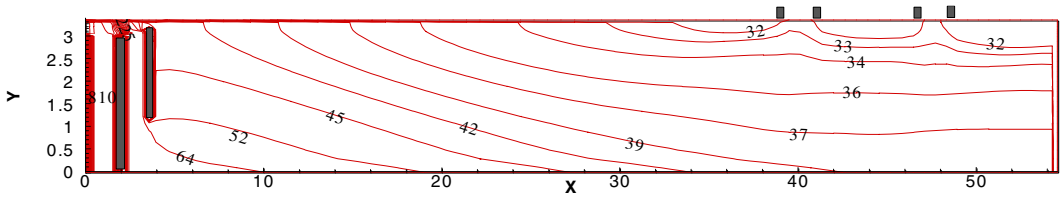

(b) Suspended solid distribution (Uin=0.23cm/sec, Cin=900ppm)

FIG. 9. Flow pattern as the change of outlet configuration.

Distribution of Radiotracer

Radioisotope in aqua phase was injected at the end of aeration tank as a short pulse so that two component mixtures of tracer and water were modelled to simulate experiment laterally after the flow with SS loading was stabilized.

Figure 10 shows the concentration field of radiotracer in the final clarifier. The tracer strongly mixes with ambient fluid in the distribution port where the influent is uniformly divided into top inlets without any settling of SS as shown in figure 10(a). And then tracer forms a high concentration field in the bottom due to the density effect and flows to the exit along the bottom as time goes by.

In figure 10(c) and (d), radiotracer shows high concentration behind the inlet baffle by the surface return flow and also the high concentration field slowly disappears in the bottom of clarifier. With the lapse of time, tracer behind the inlet baffle moves to the settling zone shown in figure 10(e).

When the radiotracer reaches the withdrawal zone such as figure 10(f) and (g), it diffuses upward and discharges into the effluent weirs. It is expected that lots of tracer leave out the clarifier after 3 hours, which is quite similar with the designed residence time.

Based on the observation of the behavior of radiotracer, it is considered that tracer will be detected earlier in the bottom region with high concentration than any other locations due to effect of the high bottom current.

(a) after 10 min

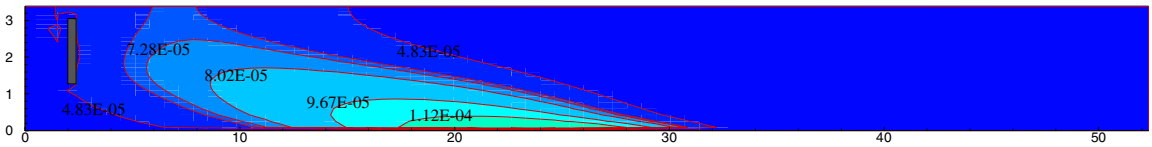

(b) after 30 min

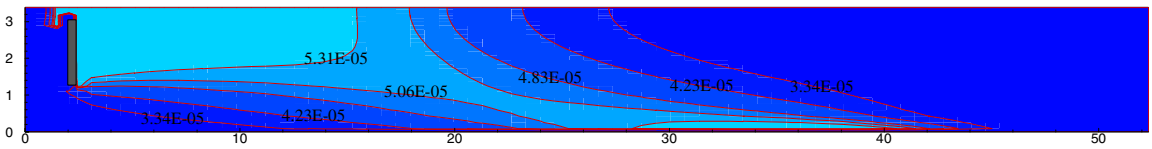

(c) after 60 min

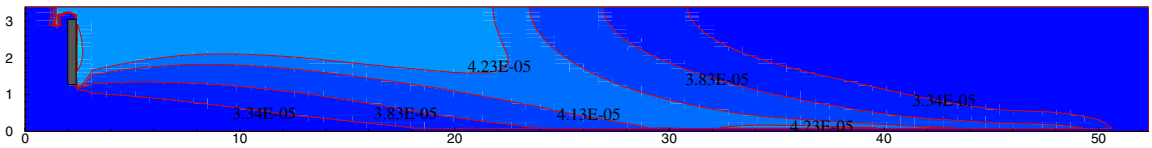

(d) after 90 min

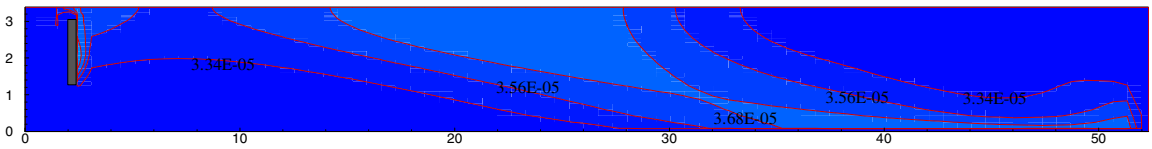

(e) after 120 min

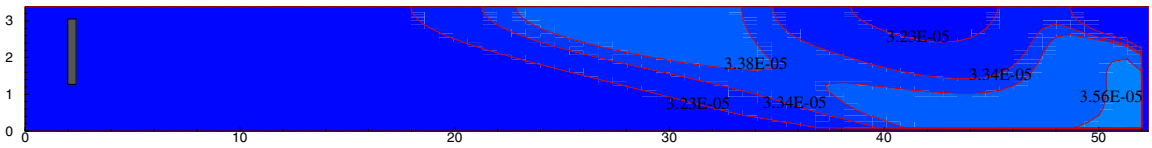

(f) after 150 min

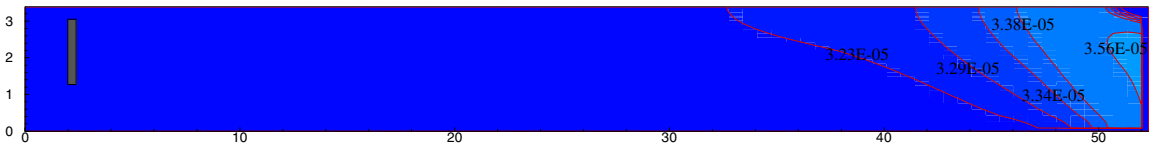

(g) after 180 min (designed retention time)

FIG. 10. Tracer distributions with the elapsed time.

5. RTD ANALYSIS AND MODEL VALIDATION

A few tracer experiments were conducted on the final clarifier in a wastewater treatment plant, Korea to validate the developed CFD model. ^{131}I as a tracer was used and injected as a pulse at the end of aeration tank located right ahead of final clarifier. Detection was performed at 20 points in the clarifier, including the inlet (point 20) and the exhaust opening (point 19) as shown in figure 11. Detection was performed far away from the centerline because the scrapper circulating the whole clarifier to remove scum on top and settling solids on the bottom of the clarifier. The contribution of the background radiation to data was eliminated before the decay correction that makes the radiation counts independent on time.

Table II shows the flow rate introduced into each clarifier during the experiment where the flow rate was fluctuated as time. Average theoretical velocity was calculated at 0.0023m/sec of which value used as the fixed inlet boundary for the execution of model. For more accurate prediction, fluctuations of influent were directly reflected on the transient inlet boundary, which compared with the fixed one afterwards.

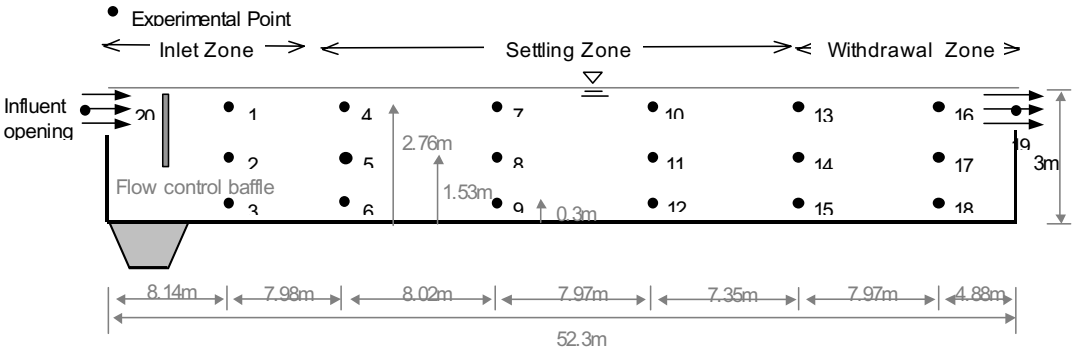

FIG. 11. Experimental points in the rectangular clarifier.

TABLE IV. INFLUENT FLOW RATE WITH TIME

Date	Hour	Flow rate to 36 clarifiers (m^3/3hrs)	Flow rate (m^3/sec)	Average theoretical velocity (m/s)
June 4	15:00~18:00	23,000	0.059	0.002
	18:00~21:00	26,600	0.068	0.003
	21:00~24:00	28,100	0.072	0.003
June 5	00:00~03:00	21,400	0.055	0.002
	03:00~06:00	17,500	0.045	0.002
	06:00~09:00	16,100	0.041	0.002
	09:00~12:00	23,300	0.060	0.002
Total flow rate (m^3/3hrs)		7,429	0.019	0.001
Average theoretical velocity (m/s)		0.0022	0.060	0.002

Average theoretical flow through velocity, U = Q / WD

Figure 12 and 13 shows RTD profiles where solid and dotted lines represent the experimental RTD and the predicted RTD, respectively. Channel number (CH) means the detection location of radiotracer along the horizontal direction with various depths.

In the inlet zone, the comparison data between the predicted and measured RTDs made especially near the sidewall of clarifier is presented, since the 2-D approximation model fits better near sidewall instead of center plane. It should be noted that in the 2-D model the average inlet velocity calculated over the entire width of clarifier instead of a number of inlet ports results in decreased velocity. Thus it is not desirable to compare calculation data with the measured value near centerline.

It is estimated that the inlet zone reaches 30% of total length of clarifier from the analysis of RTD profiles. Therefore, the CHs from No. 1 to No. 6 can be included in the inlet zone as shown in figure 12. RTDs at CH1 and CH4 show a trend of slow decrease in concentration because the surface return flow re-enters, while the RTDs at CH3 and CH6 decrease in a quasi-exponential fashion by the strong bottom density current. Generally RTDs near the water surface show slow decrease and their arrival time of maximum concentration (Breakthrough time, BT) is delayed due to the return flow. But RTDs in the bottom shows early BT and the rapid decrease by the strong bottom density current.

In the settling zone, on the contrary, the developed program is evaluated near centerline located at 2.3m far away from the sidewall of clarifier in order to minimize the wall effect. The same argument can also be made to better fit by 2-D model. RTDs in figure 13 show smooth curve such as left-handed Gaussian profiles, where rapid bottom density current gradually decreases and also SS is favorable to settle down. Therefore the removal efficiency of SS can be improved as the extent of settling zone increases. From the analysis of RTDs, the settling zone comes to about 50% of total length of clarifier.

CH13~CH18 are located between the effluent top weirs so that the initial arrival time of tracer is late to other RTDs. The hydrodynamics of top effluent weirs and rear wall of clarifier influence the flow pattern, which also have an influence on the removal efficiency of SS. Therefore the performance of clarifier may be significantly affected by the configuration of outlet which can broaden the settling zone. Especially in CH16~CH17, a considerable difference between prediction and measurement appears in RTDs. The deeper the depth, the more this difference is reduced by the decrease of the impact of top effluent weirs. BT of CFD-CH20 appears about 80minutes later than that of experimental RTD.

As shown in figure 12 and 13, RTDs are generally in good agreement with the experimental RTDs at the upstream and center section but great differences are observed at the area of discharged weirs, CH16, CH17 and CH20. This is partly caused by the radiotracer detection made away form the calculated middle centerline in a clarifier because of the existence of a moving scrapper at that location. Another reason is considered as the limitation of present 2-D model to describe the complicated 3-D feature of effluent weirs on the water surface.

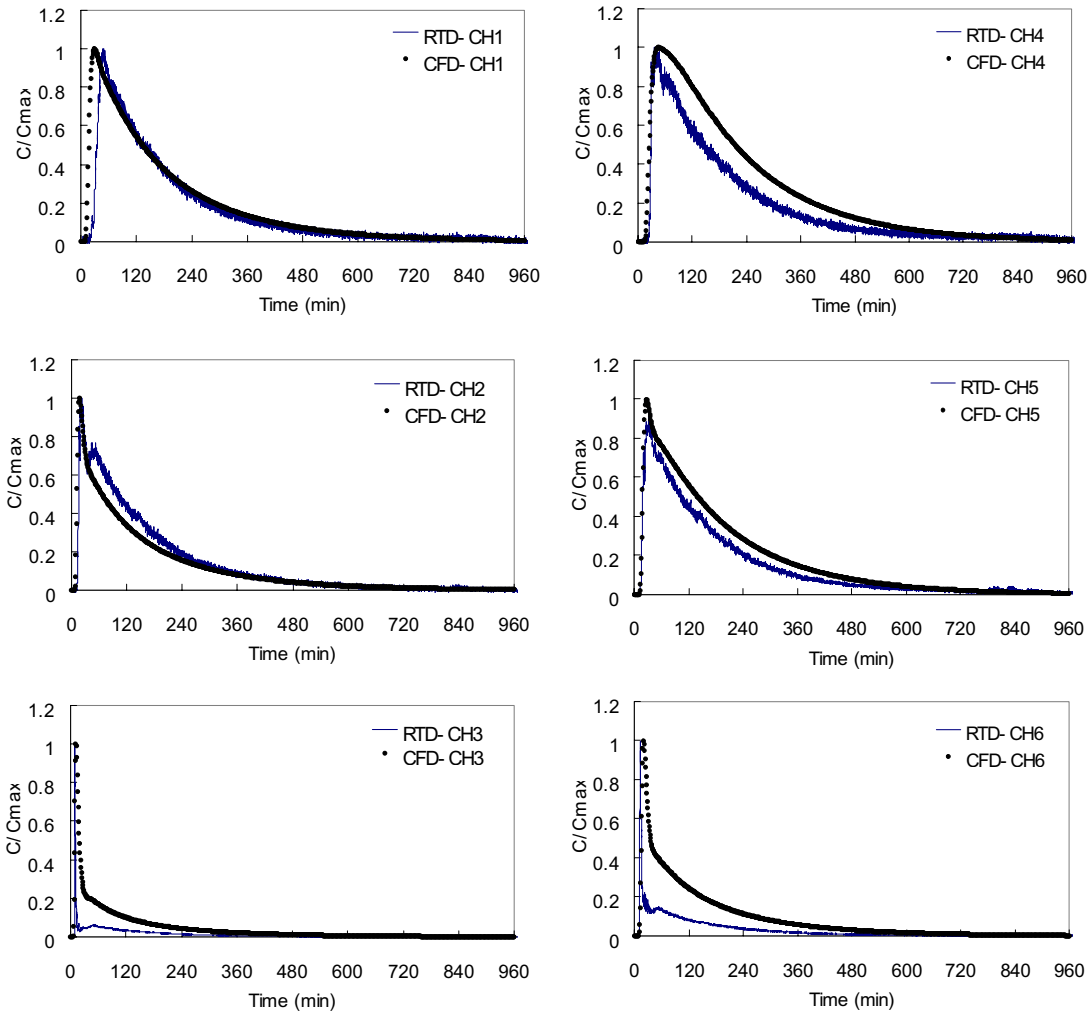

FIG. 12. Comparison of dimensionless RTDs in the inlet zone.

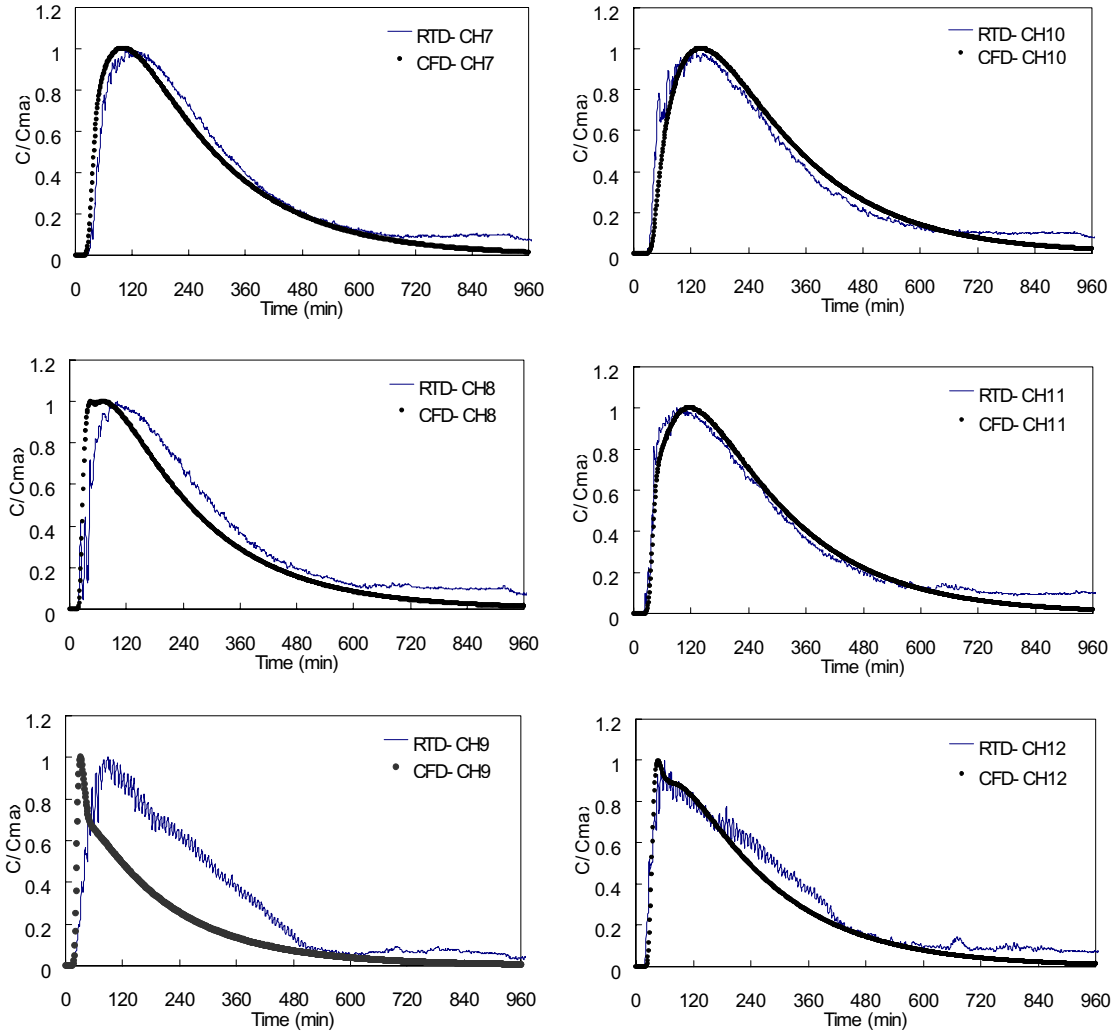

FIG. 13. Comparison of dimensionless RTDs in the settling zone.

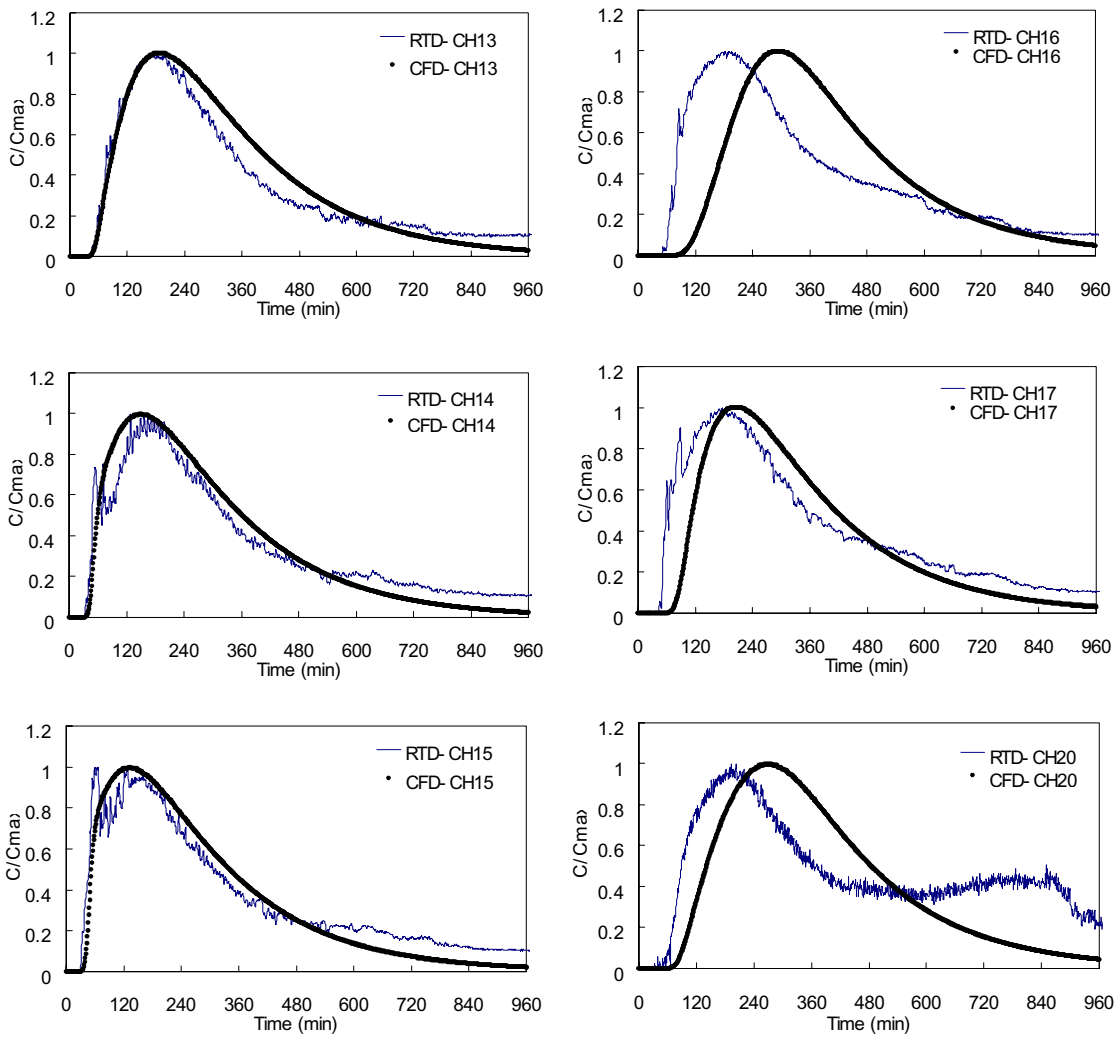

FIG. 14. Comparison of dimensionless RTDs in the withdrawal zone.

6. COMPARISON OF SETTLING MODELS

The flow field is significantly changed even by small density differences. Individual settling properties of SS are also critical for the accurate prediction of removal efficiency and solid distribution. SS distribution in the clarifier is calculated from two different settling models and then compared with each other.

Results of solid distribution with the discrete settling model (DSM) are shown in figure 15. The DSM predicts high distinct concentration for different classes of particle, which estimates lower removal rate for the slowest particles and higher removal rate for the heaviest particles. However, it yields a removal efficiency of 98.4% for the average solid distribution, which is a little bit higher than MSM because of the constant settling velocity for each particle group over the whole tank.

Figure16 shows the calculation results by using the monodisperse settling model (MSM), in which large highly-settleable SS are removed from the system before the small ones and stratified obliquely to the flow direction (Takacs et al., 1991). From comparing the streamlines shown in figure 15 (b) and figure 16 (b) it is understood that a little strong upward flow is formed in the withdrawal zone for MSM but the most of flow pattern is similar throughout the clarifier. Therefore the SS is removed in 94.3 % of the efficiency that is lower than DSM.

Comparison of two different settling models shows that solid distribution is mainly affected by settling properties of individual particles and the flow pattern in the outlet region is affected by the coupling of momentum and density. Hence, the value of settling velocity can be a key parameter to obtain reliable predictions of the removal rate.

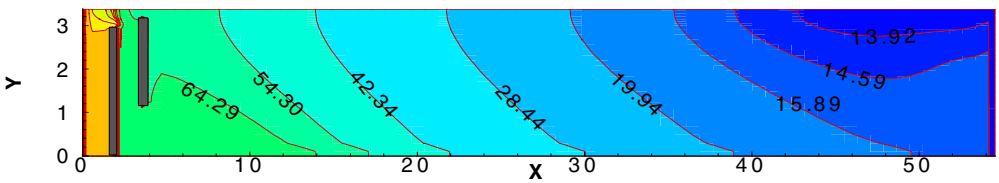

(a) Concentration field of SS

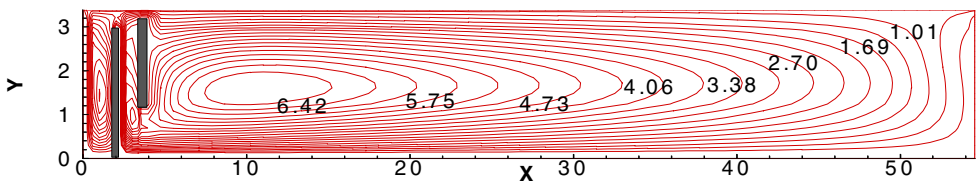

(b) Streamline contour

FIG. 15. Calculation results with DSM (Fr =0.003).

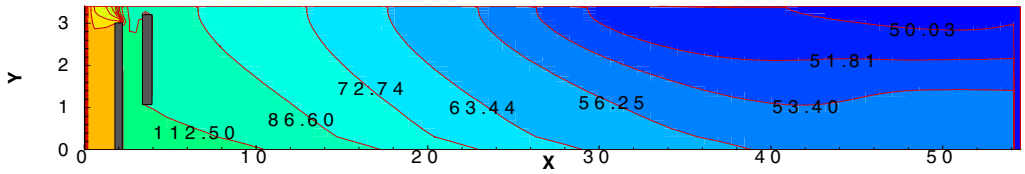

(a) Concentration field of SS

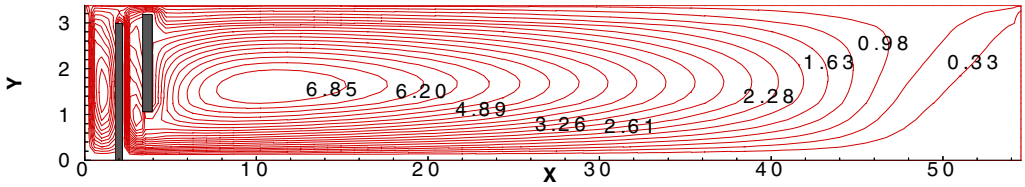

(b) Streamline contour

FIG. 16. Calculation results of MSM (Fr =0.003).

7. THREE-DIMENSIONAL CFD SIMULATION

Three-dimensional model is being set up and examined in order to simulate the complicated 3-D tank geometries of real clarifier with the help of the remarkable development in the computer technology. Especially it can describe more practically two inlet ports, outlet weirs on the water surface and sidewall of clarifier, which are difficult to be taken into account in 2-D model.

A number of achievements in simulating the clarifier have been made by introducing 3-D model. Figure 17 shows the grid generation of the 3-D clarifier with 80(L)×21(W)×13(H) where inlet and weir parts are indicated as bold lines. Some of remarkable differences are shown in the flow field compared with 2-D results. The preliminary calculation results are summarized below.

- Strength of surface return flow decreased and waterfall phenomena disappeared on the inlet section due to the high inlet velocity (increased by two order of magnitude; high Froude number)
- Formation of small recirculating flow under the vertical top weirs
- Low solid concentration in the fore part of reaction baffle
- Small entrainment of ambient fluid to the inlet zone under the baffle lip
- Upward flow near the sidewall in the inlet zone

The 3-D model should be further investigated to deal with strong buoyancy effects and the formulation of mathematical models, which requires long calculation with the difficulty of robust convergence. For this reason an appropriate turbulent model is required, combined with a computationally effective solution method, which allows a fast calculation of the coupled flow and SS concentration fields.

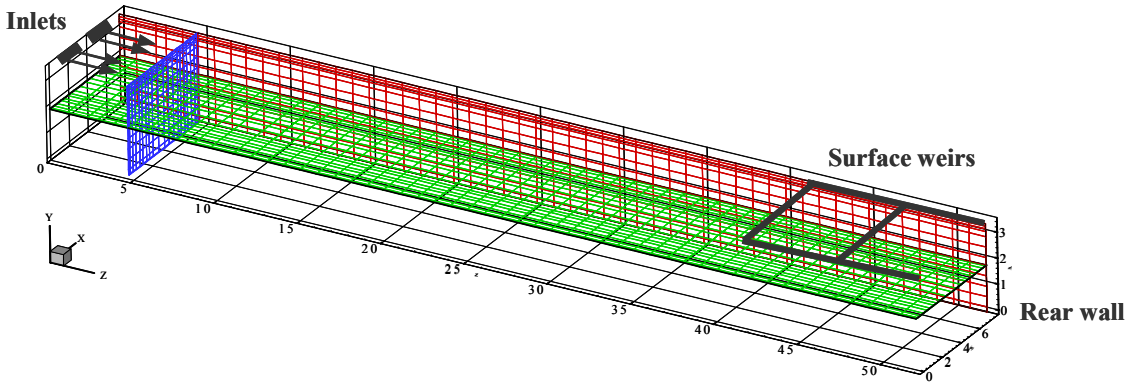

FIG. 17. 3-D grid generation of a final clarifier.

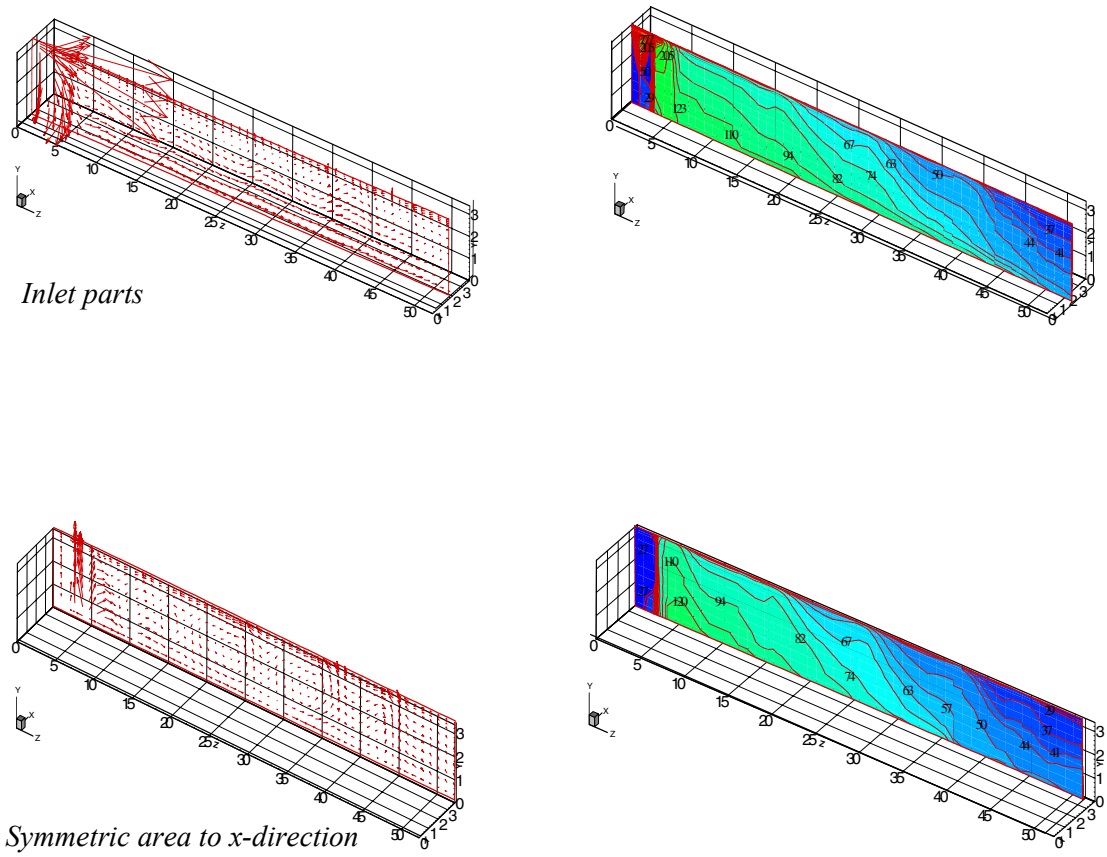

FIG. 18. Velocity vector and solid concentration fields on YZ area.

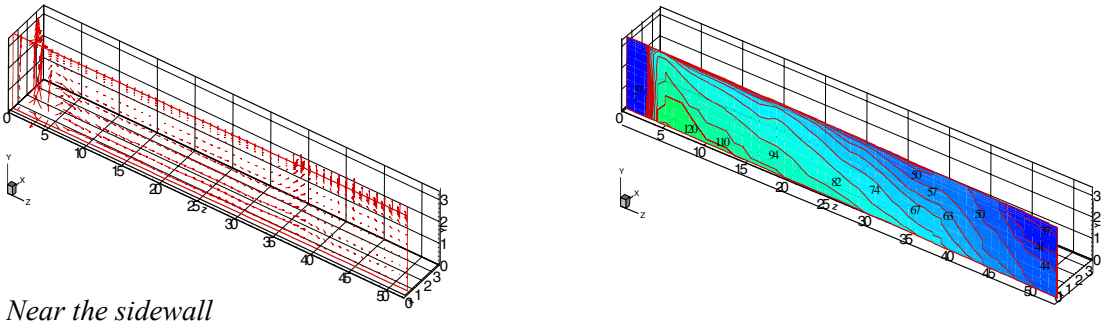

Near the sidewall

FIG. 19. Velocity vector and solid concentration fields on YZ area.

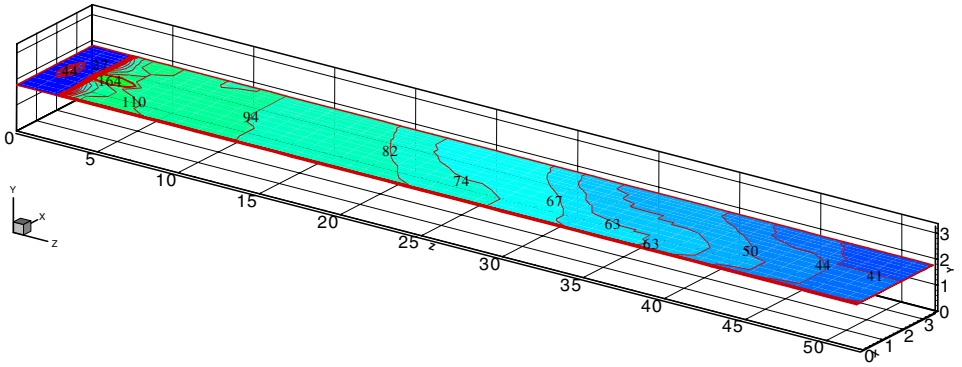

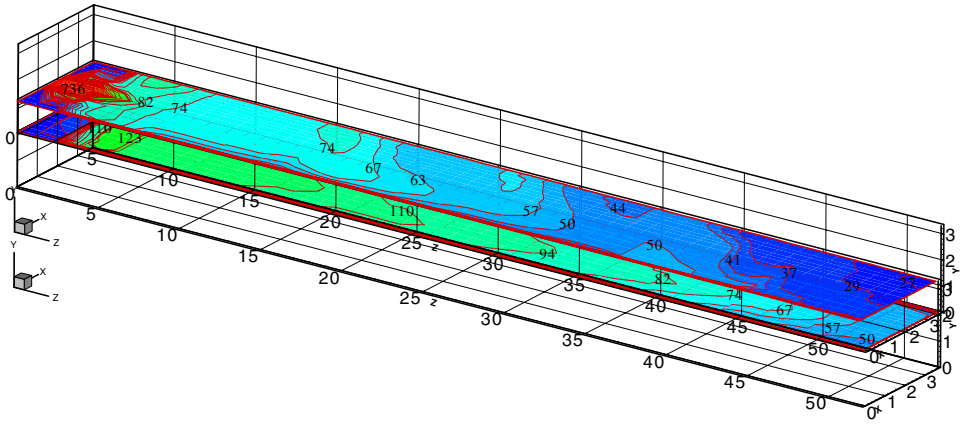

Water surface

FIG. 20. Suspended solid concentration on XZ area.

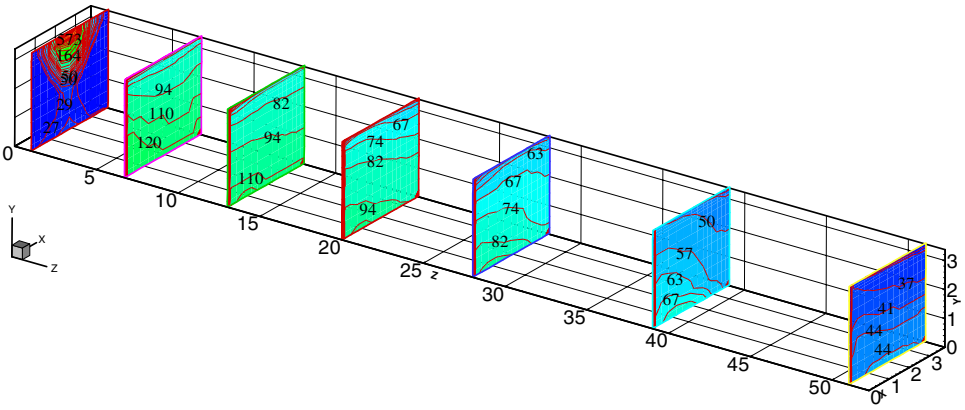

FIG. 21. Velocity vector field along the horizontal direction.

8. CONCLUSIONS

CFD simulation from 2-D model of fluid flow predicted successfully the measured concentration-time curves of radioactive tracer. In more detail, the simulated RTD profiles are generally in good agreement with the experimental RTD curves especially at the upstream and the middle-stream sections but a relatively visible difference was noted at the area of discharge weirs. The simulation predicted well the well-known characteristics of clarifier flow such as the waterfall phenomenon at the front end of the clarifier, the bottom density current in the settling zone and the upward flow in the withdrawal zone, which are induced by the density effect by the existence of suspended solid. Further the result of parametric investigation is consistent and physically acceptable.

Thus it is believed that the computational fluid dynamics (CFD) program developed in this study is considered as a viable tool for the proper design and determination of optimal operating condition of a full-scale clarifier. But a systematic, quantitative evaluation of 3-D configuration of the weir will be one of the major research topics by the development of 3-D CFD model in near future.

REFERENCES

[1] BROUCKAERT, C. J. and BUCKLEY, C. A., The use of computational fluid dynamics for improving the design and operation of water and wastewater treatment plants, Water science technology, 40(4–5) (1999) 81–89.

[2] JANG, D.S. AND H.S. KIM, CFD model development for radioisotope tracer technique, KAERI/CM-624/2002.

[3] KIM, H.S., M.S. SHIN, S.I. LEE and JANG D.S., Numerical study for a secondary circular clarifier with density effect, WAPDEC, New Delhi, India (2002).

[4] PARK, B.S., K.M. KIM, W.Y. SONG, D.S. JANG AND O.H. KWAN, Development and application of a computer program for the analysis of heat transfer and fluid flow of water body: lake and primary clarifier, J. of Korea Water Resources, 29(6) (1996) 141–154.

[5] LEE, E.J., B.S. PARK, D.S. JANG, and S.I LEE, A numerical study on the design of primary clarifier; SS concentration and FTC, J of KSEE, 18 (11) (1996) 1335–1346.

[6] LYN, D.A., STAMOU, A.I. AND RODI, W., Density currents and shear-induced flocculation in sedimentation tanks, Journal of hydraulic Engineering, 118(6) (1992) 849–867.

[7] MAZZOLANI, G., PIROZZI, F. AND D'ANTONOI, G., A generalized settling approach in the numerical modeling of sedimentation tanks, Water science technology, 38(3) (1998) 95–102.

[8] MCCORQUODALE, J. A. AND ZHOU, S., Effect of hydraulic and solids loading on clarifier performance, Journal of hydraulic research, 31(4) (1993) 461–478.

[9] PATANKAR, S. V., Numerical heat transfer and fluid flow, McGraw-Hill Company (1980).
[10] STAMOU, A. I., Modelling of settling tanks – a critical review, Invited paper, pp.305–312 (1994).
[11] STAMOU, A. I. AND RODI, W., Numerical modeling of flow and settling in primary rectangular clarifiers, Journal of hydraulic research, 27(5) (1989) 665–682.
[12] TAKACS I, PATRY G. G. AND NOLASCO D., A dynamic model of the clarification – thickening process. Wat. Res., 25(10) (1991) 1263–1271.
[13] WELL, S. A. and LALIBERTE, D. M., Winter temperature gradients in circular clarifier, Water environment research, 70(7) (1998) 1274–1279.
[14] ZHOU, S. AND MCCORQUODALE, J. A., Influence of density on circular clarifiers with baffles, Journal of Environmental Engineering, 118(6) (1992a) 829–847.
[15] ZHOU, S. AND MCCORQUODALE, J. A., Modeling of rectangular settling tanks, Journal of Hydraulic Engineering, 118(10) (1992b) 1391–1405.

CONRIBUTIONS TO THE CRP INTEGRATION OF RTD TRACING WITH CFD SIMULATION FOR PROCESS VISUALIZATION AND OPTIMIZATION

R. GARDNER, A. SHEHATA, CH.HUFFMAN, V. METWALLY, W. GUO
Center for Engineering Applications of Radioisotopes,
Department of Nuclear Engineering, North Carolina State University,
Raleigh, North Carolina, United States of America

Abstract

Four contribution areas have been treated during the three years of this CRP. In the first year the contribution was entitled "On Combining and Experimentally Verifying the CFD and RTD Approaches by Monte Carlo Simulation". That work was based largely on a paper that appeared earlier in Nuclear Science and Engineering. In the second year the contribution was entitled "Improving the Radioactve Particle Tracking (RPT) Technique by Dual Energy and Nonlinear Inverse Analysis Approaches". In the third year the two contributions were on: (1) RTD and Other Tracer Experiments on a Single Vessel for CFD Evaluation and (2) a Dynamic Radioactive Particle Tracker. The first two contribution areas for the first two years are reviewed here in abbreviated form since they were covered in detail previously. The second two are covered in more detail here since they have not been treated previously.

1. OBJECTIVE OF THE RESEARCH

The recent success of computational fluid dynamics (CFD) has opened up the possibility of being able to predict the flow and dispersion of fluids in process vessels such as fluidized beds and other unit processes. However, CFD still suffers from requiring treatments that are not exact, so that it is desirable to benchmark it with experiments. Therefore, it seemed prudent to use radioactive tracer techniques, particularly those related to residence time distribution (RTD) methods, to benchmark and augment the CFD approach. This has led to the present IAEA Cooperative Research program (CRP) to investigate methods in which the two methods can be used to enhance each other.

2. REVIEW OF FIRST TWO YEARS

The Center for Engineering Applications of Radioisotopes (CEAR) became interested in this objective. The first idea that emerged was the use of Monte Carlo simulation to implement CFD results in such a way that the use of the fundamental information generated by CFD could be used in an appropriate Monte Carlo simulation that produces RTD results that could be used to compare with the radioactive tracer method for measuring RTD. Some work that had been done previously on the Monte Carlo simulation of tracer flow [1] was the basis for this idea.

The second idea was on making some possible improvements to the Radioactive Particle Tracking (RPT) approach. This approach has been developed primarily by chemical engineers that probably have limited previous experience in radiation detection, but have the greatest need for the RPT approach.

During the second year of the CRP a group of students in the course Nuclear Engineering 726, Radioisotope Measurement Applications, took this on as a course project. They had the ideas that: (1) a dual energy approach would be useful and (2) a nonlinear inverse solution augmented by Monte Carlo simulation could be implemented for improved accuracy. These two ideas were investigated and reported on in the second CRP meeting. It was concluded that the first idea would give additional useful data that could be used for improved accuracy or it could be used to reduce the number of detection systems required for the same accuracy. It was concluded that this second idea would give improved accuracy. During this work the problem of detection system dead time correction was identified as a major problem area.

3. THIRD YEAR CONTRIBUTION — TRACER EXPERIMENT

At the second year meeting of the CRP it was suggested that it would be good to do an experiment on a simple yet representative process with radioactive and dye tracers for comparing with CFD calculations. After discussion with the CRP members the author was drafted to do the experiment and the group collectively discussed the specifics of what should be done. It was decided that the process should be a simple right circular cylinder filled with water with an inlet at the bottom on one side and an outlet at the top on the other side. An impulse tracer injection was to be made via a straight pipe that is at least 100 diameters in length before reaching the cylinder. The resulting apparatus is shown in Fig. 1.

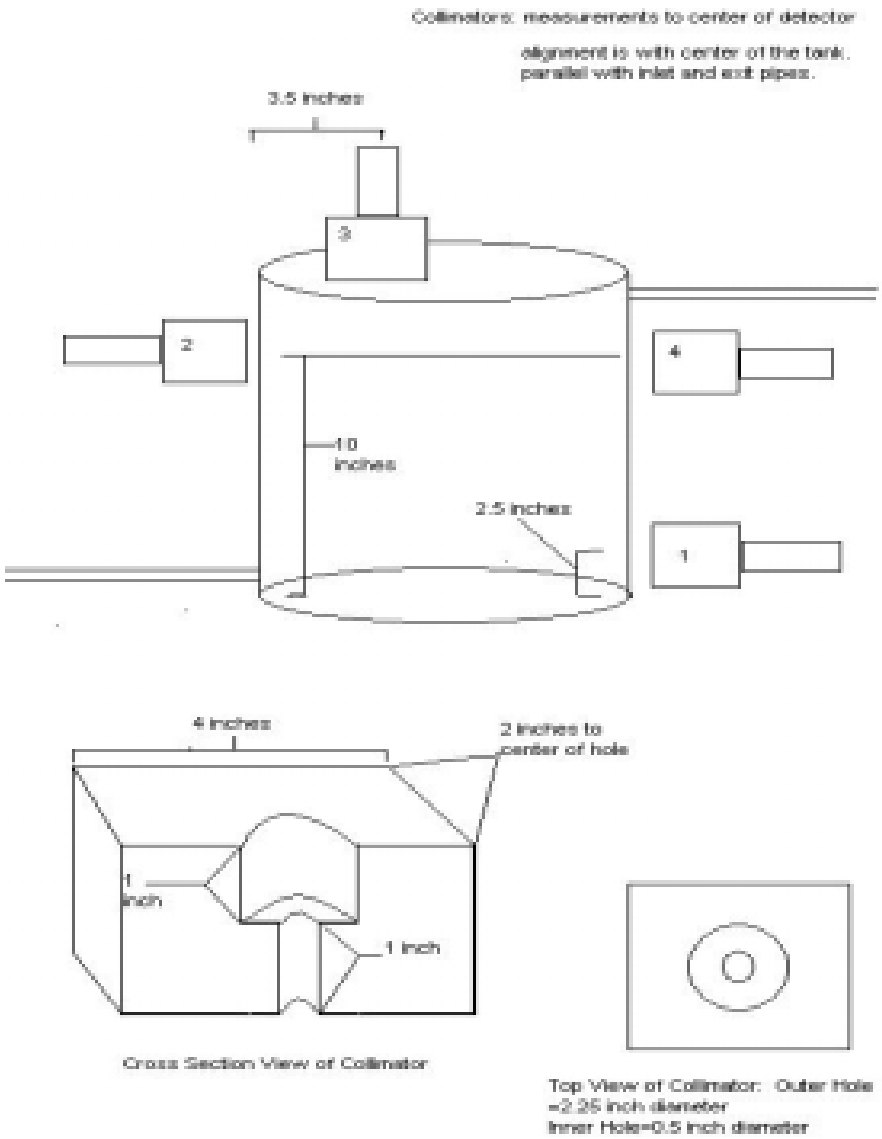

FIG. 1. Drawing with Dimensions of Test Apparatus.

A number of other suggestions were made for things like insuring that the cylinder is completely filled and these were either followed or alternative solutions were employed.

The results of the tracer dye experiments showed that the tracer enters at the bottom left of the cylinder at the inlet and moves to the right bottom side while expanding. It hits the right side and moves upward while still expanding. Then it hits the top and begins to move back to the left. At the time it hits the top it begins delivering tracer to the exit pipe located there at a higher concentration than the average (amount in the cylinder divided by the cylinder volume) would be. It continues to move to the left until it hits the left hand side at the top. At about that point the tracer begins to look as if it is uniformly distributed within the cylinder and no more movement can be discerned after that time. A radioactive tracer was used at the same time as the dye tracer and the results of the radiation detection for that part of the experiment are consistent with the qualitative results of the dye tracer experiment. That is, the counting rate initially exhibits a pulse that quickly decreases to a counting rate that is exponential in shape as a perfect mixing model would predict. A sample experimental plot illustrating this is shown in Fig. 2.

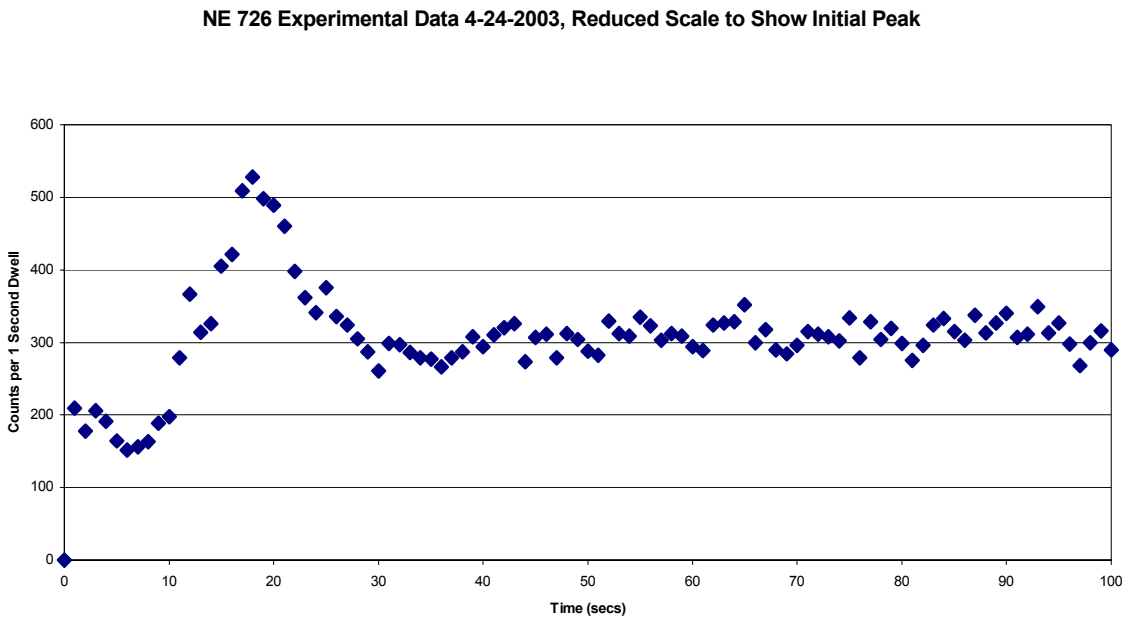

FIG. 2. NE 726 Experimental Data 4/24/03, Reduced Scale to Show Initial Peak

All these results were provided to Mrs. Tu, Patwardhan, Berne, Thyn, Bjornstad, Jin, and Thereska on a CD for intercomparison. Included on the CD were movies of the dye tracer injection experiment and plots and tables of the counting rate data from the radioactive tracer experiments.

4. THIRD YEAR CONTRIBUTION – NEW/OLD RPT APPROACH

The authors had previously located an article by Gatt [2] on an alternative hardware and method for radioactive particle tracking (RPT). There were no details in that article about the hardware and method used for RPT, but there were references to reports not in the open literature. Those reports were tracked down by our interlibrary loan department, but were also found not to contain any of the details that we desired.

However, there was a reference in those reports to another internal report to the people that actually developed the hardware and methods. Our interlibrary loan department was finally able to also track down that report [3] and it gave most of the information that we needed.

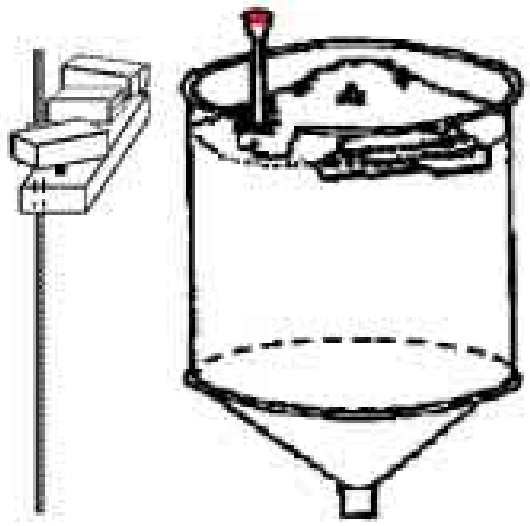

FIG. 3. Schematic drawing of the new approach for radioactive particle tracking (RPT).

This new/old idea is essentially that only three detection systems are used that are collimated and capable of movement in three dimensions to give three directions of the radioactive particle being tracked. The three detection systems are mounted on a movable platform. With the three resulting directions that give the maximum counting rate in each case one can obtain the radioactive particle position. The new part of this idea is that modern techniques can be used to obtain the angular positions of the detection systems when maximum counting rates are obtained rather than the techniques used in 1965 which were largely manual. These modern techniques include the use of encoders that are read with lasers and provide very accurate and fast operation. A Lab View system has been purchased that can be programmed for optimal operation.

This system has been designed and constructed and is presently being tested. It will serve as the PhD thesis of one of the authors (AS). The application of interest is the same as that for the previous inventors – study of the flow in a pebble bed reactor. It has the advantages that: (1) large numbers (80 or more have been reported for some systems) of detectors are not required and (2) the problem of the previous systems of detector dead time should be either eliminated or at least greatly reduced.

An extensive error analysis is being performed for this new/old approach. The details of this are given in the oral presentation for this project.

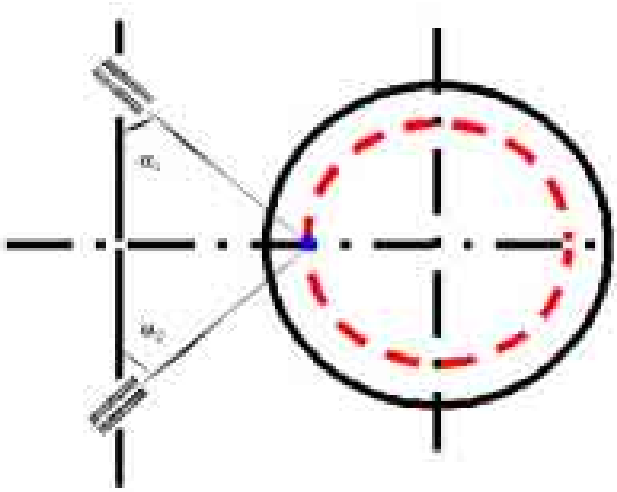

FIG. 4. Schematic representation of the new approach for RPT for the two horizontal detection systems.

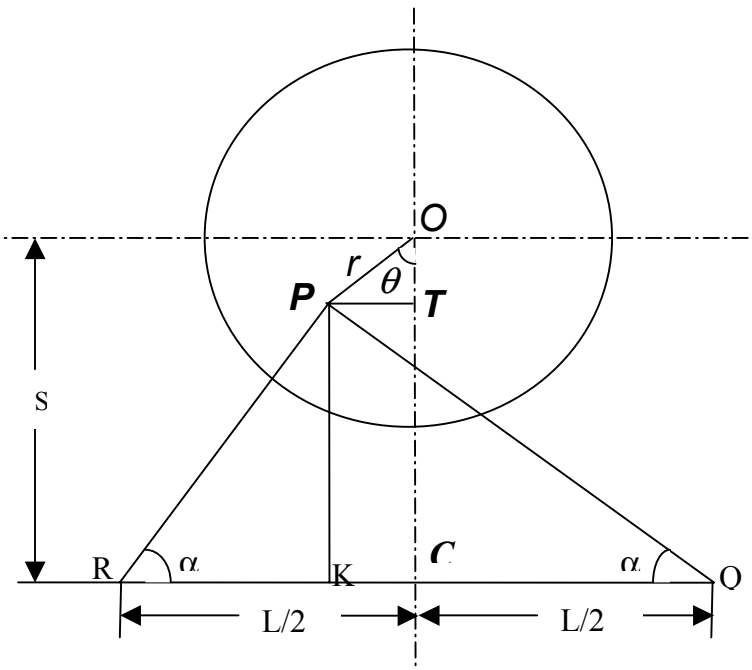

FIG. 5. Schematic diagram of the parameters necessary for obtaining the r, theta positions of the radioactive particle.

REFERENCES

[1] GARDNER, R.P., C.L. BARRETT, W. HAQ, AND D.E. PEPLOW, "Efficient Monte Carlo Simulation of ^{16}O Neutron Activation and 16N Decay Gamma-Ray Detection in a Flowing Fluid for On-Line Oxygen Analysis or Flow Rate Measurement", Nuclear Science and Engineering, 122 (1996) 326–343.

[2] GATT, F.C., "Flow of Individual Pebbles in Cylindrical Vessels", Nuclear Engineering and Design, 42 (1977) 265–276.

[3] GEESON, C.T. AND C.D.G. SHAW, "Scanner Control Unit", Australian Atomic Energy Commission Research Establishment, Internal Report of A.A.E.C., Lucas Heights, June 1965.

Annex
CFD & RTD EDUCATIONAL PACKAGE

1. OVERVIEW OF FEATURES OF THE PACKAGE

In order to promote integration of CFD and RTD tracer techniques, a recommendation was made in this CRP to develop an education package on CFD-RTD with lecturing materials and simple case studies that will benefit to CRP participants and other tracer groups. In this respect, the features of the package have included:

- A simplified CFD computer code for solving the partial differential equations for flow fields including the flow velocities, pressure and temperature and tracer concentrations;
- A simplified RTD computer code for solving the mathematic equations based on RTD concepts for studying flow fields in various configurations;
- A user-friendly interface for using both CFD and RTD computer codes;
- Basic knowledge of CFD and RTD in the form of lecture notes using simplified terms integrated into a user-friendly interface (web-based);
- Five flow cases as examples in tutorials for practicing the use of the CFD code and learning about CFD;
- Several flow cases as examples in tutorials for practicing the use of the RTD code and learning about RTD.

Because the user-friendly web-based interface provides an easy access to materials and future additions to the package, the developed package allows the lecturers more effectively conducting their training courses or workshops to teach the basic knowledge, and allows students or users more easily learning the CFD and RTD knowledge and practicing computer software's. The following presents the examples of the developed CFD&RTD Education package to illustrate the main features of this package.

2. EXAMPLES OF THE PACKAGE

A CD contains the developed CFD-RTD Education Package with the instruction of installation. The package includes both lecture and tutorial materials and computer codes. When click "Introduction to CFD", a sub-web page with a list of lectures allows the participants or users to learn about the CFD, such as, What is CFD, Why CFD, What CFD provides and How CFD works (Fig.1). The package also provides the basic concept about the integration of CFD with RTD and their interaction. In the lectures, the package provides three levels of CFD lecture notes. The following five lectures can be delivered in order to teach or learn the basic knowledge of CFD through the use of this package:

- Introduction to CFD
- Fundamentals of CFD (Elementary CFD)
- How to use a CFD code (Elementary CFD)
- Turbulence Modeling (Intermediate CFD)
- Modeling of Industrial Multi-Phase Flows (Advanced CFD).

FIG. 1. Sub-web page and lecture notes of Introduction to CFD.

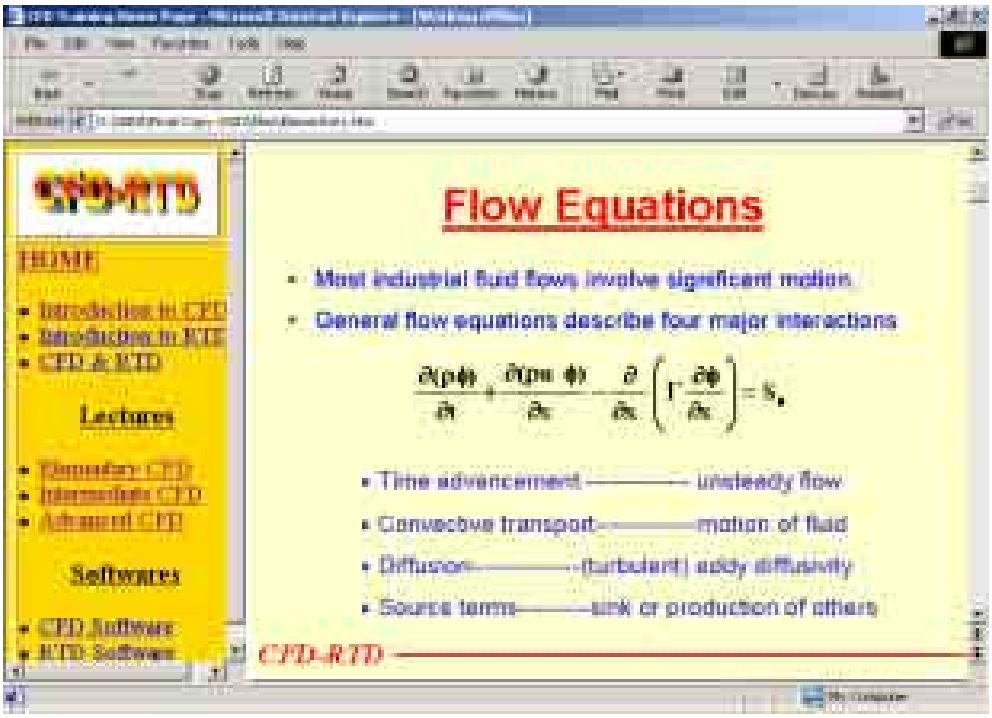

FIG. 2. Fundamentals of the CFD.

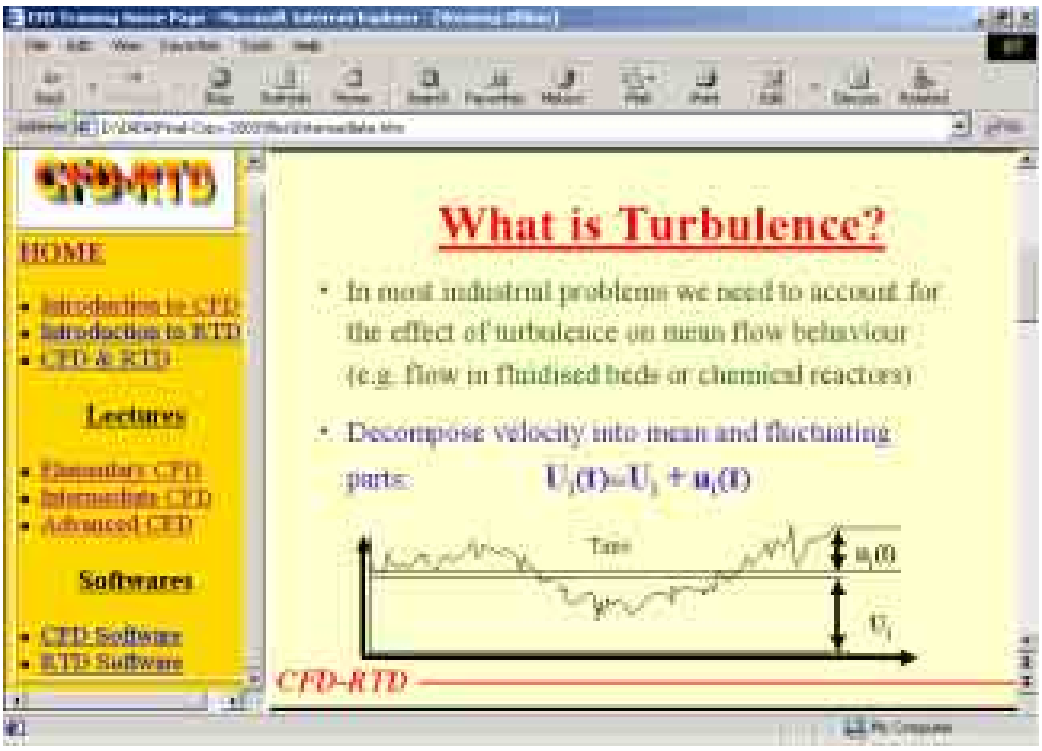

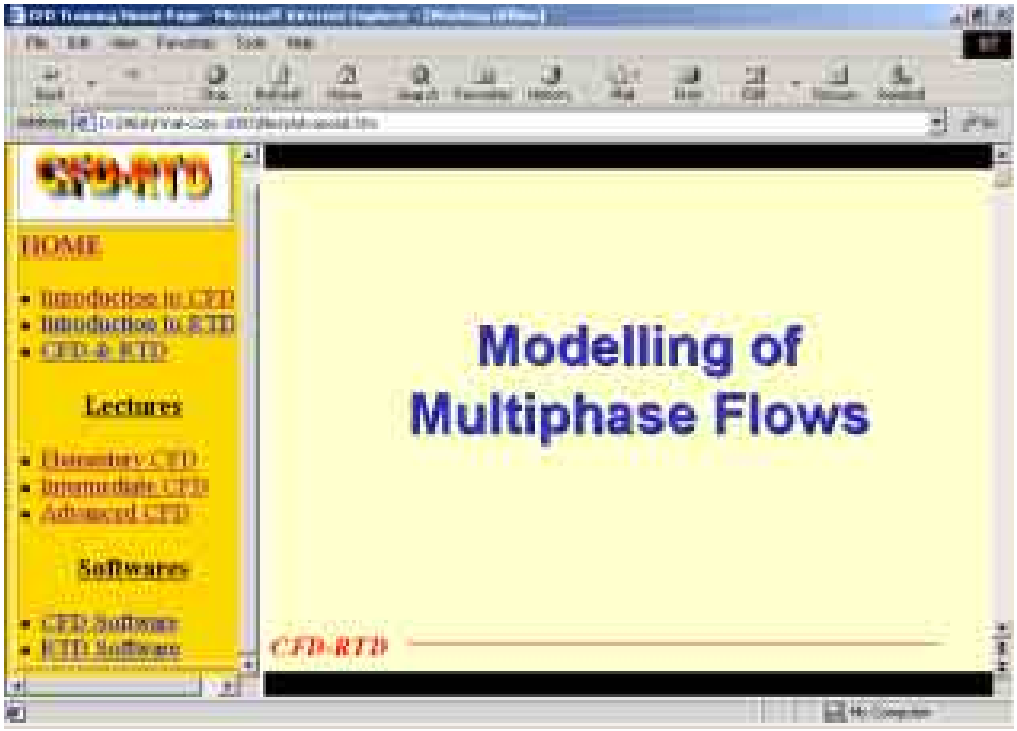

FIG. 3. Modelling of multiphase flows.

It is important that the participants or users can learn how to use a CFD computer code through the hands-on tutorials for practice. Thus, the following five tutorials (Fig.4) were developed for the participants to practice the use of CFD4RTD (short for "CFD for RTD") computer code built in the package:

- Laminar flow in a pipe
- Turbulent flow in a pipe
- Pipe flow with heat transfer
- Turbulent flow past a backward facing step
- Modeling of multi-phase flow in a ventilation room

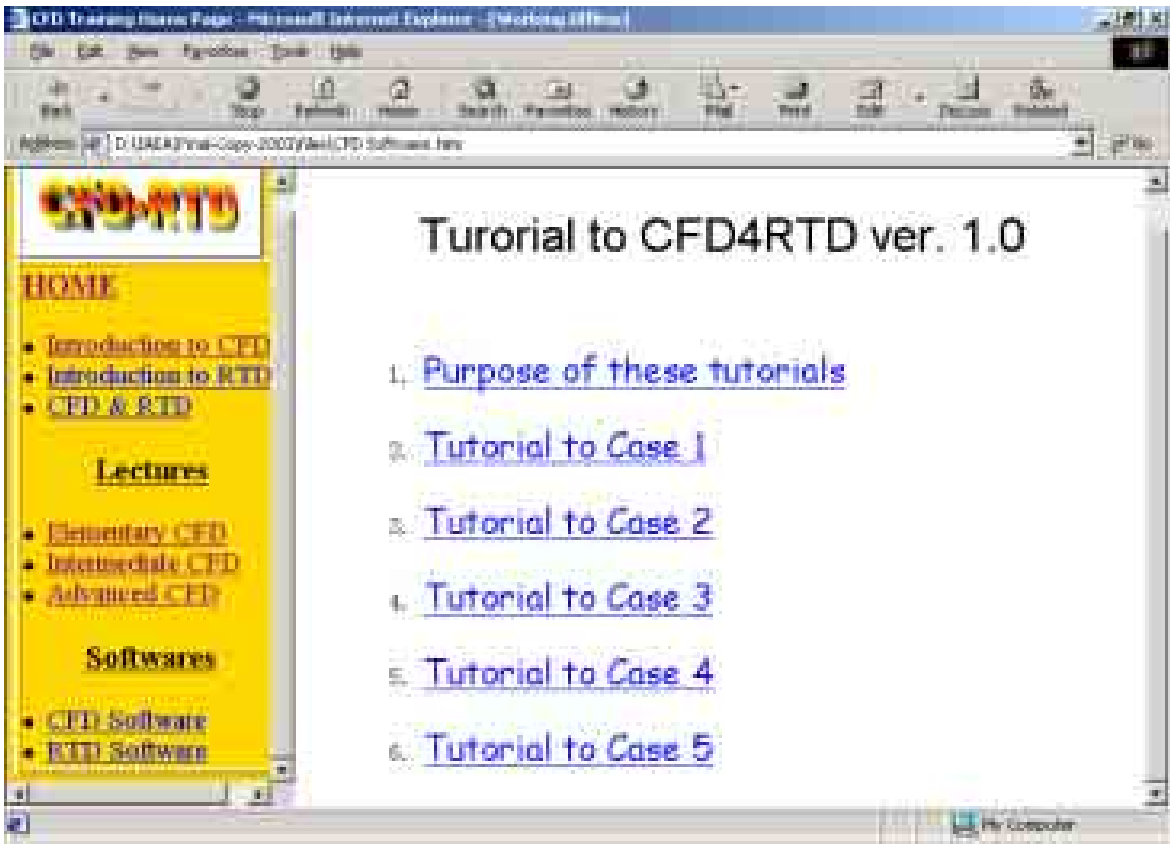

FIG. 4. Sub-web page and tutorial notes for practising the use of CFD4RTD code.

Having gone through all five tutorial materials and practiced all basic steps of using the CFD4RTD computer code as particularly designed for non CFD specialists such as tracer group practitioners (Fig.5 and 6), users should be able to use the CFD&RTD computer code by themselves through the changes of different parameters and conditions for different new simulations. The detailed flow field and tracer particle concentration distribution in the flow domain such as in a ventilation room (Fig.7) can be visualized and analysed from the simulation using the CFD4RTD computer code.

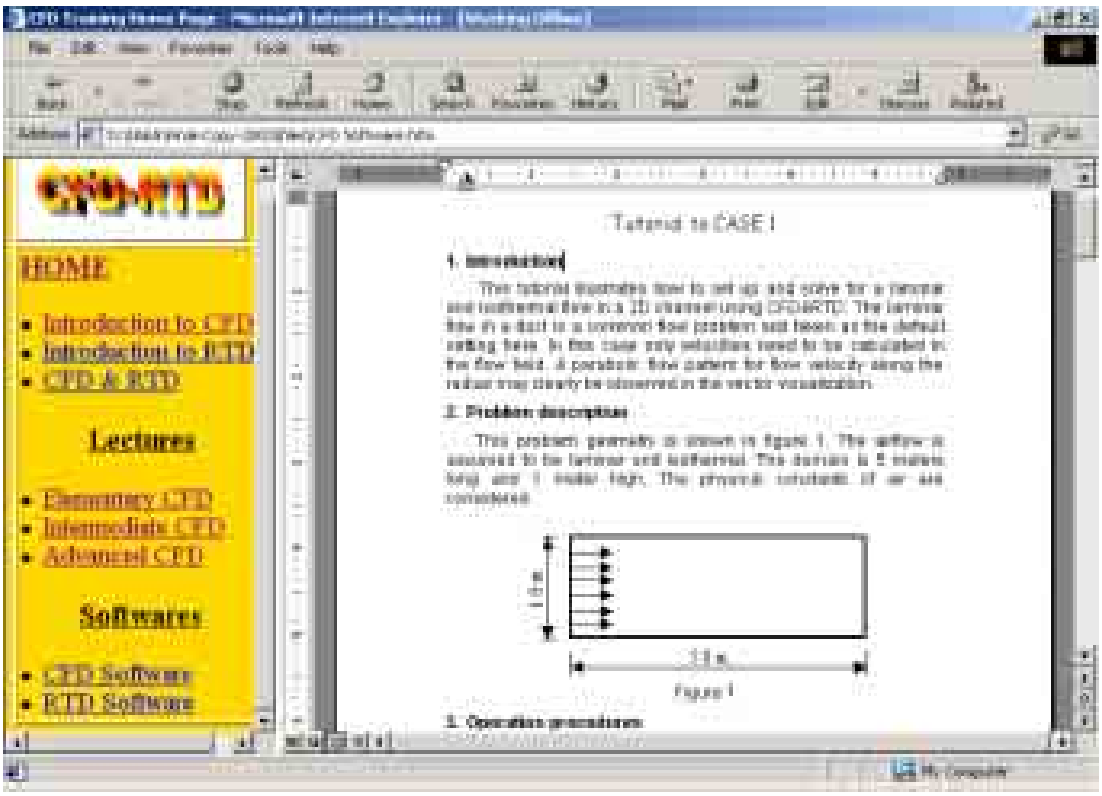

FIG. 5. Detailed tutorial notes for 5 study cases.

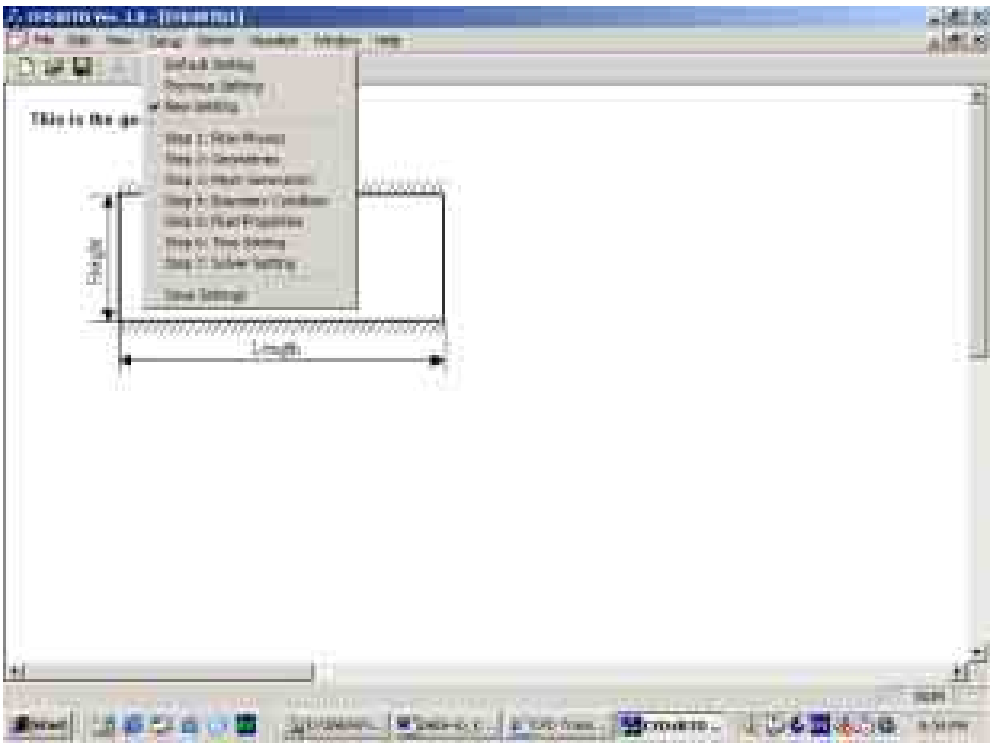

FIG. 6. Windows of the interface for using the CFD4RTD computer code.

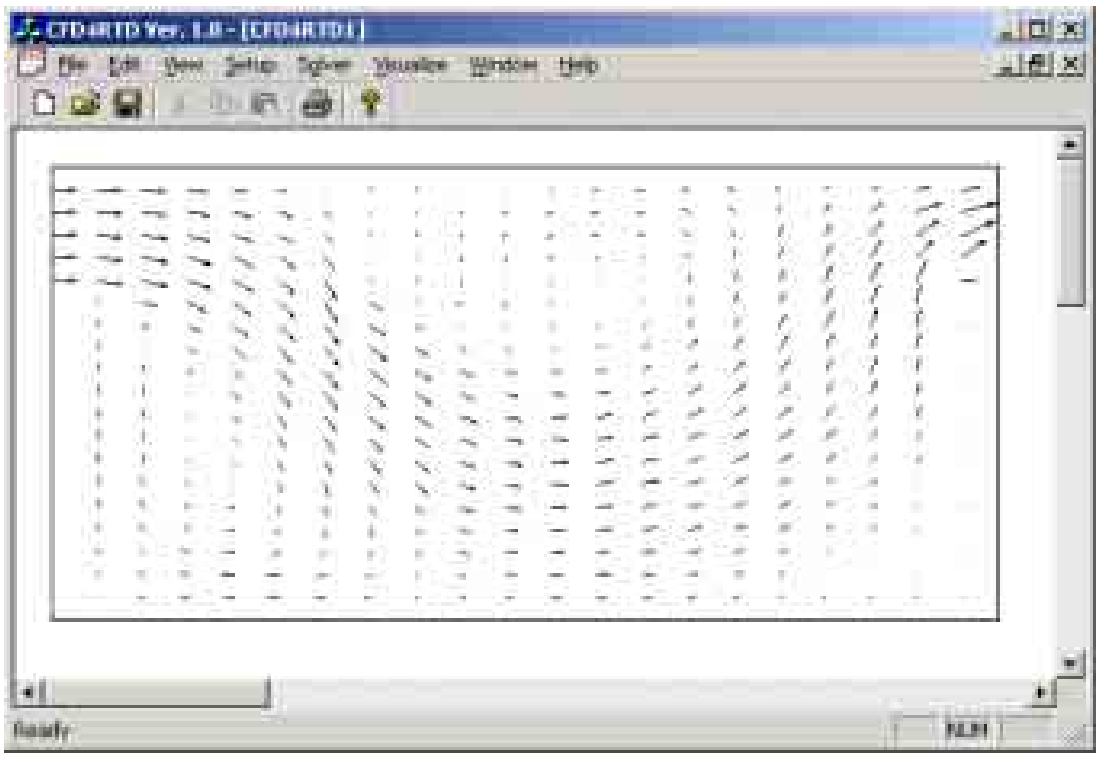

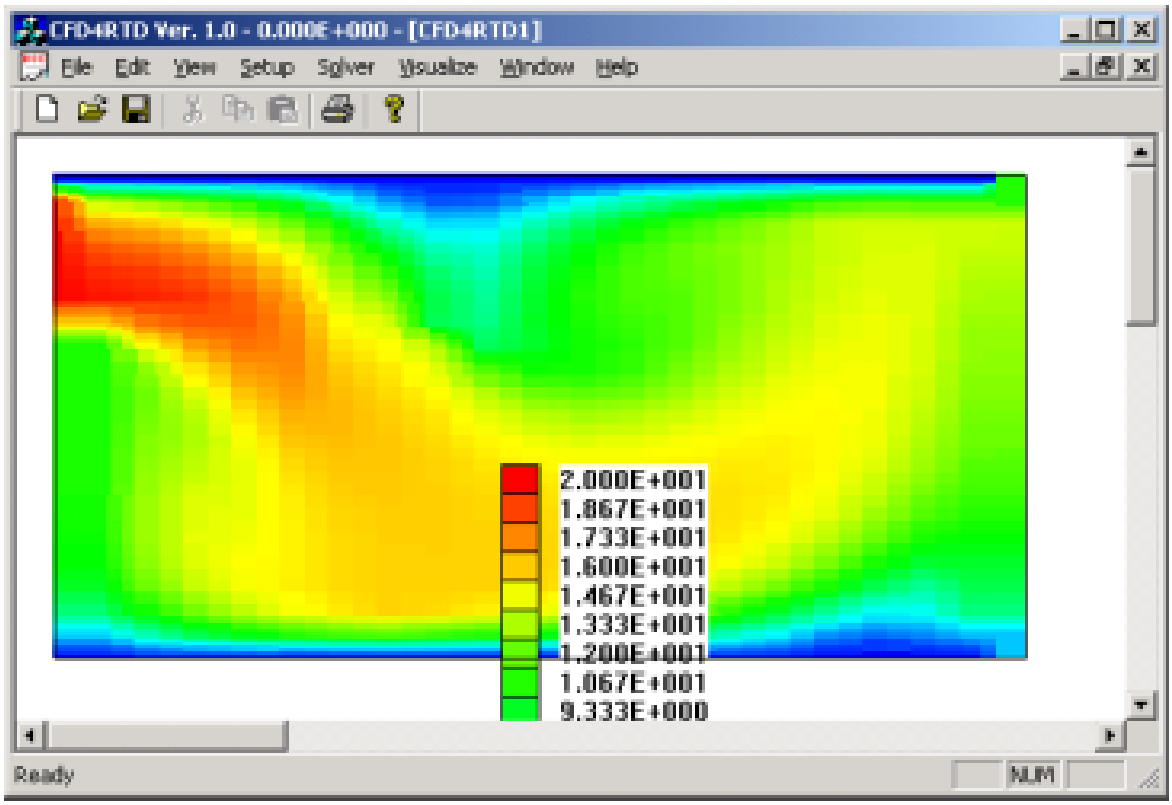

FIG. 7. Flow visualisation and analysis from the CFD4RTD computer code.

When clicking “Introduction to RTD”, a sub-web page with a list of lectures allows the participants or users to learn about the RTD, such as, How RTD Works, Multi-detector Systems, RTD for Waster Water Treatment Plant, RTD in Chemical Process and RTD from A-Z (Figures 8 and 9).

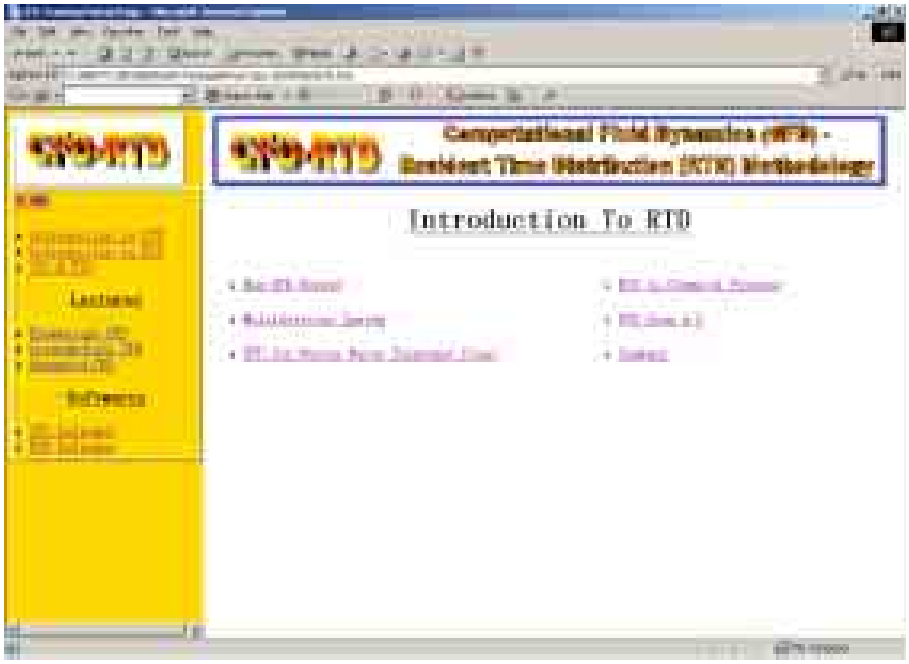

FIG. 8. Sub-web page of Introduction to RTD.

RTD From A - Z

FIG. 9. A variety of RTD applications.

RTD software was also built into the package and it was found that it is very useful not only for education purpose but also for some practical uses during RTD experiments. In particular, this software includes many optimization options and model selections that can help users have a better understanding of RTD techniques and modeling algorithms.

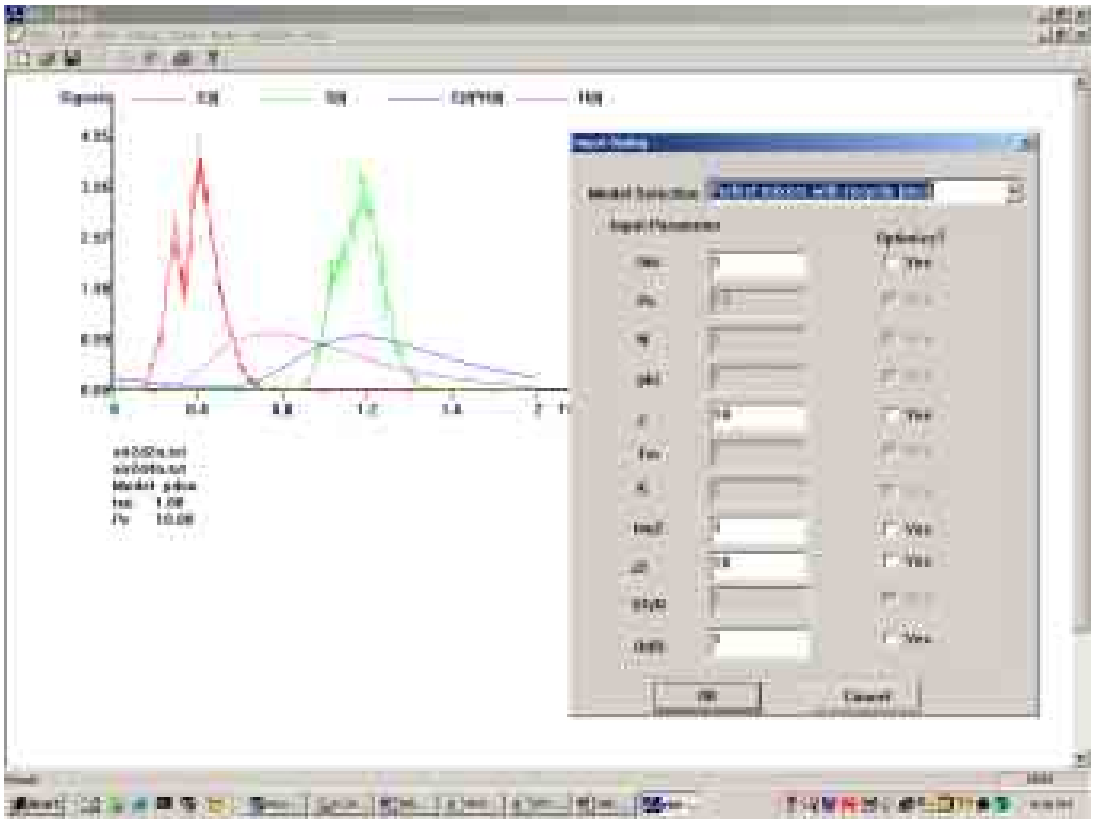

FIG. 10. User-interface of using RTD software built in the package.

3. CONCLUSION AND RECOMMENDATION ONCFD & RTD EDUCATION PACKAGE

CFD for multiphase flow has made significant strides in recent years and is rapidly becoming a useful tool for system design, scale-up and optimization. However, detailed, no-intrusive experimental data are lacking for comprehensive validation of mathematical models in CFD software for solving complex industrial problems. Radioisotope tracer techniques could play an important role in addressing this problem through RTD analysis due to its advantages over many conventional techniques. CFD simulation could also be used for RTD analysis in characterizing the basic flow behavior of the processing units or plants. The numerical tracer tests by using CFD, based on the calculated flow field, could be an effective tool in combination with the tracer experiment/field-scale measurements. RTD analysis, together with the detailed knowledge of flow and temperature distribution throughout the system, can give a more complete picture or visualization of the flow characteristics of the multiphase processing system.

The integration of CFD with radiotracer RTD techniques may become a complementary technology to be greatly beneficial for industrial applications (cost-effectively consulting and services).

In the framework of the CRP a CFD&RTD Education Package has been developed to promote the integration of these two methods. The package includes lecture notes, tutorials and computer software's for both CFD and RTD. A user-friendly web-based interface was developed to allow more effectively conducting the training courses or workshops and to allow students or users to more easily learn and practices the CFD and RTD knowledge and computer programs.

The CFD-RTD software is provided together with this TECDOC.

LIST OF PARTICIPANTS

Berne, P.	DTEN/SAT, CEA/Grenoble, France
Bjornstad, T.	Institute for Energy Technology, Kjeller, Norway
Gardner, R.P.	North Carolina State University, Raleigh, NC, USA
Jentsch, T.	Fraunhofer Institut fuer Zerstorungsfrei Prufverfahren, Dresden, Germany
Jin, Joon-Ha	International Atomic Energy Agency
Jung, Sung-Hee	Korea Atomic Energy Research Institute, Taejon, Republic of Korea
Martinez, J.G.	ICINAZ, Havana, Cuba
Moreira, R.M.	CNEN, CDTN, Belo Horizonte, Brazil
Pant, H.J.	Bhabha Atomic Research Center, Mumbai, India
Stegowski, Z.	University of Mining and Metallurgy, Krakow, Poland
Thereska, J.	International Atomic Energy Agency
Thyn, J.	Czech Technical University, Prague, Czech Republic
Tu, Jiyuan	Australian Nuclear Sciences and Technology Organization, Menai, Australia

Research Coordination Meetings

Vienna, Austria: 5–8 May 2001
Saclay, France: 15–19 July 2002
Vienna, Austria: 1–5 December 2003